NASA CR - 132546
SER-50905

Flight Investigation of Rotor/Vehicle State Feedback

By Stanley J. Briczinski

and Dean E. Cooper

Prepared under Contract No. NAS1 - 11563 by
SIKORSKY AIRCRAFT DIVISION
UNITED AIRCRAFT CORPORATION
Stratford, Conn.
for
USAAMRDL LANGLEY DIRECTORATE
and
NATIONAL AERONAUTICS AND SPACE ADMINISTRATION

TABLE OF CONTENTS

TABLE OF CONTENTS (cont.)

TABLE OF CONTENTS (cont.)

FLIGHT INVESTIGATION OF ROTOR/VEHICLE STATE FEEDBACK*

By Stanley J. Briczinski and Dean E. Cooper
Sikorsky Aircraft Division
United Aircraft Corporation

SUMMARY

Analytic and test results of the Rotor/Vehicle State Feedback Investigation indicate that feedback networks can be used successfully to simulate the important flying quality and ride comfort aspects of mechanical flapping-feathering coupled arrangements. Factors such as accuracy of tip-path-plane resolution, computer time lags, control system hysteresis, and actuator dynamics are either negligible, can be compensated for, or do not sufficiently influence the results to alter this general conclusion. A ruggedized commercial computer, installed on a CH-53A helicopter, was programmed successfully to handle a wide variety of rotor and fuselage feedback schemes and related operating logic which was investigated during the flight test phase of this study. The program cycle time was approximately twice as fast as the most demanding sampling rate studied (24 samples per revolution).

The investigation indicates that the dynamically varying first harmonic contributions (tip-path-plane coefficients) of main rotor blade flapping can be resolved from blade flapping measurements when data supplied to the resolver meet particular requirements, i.e., all or every other blade sampled at least 6 times per rotor revolution. Of the resolver techniques under consideration, the Kalman estimator was found to be the most desirable method. It yields an estimate of tip-path-plane dynamics which is acceptable for use in feedback operations even when higher flapping harmonics are present, or when measurement noise contaminates the flapping signal, as validated by test data at speeds up to 150 knots.

Those feedback schemes which showed the best results as gust alleviation methods during the analytic portion of the investigation were flight tested to determine their gust response suppression and handling qualities characteristics, and to determine the feedback gain limit based on rotor stability considerations. The pilots noticed improved ride comfort characteristics while testing the helicopter response to gust disturbances when the helicopter employed Delta-3, Oehmichen, pure pitch-cone, or normal load factor feedback. Test data showed a 30 to 50% reduction in transient normal load factor response to gust disturbances compared to the response of the basic helicopter. In flight, the

---

* The contract research effort which has lead to the results in this report was financially supported by USAAMRDL (Langley Directorate).

onset of rotor instability was typically observed when rotor feedback gain values were in the vicinity of 0.5 to 0.9 deg/deg. For a given feedback type, the handling qualities of the helicopter varied noticeably with small variation in feedback gain value.

A linear investigation conducted showed that system frequency response characteristics improve when rotor state feedback is used. An improvement in vehicle frequency bandwidth was seen, with the actual amount dependent on the specific loop closures selected. The frequency response improvements that are expected may diminish when considerations not included in the analysis are incorporated. Such factors as blade lag degrees of freedom, control system/fuselage interaction, and sensor mountings have been observed, in this and previous testing, to reduce achievable augmentation loop gains (and thus bandwidth) to values below those predicted analytically.

INTRODUCTION

The two major objectives of the Rotor/Vehicle State Feedback Investigation are:

1. Study the feasibility of using control feedback of rotor tip-path-plane motion or body state as a means of altering rotor and fuselage response in a prescribed manner.

2. Determine the practical limitations of in-flight utilization of a digital computer which conditions and shapes rotor flapping and fuselage state information as feedback signals, before routing these signals to the differential servo actuators.

Suitability of the feedback techniques under investigation is based on overall system stability and system response to control inputs. Also, the potential usefulness of estimated rotor and fuselage state feedback for reducing the response of the helicopter to gust disturbances is examined. Results of this investigation also lend insight to important considerations when incorporating a digital computer in the helicopter automatic flight control system (AFCS).

The investigation consists of two major phases - an analytic and a flight test phase. This report examines and discusses the analysis and test of various feedback schemes. The schemes considered are:

Rotor

(1) Delta-3
(2) Oehmichen
(3) Delta-3/Oehmichen
(4) Pure pitch-cone
(5) Proportional, type I
(6) Proportional, type II

Fuselage

(7) Angle-of-attack
(8) Normal load factor
(9) Pitch acceleration

Rotor and Fuselage

(10) Thrust vector control

Based on the findings of previous analytic research, the feedback schemes listed above warranted additional investigation at the time the Rotor/Vehicle feedback study began. Until now, little test work had been conducted to support existing theory or analytic findings because of the huge undertaking involved with mechanically configuring the rotor feedback schemes, or because of the unavailability of a versatile and reliable digital computer which could be used for the in-flight implementation of these rotor and vehicle feedback schemes. Also, recent discoveries in estimation techniques have increased the accuracy of predicting rotor state variables or fuselage accelerations from filtered measurement data, which is a necessary part of incorporating these feedback methods in the helicopter control system.

Because the rotor feedback schemes are based on displacement of the rotor tip path plane from its trim orientation, the analysis first investigates various methods for resolving (estimating) a tip path plane from blade flapping data. The best resolver is then incorporated in a nonlinear helicopter simulation model, which forms the basis for the analysis of the feedback systems. Linear models are obtained from the nonlinear models and are used to study the stability of the helicopter, employing various feedback systems. The feedback systems are then written into the nonlinear model, which is then used to evaluate gust alleviation characteristics, system stability, control orthogonality, and AFCS authority limits. Linear stability results are compared to the nonlinear findings.

Based on the findings of the analytic phase, feedback schemes of potential interest are selected and are tested in flight on a CH-53A (Figure 1), carrying a Digital Equipment Corporation PDP-11/R20 computer for the utilization of rotor/vehicle feedback techniques. The resulting test data are analyzed and compared to the analytic work. Conclusions are drawn about the tip-path-plane resolver, the feedback schemes, and the interaction of the helicopter/computer/control system based on the combined findings of the analytic and test portions of the study.

John Molusis prepared the estimation techniques used in the study, while Raymond Hansen conducted the eigenvalue linear stability analysis. Raymond Brand programmed the tip-path-plane resolvers and the nonlinear helicopter and control system model. Donald Fowler modified the existing control system of the helicopter to accept the computer interface, and also designed the engineer's and pilot's feedback control panels. Thomas McGeough assisted in coordinating the test program and processed the test data. Charles Reine was the program test pilot. At the time the investigation was conducted, all of the forementioned persons were engineers at Sikorsky Aircraft. Gregory Condon is the NASA/U. S. Army technical representative of this contract.

SYMBOLS

$\underline{\underline{A}}$	matrix representation of the linear model coefficients of the helicopter rotor and fuselage variables
A_{1S}	main rotor lateral cyclic blade pitch control, deg
a_{0S}	main rotor coning angle, deg
a_{1S}	main rotor first harmonic longitudinal flapping, deg
a_{2S}	main rotor second harmonic longitudinal flapping, deg
a_{3S}	main rotor third harmonic longitudinal flapping, deg
$\underline{\underline{B}}$	matrix representation of the linear model coefficients of the helicopter control variables
B_{1S}	main rotor longitudinal cyclic blade pitch control, deg
b_{1S}	main rotor first harmonic lateral flapping, deg
b_{2S}	main rotor second harmonic lateral flapping, deg
b_{3S}	main rotor third harmonic lateral flapping, deg
$\underline{\underline{D}}$	function relating the time derivatives of state of the helicopter to the values of the state variables
E	feed-forward parameter which maintains control sensitivity of a helicopter employing rotor feedback
G	normal helicopter acceleration, nondimensionalized by the acceleration of gravity
$\underline{\underline{H}}$	state variable representation of the periodic function of the helicopter
h_1	rotor feedback out-of-phase flap-pitch gain, deg/deg
h_2	rotor feedback in-phase flap-pitch gain, deg/deg
h_3	rotor feedback coning gain, deg/deg
I	identify matrix
I_{xx}	moment of inertia of the helicopter about the roll axis, slug-ft^2
I_{yy}	moment of inertia of the helicopter about the pitch axis, slug-ft^2

K_b	general feedback loop gain
K_f	general forward loop gain
K_1	Delta-3 rotor feedback gain, deg/deg
K_2	Oehmichen rotor feedback gain, deg/deg
K_3	Delta-3/Oehmichen rotor feedback gain, deg/deg
K_4	type I proportional rotor feedback gain, deg/deg
K_5	type II proportional rotor feedback gain, deg/deg
K_6	pure pitch-cone rotor feedback gain, deg/deg
K_7	angle-of-attack feedback gain, deg/deg
K_8	normal load factor feedback gain, deg/G
K_9	pitch acceleration feedback gain, deg/(deg/sec^2)
K_{10}	rotor vector control feedback gain, deg/deg
K_{11-15}	control orthogonality and sensitivity feed-forward gains, deg/in.
K_{16}	SAS roll rate feedback gain, deg/(deg/sec)
K_{17}	SAS pitch rate feedback gain, deg/(deg/sec)
L	helicopter rolling moment, ft-lb
M	helicopter pitching moment, ft-lb; also, thrust vector control model, deg/in.
M_G	component of magnitude of collective input used to simulate gust disturbance of rotor, deg
$\underline{m}$	Kalman estimator initial state covariance vector, deg^2
N	counter of the number of times the tip-path-plane resolver computer routine is solved
N_Z	helicopter normal load factor
n_b	number of blades sampled for flapping by the tip-path-plane resolver
n_s	number of times a blade is sampled for flapping by the tip-path-plane resolver, per rotor revolution

$O(s)/I(s)$	transfer function of the helicopter control (servo) system:ratio of the Laplace transform of the output at the primary servo over the input at the AFCS servo
$\underline{P}$	Kalman estimator state covariance vector, deg^2
p	helicopter roll rate, deg/sec
$\underline{Q}$	Kalman estimator process noise covariance vector (multiplied by the time interval of the solution), deg^2
q	helicopter pitch rate, deg/sec
R	Kalman estimator measurement noise covariance, deg^2
r	helicopter yaw rate, deg/sec
T	time interval between updates of the blade flapping measurements inputted into the tip-path-plane resolver (sampling interval); computer duty cycle
T_{MR}	helicopter main rotor thrust, lb
t_d	time constant for the helicopter control (servo) system delay, sec
$\underline{u}$	vector representation of the helicopter control variables
$\underline{v}$	state variable representation of the model noise and higher harmonics vector function
v_x	helicopter longitudinal velocity, ft/sec
v_y	helicopter lateral velocity, ft/sec
v_z	helicopter normal velocity, ft/sec
$\underline{w}$	state variable representation of the process noise vector function
$\underline{x}$	state variable representation of the transient rotor tip-path-plane and the fuselage vector function
x_1	state variable notation denoting the rotor coning angle, deg
x_2	state variable notation denoting the rotor longitudinal flapping angle, deg
x_3	state variable notation denoting the rotor lateral flapping angle, deg

z	state variable notation denoting blade flapping
α	main rotor angle-of-attack, deg
α_f	fuselage angle-of-attack, deg
β	main rotor blade flapping angle, deg
β'	blade flapping angle modified to include higher harmonic contribution of the tip path plane, deg
β_f	fuselage sideslip angle, deg
β_{HH}	contribution of higher harmonic of the tip path plane to blade flapping, deg
γ_{MR}	main rotor blade lag (hunting) angle, deg
δ_p	pedal input, in.
δ_x	lateral cyclic stick input, in.
δ_y	longitudinal cyclic stick input, in.
δ_Θ	collective stick input, in.
ε	error between the actual and the desired response of the helicopter using thrust vector control, deg
ζ	system damping ratio
ζ_c	system critical damping ratio
η	angle relating helicopter control orthogonality to rotor feedback gains, deg
Θ_b	fuselage pitch attitude, deg
Θ_c	main rotor collective pitch control, deg
Θ_{MR}	main rotor blade pitch (feathering) angle, deg
Θ_R	main rotor thrust orientation from a vertical reference, deg
Θ_{RM}	desired (model) main rotor thrust orientation, deg
ξ	stick feed-forward phase angle, selected by pilot, deg
τ	system time constant, sec
τ_M	time constant of the model lag in the thrust vector control system, sec

ϕ	phase angle of main rotor blades related to an arbitrarily selected blade, deg
ϕ_b	fuselage roll attitude, deg
ψ	main rotor azimuth position, referenced to an arbitrarily selected blade, rad
ψ_b	fuselage yaw attitude, deg
Ω	main rotor rotational frequency, rad/sec
ω_c	system crossover frequency, hz
ω_G	frequency of component of collective input used to simulate a gust disturbance of rotor, rad/sec
ω_η	system undamped natural frequency, rad/sec

Subscripts:

$( )_{FB}$	rotor control commanded by a rotor or vehicle feedback scheme under investigation
$( )_i$	individual main rotor blades
$( )_j$	specific instance in time during a discrete solution
$( )_o$	trim value
$( )_{FF}$	rotor control commanded by on-board stick feed-forward routine
$( )_{SAS}$	rotor control commanded by the SAS system
$( )_{TC}$	total rotor control commanded by the on-board computer routines

Miscellaneous:

(s)	denotes the frequency domain
(t)	denotes time or a function of time
$\Delta( )$	change in a parameter from the trim value
$(\dot{})$	first derivative with respect to time
$(\ddot{})$	second derivative with respect to time
$(\hat{})$	estimated or filtered value calculated by a tip-path-plane resolver, or processed by body filters

$(\underline{\ })$ vector quantity

$(\underline{\underline{\ }})$ matrix quantity

DESCRIPTION OF THE FEEDBACK SCHEMES

Three basic types of feedback concepts were under investigation in either the analytic or test portions of the study: rotor feedback, fuselage feedback, and combined rotor and fuselage feedback. These techniques close the loop on main rotor blade pitch control inputs of collective (θ_c), longitudinal cyclic (B_{1S}), and lateral cyclic (A_{1S}) - all measured relative to the shaft. The feedback control commands are functions of estimated or filtered values of the change from trim of rotor and fuselage parameters.

The method used in this study for implementing the feedback signals into the control system was to input the rotor/vehicle feedback commands through limited authority AFCS servos, which are in series with the primary mechanical system. See Figure 2. Techniques allowing for variable feedback gains were employed, in order to thoroughly study the closed-loop stability and gust alleviation characteristics of the combined rotor/fuselage/control system for individual feedback types.

ROTOR FEEDBACK

The reasons for examining the blade flapping motion feedback schemes described here are to determine the ability of each scheme to reduce the sensitivity of the rotor and fuselage to gust inputs, and to define practical limitations in implementing these schemes electronically.

Six rotor feedback schemes were chosen for investigation on the basis that they are all able, by and large, to be configured mechanically. Figure 3 shows the mechanical arrangements (and the equivalent electronic tip-path-plane feedback approximation) of each scheme. The mechanical schemes function as follows:

1. Delta-3. This technique, the most easily mechanized, changes the pitch of a blade as a function of the blade flapping displacement. (Figure 3b).

2. Oehmichen (Flapping Velocity). For a change in blade flapping, the Oehmichen coupling changes the pitch of an adjacent blade. (Because of the ninety degree relationship between flapping and flapping rate for a four-bladed rotor, the Oehmichen scheme is often referred to as flapping velocity feedback.)

   When the flapping of a blade forces a change in the pitch of the blade behind it, this mechanism is called "rearward-type" Oehmichen. (Figure 3c.) The other possibility is to affect the blade pitch ahead, in which case it is referred to as "forward-type".

3. Delta-3/Oehmichen. This scheme combines Delta-3 and Oehmichen coupling. To minimize the coning portion of the feedback, which is desirable only at low speeds, a select combination of Delta-3 and Oehmichen is required. Figure 4 shows the combinations which will satisfy the requirement. The sketch in Figure 3d reflects point D, noted in Figure 4.

4. Pure Pitch-Cone. This mechanism changes the blade pitch collectively and only for changes in coning. The amount of change is proportional to the coning angle. (Figure 3e.)

5 & 6. Proportional. This category covers combinations generally not easily configured mechanically (but many electronic combinations are possible). Feedbacks studied in this category relate primarily to pure flapping feedback to cyclic control. (Proportional cases discussed further in this report include direct tip-path-plane feedback to cyclic control for specific azimuthal relationships, referred to as Type I and Type II and described in Table I.)

This study concerns itself primarily with the electronic representation or approximation of these rotor feedback schemes. The electronic means of representing rotor feedback was selected over the use of actual mechanical techniques because the electronic technique would be easier and extremely less costly to implement in a flight test program, and would also afford greater variation in the types of feedback and feedback gains which could be studied. Because electronic versions of the feedback schemes were to be used in flight, the models used in the analytic study were derived or modified to include the electronic representation of the feedback schemes.

The tip-path-plane approximation of blade flapping is used to form the basis of the electronic rotor feedback concept. The tip path plane consists of coning (collective flapping) a_{0s}, longitudinal flapping a_{1s}, and lateral flapping b_{1s}. Therefore, all of the mechanical schemes described above can be simulated electronically, to a first order approximation, by feeding back control inputs (through swashplate deflections) which are proportional to coning and first harmonic flapping. The tip-path-plane coefficients can be resolved from blade flapping angles by estimation techniques either written into the analytic models or programmed in the on-board digital computer carried by the test helicopter in flight. The mechanical and electronic representations of a given rotor feedback type may differ somewhat from each other because the mechanical scheme will dictate appropriate blade feathering changes for all harmonic content of blade flapping, while the electronic scheme produces responses only to the estimated coning and first harmonic content of blade flapping.

Because some of the rotor feedback techniques alter or add coupling to the helicopter response to a pilot input, a means of maintaining control orthogonality is examined. This, along with sensitivity changes is attempted by using feed-forward of changes from trim values of the pilot longitudinal stick δ_y, lateral stick δ_x, and collective stick δ_θ positions.

FUSELAGE FEEDBACK

The purpose of examining body state feedback is to determine the ability of body mounted sensors to reduce sensitivity of the helicopter to gust inputs. Three fuselage feedbacks are considered:

1. Angle of Attack - modifies longitudinal cyclic.

2. Load Factor - modifies collective.

3. Pitch Acceleration - modifies longitudinal cyclic.

Standard instrumentation techniques were used to obtain measurement signals of these parameters in flight. The signals were routed to the on-board computer where they were processed by software filters before being implemented as feedback signals.

COMBINED ROTOR AND FUSELAGE FEEDBACK

The purpose of exploring a combined rotor and fuselage feedback configuration is to determine the ability to alter the dynamic response of the helicopter in a prescribed manner by using the same techniques proposed for gust alleviation. Figure 5 illustrates the thrust vector control technique selected for the rotor and fuselage feedback case. System dynamics are modified by using a simple response model M. The configuration employs both conventional vehicle feedback (body pitch attitude), and pure rotor flapping feedback. Feed-forward of the pilot longitudinal stick position is also used. If the angle between a normal to the horizon and the resultant rotor force vector is denoted by Θ_R (positive rearward), then a change in this angle may be expressed as

$$\Delta\Theta_R \cong \Delta a_{1s} + \Delta\Theta_b \qquad (1)$$

The condition desired is to permit the pilot to control the resultant rotor force vector as related to the vertical reference, where

$$\Delta\Theta_R = M\Delta\delta_y \qquad (2)$$

Similar equations exist for the lateral mode (see Table I).

Although this specific feedback scheme was chosen for study on the basis of its use of both a rotor and a body feedback signal, it also provides an opportunity to assess the control aspects of the concept of thrust vector control.

SPECIAL CONSIDERATIONS

This rotor/vehicle feedback study makes no attempt to determine optimum feedback schemes; rather it investigates the operation and determines the preferred feedback gains of feedback schemes which were of notable interest at the time when the study was begun. The primary interest in most of the schemes is in their potential as gust alleviation techniques. These schemes are not necessarily intended to increase the stability of the helicopter. Portions of both the analytic and the test investigations included the incorporation of conventional body rate feedback with some of the rotor feedback and fuselage feedback schemes in order to determine its effect on feedback gain limit, and to determine if the rate feedback provided a more stable system upon which the gust alleviation feedbacks could be evaluated. Any body rate feedback used in addition to the rotor/fuselage feedback was also inputted through the AFCS servos after being calculated within the in-flight computer.

Speaking here of rotor feedback, the operation of the electronic schemes is affected by some control system dynamics (servo and actuator lags) and possibly by some computer hardware and software oriented delays which would not be present in the equivalent mechanical schemes. Also because the electronic feedback excludes the higher harmonic blade flapping contributions which are part of the mechanical feedback, any conclusions drawn about the effectiveness of operation or of the feedback gain limitations of the electronic rotor feedback schemes studies herein may not be exactly the same for the mechanical rotor feedback counterparts.

The rotor, fuselage, and thrust vector control feedbacks, as well as the control orthogonality feed-forward and the conventional feedback, are all summarized in Table Ia. Table Ib illustrates the specific rotor schemes under investigation. These tables present the feedback input parameters and the general gains associated with each scheme. When studying any one of the feedback schemes, all gains of the other schemes are set to zero, except for any feed-forward or conventional feedback desired.

ANALYTIC INVESTIGATION

TIP-PATH-PLANE RESOLVER STUDY

Several methods are presented here for estimating a tip path plane from flapping and evaluating the accuracy of the estimation. The results of the tip-path-plane resolver study are presented and discussed, including selection of the most suitable method and the effects of various parameters on tip-path-plane estimation.

Procedure and Analysis

Tip-path-plane concept. - The rotor feedback techniques under investigation are based on a flapping coefficients representation of the rotor: in particular, the tip-path-plane approximation of rotor state. The problem of determining the flapping coefficients of the rotor can best be understood by examining the solution to the flapping of each blade as sine and cosine functions with time-varying coefficients:

$$\beta_i(t) = a_{os_i}(t) - a_{1s_i}(t)\cos(\Omega t + \phi_i) - b_{1s_i}(t)\sin(\Omega t + \phi_i) - a_{2s_i}(t)\cos 2(\Omega t + \phi_i) + \ldots. \quad (3)$$

where the subscript i denotes each individual blade, Ω is the rotational frequency of the rotor, and ϕ_i is the angle of an individual blade with respect to a selected reference blade. Equations (3) represent the Floquet description of blade flapping. A Floquet concept permits the solution of linear differential equations with periodic coefficients to be written as the products of transient and periodic functions. The greater the number of harmonics of blade flapping included in equations (3), the more accurate they become.

For a trimmed rotor, the coefficients of equations (3) are constant, and the corresponding coefficients for each blade are identical. In a transient, the coefficients are time varying and different for each blade.

The tip-path-plane approximation restricts the time-varying coefficients of the corresponding periodic function of each blade to be identical, rather than different from one another, and assumes a first harmonic representation of flapping. The tip-path-plane expression for flapping thus is

$$\beta_i(t) = a_{os}(t) - a_{1s}(t)\cos(\psi + \phi_i) - b_{1s}(t)\sin(\psi + \phi_i) \quad (4)$$

where ψ is the main rotor azimuth position, referenced to the blade selected as i = 1 and is equal to Ωt. The coning and rotor flapping coefficients of the tip path plane are time-varying for this model, but it assumes a steady state rotor solution at each instant of time at which the tip path plane is evaluated.

Both a Fourier analysis and the Kalman estimator technique are candidates for resolving the tip path plane from blade flapping measurements.

Fourier analysis. - Using equation (4), $a_{os}(t)$, $a_{1s}(t)$, and $b_{1s}(t)$ can be estimated from values of $\beta_i(t)$ by calculating the Fourier coefficients of a Fourier series. At any time t_1, equation (4) is a Fourier series, and the coefficients can be calculated from

$$a_{os}(t_1) = \frac{1}{2\pi}\int_0^{2\pi} \beta(\psi)d\psi$$

$$a_{1s}(t_1) = -\frac{1}{\pi}\int_0^{2\pi} \beta(\psi)\cos(\psi + \phi)d\psi \qquad (5)$$

$$b_{1s}(t_1) = -\frac{1}{\pi}\int_0^{2\pi} \beta(\psi)\sin(\psi + \phi)d\psi$$

At each time instant, however, only a small, discrete number of flapping values are present around the azimuth. If n_b represents the number of blades sampled for flapping, and since each blade is assumed to follow equation (4), then at any fixed instant of time n_b values of flapping are available around the rotor azimuth (o to 2π). Replacing integrals with summations yields:

$$a_{os}(t_1) = \frac{1}{n_b}\sum_{i=1}^{n_b} \beta_i(t_1)$$

$$a_{1s}(t_1) = \frac{-2}{n_b}\sum_{i=1}^{n_b} \beta_i(t_1)\cos(\Omega t_1 + \phi_i) \qquad (6)$$

$$b_{1s}(t_1) = \frac{-2}{n_b}\sum_{i=1}^{n_b} \beta_i(t_1)\sin(\Omega t_1 + \phi_i), \quad i = 1, \ldots, n_b$$

Equations (6) represent the coefficients of the discrete Fourier series at any time instant t_1.

Kalman estimator. - As with the Fourier method, the Kalman estimation solution begins with equation (4). To achieve compatibility with the state variable notation used in Kalman estimating, equation (4) is rewritten as

$$z_i(t) = x_1(t) + x_2(t)\cos(\Omega t + \phi_i) + x_3(t)\sin(\Omega t + \phi_i) \qquad (7)$$

where

$$z_i(t) = \beta_i(t), \quad i = 1, \ldots, n_b$$
$$x_1(t) = a_{os}(t)$$
$$x_2(t) = a_{1s}(t)$$
$$x_3(t) = b_{1s}(t)$$

Equation (7) may be expressed in vector form as

$$\underline{z}(t) = \underline{\underline{H}}(t)\,\underline{x}(t) + \underline{v}(t) \tag{8}$$

where $\underline{\underline{H}}(t)$ represents the periodic function, while $\underline{x}(t)$ denotes the transient time-varying function. Equation (8) is referred to as a measurement equation. $\underline{v}(t)$ is used to model noise and higher harmonics omitted from the first harmonic representation of the rotor, both of which might be included in the value of flapping input to the Kalman estimator.

The time derivative of the state variable, denoted by $\dot{\underline{x}}(t)$, is

$$\dot{\underline{x}}(t) = \underline{\underline{D}}\underline{x}(t) + \underline{w}(t) \tag{9}$$

where $\underline{w}(t)$ is called the process noise. If no *a priori* assumptions are made about the behavior of $\dot{\underline{x}}(t)$, then the function $\underline{\underline{D}}$ is written as zero, and $\dot{\underline{x}}(t)$ is represented just as noise. Equation (9) becomes simply

$$\dot{\underline{x}}(t) = \underline{w}(t) \tag{10}$$

Before measurement, and in a transient condition, it cannot be assumed that anything is known about the variation of $\underline{x}(t)$ from trim. Therefore the process noise, which represents the rate of change of $\underline{x}(t)$, is usually modeled as white noise. The process noise does not necessarily represent an error in any measurement, but represents unknown modeling errors.

Equations (8) and (10) are in a form suitable for use with the Kalman estimation technique. The Kalman estimator is easily implemented for on-line filtering via digital computer programming and provides the optimum estimates, $\hat{\underline{x}}(t)$, of the tip-path-plane coefficients. The Kalman estimator equations for the tip-path-plane model presented below are in a form for the "discrete data points" solution required by digital computer methods.

Let T be the time interval between updates of the flapping values inputted to the Kalman estimator. Then

$$T = (2\pi)/(\Omega n_s) \tag{11}$$

where n_s is the number of times a blade is sampled for flapping per rotor revolution. If N is the number of times the Kalman estimator has been solved, then (NT) designates a present value in the solution, (NT-T) designates the most recent value, and (NT+T) represents an update of the latest value in the solution. Let t_o denote values at the trim condition. Then the discrete form of the Kalman estimator solution, which works with changes from trim or initial values, is

$$\begin{aligned} P_1(NT) &= m_1(NT)/(1 + n_b m_1(NT)/R) \\ P_2(NT) &= m_2(NT)/(1 + n_b m_2(NT)/2R) \\ P_3(NT) &= m_3(NT)/(1 + n_b m_3(NT)/2R) \end{aligned} \tag{12}$$

$$\Delta x_1(NT) = \Delta x_1(NT-T) + \frac{P_1(NT)}{R}\left[\sum_{i=1}^{n_b} z_i(NT) - n_b\left\{\Delta x_1(NT-T) + x_1(t_o)\right\}\right]$$

$$\Delta x_2(NT) = \Delta x_2(NT-T) + \frac{P_2(NT)}{R}\left[\sum_{i=1}^{n_b} z_i(NT)\cos(\psi + \phi_i) - \frac{n_b}{2}\left\{\Delta x_2(NT-T) + x_2(t_o)\right\}\right] \qquad (13)$$

$$\Delta x_3(NT) = \Delta x_3(NT-T) + \frac{P_3(NT)}{R}\left[\sum_{i=1}^{n_b} z_i(NT)\sin(\psi + \phi_i) - \frac{n_b}{2}\left\{\Delta x_3(NT-T) + x_3(t_o)\right\}\right]$$

$$\begin{aligned} m_1(NT+T) &= P_1(NT) + Q_1 \\ m_2(NT+T) &= P_2(NT) + Q_2 \\ m_3(NT+T) &= P_3(NT) + Q_3 \end{aligned} \qquad (14)$$

where the $\underline{P}$, $\underline{m}$, $\underline{Q}$, and R terms are covariances. (See Appendix A for a more detailed derivation of these equations.)

The only simplification used in the derivation of the Kalman estimation solution, which is reflected in equations (13), pertains to the location of the blades in the main rotor that may be sampled for values of flapping during each calculation. Equations (13) are exactly correct only if flapping is sampled from any combination of three (3) or more blades of the rotor, provided that the selected blades are all equally spaced. This restriction allows many sinusoidal terms in the solution to be identically zero, thereby producing a Kalman tip-path-plane resolver small enough for on-line, real-time use.

The covariance terms appearing in equations (12) through (14) represent the possible or anticipated variations in values used or calculated by the Kalman estimator. The covariances provide the estimator with guidelines for evaluating the accuracy of each datum it handles, thus effectively determining a weighting factor for each datum point in the filtering process. The state covariance $\underline{P}$ and the initial state covariance $\underline{m}$ are calculated within the Kalman estimator as functions of the process noise covariance $\underline{Q}$ and the measurement noise covariance R. The latter two covariances are preselected input constants for equations (12) through (14).

In equations (13), P/R act as weighting factors of the most recent value of the tip-path-plane coefficients determined from the latest flapping values. These weighting factors are a function of Q and R. The ratios R/Q are effective filters in the Kalman estimator. The ratios are constant and are determined from input data. The effective weighting factors in the Kalman estimator are calculated on every pass through the estimator.

Figure 6 is a flow diagram illustrating the Kalman estimation solution. Proper operation of the estimator requires a trim solution as a first step. After the trimmed tip path plane has been resolved, the rotor can then be disturbed to begin a dynamic analysis. The trim solution requires Q to be set to zero, because there are no rates (all time derivatives of state are zero), and the process noise covariances are defined as the variations in rates.

Although the Kalman estimator developed above includes the tip-path-plane assumption, the Kalman estimator technique can also be applied to the problem of obtaining optimum estimates of the coefficients in equation (3) for each blade. Higher harmonics can also be included if more detailed representation of the rotor is desired. Although accuracy is expected to increase, the size and computation time of the solution would also increase.

Resolution methods under consideration. - Three methods of resolving the rotor tip path plane from blade flapping are considered:

1. Static Fourier resolver

2. Time-varying Fourier analysis

3. Kalman estimator technique

Although the static and time-varying Fourier methods can be derived independently, they both prove to be no more than special cases of the Kalman estimator.

The coning equation of the Kalman resolver is used here to illustrate the application and the generality of the Kalman estimator solution. Using familiar rotor notation, the first portion of equations (13) may be rewritten as

$$\Delta\hat{a}_{os}(t_n) = \Delta\hat{a}_{os}(t_{n-1}) + \frac{P_1 n_b}{R}\left[a_{os}(t_n) - \left\{ \Delta\hat{a}_{os}(t_{n-1}) + \hat{a}_{os}(t_o) \right\} \right] \qquad (15)$$

where the cap ($\hat{}$) indicates an estimated or calculated value, no cap indicates an actual or measured value, and (t_{n-1}) and (t_n) indicate the previous and updated values, respectively. Because

$$\hat{a}_{os}(t_{n-1}) = \hat{a}_{os}(t_o) + \Delta\hat{a}_{os}(t_{n-1}) \qquad (16)$$

equation (15) may be rewritten as

$$\Delta\hat{a}_{os}(t_n) = \Delta\hat{a}_{os}(t_{n-1}) + \frac{P_1}{R} n_b \left[a_{os}(t_n) - \hat{a}_{os}(t_{n-1}) \right] \tag{17}$$

In equation (17), $[a_{os}(t_n) - \hat{a}_{os}(t_{n-1})]$ is the estimated increment by which coning has changed between times t_{n-1} and t_n. This value added to $\Delta\hat{a}_{os}(t_{n-1})$ yields the estimated total difference of coning at time t_{n-1} from the trim value. Notice that the amount added to $\Delta\hat{a}_{os}(t_{n-1})$ is a function of the weighting factor P_1/R. The weighting factor is, in turn, a function of Q_1 and R.

If Q is set to zero, then P/R tends to zero as time increases. This condition (Q = 0) represents the static Fourier solution. Checking the flow diagram of Figure 6 shows that this pure Fourier analysis is used by the trim Kalman estimation solution.

From equations (12), (13), and (14), as R/Q tends to zero, P/R tends to $1/n_b$ or $2/n_b$ in the limiting case. For this case equations (13) reduce to equations (6) (after the respective trim values have been added to the left-hand side of equations (13)). Thus the Kalman estimator can be reduced to the time-varying Fourier solution by assigning appropriate values to the Q and R inputs. The time-varying Fourier analysis has a constant weighting factor of 100%; thus, it totally accepts each datum it reads regardless of contamination that may be present on the flapping signal. The Kalman estimator, on the other hand, calculates the weighting factor each pass through the solution whenever appropriate covariance information is inputted initially.

Evaluation of resolver methods. - The rotor feedback schemes chosen for investigation all operate on estimates of the first harmonic representation of the rotor tip path plane. In flight, these estimates are derived from blade flapping measured at the flapping hinge of the rotor blades. The analytic tip-path-plane study is concerned, therefore, with determining how well the resolution methods can approximate the rotor tip path plane, and in selecting the most desirable resolver to be incorporated into the rotor feedback logic.

The tip-path-plane resolver methods are incorporated into the rotor solution of the nonlinear model simulation program called GENHEL. GENHEL is a general purpose flight dynamics program developed for hybrid computers at Sikorsky Aircraft. The specific rotor solution, called GRP, which is part of the GENHEL solution, is solved independently of the fuselage in a Rotor Only mode for the purpose of studying the operation of each tip-path-plane resolver. GRP uses a blade element method for independently calculating the flapping of each main rotor blade about the flapping hinge. GRP does not include any blade bending degrees of freedom or blade lag motion. There are no tip-path-plane or harmonic restrictions in the flapping degrees of freedom.

A baseline case is established for comparing the performance of the resolvers. In flight, the selected resolver must distinguish the first harmonics of flapping from any noise in the flapping signal, whether it be due to a measurement error introduced by the instrumentation device, or to the presence of higher harmonics. Therefore, the analysis includes provisions for adding a higher harmonic signal to the flapping of any blade calculated by GRP. This enables the resolvers to be tested for their ability to filter noise that could contaminate the first harmonic flapping signal. Figure 7 illustrates this technique. The higher harmonics contamination, which can be used if desired, is:

$$\beta_{HH}(t) = -a_{2s}\cos 2(\Omega t + \phi_i) - b_{2s}\sin 2(\Omega t + \phi_i) \\ -a_{3s}\cos 3(\Omega t + \phi_i) - b_{3s}\sin 3(\Omega t + \phi_i) \tag{18}$$

where a_{2s}, b_{2s}, a_{3s}, and b_{3s} are any selected input constants. Regardless of higher harmonics or noise present, the tip-path-plane resolvers are required to reproduce only the first harmonic contributions of flapping.

The tip-path-plane coefficients a_{os}, a_{1s}, and b_{1s} are defined in terms of flapping and are not explicit or necessary parts of the solution of the rotor equations of motion. Since the rotor solution of the nonlinear analytic model does not solve the tip path plane explicitly, the performance of the resolvers must be checked against the baseline (GRP), using the flapping calculation. After the tip path plane is resolved from the flapping values (β_i) using GRP, the estimated tip-path-plane coefficients are used to reconstruct flapping according to the equation

$$\hat{\beta_i}(t) = \hat{a}_{os}(t_o) + \Delta\hat{a}_{os}(t) - \left[\hat{a}_{1s}(t_o)+\Delta\hat{a}_{1s}(t)\right]\cos(\Omega t+\phi_i) \\ - \left[\hat{b}_{1s}(t_o) + \Delta\hat{b}_{1s}(t)\right]\sin(\Omega t +\phi_i) \tag{19}$$

where the coefficients are written as the sum of a trim value and a difference from trim. Time histories of $\beta_i(t)$ (not containing the contamination contribution) and $\hat{\beta}_i(t)$ (estimated from contaminated data, if used) are compared for the purpose of evaluating the efficiency of the Fourier and Kalman resolver methods.

Discussion of Results

General trim and dynamic solutions. - The configuration of the CH-53A used for the analytic tip-path-plane resolver study is 35,000 lbs, flying at sea-level, standard temperature conditions. The general performance of the tip-path-plane resolver methods is evaluated at the aft center-of-gravity location, because the tip path plane for this condition is composed basically of relatively large first harmonic terms. All six blades are sampled 24 times per rotor revolution. Forward speeds investigated are hover, 100 kts, and 150 kts.

Figure 8 illustrates the trim and dynamic operation of the static Fourier resolver. This method can be applied dynamically by selecting an input value of $\underline{Q} = 0$ for the Kalman estimation solution (refer to Figure 6). Comparing the estimated value of the total flapping of blade 1 ($\hat{\beta}_1$) with the actual value calculated by GRP (β_1), shows poor correlation. As expected, this static Fourier method, when applied to a dynamic solution, quickly fails to manipulate any changing input data.

Performance of the time-varying Fourier resolver and the Kalman resolver is shown in Figures 9 and 10. The covariances for the Kalman resolver of Figure 10 are $\underline{Q} = 100$ deg^2 and $R = 1$ deg^2. No stability augmentation is employed in the resolver analysis. The resolver methods comparison, therefore, should be based on performance over only a short time interval following the pulse input to the rotor. Figures 10 and 11 indicate that both the time-varying Fourier and the Kalman resolvers reproduce flapping well. The apparent discontinuity in tip-path-plane coefficients observed in the Kalman solution when going into the dynamic mode is only a change in the variable calculated by this method. Prior to the pulse input, the coefficients are trim values; after the input, they represent changes from the trim values.

All three resolver methods show the same trim solutions, because all three methods reduce to the identical solutions in the trim mode. Based on the results illustrated by Figure 8, the static Fourier method is eliminated as a candidate for dynamic tip-path-plane resolution.

Both the time-varying Fourier and Kalman resolvers show the same degree of accuracy at hover and at 150 kts as is shown at 100 kts. Both methods appear to work well even when rotor blade excursions far from trim are encountered.

Some frequency response data are obtained by exciting the rotor with sinusoidal control inputs at various frequencies up to 3 cycles per revolution. These data show that $\hat{\beta}_1$ estimated by both methods reproduce β_1 well, and that the tip-path-plane coefficients estimated by both the time-varying Fourier and Kalman resolvers reflect the input frequency through all frequencies studied. No appreciable increase in phase lag between β_1 and $\hat{\beta}_1$ is observed through an input frequency of 3 cycles per revolution.

Number of blades sampled. - Figures 11 through 15 are examples of the performance of the Kalman method tip-path-plane resolver as a function of the number of blades sampled. (This evaluation is conducted at a helicopter loading for which the tip path plane is composed primarily of first harmonic contributions.) The sampling rate is 24 per revolution. Estimates of total flapping are compared with the actual values for two blades. Blade number 2 represents a blade that is not monitored for flapping for those cases in which fewer than 6 blades are sampled. The time histories shown in Figure 11 act as a baseline, since all blades are sampled for this case. It is noted here that the programmed form of the Kalman estimator is not rigorously exact for the blade sampling used by the cases represented in Figures 12, 13, and 15.

All cases sampling a reduced number of blades show the same trim tip path plane, while the dynamic solutions show noise in the estimated tip-path-plane coefficients. The reproduction of β_1 by the estimator is impaired for cases sampling four and two blades. The flapping reproduction of an unmonitored blade is acceptable when three equally spaced blades are sampled.

Although the comparison of $\hat{\beta}_1$ and β_1 is useful in evaluating the resolver methods, conclusions on the effectiveness of the resolution techniques must ultimately be drawn from the estimated tip-path-plane coefficients (because the rotor feedback schemes operate on these parameters). Therefore only the three-blade sampling case merits consideration as an acceptable alternative to sampling all of the rotor blades. Figure 14 shows some noise in the flapping coefficients even for a three-blade sampling solution. The noise is due to improper handling of second or higher harmonics contributions of the blade flapping. It will be shown in a following section that this effect can be filtered from the estimated coefficients through proper selection of the covariances $\underline{Q}$ and R in the Kalman estimator.

In the event of a flapping measurement failure on one blade (or possibly more) in flight, the three-blade sampling technique could be selected. It would yield the most accurate tip-path-plane estimate possible under these conditions, if appropriate covariance values are used by the Kalman estimator. The three-blade sampling solution is further investigated with respect to complete system operation as part of the nonlinear stability analysis (and briefly in the test section) appearing later in this report.

Figure 16 is an example of the effect of number of blades sampled on the time-varying Fourier resolver solution, showing the three-blade sampling case. The time histories of $\hat{a}_{1s}$ and b_{1s} in this figure show that a great deal of the signal noise or higher harmonic content of flapping may be included in the first harmonic flapping coefficients solved by the time-varying Fourier equations, depending on the number and location of blades sampled. This is due to the fact that the Fourier solution accepts the complete flapping signal at every discrete time interval (i.e., it has no filtering capability).

Sampling interval. - The effect of the number of flapping samples used by the resolvers is studied by sampling twelve and six times per revolution. These estimated tip-path-plane coefficients are then compared with the corresponding values determined with 24 samples per revolution. All six blades are sampled during these solutions, and a tip path plane composed primarily of first harmonic terms is considered. Figure 17 shows the time histories of both the time-varying Fourier and the Kalman estimated coefficients obtained when blade flapping is sampled 24 times per revolution. Figures 18 and 19 show the coefficients estimated by the Kalman resolver for twelve and for six samples per revolution, respectively. Figure 20 gives coefficients for the time-varying Fourier resolver sampling six times per revolution. Either set of the estimated coefficients of Figure 17 can be selected to act as a baseline for comparing the coefficients shown in Figures 18 through 20.

The trim values and the transient dynamic values of the tip-path-plane coefficients estimated by either the time-varying Fourier or the Kalman resolver appear accurate, with no measurable noise, for the sampling intervals studied. The effect of sampling interval on overall helicopter stability produced by the rotor feedbacks is evaluated in the nonlinear analysis and the test section, both presented later.

Noise and effective filtering. - To evaluate the ability of the time-varying Fourier and Kalman resolvers to separate the first harmonic tip-path-plane contributions from flapping data contaminated with noise, higher harmonics are added to the flapping input to the resolvers according to equation (18). The blade flapping is then reconstructed from the estimated coefficients and compared with the original flapping. Figure 21 shows the results when the Kalman method is used with covariances of $\underline{Q} = 1 \text{ deg}^2$ and $R = 100 \text{ deg}^2$. The case using the time-varying Fourier analysis is illustrated in Figure 22. The results show that a less noisy tip path plane and a more accurate reproduction of blade flapping are estimated when the Kalman method is used by the resolver (β_1 and $\hat{\beta}_1$ should be compared in Figures 21 and 22).

The Kalman estimation method provides the user with an effective filter that is inherent to the method. The amount of effective filtering provided by the Kalman resolver is determined by the input values selected for covariances $\underline{Q}$ and R. Figure 23 illustrates a case where R/Q = 100. Figure 24 illustrates R/Q = 1/100. For both cases, three blades are sampled six times per revolution. (No contamination is added to flapping for these cases.) With little effective filtering (R/Q = 1/100), the estimated tip-path-plane coefficients become unacceptably noisy.

Because the Kalman solution approaches the time-varying Fourier solution as R/Q tends to zero, the time histories in Figure 24 imply that the time-varying Fourier resolver may lose accuracy as the number of blades sampled is reduced. Although the blade flapping of the case shown in Figure 24 is composed primarily of first harmonic terms, other harmonics are also present. For each discrete calculation, the Fourier solution fits all harmonics to the first harmonic approximation. For some particular combinations of blade sampling and higher harmonic content, the improperly handled higher harmonic effects will add identically to zero within the Fourier calculation of the first harmonic coefficients. For other combinations, these effects do not add to zero and the first harmonic coefficients exhibit the effects of the higher harmonic components. ($\hat{a}_{1s}$ and $\hat{b}_{1s}$ in Figure 24 are examples of second harmonic effects being carried on the first harmonic signals at a 3/rev characteristic frequency.)

Higher harmonics contamination of the first harmonic coefficients, as a function of the number of blades sampled and particular higher harmonic content of flapping, also occurs when the Kalman method is used. However, through proper selection of covariance values inputted into the Kalman estimator, this type of contamination of the tip-path-plane coefficients can be reduced to negligible proportions. Figure 25 illustrates the performance of the Kalman estimator (R/Q = 100) when only three blades are sampled 24 times a revolution while the input data are contaminated with higher harmonics.

At a neutral center-of-gravity location, the first harmonic contributions of flapping may be three to four times smaller than they are at an aft or forward center-of-gravity location. The tip-path-plane coefficients estimated by the Kalman method can be expected to become less accurate as the magnitudes of the higher harmonics and the first harmonics of flapping approach each other, even if a large amount of effective filtering (R/Q) is used. A more accurate estimate of the first harmonic terms could be obtained if second or higher harmonics were included in the Kalman estimation solution. Adding the higher order terms to the estimator equations would increase both the computer core requirement and the execution time of the resolver program.

Phase lag. - Estimated blade flapping ($\hat{\beta}_1$) time histories are compared with the actual blade flapping (β_1) at various forward speeds, to determine if any phase lag is created by the Kalman estimation technique used by the tip-path-plane resolver. Because $\hat{\beta}_1$ is reconstructed from $\hat{a}_{os}$, $\hat{a}_{1s}$, and $\hat{b}_{1s}$, the phase lag between $\hat{\beta}_1$ and β_1 yields some insight to the phase lag of the estimated tip-path-plane coefficients. Covariance values of $Q = 1$ and $R = 100$ in the Kalman estimator are of particular interest in the phase lag analysis. Studying the time history data collected during the tip-path-plane resolver investigation indicates that the resolver itself does not introduce any significant phase lag between β_i and $\hat{\beta}_i$ for the number of blades sampled, sampling rate, or covariance values which were studied.

If the Kalman estimator is rearranged and expressed in the form of a low pass filter (in the limit as time tends to infinity), the time constant for the equivalent first order lag can be determined. Then turning to a frequency response analysis, an approximate phase lag and magnitude ratio of the tip-path-plane coefficients can be determined as a function of number of blades sampled, sampling interval, and covariance values. Through proper selection of covariance values, the time-varying Fourier solution can also be duplicated. Conducting such an analysis for an input frequency of approximately 0.4 Hz shows that the phase lag and amplitude reduction of the actual tip-path-plane coefficients are insignificant for the Fourier method sampling six or three blades either 24, 12 or 6 times per revolution, and for the Kalman estimator ($R/Q = 100$) sampling six blades 24 times per revolution. (The input frequency of 0.4 Hz represents the dominant regressing mode of rotor flapping, evident in the estimated tip-path-plane coefficient time histories.) Unlike the Fourier method, the frequency response analysis indicates that a larger phase lag (50 deg) and amplitude reduction (35%) occur when fewer blades (3) are sampled less frequently (24/rev) by the Kalman technique. Actually very little change in the coefficients is seen when looking at the more appropriate data provided in the time histories of $\hat{a}_{os}$, $\hat{a}_{1s}$, and $\hat{b}_{1s}$ in Figure 23, when compared to Figure 24 (if the higher harmonic variation in coefficients is not considered in the latter figure).

The above discussion of phase lag pertains only to the effect of the resolver method on the phase relationship between actual and estimated rotor parameters. The effect of lags due to other components of the total feedback system are discussed later in this report.

Selection of a Resolver

Because flapping data sampled in flight and supplied to the tip-path-plane resolver may be noisy or because the rotor flapping data are likely to contain higher harmonic components, the Kalman estimator method is selected to produce tip-path-plane coefficients needed by the rotor feedback schemes. The Kalman estimation method provides a filter, and the user can effectively select the cutoff frequency by inputting proper values of covariances. Both the Kalman and Fourier methods lose accuracy with an increasing ratio higher harmonic to first harmonic components of flapping, or in a reduction of the number of data points sampled per revolution (particularly if the number of blades sampled is reduced). But the loss in accuracy can be controlled and minimized by the user employing the Kalman estimator. The condition at which the Kalman estimator method yields least accurate results is when the first harmonics of the tip path plane are minimal, and the blade flapping is composed of relatively large values of higher harmonics of the tip path plane, or the flapping data are contaminated by measurement errors. Even then, the Kalman estimator technique yields a better estimate than the time-varying Fourier analysis and can minimize both random interference and unwanted bias error.

LINEAR STABILITY STUDY

The stability characteristics of the CH-53A employing each of the rotor tip-path-plane, fuselage, and combined rotor and fuselage feedbacks are initially analyzed using linear techniques. The derivation of the linear models, the stability analysis, and the general results of this analysis are presented here.

Linear Analysis

Linear models of the CH-53A at the desired flight conditions are obtained from the nonlinear GENHEL analytic model by means of a system identification program developed at Sikorsky. GENHEL, which models the CH-53A helicopter with six coupled fuselage degrees of freedom and six blade flapping degrees of freedom, also has provisions for representing a detailed mechanical and electronic control system.

Since the feedbacks under investigation depend on the tip-path-plane coefficients, the linear model must have rotor dynamics isolated from the fuselage and must express the rotor dynamics explicitly in terms of the tip-path-plane variables and their time derivatives. The nine degree-of-freedom linear model selected for use in this analysis consists of six body linear and angular degrees of freedom and three rotor tip-path-plane degrees of freedom. The body and tip-path-plane accelerations resulting from small perturbations from the trim values of the fuselage, rotor, and control variables are equal

to the sums of the product of each perturbation and its corresponding coefficient. In vector and matrix notation, this can be expressed as:

$$\dot{\underline{x}} = \underline{\underline{A}}\,\underline{x} + \underline{\underline{B}}\,\underline{u} \tag{20}$$

where $\underline{x}$ and $\underline{u}$ are the helicopter and control variables, respectively, and $\underline{\underline{A}}$ and $\underline{\underline{B}}$ represent the coefficients of these variables.

The system identification method, employing a least squares estimator technique, is used to obtain constant coefficients of the linear model that represent the change in acceleration per unit change in state variable. The technique for obtaining the linear model is shown in Figure 26. After the GENHEL model has been trimmed, control inputs are used to excite GENHEL. Techniques analogous to the tip-path-plane resolver routines are added to the program which estimate first and second time derivatives of the first harmonic tip-path-plane motion from blade flapping velocity and acceleration data (in the same way in which the tip-path-plane is estimated from flapping displacement data). The values of the difference from trim of the rotor and body variables and their time derivatives, as well as the control inputs are continuously updated as they change with time and are supplied to the system identifier. The identifier then evaluates all data and calculates the coefficients that best approximate the time history data supplied to it, within the restriction of the linear model representation selected. A more detailed description of the system identification technique is found in Reference 1.

Tables II, III, and IV present the coefficients identified at hover, 100 kts, and 150 kts. The rows of these tables represent the time derivatives of the state variables, which are the body and tip-path-plane accelerations. The columns of the tables designate the state variables and rotor controls, of which the equations of motion are functions. The coefficients are for the basic helicopter with no stability feedback.

The total stability of the CH-53A at 33,500 lbs and aft cg (348 fscg) is considered in the stability analysis. An effective filter of R/Q = 100 is used with the tip-path-plane resolver, because filtering in this manner in flight is anticipated to remove measurement error from the blade flapping signal. The three speeds under study cover the test speed range of the CH-53A.

To evaluate the accuracy of the nine degree-of-freedom model used in the linear stability analysis, the model is inputted into a time history program and excited by a control input. The resulting response is compared with the response of the GENHEL program for the same excitation input (Figure 27). The three time histories show the six body acceleration responses obtained by disturbing the nonlinear GENHEL model and the nine and six degree-of-freedom linear models with identical inputs. The short term, high frequency dynamics, which are due to the rotor transient response predicted by GENHEL, are reproduced by the nine degree-of-freedom linear model, but not by a six degree-of-freedom linear model.

The linear models presented in Tables II, III, and IV may be algebraically reduced to six degree-of-freedom models by making a quasi-static rotor assumption. Having done so, many of the coefficients of the reduced model assumed values almost identical with the values of the corresponding conventional stability derivatives. (These conventional derivatives are the partial derivatives of the linearized equations of motion.) More information about the capabilities of various types of linear models is found in Reference 2.

A linear stability analysis is performed to assess the feasibility of the various feedback schemes. This establishes the basic trends for the closed-loop systems considered, and determines approximate values for the stability boundaries. This linear analysis incorporates third-order servo dynamics on each control channel of the nine degree-of-freedom identified analytical models, includes inter-channel mixing, and closes the loops. The results are presented as root locus plots.

The CH-53A control system transfer functions for the longitudinal cyclic, lateral cyclic, and collective pitch channels take the form

$$\frac{O(s)}{I(s)} = \frac{\omega_n^2 e^{-t_d s}}{(s^2 + 2\zeta_c \omega_n s + \omega_n^2)(\tau s + 1)} \tag{21}$$

where $O(s)$ is the output of the primary servo, $I(s)$ is the input of the AFCS servo, and τ and t_d are the time constants of the servo system lag and servo system delay, respectively. For the CH-53A control system, approximate values are $\omega_n = 95$ rad/sec, $\zeta_c = 0.2$, $\tau = 0.02$ sec, and $t_d = 0.02$ sec.

The exponential can be approximated as:

$$e^{-t_d s} \cong \frac{1 - (t_d/2)s}{1 + (t_d/2)s} \tag{22}$$

Hence, the servo dynamics can be represented as a fourth-order system for each channel. To reduce the order of the system without imparing the accuracy of the results, it was found reasonable to neglect $(1 + (t_d/2)s)$ in the denominator.

Due to the simultaneous variation of feedback loops, the resulting locus of roots must be carefully interpreted. The locus does <u>not</u> follow single loop feedback closure rules except under special circumstances and should be analyzed either as a succession of single loop closures or as a parametric variation.

Discussion of Eigenvalue Results

The open loop poles for hover, 100, and 150 knots are presented in Figures 28, 29, and 30. The three rotor tip-path-plane modes are referred to as the flapping-advancing mode, flapping-regressing mode, and flapping-coning mode. The remaining helicopter roots correspond to the conventional six degree-of-freedom rigid body modes. When servo dynamics are included in the system, a high frequency oscillatory mode and an aperiodic convergence mode appear for each channel. Velocity variation has only slight effects on the flapping-regressing mode and the flapping-coning mode, whereas the flapping-advancing mode shows a significant increase in frequency and damping from 100 to 150 knots.

Representative plots for each of the specific closed-loop feedback schemes are presented in Figures 31 thru 40. All plots correspond to a loading of 33,500 lbs at aft cg (348 fscg), 100 knots, and are shown for the most critical case which includes the servo dynamics. SAS is excluded. Incorporation of the servo dynamics has a significant effect on the rotor tip-path-plane closed-loop roots, in that the rotor root trends with servos always indicate a less stable behavior than the trends without servos. The servos have a relatively insignificant effect on the rigid body modes. On the other hand, standard pitch and roll rate stability augmentation will stabilize the lower frequency rigid body modes but leave the rotor modes virtually unaffected.

Discussion of the actual stability boundaries, gain values and frequency of instability is included under the presentation of the nonlinear results.

Vehicle Frequency Response and Model - Following Systems

A brief assessment of the useable frequency range for the overall system is undertaken in this study. The frequency characteristics of the actuators, rotor flapping motion, and vehicle motion are studied individually and combined using a simple hover model. The transfer function representations of the rotor and the fuselage used for this study are

$$\text{rotor: } \frac{(s^2 - 2\zeta_1\omega_{n1}s + \omega_{n1}^2)}{(\tau_1 s + 1)(s^2 + 2\zeta_2\omega_{n2}s + \omega_{n2}^2)}$$

$$\text{fuselage: } \frac{(CP/D)(s^2 - 2\zeta_1\omega_{n1}s + \omega_{n1}^2)}{(\tau_1 s + 1)(\tau_2 s + 1)(s^2 + 2\zeta_2\omega_{n2}s + \omega_{n2}^2)}$$

where τ_1 is the inverse of the product of the rotor angular velocity and the rotor Lock number, τ_2 is the helicopter moment of inertia divided by the helicopter damping, and CP/D is the control power divided by helicopter damping. The servos are represented by a transfer function like equations (21) and (22).

Both open-and closed-loop situations are studied. The frequency characteristics for the basic system are shown in Table V for the various transfer functions.

The combined AFCS servos and primary servos have a high (phase) crossover frequency (11 hz), but as the rotor is added to the system, this drops to about 4 hz; the inclusion of body motions (rate) further reduces this to about 2 hz. Looking at body attitude rather than rate results in a crossover frequency of 0.3 hz. The addition of vehicle damping does offer some improvement in attitude response, in terms of both crossover and gain margin; however, stability considerations limit the possibility of any high loop gain. The cutoff frequency associated with the classic bandwidth definition, also shown in Table V, has a more pronounced reduction as more elements of the system are added open-loop.

A low gain closed-loop solution (with a unity gain feedback) does not improve the crossover frequency of the actuator/rotor system, although the phase shift at 1 hz is reduced from 48° to 28°. However, while the crossover frequency remains at about 4 hz, the bandwidth, or cutoff frequency, does show an improvement: from 2.4 to 5.4 hz. If stability considerations would allow for larger loop gains, then some improvement in crossover frequency (ω_c = 11 hz) is possible as seen for the case of a forward gain of 5.0 deg/deg. Gain levels of five, however, are not possible (because of stability considerations) and this case is shown only for comparison purposes. At the theoretically maximum allowable gain of 2.5 deg/deg, an improvement in bandwidth is provided and an improvement in the system lag is noticable between 0.1 and 4 hz.

If it is intended that the helicopter control system include a model-following capability, then the ability to respond at high frequencies is certainly desired. For example, to simulate a helicopter of smaller size, a test helicopter must respond at frequencies higher than, for example, 1 hz. Model-following systems usually use angular rate as the basic feedback loop. It is seen in Table V that the crossover frequency for a rate controller (rate feedback) is approximately 2 hz. The gain margin for this case is roughly 3.5 according to the analysis. Thus, based on an analysis using a rotor with only flapping dynamics, one would expect that relatively high values of feedback gain could be used. However, such is not the case. Other factors, including blade lag degrees of freedom, control system interaction with the airframe, and sensor mounting contribute to limiting the achievable gains. Figure 41 shows the approximate upper levels of gain obtained from theoretical and experimental sources. The data shown are based on a critical damping ratio of approximately 0.2. The inclusion of the servo dynamics is important in determining the allowable gains; however, there still remains a sizable difference in predicted and actual gain limits. Of the factors not included, the blade lag degrees of freedom are suspected as being quite important. Analytic data from recently completed work unrelated to this study show that the inclusion of lag degrees of freedom can reduce by one half the theoretically achievable SAS gain.

The results of this brief frequency investigation indicate that closing the basic actuator/rotor flapping loop can provide better response characteristics. Further variations of minor loops and lead networks have not been investigated and might provide further improvement. To utilize the improvements in response from this feedback loop however requires that the unknown factors which affect the general ability to use high gain feedbacks become better understood.

NONLINEAR STUDY

A nonlinear investigation is undertaken to quantitatively study the interaction of the rotor/vehicle feedbacks with the complete helicopter, composed of rotor, fuselage, and control system. The nonlinear approach is employed in the detailed study of gust alleviation capabilities, the effect of the feedback schemes on system stability, the effect of control system authority limits on the operation and evaluation of the feedback schemes, and the ability to maintain control orthogonality using feed-forward loops.

The nonlinear investigation uses the GENHEL model of the CH-53A with a loading of 33,500 lbs and aft (348 fscg) center-of-gravity location. The aft cg loading condition is considered exclusively in the nonlinear analysis because it represents the loading condition which is most sensitive to gust disturbances and which generally has the poorest stability characteristics. The Kalman estimator tip-path-plane resolver is also added to the helicopter simulation, with covariance values of $\underline{Q}$ = 1 deg^2 and R = 100 deg^2 given particular consideration. All of the feedback and feed-forward logic needed for the investigation is programmed, along with an accurate description of the CH-53A control system. All six main rotor blades are sampled 24 times per revolution (except as noted). The complete nonlinear helicopter model is programmed on the Digital Equipment Corporation PDP-10 computer at Sikorsky Aircraft. The individual analyses performed for each topic under investigation are described in the following sections.

Nonlinear Control System Model Description

Figure 42 illustrates the CH-53A control system which is represented in the nonlinear helicopter model used in the analytic study. Most of the components cannot be represented by anything other than nonlinear means. The components of the control system programmed in the GENHEL CH-53A model are:

1. Stick sensitivity. To maintain an accurate evaluation of the feedback logics under investigation, control inputs to the helicopter are initially inputed at the stick in the model. The correct control range combined with the available stick displacements provide an accurate stick sensitivity which is expressed as a linkage ratio of degrees commanded to the AFCS servo per inch of stick displacement. The stick sensitivity is corrected for any deadband in the controls. All data are obtained from CH-53A rigging data.

2. Stability augmentation system (SAS). In addition to programming the rotor/vehicle feedback and the control orthogonality feedforward logic, the conventional inner-loop rate feedback for the CH-53A is programmed, with the option available to select any gain, including zero which would exclude this feedback completely. Only an inner-loop capability of the rate feedbacks is programmed to provide basic stability during evaluation of the rotor/vehicle feedbacks, and the authority limits of the total SAS command are monitored to assure that they are not saturated by the conventional feedback. Logic to maintain the proper authority limit of the actuator command is also included.

3. AFCS servos. The sum of the control input from the pilot and total command from the AFCS are summed to duplicate the output of the AFCS servo. The output command from this servo is checked, and adjusted if necessary, to guarantee the proper representation of the AFCS servo limits.

4. Control coupling. The control coupling provided by the mixing unit of the CH-53A is duplicated in the nonlinear simulation. The command from the mixing unit is checked, and adjusted if necessary, to assure that the control ranges (control stops of the primary servo) are not exceeded.

5. Servo dynamics. The lag introduced by the servo system is quite accurately approximated by equation (21) and is described in the Linear Analysis Section of this report. This servo system representation, including the exponential expression for the servo delay in equation (21) is programmed on the PDP-10 digital computer using the Z - transformation technique. The transfer function expressed by equation (21) is interpreted in the nonlinear simulation as the transport lag between an input signal at the AFCS servo and the output of the signal from the primary servo. Equation (21) was established to best represent existing CH-53A test data.

6. Hysteresis. Before the lagged servo signal is permitted to go to the swashplate, it is corrected to represent the net hysteresis of the CH-53A control system. While it is more correct to apply the hysteresis as it occurs between the specific servos, it was not done because of an inadequate breakdown of this information. By applying it at the output of the primary servos, the analysis is most conservative. The hysteresis ranges programmed for each of the controls are obtained from existing CH-53A test data.

7. Swashplate rotation. Due to main rotor blade offset and other dynamic phenomena, the precession angle of the articulated rotor is not exactly 90°. Therefore, the swashplate must be rotated in order to create the proper phase between control inputs commanded by the primary servos and the blade pitch angles which will provide the most desirable relationship between control inputs and

helicopter response. Such a swashplate representation is included as a final control modification within the control system of the CH-53A nonlinear model used in this study.

Table VI presents the pertinent values which describe the CH-53A control system. Based on the existing test data and digital computer solution techniques, the control system programmed for the nonlinear feedback investigation is considered to be an excellent model of the actual system of the CH-53A.

Gust Alleviation Capabilities

Procedure and analysis. - The load factor response of the helicopter to a gust disturbance is obtained from a static variation of the nonlinear model. The change in main rotor thrust and total helicopter pitching moment per unit change in rotor angle of attack are used as measures of gust sensitivity. The response expressions $\Delta T_{MR}/\Delta\alpha$ and $\Delta M/\Delta\alpha$ are obtained from GENHEL by first trimming the helicopter, and then inputting a unit step into the fuselage angle-of-attack and allowing the rotor to attain a new steady state. All other body variables are held at their trim values during this process. Due to the re-trimming of the rotor which characterizes this technique, it is referred to as a quasi-static solution.

The two response expressions are obtained for each rotor and fuselage feedback under investigation, over a range of gain values for each scheme. For comparative purposes these expressions are also obtained for the basic rotor configuration, employing no feedback, which acts as a baseline case. For the baseline condition, the vehicle response to a sharp-edged gust is characterized by a notable increase in load factor by a nose-up pitch response. The most desirable gust alleviation feedback schemes and the corresponding gain values are those which produce small values of $\Delta T_{MR}/\Delta\alpha$ while simultaneously maintaining a satisfactory pitching moment response, characterized by low or negative values of $\Delta M/\Delta\alpha$. The gust alleviation evaluation is conducted at the most critical condition, which is high speed (150 kts).

In order to compare the effectiveness of each feedback scheme for reducing the transient load factor response to a gust disturbance, as compared to the alleviation predicted by the quasi-static technique described above, a dynamic analysis is also conducted. The helicopter is initially trimmed, and then a gust of short duration with a selected amplitude, frequency, and shape is inputted into GENHEL. The resulting time histories of rotor thrust, load factor, and pitching and rolling moments are studied. Comparisons of the dynamic time histories for each feedback scheme are made against the basic rotor dynamic response. The dynamic analysis is conducted at only one specific gain for each feedback type. Comparisons are made to the quasi-static gust alleviation characteristics at the specific gain for each scheme in order to obtain qualitative information relating the quasi-static results to the expected transient results.

Discussion of results. - Figures 43 through 46 present the static gust alleviation characteristics of the rotor and fuselage feedback schemes as a function of feedback gain values. At certain gain values for most of the feedback techniques the rotor solution diverged and the plots were terminated prior to this point. This is not indicative of a rotor instability; an instability is generated because of the restriction of the helicopter motion which has been included in the GENHEL program for the quasi-static gust analysis. A specific stability analysis is presented in the following section of the report. In Figures 45 and 46 the derivatives determined while using load factor and angle-of-attack feedbacks are calculated only through gain values of 2.5 deg/G and 2.5 deg/deg respectively; no rotor divergence was exhibited through these gain values.

As can be seen in Figure 43, the Delta-3, Oehmichen, and pure pitch-cone rotor feedbacks all provide a significant decrease in rotor response to a gust disturbance in comparison to the basic rotor, while also providing a favorable improvement in pitching moment response. For a gain of 1.0 deg/deg, all three schemes reduce the thrust response to approximately 50% of the value found when using no feedback. At higher gain values, the pure pitch-cone feedback yields as little as 30% of the transient response expected with no feedback. The combined Delta-3/Oehmichen feedback is not as effective as the other three feedbacks shown in Figure 43.

Both types of the proportional rotor feedbacks under study show much less efficiency in producing ride comfort characteristics, compared to the other types of rotor feedbacks. Figure 44 shows that for a particular range of gains the proportional, type I feedback actually increases the transient load factor of the helicopter.

Figure 45 illustrates that the load factor feedback reduces the gust response of the helicopter rather linearly with gain. Pitch acceleration provides a similar reduction. Figure 46 presents the characteristics of the fuselage angle-of-attack feedback. At a gain of 1.0 deg/deg, the quasi-static analysis predicts the transient load factor response is reduced to zero, but at gains greater than 0.4 deg/deg the pitching response changes direction, compared to the familiar response of the basic configuration.

In the dynamic situation, the magnitude of the reduction in transient load factor provide by rotor or vehicle feedback is a function of the characteristics of the gust which disturbs the system. Analysis of the dynamic cases investigated indicate that the practical gust alleviation provided is smaller than predicted by the quasi-static analysis. For this discussion, gust alleviation is defined as the percent reduction in load factor for a feedback case over the baseline rotor. For example, for a gust shaped as one cycle of a "sine-squared" function (with an amplitude of 30 ft/sec and a frequency of 1.58 hz), the reduction in load factor obtained using the dynamic analysis is only half of what is predicted by the quasi-static analysis. In the GENHEL program there presently is no provision for the gust to gradually penetrate the rotor, so these dynamic results are somewhat conservative. Also, the particular gust described here disturbs the rotor very rapidly, and is representative of a "worst case" condition which might occur in flight.

The dynamic gust analysis also shows that the transient pitch and roll oscillatory response of the helicopter to a gust disturbance decreases in magnitude when rotor or fuselage feedback is used, but these responses usually die out more slowly when compared to the case with no feedback. This is true because rotor feedback typically reduces the damping of the system. The quasi-static disturbance technique is used to obtain roll damping and pitch damping expressions for the CH-53A, from the GENHEL simulation. Figure 47 shows how these terms vary with feedback gain for two rotor feedback schemes. The variation of damping with feedback gain for the Oehmichen scheme is representative of most rotor feedbacks, showing a decrease in damping with an increase in gain. The plot for Delta-3 in Figure 47, however, indicates that over a particular gain range this scheme provides an increase in damping while de-sensitizing the rotor. Damping lost due to rotor feedback in most situations can be replaced by using an appropriate amount of conventional body pitch rate or roll rate feedback in conjunction with the rotor feedback, if desired. AFCS authority is not expected to be saturated in the event that both rotor and conventional rate feedbacks are used, because for stabilizing gains the control contributions demanded by these two feedbacks are primarily in opposite directions.

While de-sensitizing the rotor to produce desirable gust alleviation characteristics, most of the rotor and vehicle feedbacks destabilize the overall dynamics with increasing values of feedback gain. Therefore the gust alleviation analysis presented in this section, and the stability analysis of the following section must both be considered before finally selecting practical feedback gain limits for the schemes being studied.

Stability vs Gain

Procedure and analysis. - The nonlinear analysis for determining how the rotor and vehicle feedback concepts affect system stability begins by trimming the GENHEL model, employing a particular feedback scheme and value of gain. From a trimmed condition, the helicopter is disturbed by a pulse control input, originating at the pilot's stick. (Because the helicopter degrees of freedom are highly coupled, any control input will eventually excite unstable modes.) Time histories of the rotor and fuselage motion, and the commands from the feedback and stabilization systems resulting from the disturbance, are calculated by the GENHEL program. A stick-fixed solution is employed, with no control inputs applied after the pulse disturbance, except for those commanded by the feedback scheme under investigation, and by the conventional rate feedback stabilization system. The time histories are studied, and the procedure is repeated for different feedback gain values until an instability is observed. The limiting gain value, based on stability criteria, is established in this manner.

The procedure outlined above is conducted at three speeds (hover, 100 kts, and 150 kts) for each rotor and fuselage feedback concept. The lowest limit of feedback gains found is taken as the limiting value for the particular feedback concept. Stability is not dependent on the feed-forward loop, and so it is not included in the stability analysis.

Hysteresis and servo system lags (described by the servo dynamics model) are integral parts of the helicopter control system, and will be present when the rotor feedback schemes are implemented electronically. Therefore they are included in most of the cases studied in the stability analysis. Conventional roll and pitch rate feedback is also included in most of the stability analysis, because it was assumed that it would be needed in flight to provide net stability while evaluating the feedback schemes.

Variations in the helicopter trim attitude, the type and size of the disturbing control input, and feedback authority limits are made in some of the cases under investigation to determine the effect that these parameters have on the stability limiting feedback gain values. For the same purpose, hysteresis, servo system lags, and conventional rate feedback are separately excluded in some cases. The number of blades sampled by the tip-path-plane resolver, and the sampling interval are also varied to determine how these parameters change the rotor feedback gain at which instability occurs.

Discussion of results. - Nature of instability: Taken individually, none of the rotor or fuselage feedback schemes under investigation are adequate for stabilizing the helicopter. Conventional roll and pitch rate feedback is used to bring the helicopter near enough to neutral stability to allow the short term rotor stability characteristics (which are affected by the gust alleviation feedback) to be evaluated without being mistaken for effects of longer term fuselage motion.

Upon examination of the time histories, all of the instabilities exhibit themselves as a continuous oscillation of the control input commanded by the feedback logic. Due to the authority limit restriction imposed on this input, this parameter does not diverge; instead it oscillates back and forth against the fixed limits and continues in this limit cycle. Because the servo actuator restricts the size of the control input, blade flapping does not diverge immediately. But the continuous oscillation of the feedback control against its limits at frequencies which are usually quite high, is an unsatisfactory situation in itself.

The time histories show that most of the rotor and fuselage feedbacks interact with the conventional rate feedback, causing the rate feedback input to the control system to become oscillatory divergent when a particular rotor or fuselage feedback gain value is reached. For some of the rotor/vehicle feedback types or flight conditions simulated, this limiting gain value was found to be smaller than the limiting value determined when no body rate feedback was used; however, the difference was typical less than 10%. At the time when the nonlinear analysis was conducted, it was thought that body rate feedback would be employed in flight while evaluating the rotor/vehicle feedback schemes. Therefore most of the nonlinear stability data were collected for this condition.

Effect of AFCS: The authority limit imposed on the feedback commands, by the servo actuators, is included to make the stability evaluation of the feedback concepts relate as much as possible to the situation which exists during the flight test. Time histories studied with feedback gains selected

below the limiting value show that the rotor response and the control input signal converge whether 100% or as little as 2% authority limit is used. If a gain above the limiting value is selected and 100% authority limit is used, the control input signal commanded by the feedback diverges; if a reduced limit is used, the signal continuously oscillates against the limits.

Under actual flight conditions, both the gust alleviation and any conventional feedbacks must work within the authority limits of the AFCS actuators. For stable gust alleviation feedback schemes, the nonlinear results show that sufficient authority exists so that these schemes can be properly evaluated in flight. The only situation where authority is saturated is when the overall solution is unstable.

Feedback gain limits: Figures 48 and 49 are presented as examples of the time history approach used for determining the stability limiting feedback gain values. Both time histories are for the CH-53A at 150 knots, employing Delta-3 feedback. In Figure 48, blade flapping and the control inputs commanded by the Delta-3 and the conventional feedbacks all converge following the disturbing input, and represent a stable system for a feedback gain value of $K_1 = 1.75$ deg/deg. Figure 49 shows an instability when $K_1 = 1.85$ deg/deg, as indicated by the continuous oscillation of A_{1s} and θ_c commanded by the rotor feedback, and the divergence of flapping and of the B_{1s} signal commanded by pitch rate feedback. The limiting gain therefore lies between 1.75 and 1.85 deg/deg for Delta-3 feedback.

Table VII presents a summary of feedback gain limits and the corresponding frequency at the point of the instability for each scheme, determined in the manner described above. These data are accumulated for the CH-53A at 33,500 pounds and aft cg (348 fscg), initially trimmed at zero roll attitude. Conventional roll and pitch rate feedbacks, having respective gain values of $K_{16} = -0.3$ deg/(deg/sec) and $K_{17} = 0.3$ deg/(deg/sec) are used in conjunction with the feedbacks under study. AFCS actuator authority limits of 10% are imposed on the gust alleviation feedback signals. (No restriction is imposed on the conventional feedback signal.) With rotor feedback concepts, the Kalman estimator tip-path-plane resolver is used, with covariance values of $\underline{Q} = 1$ deg^2 and $R = 100$ deg^2, and which samples six blades 24 times per revolution. The complete helicopter control system is modeled, including servo system lags and hysteresis.

The presence of the conventional rate feedback has only a negligible effect on the gust alleviation limit feedback gain. Time histories of cases which did not use body rate feedback (with the body fixed at its trim attitude in the program to prevent fuselage modes of instability from appearing in the dynamic response) show that the instabilities caused by the gust alleviation feedback occur at approximately the same gain values as they do when the fuselage roll and pitch rate feedbacks are used.

For each feedback scheme, the limiting gain listed in Table VII is based on the condition resulting in the lowest gain necessary to drive the system unstable. Figure 50 represents the same condition as Figure 49 except

the airspeed is 100 knots rather than the 150 knots associated with Figure 49. Maximum speed is usually, but not always, the most critical condition, as indicated in Table VII.

The feedback gain limit is a function of several other helicopter parameters, in addition to velocity. The initial trim is one example of such a parameter. Figure 51 presents time histories for the CH-53A at 150 knots, employing Delta-3 feedback with a gain of K_1 = 1.65 deg/deg. In this case the helicopter is initially trimmed with zero sideslip. The system is unstable at this gain value. Figure 48 shows that when the helicopter is initially trimmed at zero roll attitude, the helicopter employing Delta-3 feedback is still stable at a gain of K_1 = 1.75 deg/deg. The difference here is due, most likely, to the difference in trim value of blade flapping (and therefore rotor tip path plane) between the two cases. Because the feedback gain limits are dependent on a number of parameters and conditions, they should be considered as only somewhat approximate. In any event, testing should start with considerably lower gains.

Number of blades sampled : Cases were run employing rotor feedback in which the tip-path-plane resolver sampled every other blade of the rotor 24 times per revolution. An example of the time histories obtained for these cases is shown in Figure 52, using Delta-3 feedback, with a gain of K_1= 1.75 deg/deg. Comparing the time histories in this figure to those of Figure 48 indicate that a lower limiting gain is found when 3 blades are sampled. In general, the limiting gain value is about 10% lower when only every other blade is sampled. The control signal commanded by the rotor feedback also contains some noise contamination when every other blade is sampled in the nonlinear analysis.

Sampling time interval: The effect of the sampling time interval of the tip-path-plane resolver and rotor feedback logic was studied. Results indicate that when all six blades are sampled either 12 or 6 times per rotor revolution, the limiting feedback gain increases. (For example, for the Delta-3 scheme the limiting gain value is about 2.25 deg/deg when the sampling interval is 12 per revolution, and approximately 3.0 deg/deg when the sampling interval is a 6 per revolution.) However, it was difficult to proceed to the dynamic response condition in order to find the gain limits because whenever the sampling interval was reduced to 12 or 6 times per revolution, the trim solution of the tip-path-plane coefficients behaved in a peculiar and unpredictable manner, often exhibiting unstable (diverging) characteristics. Therefore a conclusion about the effect of the sampling interval is not drawn based on the results of the nonlinear analysis.

System lags and delays: Control system lags and time delays (as well as hysteresis), inherent to the servos and servo actuators, affect the value of the limiting feedback gain, and therefore affect the ultimate performance of the gust alleviation feedback schemes. This fact is illustrated by the time histories of Figure 53. These are the time histories of a case in which Delta-3 feedback with a gain of K_1 = 2.0 deg/deg was used, but the control system hysteresis and servo lags were omitted. Here, Delta-3 feedback has not caused the system to be unstable at this gain value (the long term non-oscillatory divergence seen in Figure 53 is due to the inability of the conventional

rate feedback to restrain the fuselage motion). With hysteresis and servo lags the limiting feedback gain was established at 1.80 deg/deg for this type of feedback. (Most of the decrease is due to servo lags.) The limiting gain is usually higher when these control system lags are omitted.

In the Tip-Path-Plane Resolver Study section of this report it was mentioned that any phase lag associated with the Kalman solution appeared to be negligible. Other possible computer related lags and delays include those associated with the program cycle time, the input/output devices, and any hardware or software filters used to process measurement signals as they enter the computer. These lags cannot be eliminated, but can be reduced by using efficient programming, fast computers, and fast input/output devices. A true mechanical representation of the rotor feedback schemes would not contain the lags due to hysteresis, servo dynamics, or any computer related delays. These lags are included for the cases analyzed and summarized in Table VII. The rotor feedback data of Table VII presents gain limits for the electronic representation of these schemes. For pure mechanical rotor feedback, the elimination of hysteresis and servo lags alone is expected to increase the gain limit values by about 30% over those shown in the table.

Comparison to linear results: The linear stability analysis of the feedback systems show many of the same trends and qualitative results which were determined by the nonlinear analysis. Some of these include the decrease in rotor stability with increase in feedback gains, and the effects of conventional rate feedback (SAS) and servo system lags on stability boundaries. The linear analysis also produced useful open-loop data, indicating rotor, rigid body, and control system characteristic modes.

The limiting values of feedback gain predicted by the linear stability analysis were not in close agreement with those values predicted by the nonlinear analysis. Typically the limits predicted by the linear analysis were about twice as high as the corresponding nonlinear values. Therefore, in order to avoid possible confusion with the more conservative restraints determined by the more accurate nonlinear analysis, the limiting feedback gain values predicted by the linear stability analysis are not presented.

A few possible explanations for the quantitative differences resulting from the linear closed-loop analysis are briefly mentioned here. The coefficients of the helicopter variables of the linear model were assumed to be constant with time, and were identified based on this assumption. Reference 3, which investigates various techniques for describing rotor flapping, indicates that a constant coefficient linear model does not accurately predict closed-loop system characteristics; more accurate results are anticipated if a model with periodic coefficients is used. Another explanation for the inaccuracy of the closed-loop linear results may be due to the fact that the rotor modeled by the tip-path-plane coefficients in the linear solution was composed of only first harmonic terms. Therefore the feedback had to deal with much simpler and more predictable rotor motions in the linear analysis than it did in the nonlinear analysis (where the actual rotor motion was not restricted to a first harmonic tip-path-plane approximation). For this reason the feedbacks may have been effective through higher gain values during the linear analysis than they were for the more complicated nonlinear approach.

Control Orthogonality

When the pilot inputs a control at the cyclic and/or collective stick the helicopter should respond initially in a familiar manner, based on typical helicopter response characteristics (i.e., basically orthogonal control moments). Control orthogonality refers to a desired relationship between pilot cyclic control inputs and the resulting moment (angular acceleration) response of the helicopter - longitudinal cyclic control inputs (δy) should initially produce a pure pitching moment (M), while lateral cyclic control inputs (δ_x) should initially produce only a rolling moment (L). The modified rotor and fuselage response produced by rotor feedback is, however, desired whenever the helicopter is disturbed by gusts. Therefore the rotor feedback logic must be capable of distinguishing between tip-path-plane disturbances requested by the pilot and tip-path-plane disturbances resulting from gust inter-action with the rotor, or other excitations. This can be accomplished with the aid of feed-forward of control stick inputs.

A complex coordinate analysis of rotor tip-path-plane motion was used to determine the values of feed-forward gains (as designated in Table I) which must be used in conjunction with specific rotor feedbacks in order to maintain control orthogonality. The resulting equations which establish the necessary feed-forward gain values:

$$K_{11} = \frac{\Delta A_{1s}}{\Delta \delta_x} \quad (E \cos\eta - 1) \tag{23}$$

$$K_{12} = \frac{\Delta B_{1s}}{\Delta \delta_y} \quad (E \cos\eta - 1) \tag{24}$$

$$K_{14} = \frac{\Delta B_{1s}}{\Delta \delta_y} \quad (-E \sin\eta) \tag{25}$$

$$K_{15} = \frac{\Delta A_{1s}}{\Delta \delta_x} \quad (E \sin\eta) \tag{26}$$

$$K_{13} = \frac{\Delta \theta_c}{\Delta \delta_\theta} h_3 \tag{27}$$

where

$$\eta = \arctan \frac{h_2}{(1 + h_1)^2} \tag{28}$$

$$E = \left[(-h_2)^2 + (1 + h_1)^2 \right]^{1/2} \tag{29}$$

These feed-forward gains are functions of the rotor feedback gain values, and control linkage ratios (control angle commanded at the servo actuator per unit control stick displacement). In addition to maintaining control orthogonality, these feed-forward gains are also used to maintain constant control sensitivity (magnitude of moment response per unit stick input).

In order to verify equations 23 through 29, the quasi-static disturbance technique is applied to the GENHEL model. The CH-53A is trimmed in hover and is disturbed by a one inch step input of either the lateral or longitudinal cyclic stick. This is done for three conditions: (1) the basic rotor, employing no feedback or feed-forward; (2) Delta-3 feedback with $K_1 = 0.5$ deg/deg and no feed-forward; and (3) Delta-3 feedback with $K_1 = 0.5$ deg/deg, and application of the appropriate feed-forward. The resulting rolling and pitching moment responses are shown in Figure 54. The results indicate that feed-forward properly maintains control orthogonality during the short term response of the helicopter, whenever rotor feedback is employed in the system. The steady state response data obtained from GENHEL is short term data (i.e., it is not instantaneous response data, nor is it long term response data). The short term response here is of about one to three rotor revolutions in duration, and provides acceleration cues which are easily recognized by the pilot.

The feed-forward gains specified by equations 23 through 29 are not functions of forward speed. Figure 55 illustrates the effectiveness of these feed-forward solutions (which are rigorously exact only in hover) at 150 kts. The results shown in Figures 54 and 55 indicate that feed-forward adequately maintains control orthogonality and constant control sensitivity over the entire speed range of the helicopter.

Thrust Vector Control

The thrust vector control scheme selected for study as a combined rotor and fuselage feedback control concept was described earlier, with the block diagram for the system appearing in Figure 5. The positioning of the rotor tip path plane relative to the vertical has been considered as a control scheme in the past, but since as adequate measurement of tip path plane was not available, no known success was ever achieved with such a feedback system. The stick position lead network shown in Figure 5 was included in the analytic study because it would be present in an experimental flight test configuration, unless major control system modifications were made to the test helicopter.

In the longitudinal mode, as an example, the rotor vector control scheme allows the pilot to control the resultant fore-and-aft force of the helicopter, independent of the fuselage attitude. The control stick in this case controls a simple model

$$\frac{\Theta_{R_M}}{\delta_y} = \frac{M}{(\tau_M S + 1)} \qquad (30)$$

where Θ_{R_M} is the desired angle $\Delta\Theta_R$ (see equation (1)) which is calculated by the model, and τ_M is the time constant of the model lag.

Typically, model-following schemes such as this one provide a lead network which routes a stick signal past the model and inputs it directly to the servos. By doing this, the dynamic response error can be minimized for models, which generally would include some dynamic lags. Specifically, for model-following it is desirable that the response characteristics of $\Theta R/\Theta_{R_M}$ be as good as or better than the model response Θ_{R_M}/δ_y. The Θ_R/Θ_{R_M} response is a measure of the ability of the closed loop system, exclusive of the model, to respond to any specific command inputs.

In this study, the model is kept quite simple. The model lag τ_M is set at zero which eliminates the need for lead shaping. Justification of this simple model is based on the fact that force rather than attitude is the desired output, and for this reason the pilot desires as rapid a response as the helicopter will generate. Thus, the lags of the closed-loop rotor/vehicle are the only factors in the resulting response dynamics. Therefore the actual response characteristics of the physical closed-loop system must be found.

A brief assessment of the usable frequency range for various elements of the combined control, rotor, and fuselage system has been discussed previously, and is shown in Table V for the various transfer functions. The thrust vector control scheme, which employs both attitude and rotor flapping feedback, has an open-loop crossover frequency of 4.2 hz (similar to the case of only the servos and the rotor flapping). Figure 56 shows the response amplitude and phase for the closed-loop rotor force control system for gains of .25, 1.0 and 5.0 deg/deg. While the gain of 5.0 causes the system to be unstable, it is included to show the improved tracking which results from the higher loop gain.

The stability of this feedback system is predicted to be positive for loop gains to approximately 2.5 deg/deg. This level of gain, while not sufficient to provide accurate model-following (low value of ε) for rapid control motions, is adequate for good control. The signal error ε is approximately proportional to the inverse of the loop gain, and since the value of K_{10} is limited to relatively low values, some Θ_R error will result. This error will be most noticeable for the higher frequency inputs (0.4 to 4.0 hz). The longer term response (<0.4 hz) for this case of thrust vector control should be quite adequate however. This gain limitation will affect all closed-loop helicopter schemes quite similarily. In fact, as was discussed earlier under the Frequency Response section, it is quite probable that only a fraction of the predicted gain will be achievable.

At 150 kts, the stability analysis using time histories produced by the GENHEL program indicate that the helicopter employing the thrust vector control scheme is stable for gain values of K_{10} between 1.0 and 2.0 deg/deg. No conventional SAS (body rate feedback) is used in this analysis; the rotor and fuselage are both stable within this gain range using only thrust vector control feedback. For gain values below 1.0 deg/deg, the model cannot track the

helicopter fast enough, and a net fuselage instability results. For gains above 2.0 deg/deg, the feedback signal to the cyclic control reaches a limit cycle, and the rotor diverges.

FLIGHT TEST INVESTIGATION

A flight test program was conducted to verify the analytic findings for several of the feedback schemes, and to determine the efficiency of operation of a digital computer incorporated as part of the helicopter control system. A bailed Navy CH-53A (Bu. No. 153718) was used in this test program (Figure 1). The following sections of the report describe the set-up of the helicopter/computer/control system and the equipment used, the test procedure, and the conditions studied. The data reduction techniques used are discussed, and the test results and conclusions are presented.

SYSTEM COMPONENTS AND OPERATION

Instrumentation

Figure 57 shows the basic instrumentation on the test helicopter. The helicopter was instrumented to record the following parameters during flight:

Roll attitude
Pitch attitude
Yaw attitude (heading)
Roll angular velocity
Pitch angular velocity
Yaw angular velocity
Roll angular acceleration
Pitch angular acceleration
Yaw angular acceleration
CG lateral acceleration
CG longitudinal acceleration
CG normal acceleration
Pilot-station normal acceleration
Airspeed
Fuselage angle-of-attack
Fuselage sideslip angle
Lateral stick position
Longitudinal stick position
Collective stick position
Pedal position
Lateral AFCS servo output
Longitudinal AFCS servo output
Collective AFCS servo output
Directional AFCS servo output
Main rotor blade flapping - six blades

Main rotor blade pitch (feathering) - three blades
Main rotor blade lag (hunting) - three blades
Sine of rotor azimuth
Cosine of rotor azimuth
Rotating star load (at one push rod)

The attitudes and angular velocities were measured with gyros, angular and linear accelerations with accelerometers, airspeed with a pressure transducer, angle-of-attack and sideslip with vanes, stick and AFCS servo positions with potentiometers, star load with a strain gage, and rotor azimuth functions with a transducer. The blade motions were measured with angulators. The installation of a yaw boom and a main rotor slip ring arrangement was required on the test helicopter to accommodate some of the instrumentation.

All measurements were made with conventional "off-the-shelf" instrumentation. Sensitivities selected and calibrations performed during the rotor/vehicle flight test investigation produced the same degree of accuracy in measurements as produced in any typical test program.

The parameters measured were all recorded on FM analog tape system. In addition to these 39 signals, nine outputs from the on-board computer were recorded on the tape, including the three commanded control inputs fed to the AFCS servo actuators by the programmed routines. The other six computer outputs recorded on tape are selected parameters for monitoring the operation of the programmed routines, and are described later.

Computer and Related Peripheral Devices

A Digital Equipment Corporation PDP-11/R20 computer and related peripheral equipment were obtained for the test portion of the investigation. The selection of this computer (Figure 58) was based on its speed, reliability, cost, and the associated software systems which allow for relatively quick and easy programming and debugging.

The resolver and feedback routines, equations, and logic programmed in PDP-11/R20 are similar to those which were programmed in the PDP-10 for the analytic investigation. Routines and calculations added to the in-flight programming, not included or discussed earlier in the analytic section of this report, are a low-pass body filter, a computer generated "gust" input, and a pilot-selected modification of the stick feed-forward input. The low-pass filter was programmed to allow the selection of a different cutoff frequency for each fuselage parameter passing through the filter being used as a feedback signal. The gust simulated by the computer in flight is created by commanding a time-varying collective control input to the rotor according to the equation

$$\theta_C = M_{G_1} \sin \omega_{G_1} t + M_{G_2} \sin \omega_{G_2} t + M_{G_3} \sin \omega_{G_3} t \qquad (31)$$

where M_{G_1}, M_{G_2}, and M_{G_3} represent magnitudes of collective control inputs and ω_{G_1}, ω_{G_2}, and ω_{G_3} are the corresponding frequencies of the inputs. Both the magnitudes and the frequencies are input variables for the in-flight "gust" generator routine. The stick feed-forward equations used in flight to calculate the control inputs necessary for maintaining control orthogonality and constant sensitivity differ slightly from the feed-forward equations described in Table I. The feed-forward equations programmed in the PDP-11/R20 allow the pilot to alter the phase relationship of the control inputs, governed by the feed-forward gains, according to the equations

$$A_{1S_{FF}} = (K_{11}\cos\xi - K_{15}\sin\xi)\Delta\delta_x + (K_{14}\cos\xi - K_{12}\sin\xi)\Delta\delta_y \qquad (32)$$

$$B_{1S_{FF}} = (K_{15}\cos\xi + K_{11}\sin\xi)\Delta\delta_x + (K_{12}\cos\xi + K_{14}\sin\xi)\Delta\delta_y \qquad (33)$$

The angle ξ is a variable, selected by the pilot in flight. Changing ξ is equivalent to rotating the swashplate for the stick feed-forward portion of the control signal.

The computer program was set up to operate in four basic modes:

IC - The initial condition mode. In this mode the input variables (feedback type and gain values, covariances and cutoff frequencies, number of blades sampled, sampling time interval, and "gust" generator magnitudes and frequencies) are read by the computer while the helicopter is being trimmed by the pilot.

TRIM - In this mode, trim values of all feedback parameters are measured or calculated and stored in memory for subsequent use.

OPERATE - The dynamic operate mode. Control inputs are calculated based on deviations from the trim condition, and are routed to the control system. All schemes are evaluated in this mode.

DDT - The hold mode. Program can be investigated or modified in this mode using the DDT (Dynamic De-bugging Technique) program, which is stored in the PDP-11/R20. No interaction occurs between the helicopter and the computer in this mode.

Body roll and/or pitch rate feedback can be calculated within the computer and may be used, if desired, to replace the conventional SAS (Stability Augmentation System) of the helicopter by selecting the SAS mode of the computer program. (The conventional helicopter SAS becomes inoperative whenever the computer is engaged by the control system.) When selected, the SAS mode relays body rate feedback inputs to the control system if the IC, TRIM or OP mode is in use, but not when the DDT mode has been selected. Rotor or fuselage feedback, stick feed-forward, or computer generated "gust" inputs are relayed to the control system only when the OP mode has been selected.

A paper tape reader was installed on the helicopter so that the feedback program could be loaded in the computer quickly before a flight, and to provide the capability of re-loading the program in flight in case it was lost within the computer memory while airborne. The in-flight version of the rotor/vehicle feedback computer program was first prepared using the DEC PDP-10 hybrid computer. The PDP-10 version of the program was then converted to a form acceptable to the PDP-11/R20 using an emulator routine. A paper tape copy of the resulting program was then made and was loaded in the PDP-11/R20 via the paper tape reader. This indirect technique of programming the in-flight computer required less time and effort than programming the PDP-11/R20 directly (which requires the use of assembly language.)

An electronically operated teletype, shown in Figure 59, was installed on the test helicopter in order to add flexibility of operation while in flight. The teletype was carried on the helicopter to permit detailed inspection of computer program operation and calculation, and to change the values of some input variables.

The measurement signals supplied to the computer for use in the resolver, filter, or feedback calculations, and the potentiometer settings of the feedback gain and other input values were inputted to the computer through analog-to-digital converters. Eighteen measurement signals were split so that they could be inputted into the computer, in addition to being recorded on tape. These signals were the flapping angle of all six blades; sine and cosine of the rotor azimuth; lateral, longitudinal, and collective stick position; roll and pitch attitude; roll and pitch rate; normal load factor; pitch acceleration; and angle-of-attack. These signals were amplified to voltage magnitudes acceptable to the PDP-11/R20.

Digital-to-analog converters were used to relay the total computer-calculated control signals to the lateral cyclic, longitudinal cyclic, and collective channels of the AFCS, and to relay eight computer calculated parameters to a direct write device carried on the helicopter. The three commanded control signals and six of the signals sent to the direct write device from the computer were split, and these nine computer originated parameters were also recorded on the analog tape.

The direct write device installed on the helicopter was an eight channel hot pen recorder. At any time during a flight, the engineer could immediately monitor the time histories of eight parameters originating from the computer. A routine was programmed in the PDP-11/R20 which conditioned and sent the signals of a set of eight pre-selected parameters to the direct write recorder. Eight different sets of parameters were available, and the particular set exhibited on the recorder could be selected by the engineer before each test maneuver was flown. The parameters available at the pen recorder were pre-programmed combinations of eight of the following:

Signals received by the computer -

Roll attitude
Pitch attitude
Blade flapping (6 blades)
Sine of rotor azimuth
Cosine of rotor azimuth
Roll angular velocity
Pitch angular velocity
Lateral stick position
Longitudinal stick position
Collective stick position
Angle-of-attack
CG normal load factor
Pitch angular acceleration

Parameters calculated within the computer -

Tip-path-plane coefficients (3)
Re-constructed blade flapping (2 blades)

Control inputs calculated within the computer -

Rotor/fuselage lateral cyclic
Rotor/fuselage longitudinal cyclic
Rotor/fuselage collective
Body rate lateral cyclic
Body rate longitudinal cyclic
Stick feed-forward lateral cyclic
Stick feed-forward longitudinal cyclic
Stick feed-forward collective
Gust generator collective
Total lateral cyclic
Total longitudinal cyclic

Feedback Control Units and Control System Modifications

An engineer rotor/vehicle feedback control unit and a pilot monitor/control panel were built especially for the flight test investigation. Both units are shown in Figure 60 (where the pilot panel has been placed on top of the engineer control unit).

The engineer control unit provides a common interface between the computer and the sensor inputs from the instrumentation, the flight engineer, the recording equipment, and the helicopter control system. The sensor inputs from instrumentation are routed to a connector on the back of the control unit. The signal wires are connected to input test jacks on the front panel and also to the computer analog-to-digital converter input pins. Potentiometer knobs on the front panel provide variable signal sources to the analog-to-digital converter (a potentiometer knob on the pilot monitor panel provides

a similar signal). All potentiometer signals are available at test jacks on the front panel. The knobs are used to input selected feedback gains and other related variables into the computer program.

Hardware filters (R-C circuits) were provided within the control unit to filter out the high frequency content of the instrumentation signals supplied to the computer. The high frequency content did not come from the sensor itself, but originated from the signal conditioning which was necessary in order to record these same signals on the FM analog tape recorder. The hardware filtering provided a cutoff frequency of 40 Hz.

Discrete switches on the front panel control one 16 bit word in the computer for mode control, while lamps on the panel indicate computer modes, overflow conditions, saturated AFCS authority, and duty cycle overrun. Three voltometers were built into the unit, and are located on the engineer control panel.

The digital-to-analog converter output channels are connected to output test jacks on the panel. Three channels are also fed to the pitch, roll, and collective servo valve driver circuits.

Most of the interface between the computer and the AFCS is done at the engineer control unit. A valve driver receives the computer generated signal current, and its output is controlled by a relay circuit. When the circuit is de-energized, the conventional AFCS channel 1 outputs (such as SAS outputs) are connected to the servo. The computer engage switch on the engineer control panel and on the pilot monitor panel cause a latch circuit to be set when either switch is pressed. When the latch is set, the relay circuit transfers the AFCS outputs to a dummy load and connects the computer valve driver outputs to the servo. There is no connection between this computer engage system and the computer mode switches. The supply voltage to the engage latch circuit runs in series through normally closed computer release switches on the pilot and copilot cyclic sticks. When either switch is pressed, power is removed from the latch and also the relay circuit, and the AFCS channel 1 outputs are then connected to the AFCS servo. Existing control system circuitry, and circuitry provided in the feedback control unit, as well as routines programmed in the computer, provide smooth transition and fade-in of signals originating from either the computer or the conventional AFCS, as long as the control system and computer control options are selected in the proper and prescribed manners.

The safety of flight for the computer/control system is provided by the operation of the engage - disengage function which is completely independent of the computer and the use of the limited authority AFCS servo-actuators. No automatic shutdown can be provided because the entire control system (incorporating the computer) is single channel. However, the engage latch and relay circuit provides immediate release capability at the pilot's finger tip; the computer outputs immediately go to zero when the computer release switch is pressed.

The pilot monitor panel was installed in the cockpit, between the pilot and copilot locations. This panel has the computer engage switch, the computer IC and SAS mode switches, the feed-forward coupling potentiometer knob, and computer mode indicator lights. The pilot has control of the IC mode and has the option to select the computer calculated body rate feedback (SAS mode), if desired. These two modes are also under the control of the flight engineer at the engineer control unit panel located in the cargo area of the helicopter. (The flight engineer alone has control of the TRIM, OPERATE, and HOLD program modes.)

The computer release switches were incorporated into both the pilot and the copilot cyclic stick grips. These switches are normally closed momentary switches which supply 28 vdc power to the latch circuit and the engage relay circuit. Failure of such a switch would make it impossible to engage the computer outputs. This would result in normal operation of the channel 1 AFCS.

The conventional CH-53A AFCS servos and the AFCS amplifiers are used as part of the rotor/vehicle feedback control system. The pitch and roll cyclic AFCS servos have dual actuators, while the collective AFCS servo has a single actuator. The computer/control system interface modifications were made so the feedback schemes could be operated and evaluated whenever the channel 1 AFCS is operative and the channel 2 AFCS is not operative (the ON - OFF AFCS mode). The dual actuators are operated with only one actuator engaged, as selected at the AFCS control panel servo switch. The collective electronics are single channel. The pitch and roll AFCS electronics are dual channel and normally are operated in the ON - ON AFCS mode, with each channel feeding each of the two coils on the servovalve of the engaged servo. It is possible to fly the CH-53A up to 150 kts with only one channel of the dual electronics operating. In this program the PDP-11/R20 was installed as a single channel controller, and the flight envelope was restricted for single channel AFCS operation (150 kts airspeed).

On the test helicopter, the normal AFCS #1 electronic signals are interrupted at the amplifier outputs and replaced by a separate set of signals from the PDP-11/R20 computer. Thus, the normal AFCS control panel, flight director, and servos have the computer control signals on the #1 channels and on the single collective channel. The AFCS #1 engage switch interrupts the pitch and roll computer inputs if turned off. For proper operation, the flight director is set in the AFCS mode so that the #1 AFCS signals and collective and yaw signals are displayed on the corresponding indicators. Then the computer inputs are displayed on the pitch, roll, and collective indicators whenever the computer signals are engaged by the latch and relay circuits.

The AFCS stick trim system remains operative in the usual way. However, the roll attitude input was re-wired so that it could be disabled for a rotor/vehicle feedback test flight, otherwise the outer-loop roll attitude hold function could saturate the AFCS authority available to the feedback schemes under investigation. The normal yaw AFCS is available whenever selected; however the altitude hold techniques are inoperative within the modified control system.

TEST PROCEDURE

Prior to each flight, a thorough check of the helicopter/computer/control system was conducted. Instrumentation was calibrated, and signal sensitivities inputted at the computer were checked. Selected check case input values were loaded into the program, and the commanded control outputs at the digital-to-analog converters (feeding the AFCS servo actuators), and the outputs at the pen recorder were compared to the expected calculated values.

Once in flight, all of the sensor signals inputted to the computer, which would be used as parameters in the feedback logic, were checked to determine if they were acceptable before closing any feedback loops. These signals were also frequently checked during the duration of the flight.

The engineer on board the helicopter monitored the system response during and after each maneuver by observing the pen recorder outputs, and, on occasion, by checking signals at the test jacks on the control unit panel, or by reading values calculated within the program using DDT and the teletype. After each maneuver, the flight engineer discussed the performance of the particular feedback studied with the pilot, and subsequently selected the feedback type and gain to be evaluated next. A computer programmer was also on board during each flight, and assisted the flight engineer by operating the computer equipment, and by setting the selected program input variables and modes at the control unit panel or through the teletype.

When the helicopter was trimmed at the desired speed and altitude at the beginning of a flight, the pilot zeroed the conventional SAS inputs to the AFCS servos (using the CG trim wheel). The pilot then switched from the ON - ON to the ON - OFF AFCS mode, thus readying the AFCS servos for the commanded control signals originating from the computer.

The typical sequence of selection of control system options and computer program modes made in flight during a test maneuver was as follows: As the pilot held the helicopter near the trim condition, potentiometer and teletype inputs were made by the programmer and read by the computer program in the IC mode. The pilot then engaged the computer. The programmer then selected the TRIM mode, and the engineer monitored the sensor input signals to the computer in trim, or the estimated trim tip-path-plane coefficients. The programmer then selected the OPERATE mode, after notifying the pilot that he was doing so. The pilot then gave the engineer a cue to begin to record data on the tape system before performing the desired maneuver. At the completion of the maneuver, the pilot selected the IC mode or pressed the computer release switch to terminate the rotor/vehicle feedback signals and any associated signals to the AFCS servos originating from the computer. This procedure was repeated for each test condition.

Eight and one-half hours of Rotor/Vehicle Feedback flight testing were conducted as outlined in Figure 61. All testing was done at light gross weight (33,000 to 35,000 lbs) and aft center-of-gravity location (346 to 348 fscg). Closed loop testing was restricted to those feedback schemes which showed the best results based on the analytic investigation, and whose

computer input signals, originating from the sensors, appeared acceptable for closed-loop operation. These schemes were Delta-3, Oehmichen, pure pitch-cone, type II proportional, and normal load factor. The particular subjects investigated during the test, and the feedback types used in these studies are specified in Table VIII. Pulse or step inputs by the pilot were used to study the operation of the tip-path-plane estimator and the low pass body filter, and to determine stability and handling qualities characteristics of the helicopter when employing selected feedbacks. Small disturbances from trim were used by the pilot to excite the helicopter in order to determine feedback gain limits. The computer generated "gust" input was used to evaluate the gust alleviation characteristics of selected feedback schemes.

DATA REDUCTION

A digital tape composed of 40 of the 48 parameters recorded in flight on analog tape was made at the ground stations facility following each flight. The analog tape data were scanned at a sample rate of either 20 or 60 per second and were recorded on digital tape. The following parameters were digitized:

At 60 samples per second -

- Blade flapping (6 blades)
- Sine of rotor azimuth
- Lateral AFCS servo output
- Longitudinal AFCS servo output
- Collective AFCS servo output
- Directional AFCS servo output
- Total computer commanded longitudinal cyclic control
- Total computer commanded lateral cyclic control
- Total computer commanded collective control
- Computer originated signals to pen recorder (6)
- Push rod load
- Blade hunting (3 blades)

At 20 samples per second -

- Roll attitude
- Pitch attitude
- Roll angular velocity
- Pitch angular velocity
- Yaw angular velocity
- Roll angular acceleration
- Pitch angular acceleration
- Yaw angular acceleration
- CG normal acceleration
- Airspeed
- Fuselage angle-of-attack
- Fuselage sideslip angle
- Lateral stick position

Longitudinal stick position
Collective stick position
Pedal position

The roll, pitch, and yaw angular acceleration signals were the only parameters which were filtered at the ground station during the digitization process. A 1 Hz filter was used on these parameters because of the high noise content of the analog signals.

Feedback systems which rely on rotor parameters could introduce high frequency inputs to the control system, which could highly influence the performance of the feedback type and the stability of the system. In order to see such effects in the data, if it were present, a high sampling rate of key parameters was selected whenever possible in the digitization process. A high sampling rate also minimizes the problem of data aliasing associated with discrete sampling and filtering processes.

An existing ground station computer routine was used to automatically plot time histories. Plots of each of the 40 digitized parameters were developed for those test cases chosen for closer scrutiny after the completion of the test program. These time histories were displayed on a cathode ray tube (CRT), and hard copies were made from the displays. On the CRT plots, 20 data points appear for each second of the time history of those parameters which were sampled during the digitization process at 20 times per second; 30 data points per second of time history appear on the CRT plots for those parameters which were sampled during the digitization process at 60 times per second.

Prior to processing the CRT plots, oscillograph plots of all of the analog data recorded during every flight were made. The portion of the time history data plotted on the CRT display was selected after studying the oscillograph rolls. The time histories of the eight parameters plotted in flight on the pen recorder were also used as necessary, in analyzing the conditions tested.

Figure 62 serves as an example of the form of the CRT plotted time history data of the 40 digitized parameters, for one of the cases selected for detailed study.

TEST RESULTS

Helicopter and Instrumentation System Operation

In general, the testing proceeded well, without incurring any major difficulties related to the system hardware or the feedback related computer software. However some hardware problems associated with the test helicopter slowed the test investigation, which ultimately prevented some subjects of interest from being tested as thoroughly as planned. A number of Rotor/Vehicle Feedback Investigation flights were either aborted before takeoff or were terminated prematurely because cockpit instrumentation indicated unsafe engine

temperature and oil pressure conditions. Repairs were made to a hydraulic reservoir, the heater, and a fuel line, and the auxiliary power unit had to be replaced after ingesting a wire screen during the test program.

Other problems related to the operating status of the test vehicle may have influenced the rotor response and handling characteristics of the helicopter during the test. It was suspected that the rotor had a marginally acceptable blade lead-lag motion damper, and that the blade tip-path-plane was not tracking as accurately as it could have. The lack of readily available spares, a limited budget, and a limited schedule prevented these problems from being thoroughly checked and corrected. The rotor response and handling characteristics of the helicopter were also affected by the gusting wind conditions which prevailed during the period which the flight testing was conducted.

On most occasions, the measurement sensor signals provided to the computer and to the tape system functioned acceptably. In two instances all of the sensor signals relayed to the computer sustained a type of bias or hardover. The duration of this condition was about five minutes for one instance, and about five seconds for the other, but the response of the helicopter resulting from these effective hardovers was not unacceptable, due to the 10% AFCS authority limit. The cause of these apparent hardovers was not known, although evidence indicated that it was an instrumentation related problem rather than computer related. The hunting angle signal for one of the blades did not function properly during any of the flights. An effort was made to correct this signal, but it could not be done within the time frame to which the test program was restricted. On certain flights, some signals or the corresponding tape system tracks were not operating properly, but these signals were never those which were also used by the feedback loops within the PDP-11/R20.

Computer System Operation

The PDP-11/R20 computer functioned well during the flight test program. The computer accepted loading of the program via the paper-tape reader every time except when the paper-tape reader malfunctioned. Once airborne, the program was never lost in memory. The program was easy to enter using the DDT routine in flight, which was important for making some input changes and for investigating any phase of operation of the program itself.

One important reason why the computer never lost the program was that the power supplied to the computer system was always acceptable to the components of that system. The computer equipment was run off the normal aircraft power supply, provided by one of the primary ac buses. Two inverters were installed to supply the computer and peripheral equipment with 12 amps of current at 60 Hz. No other preparation was necessary to supply proper power to the computer. Power surges large enough to force the PDP-11/R20 to shut itself off were never encountered. Although not sufficient to run all of the computer related equipment at one time, 12 amps was enough current to run as much of the equipment that was needed simultaneously at any time during the entire test program.

The 4000 word memory of the PDP-11/R20 was sufficient to store all of the feedback and related routines, the program mode and input/output logic, and the DDT routine, although almost no room remained in the memory core after everything was loaded. It was estimated that one complete pass through the entire program required about 0.008 sec. The duty cycle required by the PDP-11/R20 to execute the feedback program therefore was approximately twice as fast as the sample rate used most frequently during the testing (24 samples/ revolution).

During the course of the test program, only one significant computer-oriented hardware problem arose. This was the malfunction of a digital-to-analog converter (DAC). The DAC that failed was the one that relayed the commanded computer signal to the longitudinal AFCS servo-actuator. The problem was quickly corrected by a program change and a wiring modification made to the control unit panel - the combination of which re-routed the computer commanded longitudinal control signal through an extra DAC which was included in the computer/control system interface. No problems involving the computer software systems occured during the test program.

With the exception of the one analog-to-digital converter which failed, the peripheral equipment used for interaction with the computer all functioned well within the helicopter environment and in flight, and only a few minor problems were incurred. The paper tape reader operated in a sluggish manner when it became cold and dusty on-board the helicopter. It required some effort for the programmer to type accurately into the teletype while in flight because of the helicopter motions he was subject to, but the teletype itself did not type any unwanted characters due to the vibrations. At 150 kts, the vibration of the helicopter caused a few of the pens of the pen recorder to shake badly, and they did not contact the paper properly, therefore failing to accurately display some parameters in flight.

Tip Path Plane Resolution

A significant portion of the flight testing pertaining to the operation of the tip-path-plane resolver was conducted in the open-loop condition because the closure of any feedback loops has no effect on the tip-path-plane resolver.

At all speeds tested (hover, 100, and 150 kts) the trim tip-path-plane coefficients were calculated within two or three rotor revolutions whether 6, 5, or 3 blades were sampled, or whether the sampling rate was 24, 12, or 6 times per revolution. These results were predicted by the analytic investigation.

In flight, the trim and the dynamic tip-path-plane coefficients carried a small (approximately ± 0.10 deg) oscillatory component which was not evident in the analytic solution. The flapping signal of one of the blades was purposely biased by 0.40 deg as it entered the computer for a few cases to determine if a biased signal or an out-of-track condition was responsible for the 1/rev component on the coefficients. The biased conditions had no noticeable effect on the 1/rev component. This oscillatory component was too small

to be recognized in closed-loop conditions for levels of rotor feedback gain values such as those tested in this program, and had no apparent influence on any of the test results.

The effect of the covariance values on the resulting estimated tip-path-plane coefficients was studied for R/Q ratios of 1/25, 1, 25, 100, and 500. With one exception, no significant variation in the coefficients was noticed for different covariance values. The exception was when R/Q was set to 1/25, the estimated coning coefficient became zero. This result was checked on three separate occasions in flight, always yielding the same result. For this particular covariance ratio, it was difficult to verify if the values of the lateral and longitudinal flapping values were reduced, due to the small magnitude of these coefficients and the inaccuracy associated with the resolution of these data.

A covariance ratio of R/Q = 100 was used for estimating all three coefficients in most of the cases studied. Figure 63 is an example of the variation in tip-path-plane coefficients from trim as estimated by the Kalman filter method. Also shown is the stick input which is responsible for the tip-path-plane motion.

Whenever the sampling rate was reduced from 24 to 12 or 6 per revolution, or whenever the number of blades sampled was reduced from 6 to 3, the estimated tip-path-plane coefficients were acceptable. In some instances the values of the coefficients estimated for a reduced sampling rate or number of blades varied slightly from the values determined for the condition serving as a baseline. Sampling 5 blades was unacceptable; an oscillatory content (about $\pm$ 0.90 deg at approximately 1/rev) appeared on the coefficients which was of the same order of magnitude as the true coefficients themselves. The test results with regard to sampling rate and number of blades sampled agreed with the analytic results.

In hover and at 100 kts the first harmonic assumption of the composition of flapping used in the tip-path-plane resolver appeared accurate, accounting for 90 to 100% of the blade motion. This result is seen in Figures 64 and 65, where the actual flapping signal of a blade is compared to the flapping value reconstructed in flight from the estimated tip-path-plane coefficients within the computer. Figure 66 shows the same parameters at 150 kts. At this speed the first harmonic (tip-path-plane) assumption loses accuracy, failing to account for up to 30% of the peak flapping motion. The Kalman estimator was expected to account for only the first harmonic contributions of flapping (since it was derived on such an assumption), and appeared to estimate these components of flapping well at the three speeds investigated. The tip-path-plane coefficients at 150 kts did not have a high content of noise, and these signals were used successfully in closed-loop solutions.

When the peaks of the reconstructed blade flapping ($\hat{\beta}_{MR}$) were compared to the peaks of the sine or cosine functions of the rotor azimuth for the cases tested in flight, no distinguishable difference in the time of occurance of the peaks was seen. This indicates that the Kalman method and the specific technique used for programming the Kalman resolver do not introduce any significant phase lag into the first harmonic solution of flapping.

Helicopter Handling Qualities and Feedback Gain Limits

The computer loop was closed in flight to study the characteristics of the feedback schemes selected for investigation. The feedback gain limits (as determined to be marginally acceptable by the pilot) were found by starting with some specific gain value, for a specific feedback type. Successive cases were then flown at increasing gain values until the pilot noticed either a self-excited rotor or fuselage instability, or a self-sustained motion of the rotor or fuselage following a very small stick input. Once such a gain limit was determined, the value of the feedback gain was reduced slightly, and a pulse input of approximately 5% magnitude and 1 sec duration was applied at the stick to evaluate the stability and handling qualities of the combined helicopter/feedback system. Some cases were also flown in which the pilot interacted with the system, flying the helicopter for several minutes for the purpose of more closely examining the handling characteristics created by specific feedback types.

Feedback gain limits. - The feedback gain limits determined for the feedback schemes tested in flight are presented in Table IX for the forward speeds at which the schemes were tested. These limiting values of rotor feedback gains exhibited themselves as either a sustained rotor tip-path-plane spread, a rotor tip-path-plane wobble, or an oscillatory lateral-directional helicopter acceleration. For example, Figure 67 shows two sets of time histories of a longitudinal stick input and the corresponding yaw acceleration response. Both sets of data were gathered during the test program: the first for the basic helicopter, and the second for the helicopter employing Delta-3 feedback (0.6 deg/deg). The feedback gain used in the latter case is a limiting value, and the resulting directional yaw response can be compared to the basic helicopter response whereas approximately the same input was used in both cases. The normal load factor feedback scheme created a self-excited vertical bounce (at approximately 2.75Hz) at the limiting condition.

The flight testing showed that the effect that Delta-3 feedback has on the handling qualities of the helicopter depends on the particular gain value used. In particular there is a range of gain values for which the damping of the helicopter increases. This result was predicted by the analytic study. Figure 68 shows the roll and pitch response of the basic helicopter (with no conventional SAS) to a longitudinal stick pulse input. Figures 69, 70, and 71 show the roll and pitch responses to similar inputs when Delta-3 feedback is used with gains of 0.2, 0.4, and 0.6 deg/deg respectively. For these cases, the damping characteristics of the helicopter appear to be worse, better, then worse again in comparison to the basic helicopter. The pilots who flew the Delta-3 feedback cases felt that when a feedback gain of $K_1 = 0.4$ deg/deg was used, the damping and the pilot workload improved in comparison to the basic helicopter without conventional SAS, although they were not as good as for the basic helicopter with SAS.

Body pitch acceleration and fuselage angle-of-attack feedbacks were not tested in flight. The signals for these two parameters, as conditioned by available filters, appeared unacceptable for closed-loop operation. The angle-of-attack signal originating from the sensor was choppy. The pitch

acceleration signal was extremely noisy, even after passing through the 40 Hz hardware filter provided at the engineer control unit. A cutoff frequency of 1 Hz was needed by the software low pass filter (programmed in the computer) to reduce the high noise content of the pitch acceleration signal by a considerable amount. The flight schedule did not allow for an investigation of the closed-loop response of a feedback system employing this signal. The schedule also did not allow for the development and testing of a Kalman filtered pitch acceleration feedback, although the nature of the raw acceleration signal supports the need for such an approach.

The values given in Table IX should be considered as only approximate limits for a number of reasons. The pilot felt that many of the limits would have been slightly higher if the suspected marginal blade damper would have been replaced or repaired. The lateral oscillatory acceleration may have occurred prematurely due to the interaction of this damper and blade motions due to the feedback. (The lateral oscillation was even observed in the open-loop condition in a few instances.) The limiting gain determined in the manner described above was not necessarily at an unstable condition, but rather was at a condition identified by the pilot as being marginally acceptable (stable). Random real gust inputs which occurred sporadically during the test also may have had some influence on the results presented in Table IX, making these feedback gain limits less accurate and less consistent than those limits that would have been determined under ideal test conditions with a helicopter in excellent mechanical status.

As noted earlier, at 150 kts, the estimated tip-path-plane coefficients account for less than the actual blade peak flapping motion. Under this condition, a mechanical flap/pitch arrangement would produce more blade pitch change for a particular change in flapping than would be produced by a similar electronic feedback scheme whose gain value was equal to the flap/pitch coupling ratio of the mechanical scheme. Therefore the rotor feedback gain limits determined at 150 kts may be higher than the flap/pitch coupling ratio limits of the corresponding mechanical schemes.

Effect of AFCS authority limit. - The feedback schemes at the gain values studied generally operated within the limited AFCS authority, for small and moderate aircraft excursions about the trim condition. Only in a few instances did the control signal commanded by the computer exceed the 10% authority limit. Usually a control signal greater than 1 to 2% of the total range had to be commanded by the computer before the effects of the computer signal could be seen. This was due to the hysteresis within the basic control system. Blade flapping extremes during all closed-loop feedback testing were moderate (8 deg $> \beta_{MR} >$ -2 deg), and compared to blade flapping typically seen during open-loop operation. Acceptable operation of the feedback schemes was not restricted to only very small perturbations from trim; the feedback schemes operated properly during maneuvers of approximately three minutes duration.

Comparison to analytic results. - The limiting feedback gains determined in test are two to three times smaller than those determined analytically (comparing Tables VII and IX). One reason for this difference may be due to the inexact analytic representation of the dynamics of the control system and

of the sensor characteristics. Probably a more important factor in accounting for these differences is the blade lead-lag motion degrees of freedom, which are omitted from the analytic helicopter model. The gain limits determined analytically produced an unstable system; the limits found in test produced a system which approached an unstable situation, within some qualitative safety margin.

Effect of number of blades sampled and sampling interval. - Delta-3 feedback gain limits were determined in flight at 100 kts when only 3 blades (every other blade) were sampled 24 times per rotor revolution, and when all 6 blades were sampled either 12 or 6 times per revolution. The gain limit determined for the reduced number of blades case was the same as the case sampling all blades (0.6 deg/deg). For the reduced number of samples per rotor revolution cases, the gain limit was 0.9 deg/deg when 12 samples per revolution were taken, and 1.5 deg/deg for the case in which 6 samples per revolution were taken. As the sampling rate per revolution is reduced, so is the frequency of interaction of the feedback control signals with the control system. Thus as the feedback routine is executed less frequently, the highest possible control system input frequency which can be introduced by the feedback is reduced. This may be partially responsible for the higher feedback gain limit found when the sampling rate per revolution is reduced. The dynamic response of the helicopter corresponding to a stick pulse or step input of modest size was not investigated during the test program for the reduced sampling cases, and therefore the overall effect of sampling less frequently or sampling fewer blades on helicopter handling characteristics is uncertain. Previous conventional feedback work indicates a reduction in net stability of the system whenever the number of calculations of the feedback signal per second are reduced.

Body rate feedback effects. - The gains of the body roll and pitch rate feedback, K_{16} and K_{17}, programmed within the PDP-11/R20 were varied to determine if this feedback routine could duplicate the damping characteristics created by the conventional SAS system of the helicopter. According to pilot opinion, values of $K_{16} = -0.1$ deg/deg/sec and $K_{17} = 0.6$ deg/deg/sec approximated quite well the damping characteristics of the helicopter with conventional SAS turned on. These rate feedback gains differ from those employed by the rate terms of the conventional SAS (see Table VI). The similarity in effective damping while at different rate gains is not easily explained. The fact that computer feedback is calculated by a digital system, while the conventional SAS employs an analog solution should not result in any significant effect; however, the conventional SAS does employ minor characteristic lags in its solution which are not present in the digital rate feedback. The pilot felt that the computer-programmed rate feedback was a very flexible and useful device for quickly varying the helicopter damping and investigating the resulting handling characteristics.

The computer calculated body rate feedback with gain values of $K_{16} = -0.1$ deg/deg/sec and $K_{17} = 0.6$ deg/deg/sec was used in addition to rotor feedback at two speeds for the purpose of determining how the combined operation of these feedbacks affected the handling characteristics of the helicopter. In hover the rate feedback was used with Delta-3 feedback with a gain of $K_1 = 0.4$ deg/deg. For this condition, the system response was preferred over the response of the basic helicopter (without conventional SAS).

At 100 kts the rate feedback was used with Delta-3 feedback of K_1 = 0.2 deg/deg/sec, and the pilot found the helicopter response to be unacceptable, with the roll attitude slowly diverging. Yet a Delta-3 feedback gain value of K_1 = 0.2 deg/deg was determined to be acceptable when this rotor feedback was used alone. There are two explanations for this result. First, the rotor feedback gain limit corresponding to the total system feedback gain limit would be reduced whenever the total feedback loop also includes other feedback types. Second, if some means for maintaining control orthogonality is not initially employed whenever Delta-3 is used, then the cross-coupling created by this concept is further aggravated by the body rate inputs to the control system which result in additional cross-coupled responses. For each feedback type tested in flight (for the range of gains used), the pilot was able to fly the helicopter with little difficulty even though conventional SAS or the programmed body rate feedback was not used. Therefore the bulk of rotor/vehicle feedback testing was conducted without employing body rate feedback in order to determine more realistic feedback gain limits.

System lags and delays. - The electronic feedback representation of mechanical blade flapping-feathering coupled arrangements may introduce time delays within its response which do not exist in the equivalent mechanical system. Therefore the test data gathered during this program were studied to determine if any sizeable delays were apparent and to find where they occurred. A delay could occur between the time when the tip path plane changes and the time when the sensor signals relaying this change to the computer are read by the computer. This delay is only a function of the sampling rate used, and is not apparent in any of the test data from cases employing a sample rate of 24 per revolution. (It has already been mentioned that there is no apparent software delay associated with estimating the change in the values of the tip-path-plane coefficients from changes in blade flapping values.) The test data also failed to show any sizeable delay associated with the time it takes the control signal calculated by the computer to reach the AFCS servo and be outputted by this device. There appears to be a delay of from 0.03 to 0.08 sec which occurs between the output of the AFCS servo and the change in the feathering of the blades. This delay is associated with the response characteristics of the servo system, and is the only delay representing differences in the electronic and mechanical versions of blade flapping-feathering coupled systems which is clearly evident in the test data. If the resolution of the test data were increased by additional processing, smaller delays which escaped detection during the original search through the data might be discovered. However, such delays are expected to be almost negligible in comparison to the delay introduced by the servo system.

Control orthogonality. - As expected, Delta-3 feedback introduced control cross-coupling which increased with increasing gain. The pilot was aware of the cross-coupling for gain values of 0.4 deg/deg or greater. Due to the difference in the number of degrees of control commanded per inch of lateral and longitudinal stick, and because of the difference in the moments of inertia of the helicopter about its lateral and longitudinal axes, Delta-3 feedback has different amounts of coupling in the lateral and longitudinal mode. This was very apparent to the pilot, to the extent that he felt different gains were being used in the lateral and the longitudinal feedbacks. The pilot based this opinion regarding this apparent difference on his application of lateral and

longitudinal pulse inputs at the stick. Analyzing the test data after the flight indicated that the coupled responses were proper and consistent for the particular inputs, as predicted by theory.

Attempts to restore control orthogonality through the use of stick feed-forward signals were not successful in flight. (The feed-forward feature provides an effectively altered control precession angle to accompany Delta-3 feedback.) The delay associated with the response characteristics of the servo system plays an important part in the failure to obtain control orthogonality during the test program.

The control orthogonality problem encountered in flight is best illustrated by a specific example. A forward stick input created a right roll response when Delta-3 feedback was used. When stick feed-forward was added to the same system, the helicopter initially rolled to the left and then rolled to the right for the same type of stick input. This is seen in the time history data presented in Figures 72 and 73. In Figure 72, the lateral control signal originating from the computer is only the Delta-3 rotor feedback signal. In Figure 73 the total computer lateral control signal is composed of the Delta-3 feedback signal and the stick feed-forward signal (which is also shown alone in this figure).

The reason that the roll response due to Delta-3 feedback and due to the stick feed-forward did not initially cancel when flight tested was that while statically correct they were not dynamically phased properly. Following a pilot input at the stick, there is a delay due to the dynamics of the control system (and the rotor blades themselves) before the rotor tip path plane changes. This first tip-path-plane change is sensed by the Delta-3 feedback which causes an appropriate control signal to the valve drivers. Now there is a second delay, due to the servo system, before the pitch of the blades are changed according to the feedback signal. The rotor eventually flaps due to this feathering change. This second tip-path-plane change is the expected cross-coupled effect for the Delta-3 concept. When stick feed-forward is used, the pilot input is sensed immediately by the computer, and the feed-forward signal prescribed to cancel the cross-coupled tip-path-plane change is relayed to the servo system at the same time as the pilot mechanical input. Therefore the change in the tip path plane due to the feed-forward electronic input occurs at the same time as the change in the tip-path-plane due to the initial pilot input. This means that the change in the tip path plane due to the feed-forward input occurs before the change in the tip path plane due to the Delta-3 feedback input. This delay, which was very noticeable to the pilot, was evident after studying the test data. To illustrate this point the longitudinal stick inputs and the lateral AFCS servo outputs are plotted together in Figure 74 for a test case using only Delta-3 feedback (0.6 deg/deg) and a test case using Delta-3 feedback (0.6 deg/deg) and stick feed-forward. The time difference between the control commands for these two cases can be clearly seen in this figure.

The delay between the control commands of the feed-forward and the rotor feedback was approximately a quarter of a revolution (about 0.08 sec). This was enough time for the pilot to sense two distinct roll responses. The proper

sequencing of the electronic rotor feedback and the stick feed-forward control signals needed to maintain control orthogonality could probably be attained by including a time constant in the programmed feed-forward calculation. Control orthogonality for a mechanical blade flapping-feathering coupled arrangement would not suffer from this problem and could be maintained by simple realignment of the swashplate. Oehmichen, type II proportional, and load factor feedback do not change the orthogonality of the controls, but the pilots noted a decrease in control sensitivity when these schemes were used (as well as when body rate feedback was being studied). The analytic study indicates that stick feed-forward can also be used to maintain constant sensitivity when using rotor feedback. A few cases were flown to check this, using Oehmichen feedback with stick feed-forward, but the results were inconclusive.

The rotor feedback gain limits and gust alleviation test results presented in this report are not exactly the same as those that would have been found if the equivalent mechanical systems were to have been tested. This is because of the time delay caused by the servo system while servicing the electronically simulated system, and also because the mechanical systems would response to more than just the first harmonic contributions of flapping. It should also be remembered that the feedback gain limits determined in this test program may only be approximate even for electronic rotor feedback schemes because of the marginal weather conditions that existed during most of the tests and due to the questionable lag damper.

Gust Response Characteristics

A pre-programmed computer generated signal into the collective pitch channel was used to simulate a gust disturbance of the rotor for the purpose of evaluating the gust response characteristics of various feedback schemes. The collective control signal used was governed by equation (31), with ω_{G_1}, ω_{G_2}, and ω_{G_3} set to 1.03, 4.12, and 5.15 rad/sec respectively, and M_{G1}, M_{G2}, and M_{G3} all set to 0.32 deg for all cases using the gust generator. Analytically it was determined that the collective input would generate a disturbance equivalent to a gust with peak magnitude of about 4.75 ft/sec at 100 kts and 5.75 ft/sec at 150 kts. The computer generated gust was used in lieu of attempting to use real random gusts because the identical disturbance could be used for all cases. By using a common disturbance, the comparative response characteristics of the different feedback schemes could be determined.

Figure 75 shows the collective signal which was used in the test program to generate the "gust" disturbance. Also shown in this figure is the normal load factor response of the basic helicopter to this disturbance at 150 kts.

Both the collective "gust" signal and the collective signal commanded by the feedback schemes were restricted to work within the standard AFCS authority. The test data showed that the authority limit did not hinder the operation of the feedbacks during any of the cases employing the "gust" generator. Even though the collective "gust" signal commanded by the computer was pre-determined, the feedback schemes themselves were not influenced to respond in any manner other than the manner prescribed by their governing equations. They respond in reaction to the tip path plane or load factor variations caused by the "gust".

Figure 76 presents the gust alleviation characteristics determined for the feedback schemes tested, in comparison to the characteristics of the basic helicopter. The range of the variation in normal load factor resulting from the simulated gust was determined by searching the test data for the highest and the lowest value of load factor recorded during the maneuver. This peak-to-peak load factor response was normalized by the value for the basic helicopter. Delta-3, Oehmichen, pure pitch-cone, and type II proportional rotor feedbacks (all with a gain of 0.5 deg/deg) and normal load factor feedback (with a gain of 2.0 deg/G) were compared to the gust alleviation characteristics of the basic helicopter at 100 kts. Delta-3, Oehmichen, and pure pitch cone feedbacks (each with a gain of 0.5 deg/deg) were compared to the gust alleviation characteristics of the basic helicopter at 150 kts. During the interaction of the simulated gust and the helicopter/feedback system, pilot inputs were held fixed or kept at a minimum so that only the gust alleviation characteristics of the feedback schemes would be determined without the influence of pilot inputs.

Although the simulated gust disturbance did not exactly duplicate the effect of a real gust (a real gust would generally require some finite time in which to penetrate the entire rotor disc, and would also impinge on the fuselage), the same "gust" served successfully as a baseline for all conditions tested, and the results presented in Figure 76 are believed to accurately relate the gust alleviation characteristics of the feedback schemes. (The peak-to-peak load factor response to the simulated gust was not determined for the basic helicopter employing conventional SAS, but test data for collective stick inputs indicate that this response is about 85% of the value obtained for the basic helicopter without conventional SAS.)

At 100 kts, a softened response was recognized by the pilot when Delta-3 was used, and to a lesser extent when pure pitch-cone, Oehmichen, and load factor feedbacks were used. (The test data indicate that the response when Oehmichen feedback was used was reduced approximately as much as when Delta-3 was used.) The pilot felt that the response to the disturbance when type II proportional feedback was used was about the same as for the basic helicopter. (The test data support this opinion.) This result indicates the importance of coning feedback for suppressing rotor responses to a gust which impinges the entire rotor disc. The response characteristics of the pure pitch-cone and the load factor feedbacks appeared to be very similar.

At 150 kts the simulated gust input appeared larger (as expected) to the pilot. The gust suppression characteristics of the feedback schemes were also more evident to the pilot at this speed for all three schemes tested.

CONCLUSIONS

1. Rapid, on-line estimation of the rotor tip path plane from blade flapping angles is possible both analytically and in flight, using digital computer techniques. Analytical results show that the Kalman estimator method predicts the rotor tip-path-plane coefficients more accurately than the Fourier analysis whenever the blade flapping data are contaminated with noise or are composed of significant higher harmonic content, or whenever the number of blades sampled for flapping is reduced.

2. Both the analytical and test results show that the Kalman resolver estimates tip-path-plane coefficients which are acceptable for use in feedback systems whenever the flapping signals of all the blades or every other blade of a six-bladed main rotor are sampled, and the tip-path-plane resolver routine is solved 6 or more times per rotor revolution. Some accuracy in coefficient estimation is lost as the number of blades sampled is reduced.

3. Test results show that a Kalman estimator routine which is based on only the first harmonic contributions of blade flapping yields tip-path-plane coefficients which are adequate for use in feedback systems, at speeds up to 150 kts. The Kalman estimator used was based on only the first harmonic of flapping, and it accurately predicted the first harmonic components of flapping at each of the three speeds investigated. (In hover and at 100 kts approximately 90 to 100% of the flapping is composed of first harmonic terms. At 150 kts, as much as 30% of the blade flapping content is due to higher harmonic contributions.)

4. A thorough and accurate flight evaluation of rotor tip-path-plane feedback schemes is feasible using conventional measurement devices to supply blade flapping signals to a digitally programmed tip-path-plane resolver routine. The Digital Equipment Corporation PDP-11/R20 proved to be an ideal computer for experimental investigation of feedback control techniques, and was incorporated into the standard helicopter control system with no major difficulty. Restrictions associated with the properties of standard helicopter equipment, such as a limited authority automatic flight control system, servo system lags, and control system hysteresis do not hinder the in-flight investigation of rotor tip-path-plane feedback techniques.

5. Limiting values of rotor or fuselage feedback gains exhibited themselves in flight as either a sustained rotor tip-path-plane spread, a rotor tip-path-plane wobble, an oscillatory divergent lateral-directional helicopter response, or a self-excited vertical bounce. The rotor feedback limits determined in flight were at values between 0.5 and 0.9 deg/deg. These feedback gain limits are suspected to be slightly lower than they should normally be because the rotor stability in the test program was affected by a marginal blade lag damper. The test data clearly indicated that the servo system introduced a delay in the electronic network. The stability and handling qualities characteristics created by the rotor feedback schemes may differ slightly from the characteristics which would be produced by the corresponding mechanical flapping-feathering coupled arrangements because the latter system is not affected by control system

lags and because the mechanical arrangement would also respond to higher-order components of blade flapping. The gain limits determined in flight are two to three times smaller than the limits predicted analytically, and the exclusion of blade lead-lag degrees of freedom from the model used in the analytic study is believed to be primarily responsible for this result.

6. Both the analytical and test results show that of the schemes studied, the Delta-3, Oehmichen, and pure pitch-cone coupling feedback schemes show the best results as gust alleviation techniques. For a moderate gain value of 0.5 deg/deg, the schemes reduce the load factor response to a gust by 30 to 50 percent. Helicopter normal load factor feedback with a gain of 2.0 deg/G yields gust response characteristics similar to those of pure pitch-cone rotor feedback.

7. Flight test results show that for a given rotor feedback scheme, the handling qualities of the helicopter change significantly as a function of the feedback gain value. Over a gain range sometimes as small as 0.2 deg/deg, the helicopter employing feedback can have handling qualities characteristics which are either less desirable than those of the basic helicopter (without stability augmentation), or are an improvement in comparison to the handling qualities of the basic helicopter.

8. Depending on the specific loop closures, linear analysis indicates that the use of rotor state feedback can produce increases in vehicle bandwidth. However, gain limitations, based on overall stability consideration, limit the achievable vehicle bandwidth to rather moderate amounts.

9. The nine degree-of-freedom linear model obtained by applying system identification techniques to a nonlinear helicopter model accurately reproduces the short-term, high frequency dynamics caused by rotor transient responses. While providing excellent trending information, this nine degree-of-freedom linear model produces less reliable quantitative information than nonlinear analysis when analyzing multi-loop feedback systems. A nonlinear stability analysis containing a full description of the rotor dynamics and the interaction with the fuselage is important for establishing more accurate limiting gains.

RECOMMENDATIONS

Further Analytic Investigation

1. Analytically study the influence of rotor lead-lag degrees of freedom on overall stability to determine how much more accurately stability limiting feedback gains can be predicted. Process the flight test blade hunting data through a coefficient identification program to determine the dynamic properties of these modes.

2. Using optimal control techniques, determine the best control system which employs a combination of rotor feedback and body feedback, and which provides desired gust alleviation characteristics while satisfying the total system stability requirements. A system-identified linear model based on a nonlinear helicopter model which includes the blade lead-lag degrees of freedom would be used in this study. Study the second harmonic components of blade flapping to determine if this information can be used to produce further improvement in the control system.

3. Investigate the effects of shaping of flapping data and the use of alternate actuator loops in reference to increasing helicopter frequency response and bandwidth (in order to create better model-following characteristics).

4. Use existing flight test data, processed by the Kalman Filter technique, to determine the improvement in the angular acceleration signals which is achievable.

Further Test Investigation

1. Test an optimal feedback system employing both rotor and fuselage state variables for gust alleviation and handling characteristics. Consider the use of tip-path-plane rate signals in such an optimum system.

2. Further investigate Delta-3 feedback, using a compensated (lagged) stick feed-forward signal to maintain control orthogonality. Investigate handling characteristics and feedback operation over a wide range of flight conditions including flares and large power changes.

3. Conduct flight testing in which blade lead-lag motion is resolved to provide the effective rotor center-of-gravity location. Subsequently, use this information in a compensating feedback network to determine if higher body angular rate (SAS) feedback gain limits are achievable.

4. Establish system frequency characteristics for:

- Open-loop case (basic helicopter)
- Closed-loop case with body pitch rate as the major loop
- Closed-loop case with body pitch rate as the major loop and rotor flapping as a minor loop.

APPENDIX

KALMAN TIP-PATH-PLANE RESOLVER

The Kalman filter method for estimating the rotor tip path plane was presented in the text of this report under the section entitled Tip Path Plane Resolver Study. Equation sets (12), (13) and (14) forms the basis of the analytic and flight test computer tip-path-plane resolver solution. This appendix summarizes the development and assumptions used in deriving the equations in their discrete form.

The first harmonic representation for blade flapping motion at time instance NT, where T represents the sampling interval, is

$$\beta_i\,(NT) = a_{os_o} + \Delta a_{os}\,(NT) - (a_{ls_o} + \Delta a_{ls}\,(NT))\cos\,(\Psi+\Phi_i) \qquad (A1)$$
$$-(b_{ls_o} + \Delta b_{ls}\,(NT))\sin\,(\Psi+\Phi_i) + v_i\,(NT)$$
$$, i = 1, 2, \ldots, n_b$$

where n_b is the number of blades sampled in the solution, and v_i represents zero mean white gaussian measurement noise with covariance $\underline{\underline{R}}$. Assuming the same type of instrument is used to measure flapping for each blade, $\underline{\underline{R}}$ becomes a diagonal matrix with each element having the same variance R.

The trim tip-path-plane coefficients are represented by a_{os_o}, a_{ls_o} and b_{ls_o} and the perturbations motion from trim are Δa_{os}, Δa_{ls} and Δb_{ls}. The perturbation motion from trim can be represented in discrete form by

$$\Delta a_{os}\,(NT) = \Delta a_{os}\,(NT-T) + w_1\,(NT-T) \qquad (A2)$$
$$\Delta a_{ls}\,(NT) = \Delta a_{ls}\,(NT-T) + w_2\,(NT-T)$$
$$\Delta b_{ls}\,(NT) = \Delta b_{ls}\,(NT-T) + w_3\,(NT-T)$$

where w_1, w_2 and w_3 represent zero mean white gaussian process noise with covariance $\underline{\underline{Q}}$.

The state variable formulation (with the designations NT and NT-T being replaced by j+1 and j respectively) for equations (A2) and (A1) respectively are

$$\underline{x}_{j+1} = \underline{x}_j + \underline{w}_j \qquad (A3)$$
$$\underline{z}_j = \underline{\underline{H}}_j\underline{x}_j + \underline{\underline{H}}_j\underline{x}_o + \underline{v}_j \qquad (A4)$$

where for a 6 bladed rotor;

$$\underline{\underline{H}}_j = \begin{bmatrix} 1 & -\cos(\psi+\Phi_1) & -\sin(\psi+\Phi_1) \\ 1 & -\cos(\psi+\Phi_2) & -\sin(\psi+\Phi_2) \\ 1 & -\cos(\psi+\Phi_3) & -\sin(\psi+\Phi_3) \\ 1 & -\cos(\psi+\Phi_4) & -\sin(\psi+\Phi_4) \\ 1 & -\cos(\psi+\Phi_5) & -\sin(\psi+\Phi_5) \\ 1 & -\cos(\psi+\Phi_6) & -\sin(\psi+\Phi_6) \end{bmatrix}_j \tag{A5}$$

The Kalman filter estimates of the state variables (tip-path-plane coordinates) are given by

$$\underline{\underline{P}}_j = (\underline{\underline{m}}_j^{-1} + \underline{\underline{H}}_j^T \underline{\underline{R}}^{-1} \underline{\underline{H}}_j)^{-1} \tag{A6}$$

$$\underline{x}_{j+1} = \underline{x}_j + \underline{\underline{P}}_j \underline{\underline{H}}_j^T \underline{\underline{R}}^{-1} (\underline{z}_j - \underline{\underline{H}}_j \underline{x}_j - \underline{\underline{H}}_j \underline{x}_o) \tag{A7}$$

$$\underline{\underline{m}}_{j+1} = \underline{\underline{P}}_j + \underline{\underline{Q}} \tag{A8}$$

where $\underline{\underline{m}}_j$ represents the covariance in the estimate of the state before measurement. $\underline{\underline{m}}_o$ is a diagonal matrix and assumed to be equal to R. The superscripts T and -1 denote the transform and inverse of a matrix, respectively.

Since $\underline{\underline{R}}$ is diagonal with identical elements, equations (A6) and (A7) can be rearranged with the matrix $\underline{\underline{R}}^{-1}$ replaced with a division by the scalar R, yielding

$$\underline{\underline{P}}_j = (\underline{\underline{m}}_j^{-1} + \underline{\underline{H}}_j^T \underline{\underline{H}}_j / R)^{-1} \tag{A9}$$

$$\underline{x}_{j+1} = \underline{x}_j + \underline{\underline{P}}_j / R (\underline{\underline{H}}_j^T \underline{z}_j - \underline{\underline{H}}_j^T \underline{\underline{H}}_j (\underline{x}_j + \underline{x}_o)) \tag{A10}$$

$$\underline{\underline{m}}_{j+1} = \underline{\underline{P}}_j + \underline{\underline{Q}} \tag{A11}$$

where;

$$\underline{\underline{H}}_j^T \underline{\underline{H}}_j = \begin{bmatrix} \sum_{i=1}^{n_b} 1 & -\sum_{i=1}^{n_b} \cos(\Psi+\Phi_i) & -\sum_{i=1}^{n_b} \sin(\Psi+\Phi_i) \\ -\sum_{i=1}^{n_b} \cos(\Psi+\Phi_i) & \sum_{i=1}^{n_b} \cos^2(\Psi+\Phi_i) & \sum_{i=1}^{n_b} \cos(\Psi+\Phi_i)\sin(\Psi+\Phi_i) \\ -\sum_{i=1}^{n_b} \sin(\Psi+\Phi_i) & \sum_{i=1}^{n_b} \sin(\Psi+\Phi_i)\cos(\Psi+\Phi_i) & \sum_{i=1}^{n_b} \sin^2(\Psi+\Phi_i) \end{bmatrix} \tag{A12}$$

For a solution in which symmetrically spaced blades are being sampled, all the off-diagonal terms in equation (A12) reduce to zero, yielding

$$\underline{\underline{H}}_j^T \underline{\underline{H}}_j = \begin{bmatrix} n_b & 0 & 0 \\ 0 & n_{b/2} & 0 \\ 0 & 0 & n_{b/2} \end{bmatrix} \tag{A13}$$

Equation (A9) is initialized with the diagonal matrix m_o, and since $\underline{\underline{H}}_j^T \underline{\underline{H}}_j$ is diagonal, then $\underline{\underline{P}}_j$ remains diagonal. Thus equation (A9) is simplified to equations (12) of the text.

The simplified form of equation (A13) reduces equation (A10) to that shown in the text (equations (13)). Equation (A11) is also shown repeated in the text (equations (14)).

Equations (12), (13), and (14) shown in the text are used to complete both the trim tip path plane and the perturbation from the trim. The initializations and procedure to accomplish this is shown in Figure 6.

For a general treatment of Kalman filtering, see Reference 4.

REFERENCES

1. Molusis, J. A., Analytical Study to Define a Helicopter Stability Derivative Extraction Method, Final Report of NASA Contract NAS1-11613, August 1973.

2. Molusis, J. A., and Briczinski, S. J., "Helicopter Derivative Identification from Analytic Models and Flight Test Data", presented at the NASA Parameter Estimation Symposium, Edwards, California, April 1973.

3. Hohenemser, K. H., and Yin, S., "Some Applications of the Methods of Multiblade Coordinates", J. American Helicopter Society, Volume 17 (Number 3), July 1972.

4. Bryson, A. E., and Ho, Y-C: Applied Optimal Control. Blaisdell Publishing Co., 1969.

TABLE I. - FEEDBACK SCHEMES AND FEEDBACK GAIN NOTATION

A) FEEDBACK SCHEMES, INCLUDING GENERAL ROTOR FEEDBACK NOTATION

AFCS INPUT / AFCS OUTPUT	ROTOR TPP MOTION*			BODY STATE			THRUST VECTOR CONTROL						FEED − FORWARD			CONVENTIONAL SAS	
	Δa_{os}	Δa_{1s}	Δb_{1s}	Δa_f	ΔN_z	$\Delta\ddot{\theta}_b$	$\Delta\theta_b$	Δa_{1s}	$\Delta\delta_y$	$\Delta\phi_b$	Δb_{1s}	$\Delta\delta_x$	$\Delta\delta_\theta$	$\Delta\delta_y$	$\Delta\delta_x$	$\Delta\dot{\theta}_b$	$\Delta\dot{\phi}_b$
θ_c	$-h_3$	0	0	0	$-K_8$	0	0	0	0	0	0	0	K_{13}	0	0	0	0
B_{1s}	0	h_1	$-h_2$	K_7	0	K_9	K_{10}	K_{10}	$M{\cdot}K_{10}$	0	0	0	0	K_{12}	K_{15}	K_{17}	0
A_{1s}	0	$-h_2$	$-h_1$	0	0	0	0	0	0	$-K_{10}$	$-K_{10}$	$M{\cdot}K_{10}$	0	K_{14}	K_{11}	0	K_{16}

B) SPECIFIC ROTOR FEEDBACK SCHEMES AND NOTATION

*

ROTOR TPP MOTION FEEDBACK SCHEME	h_1	h_2	h_3
DELTA-3	0	K_1	K_1
OEHMICHEN	K_2	0	K_2
DELTA-3 / OEHMICHEN	K_3	K_3	0
PROPORTIONAL , TYPE I	0	K_4	0
PROPORTIONAL , TYPE II	K_5	0	0
PURE PITCH-CONE	0	0	K_6

TABLE II. - NINE DEGREE-OF-FREEDOM LINEAR MODEL COEFFICIENTS OF THE BASIC CH-53A IN HOVER (33,500 LB, 348 FSCG)

derivative of state \ state	v_x (ft/sec)	v_y (ft/sec)	v_z (ft/sec)	p (rad/sec)	q (rad/sec)	r (rad/sec)	ϕ_b (rad)	θ_b (rad)	a_{0S} (rad)	$\dot{a}_{0S}$ (rad/sec)	a_{1S} (rad)	$\dot{a}_{1S}$ (rad/sec)	b_{1S} (rad)	$\dot{b}_{1S}$ (rad/sec)	B_{1S} (rad)	A_{1S} (rad)	θ_{TR} (rad)	θ_C (rad)
$\dot{v}_x$ (ft/sec^2)	-0.0812	0.119	0.0282	-0.377	-0.330	-0.692	0	-32.0	35.6	1.29	-22.1	-1.26	9.78	-0.160	17.9	-11.9	-0.478	15.5
$\dot{v}_y$ (ft/sec^2)	0.0687	-0.514	-0.182	-5.34	-6.94	-11.2	31.9	0.215	5.02	0.176	43.2	3.03	30.0	-2.73	42.9	36.9	-0.962	-2.91
$\dot{v}_z$ (ft/sec^2)	0.0958	-0.143	-0.412	-1.54	0.956	-0.0300	1.85	-3.70	-270.	-11.4	-4.87	-0.354	0.376	-1.03	2.00	3.15	-0.204	-94.6
$\dot{p}$ (rad/sec^2)	0.0060	-0.0447	-0.0140	-0.287	-0.495	-0.411	0	0	-0.0275	0.0329	-1.11	-0.229	18.2	1.02	2.91	4.76	1.90	-1.92
$\dot{q}$ (rad/sec^2)	0.0082	-0.0090	-0.0066	-0.0620	-0.193	-0.219	0	0	-0.778	-0.150	4.26	0.321	0.689	0.0090	-0.248	0.622	-0.156	1.37
$\dot{r}$ (rad/sec^2)	-0.0067	0.0563	0.0117	0.425	0.193	-0.530	0	0	0.474	0.138	-0.884	-0.122	3.37	0.334	0.197	-1.89	-2.40	5.55
$\ddot{a}_{0S}$ (rad/sec^2)	-0.0357	0.0597	0.238	0.151	-0.388	-2.87	0	0	-146.	-7.73	0.862	0.187	0.516	0.0675	2.14	-0.542	-0.564	155.
$\ddot{a}_{1S}$ (rad/sec^2)	0.0625	-0.0617	0.0093	-7.36	-14.0	0.267	0	0	1.42	0.0023	-53.4	-17.4	-139.	-20.4	-108.	138.	0.658	-0.535
$\ddot{b}_{1S}$ (rad/sec^2)	-0.0567	-0.0674	0.0012	-14.4	7.50	0.192	0	0	-0.306	0.0331	145.	20.6	-53.4	-17.0	138.	107.	0.126	1.36

TABLE III. - NINE DEGREE-OF-FREEDOM LINEAR MODEL COEFFICIENTS OF THE BASIC CH-53A AT 100 KTS (33,500 LB, 348 FSCG)

state / derivative of state	v_x (ft/sec)	v_y (ft/sec)	v_z (ft/sec)	p (rad/sec)	q (rad/sec)	r (rad/sec)	ϕ_b (rad)	θ_b (rad)	a_{0S} (rad)	$\dot{a}_{0S}$ (rad/sec)	a_{1S} (rad)	$\dot{a}_{1S}$ (rad/sec)	b_{1S} (rad)	$\dot{b}_{1S}$ (rad/sec)	B_{1S} (rad)	A_{1S} (rad)	θ_{TR} (rad)	θ_C (rad)
$\dot{v}_x$ (ft/sec^2)	-.0048	.00042	.0942	-.126	-9.97	.865	0	-32.2	25.1	.0416	-24.0	-2.51	-1.91	-.49	-4.92	-4.92	-.48	26.5
$\dot{v}_y$ (ft/sec^2)	.0156	-.0567	.00216	6.63	-.659	-167.	32.2	0.054	-10.1	-.376	4.32	-.210	25.8	.923	12.0	11.9	6.67	-.708
$\dot{v}_z$ (ft/sec^2)	-.124	-.0071	-.744	-6.12	193.	4.40	0.89	-1.44	-218.	.799	-11.1	3.78	11.7	-4.49	124.	17.1	.534	-269.
$\dot{p}$ (rad/sec^2)	-.0011	-.0158	-.0099	-.172	.0170	.443	0	0	-.520	-.01	-4.56	-.472	17.8	1.07	.913	3.33	3.85	-3.45
$\dot{q}$ (rad/sec^2)	-.0005	.0023	.0016	-.0055	-.121	.0045	0	0	-.064	-.0421	3.84	.30	1.00	.104	-.352	-.0795	.0078	.66
$\dot{r}$ (rad/sec^2)	-.0016	.0081	-.0002	.111	.0594	-.728	0	0	-1.4	-.0152	-.83	-.0532	1.84	.08	-.0905	-.543	-5.17	4.7
$\ddot{a}_{0S}$ (rad/sec^2)	.0294	.0005	.432	.495	-3.97	-3.96	0	0	-168.	-13.7	19.0	.999	-16.8	-.59	-64.2	9.82	-1.94	231.
$\ddot{a}_{1S}$ (rad/sec^2)	.0891	-.0707	.0379	-8.46	-18.8	.156	0	0	89.5	3.32	-47.	-19.4	-161.	-23.7	-117.	163.	-.53	30.7
$\ddot{b}_{1S}$ (rad/sec^2)	-.0644	-.0506	-.0945	-15.2	12.1	-.72	0	0	-8.31	1.56	154.	22.8	-48.7	-17.6	163.	110.	.29	-84.

TABLE IV. - NINE DEGREE-OF-FREEDOM LINEAR MODEL COEFFICIENTS OF THE BASIC CH-53A AT 150 KTS (33,500 LB, 348 FSCG)

derivative of state \ state	v_x (ft/sec)	v_y (ft/sec)	v_z (ft/sec)	p (rad/sec)	q (rad/sec)	r (rad/sec)	ϕ_b (rad)	θ_b (rad)	a_{0S} (rad)	$\dot{a}_{0S}$ (rad/sec)	a_{1S} (rad)	$\dot{a}_{1S}$ (rad/sec)	b_{1S} (rad)	$\dot{b}_{1S}$ (rad/sec)	B_{1S} (rad)	A_{1S} (rad)	θ_{TR} (rad)	θ_C (rad)
$\dot{v}_x$ (ft/sec^2)	-0.108	0.0133	0.0627	0.287	15.6	-1.41	0.	-32.2	-22.3	-2.80	-12.1	2.88	15.7	2.16	14.2	-20.8	-1.94	29.8
$\dot{v}_y$ (ft/sec^2)	0.0594	-0.119	-0.0633	-14.6	-13.0	-254.	32.2	-0.050	86.5	4.12	-9.96	-8.14	-12.6	-6.99	-5.25	76.3	3.15	-36.5
$\dot{v}_z$ (ft/sec^2)	-.186	-0.0725	-0.859	-8.14	250.	3.67	1.35	1.19	-48.1	10.9	-50.6	-13.7	-42.6	-15.7	138.	94.9	3.58	-376.
$\dot{p}$ (rad/sec^2)	0.0286	-0.0329	-0.0206	-0.853	-4.95	0.769	0.	0.	32.4	1.52	-10.8	-3.76	2.77	-1.38	-8.76	21.9	5.16	-14.2
$\dot{q}$ (rad/sec^2)	0.0021	-0.0034	0.00231	-0.0120	-0.524	0.0428	0.	0.	1.73	0.0711	3.28	0.122	0.210	0.0266	-1.47	0.410	0.0142	0.608
$\dot{r}$ (rad/sec^2)	-0.0127	0.0126	0.0022	0.206	1.55	-1.11	0.	0.	-9.66	-0.470	1.35	1.06	5.66	0.696	3.40	-4.69	-6.41	7.75
$\ddot{a}_{0S}$ (rad/sec^2)	-0.0823	0.0860	0.468	6.95	21.2	-4.63	0.	0.	-322.	-19.7	35.2	12.8	31.2	11.9	-74.5	-72.7	-4.41	305.
$\ddot{a}_{1S}$ (rad/sec^2)	0.264	-0.467	-0.155	-34.7	-101.	3.30	0.	0.	776.	30.0	-132.	-69.1	-418.	-78.8	-266.	543.	14.2	-166.
$\ddot{b}_{1S}$ (rad/sec^2)	-0.0684	-0.162	-0.240	-23.5	11.6	-3.78	0.	0.	35.3	5.28	186.	26.5	-74.8	-28.0	230.	190.	1.82	-202.

TABLE V.– LINEAR MODEL FREQUENCY RESPONSE CHARACTERISTICS OF ROTARY WING ELEMENTS

SYSTEM	TRANSFER FUNCTION	GAIN k_b	GAIN k_f	BLOCK DIAGRAM	BANDWIDTH CUTOFF FREQUENCY (Hz)	CROSSOVER CHARACTERISTICS CROSSOVER FREQUENCY (Hz)	GAIN MARGIN db	GAIN MARGIN RATIO
Open Loop								
Servos	B_{1S}/δ_y			δ_y → SYSTEM	16.0	11.0	-1.2	0.87
Servos, rotor	a_{1S}/δ_y				2.4	4.2	8.0	2.51
Servos, rotor, fuselage rate	$\dot{\theta}_b/\delta_y$				0.08	2.1	11.0	3.54
Servos, rotor, fuselage attitude	θ_b/δ_y				-	0.30	-4.0	0.63
Servos, rotor, fuselage attitude (at twice the damping)	θ_b/δ_y				-	0.45	3.0	1.41
Closed Loop								
Servos, rotor	a_{1S}/δ_y	1.0	1.0	δ_y → K_f → SYSTEM, K_b feedback	5.4	4.3	1.5	1.19
Servos, rotor	a_{1S}/δ_y	1.0	5.0		6.5	11.0	Unstable	
Servos, rotor, fuselage rate	$\dot{\theta}_b/\delta_y$	1.0	1.0		1.8	2.1	6.0	2.00
Servos, rotor, fuselage attitude	θ_b/δ_y	0.5	1.0		0.4	0.32	-12.0	0.25
Thrust Vector Control								
Open loop	θ_R/θ_{R_M}	-	-	δ_y → M → θ_{R_M} → K_f → ROTOR → FUSELAGE → θ_R, K_b feedback	-	4.2	8.0	2.51
Closed loop	θ_R/θ_{R_M}	1.0	0.25		0.23	4.3	17.0	7.07
Closed loop	θ_R/θ_{R_M}	1.0	1.0		2.0	4.4	4.0	1.59
Closed loop	θ_R/θ_{R_M}	1.0	5.0		6.0	11.0	Unstable	

TABLE VI. - CHARACTERISTICS OF THE CH-53A CONTROL SYSTEM

Stick Range -

δ_x = 11.0 in.
δ_y = 12.23 in.
δ_Θ = 10.0 in. (including 1.0 in. deadband at low collective stick)
δ_p = 6.23 in. (with overtravel); 4.91 in. (effective)

Control Range (Primary Servo Stops) -

A_{1S} = 12.5 deg (-8.0 to 4.5 deg. for high Θ_c)
(-7.0 to 5.5 deg. for low Θ_c)
B_{1S} = 27.2 deg (-8.0 to 19.2 deg)
Θ_c = 13.0 deg (3.5 to 16.5 deg)
Θ_{TR} = 26.0 deg (1.5 to 24.0 deg for high Θ_c)
(-2.0 to 24.0 deg for mid Θ_c)
(-2.0 to 20.5 deg for low Θ_c)

Control Coupling -

1.0 deg Θ_c yields 1.0 deg Θ_{TR}
1.0 deg Θ_c yields -0.1 deg A_{1S}

AFCS Actuator Authority Limit -

A_{1S} = ±10%
B_{1S} = ±10%
Θ_c = ±10%
Θ_{TR} = ±8%

Hysteresis (Between Auxiliary Servos and Primary Servos) -

A_{1S} = ±2%
B_{1S} = ±2%
Θ_c = ±3%
Θ_{TR} = ±4%

Swashplate Rotation -

8 deg(CCW)

Conventional SAS (Inner-Loop Only) -

$$A_{1S} = -\frac{(0.224)s\Phi_b}{(0.016)s + 1}$$

$$B_{1S} = \frac{(0.32)s\theta_b}{\{(0.013)s + 1\}^2}$$

$$\Theta_{TR} = \frac{(0.83)\ s^2\psi_b}{(1.8)s + 1}$$

TABLE VII. NONLINEAR MODEL STABILITY LIMITING GAIN VALUES FOR ROTOR AND FUSELAGE FEEDBACK SCHEMES

Feedback Scheme	Lowest Limiting Gain	Speed (Kts)	Highest Feedback Frequency (HZ)
Delta-3	K_1 = 1.8 deg/deg	150	3.0
Oehmichen	K_2 = 1.60 deg/deg	100	3.0
Delta-3/Oehmichen	K_3 = 1.10 deg/deg	150	3.5
Pure Pitch-Cone	K_6 = 1.80 deg/deg	150	3.0
Proportional, Type I	K_4 = 1.85 deg/deg	150	1.0
Proportional, Type II	K_5 = 1.60 deg/deg	100	3.0
Angle-of-Attack	K_7 = 1.50 deg/deg	150	0.5
Load Factor	K_8 = +10.0 deg/G	100	9.0
Pitch Acceleration	K_9 = 0.35 deg/(deg/sec^2)	150	18.0

TABLE VIII. - CONDITIONS INVESTIGATED DURING ROTOR/VEHICLE STATE FEEDBACK FLIGHT TEST PROGRAM

Purpose	Computer Loop	Speed	Number of Blades Sampled	Samples Per Revolution	TPP Covariance Ratio, or Body Filter Cutoff Frequency	Feedback Type
TPP estimate	open	hover	6	24	1/25, 1, 25, 100, 500	NA
TPP estimate	open	100,150 kts	6	24	100	NA
TPP estimate	open	hover, 100,150	6	12, 6	100	NA
TPP estimate	open	hover, 100,150	3	24	100	NA
TPP estimate	open	hover	5	24	100	NA
body filter	open	hover	NA	NA	N_Z, α_f, $\ddot{\theta}_b$: 3, 5 Hz	NA
body filter	open	100 kts	NA	NA	N_Z, α_f, $\ddot{\theta}_b$: 5 Hz	NA
body filter	open	150 kts	NA	NA	N_Z, α_f : 4 Hz; $\ddot{\theta}_b$: 1 Hz	NA
gain limit	closed	hover	6	24	100	Delta-3; Oehmichen
gain limit	closed	hover	NA	NA	4 Hz	Load factor
gain limit	closed	100 kts	6	24	100	Delta-3; Oehmichen; pure pitch-cone; proportional, type II
gain limit	closed	100 kts	NA	NA	4 Hz	Load factor
gain limit	closed	150 kts	6	24	100	Delta-3; Oehmichen; pure pitch-cone

TABLE VIII. - CONDITIONS INVESTIGATED DURING ROTOR/VEHICLE STATE FEEDBACK FLIGHT TEST PROGRAM - Continued

Purpose	Computer Loop	Speed	Number of Blades Sampled	Samples Per Revolution	TPP Covariance Ratio, or Body Filter Cutoff Frequency	Feedback Type
baseline stability	NA	hover,100,150	NA	NA	NA	Basic helicopter, with and without conventional SAS
stability	closed	hover	6	24	100	Delta-3; Oehmichen
stability	closed	hover	NA	NA	4 Hz	Load factor
stability	closed	100 kts	6	24	100	Delta-3; Oehmichen; pure pitch-cone; proportional, type II
stability	closed	100 kts	NA	NA	4 Hz	Load factor
stability	closed	150 kts	6	24	100	Delta-3; Oehmichen; pure pitch-cone
gust response	closed	100, 150 kts	NA	NA	NA	Basic helicopter, with no SAS
gust response	closed	hover	6	24	100	Delta-3
gust response	closed	100 kts	6	24	100	Delta-3; Oehmichen; pure pitch-cone; proportional, type II
gust response	closed	100 kts	NA	NA	4 Hz	Load factor
gust response	closed	150 kts	6	24	100	Delta-3; Oehmichen; pure pitch-cone

TABLE VIII. - CONDITIONS INVESTIGATED DURING ROTOR/VEHICLE STATE FEEDBACK FLIGHT TEST PROGRAM - Concluded

Purpose	Computer Loop	Speed	Number of Blades Sampled	Samples Per Revolution	TPP Covariance Ratio, or Body Filter Cutoff Frequency	Feedback Type
control orthogonality	closed	hover,100,150	6	24	100	Delta-3 with stick feed-forward
control orthogonality	closed	100 kts	6	24	100	Oehmichen with stick feed-forward
body rate fb limits	closed	hover	NA	NA	NA	Body roll and pitch rate
body rate and rotor fb	closed	hover, 100 kts	NA	NA	NA	Delta-3 with body roll and pitch rate
stability vs. sampling	closed	100 kts	6	12, 6	100	Delta-3
stability vs. sampling	closed	100 kts	3	24	100	Delta-3

TABLE IX. ROTOR AND FUSELAGE FEEDBACK GAIN LIMITS DETERMINED IN FLIGHT

Feedback	Flight Test Gain Limit		
	Hover	100 Kts	150 Kts
Delta-3	0.5	0.6	0.7
Oehmichen	0.6	0.7	0.6
Pure pitch-cone	-	0.7	0.7
Proportional, Type II	-	0.9	-
Load Factor	2.0	2.5	-

6 blades sampled, 24 times/revolution

(Limits are approximate due to marginal weather conditions and blade lag damper.)

(All gains are deg/deg except load factor is deg/G)

718
MARINES

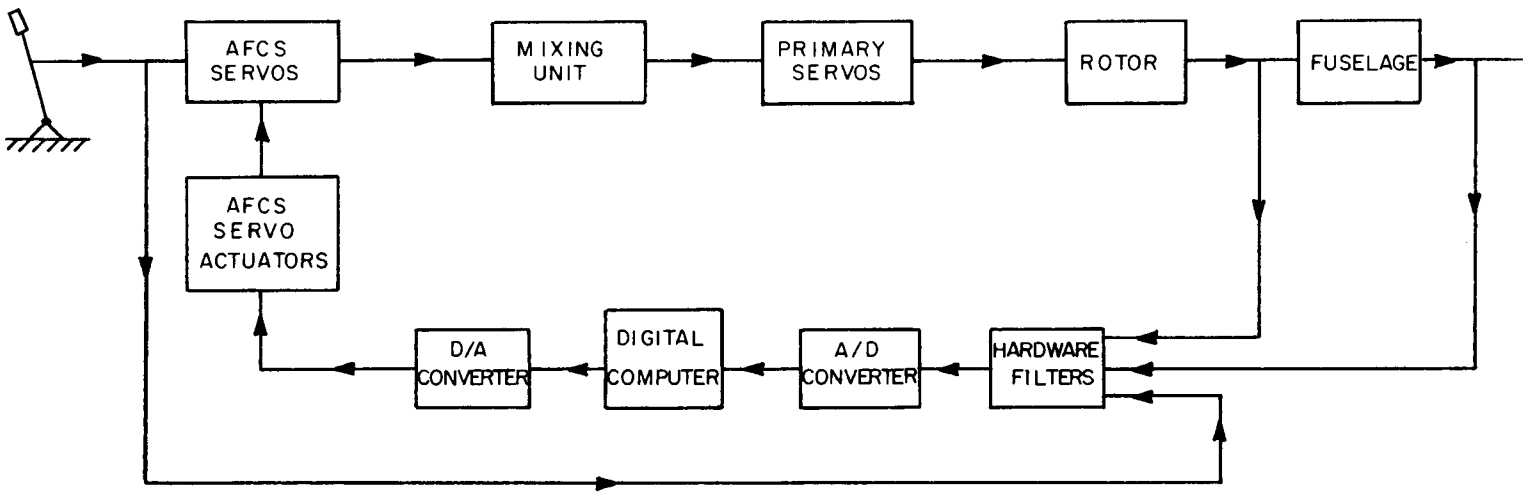

Figure 2. Incorporation of the On-board Digital Computer into the Helicopter Control System.

MECHANICAL CONFIGURATION

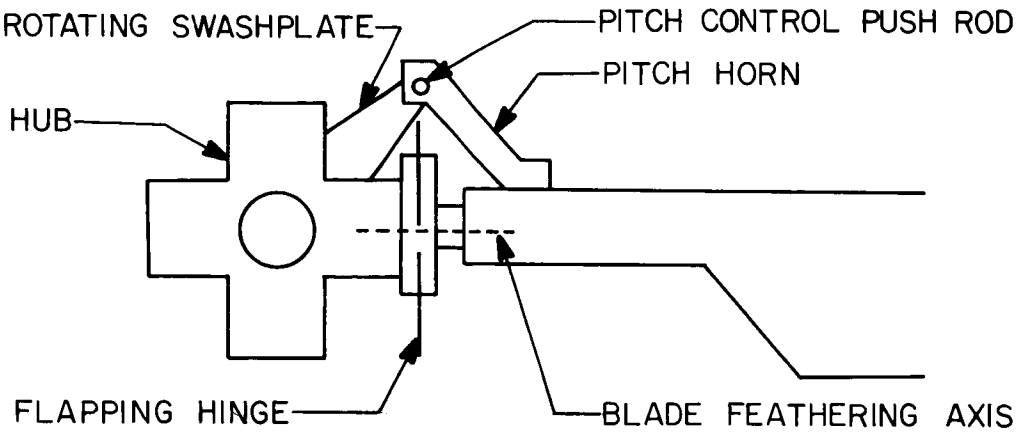

ELECTRONIC FEEDBACK REPRESENTATION

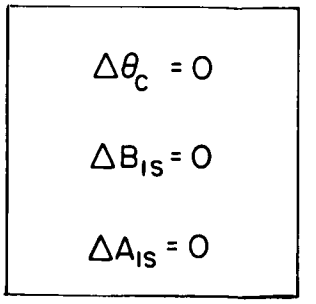

(a) BASIC ROTOR

Figure 3. Mechanical Configurations and Equivalent Electronic Representations of Rotor Feedback Schemes.

MECHANICAL CONFIGURATION

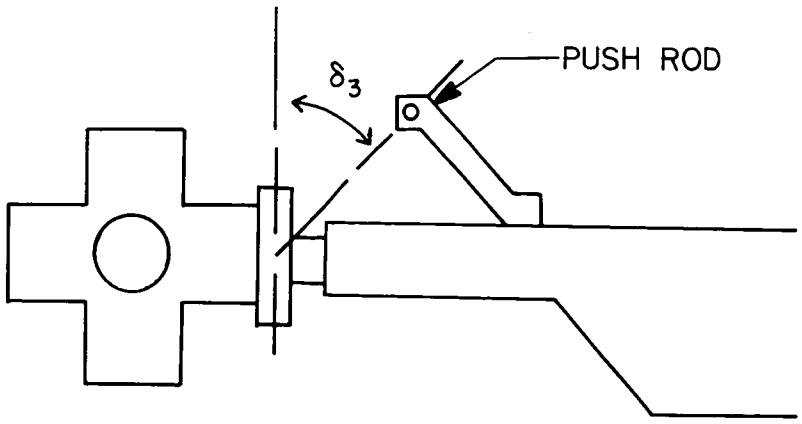

$$k_1 = \tan \delta_3$$

ELECTRONIC FEEDBACK REPRESENTATION

$$\Delta\theta_c = -k_1 \Delta a_{0s}$$

$$\Delta B_{1s} = -k_1 \Delta b_{1s}$$

$$\Delta A_{1s} = -k_1 \Delta a_{1s}$$

(b) DELTA-3

Figure 3.– Continued.

MECHANICAL CONFIGURATION

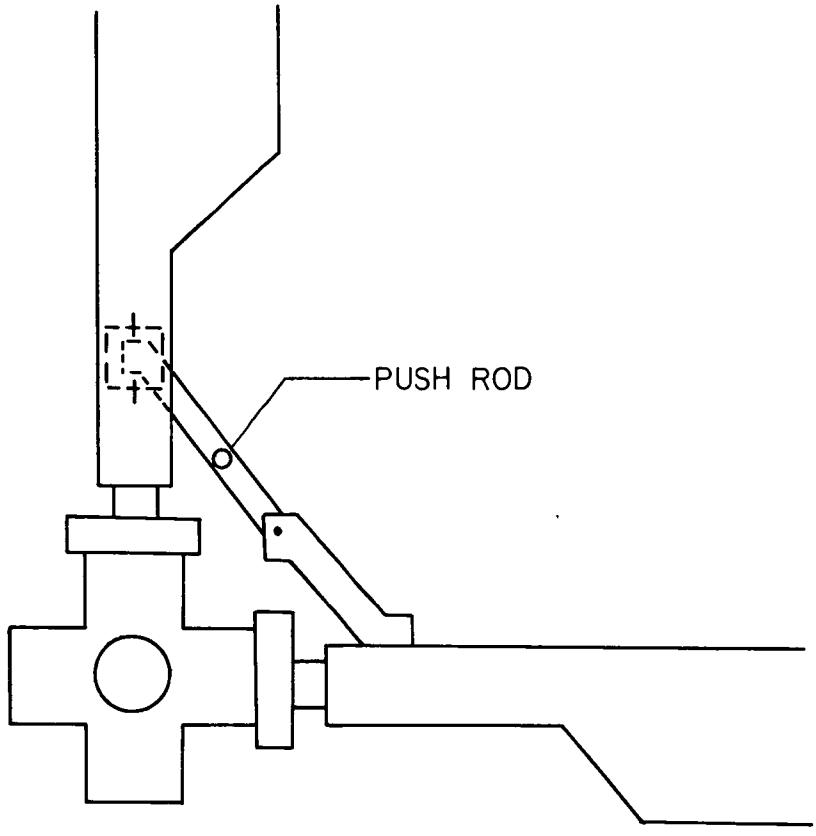

ELECTRONIC FEEDBACK REPRESENTATION

$$\Delta\theta_c = -k_2 \Delta a_{os}$$

$$\Delta B_{is} = k_2 \Delta a_{is}$$

$$\Delta A_{is} = -k_2 \Delta b_{is}$$

(c) OEHMICHEN (REARWARD TYPE)

Figure 3. — Continued.

MECHANICAL CONFIGURATION

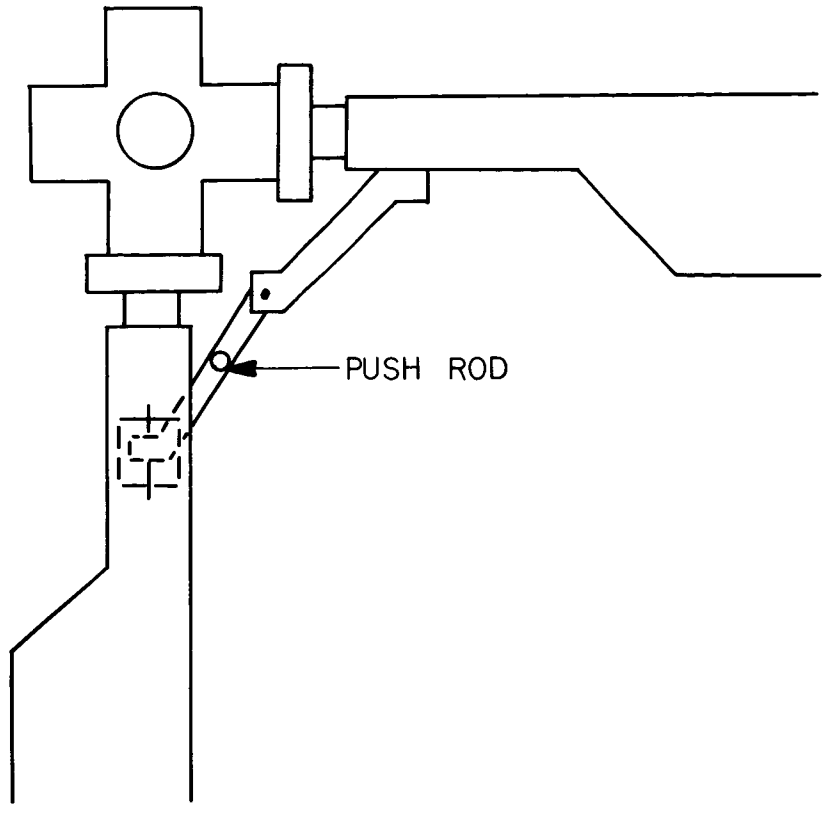

ELECTRONIC FEEDBACK REPRESENTATION

$$\Delta\theta_c = 0$$

$$\Delta B_{IS} = k_3 \Delta a_{IS} - k_3 \Delta b_{IS}$$

$$\Delta A_{IS} = -k_3 \Delta a_{IS} - k_3 \Delta b_{IS}$$

(d) DELTA-3/OEHMICHEN (FORWARD TYPE)

Figure 3.- Continued.

MECHANICAL CONFIGURATION

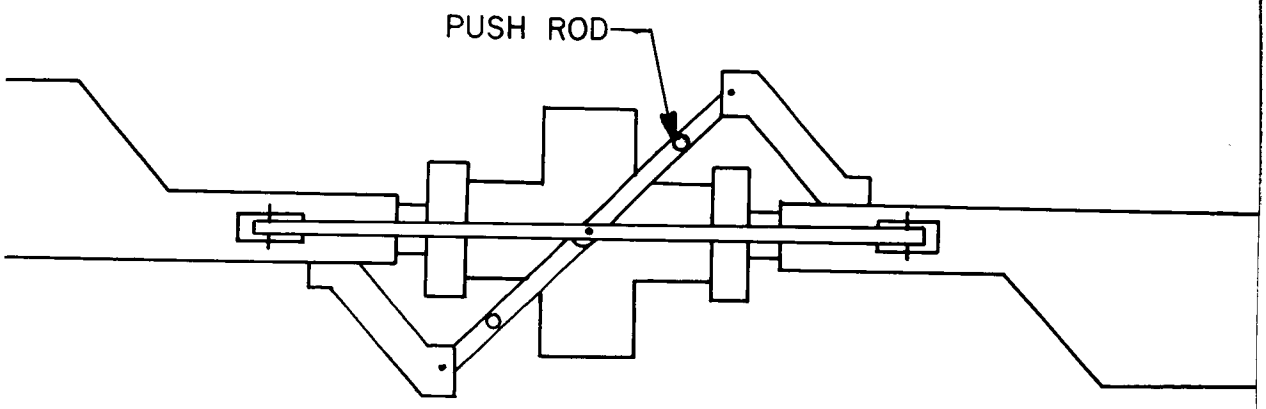

ELECTRONIC FEEDBACK REPRESENTATION

$$\Delta\theta_c = -k_6 \Delta a_{os}$$

$$\Delta B_{is} = 0$$

$$\Delta A_{is} = 0$$

(e) PURE PITCH-CONE

Figure 3. – Continued.

NO SIMPLE MECHANICAL
REPRESENTATION

ELECTRONIC FEEDBACK REPRESENTATION

$$\Delta\theta_c = -k_6 \Delta a_{os}$$

$$\Delta B_{1s} = k_5 \Delta a_{1s} - k_4 \Delta b_{1s}$$

$$\Delta A_{1s} = -k_4 \Delta a_{1s} - k_5 \Delta b_{1s}$$

(f) PROPORTIONAL

Figure 3. – Concluded.

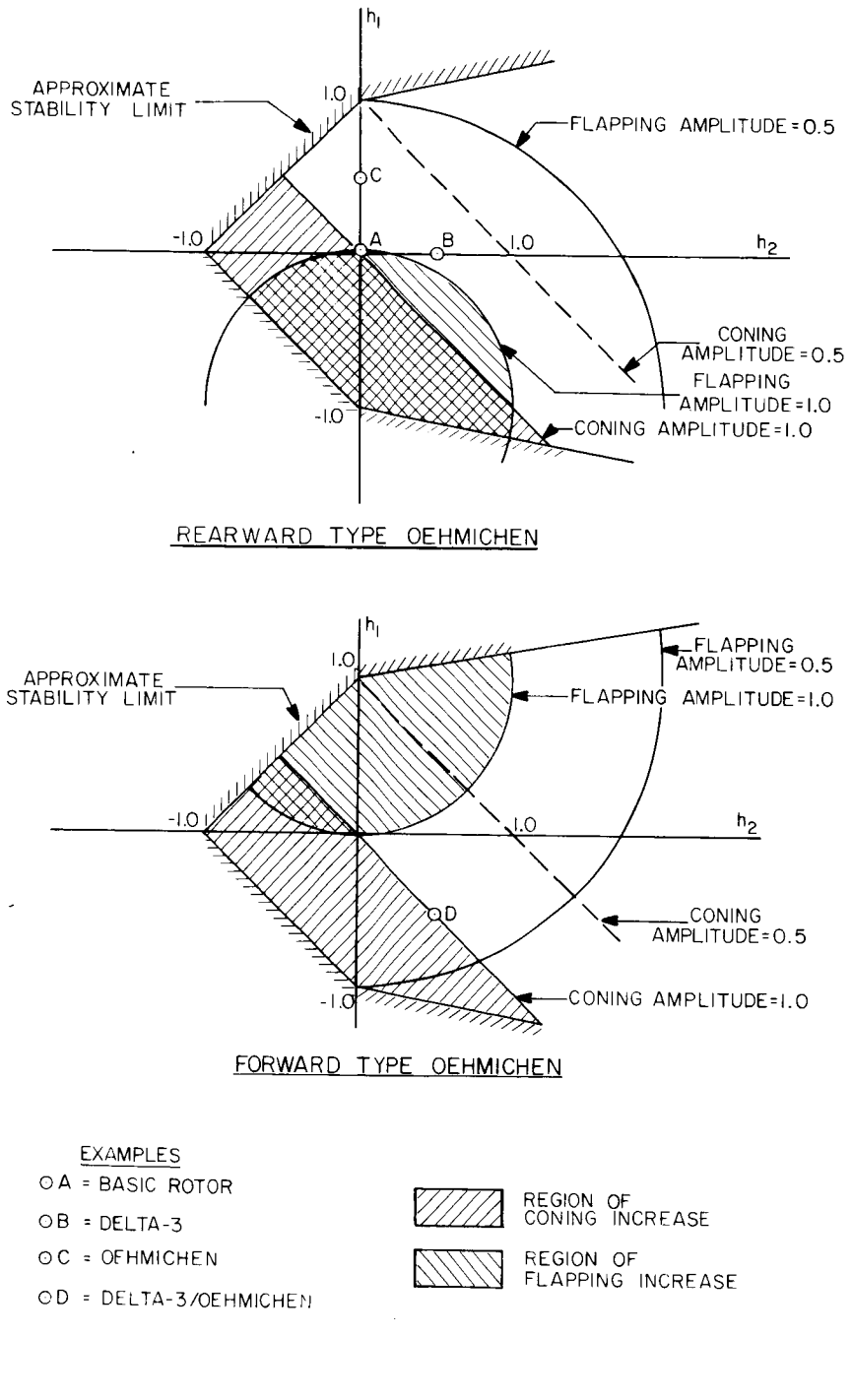

Figure 4. Typical Flapping and Coning Characteristics of Various Delta-3 and Oehmichen Feedback Combinations in Hover, for a Rotor with a Lock Number of 8.0.

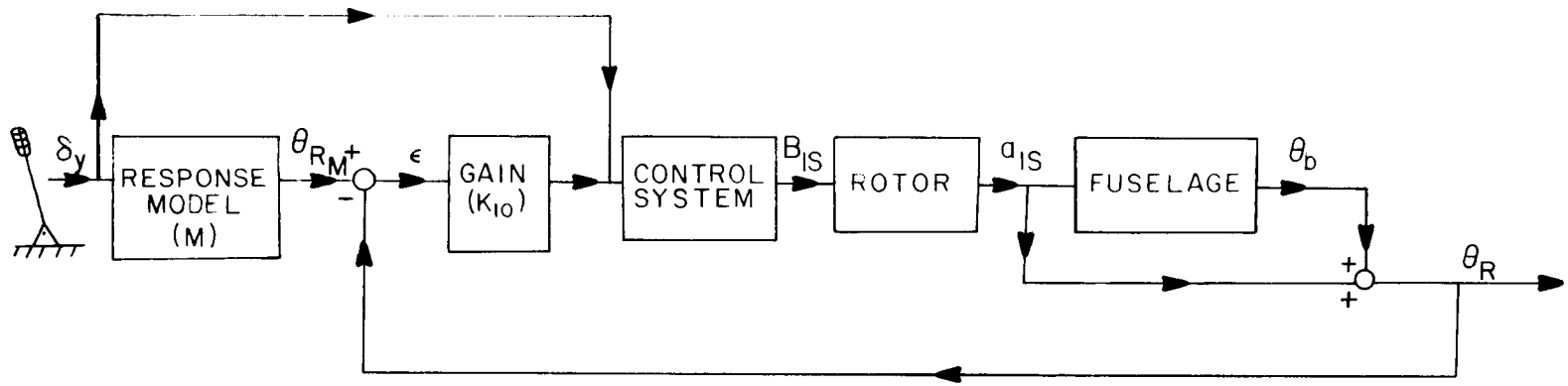

Figure 5. Thrust Vector Control Stabilization Technique (Longitudinal Mode) Used for the Combined Rotor and Fuselage Feedback Study.

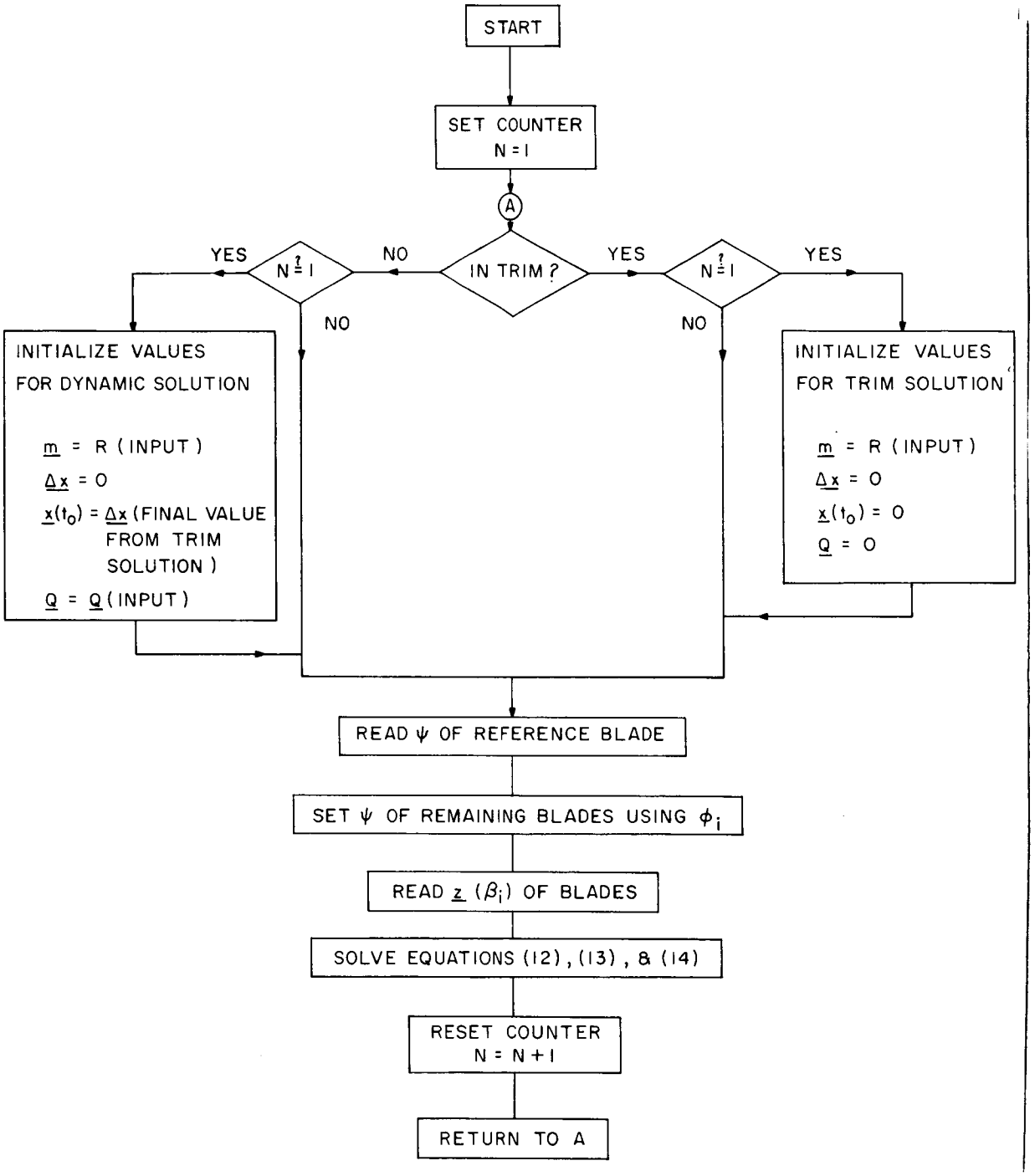

Figure 6. Flow Diagram of the Discrete Kalman Estimation Solution.

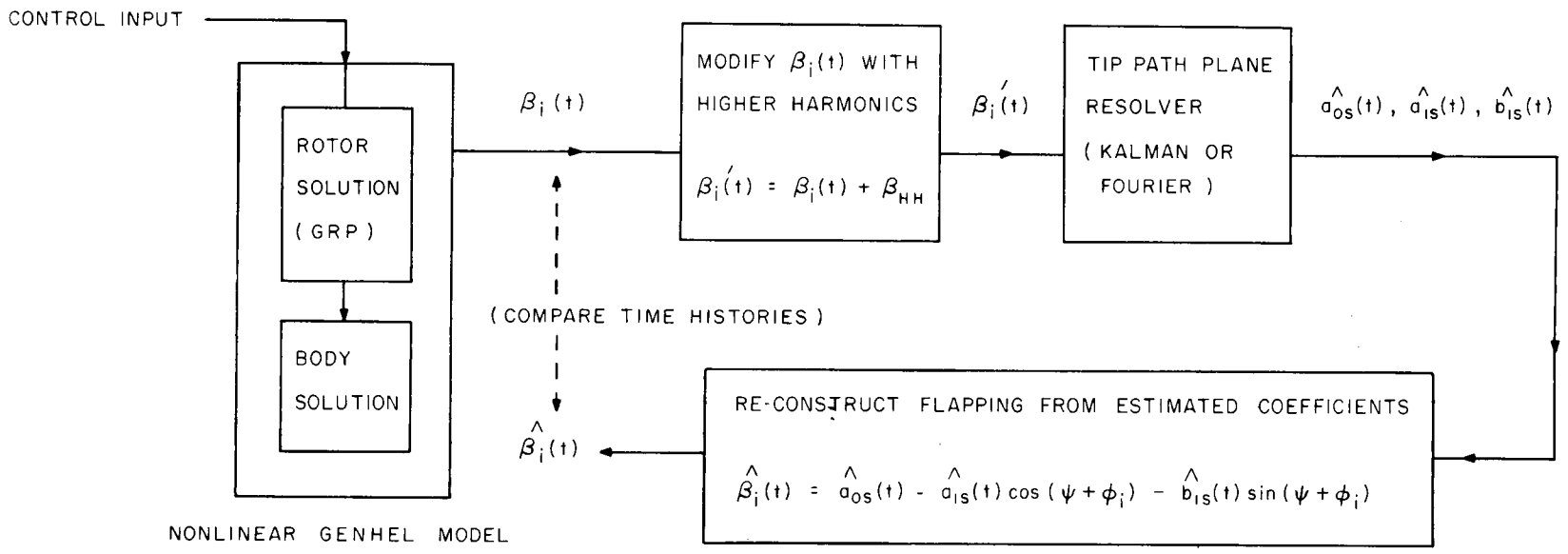

Figure 7. Analytic Method of Evaluating the Tip-Path-Plane Resolvers.

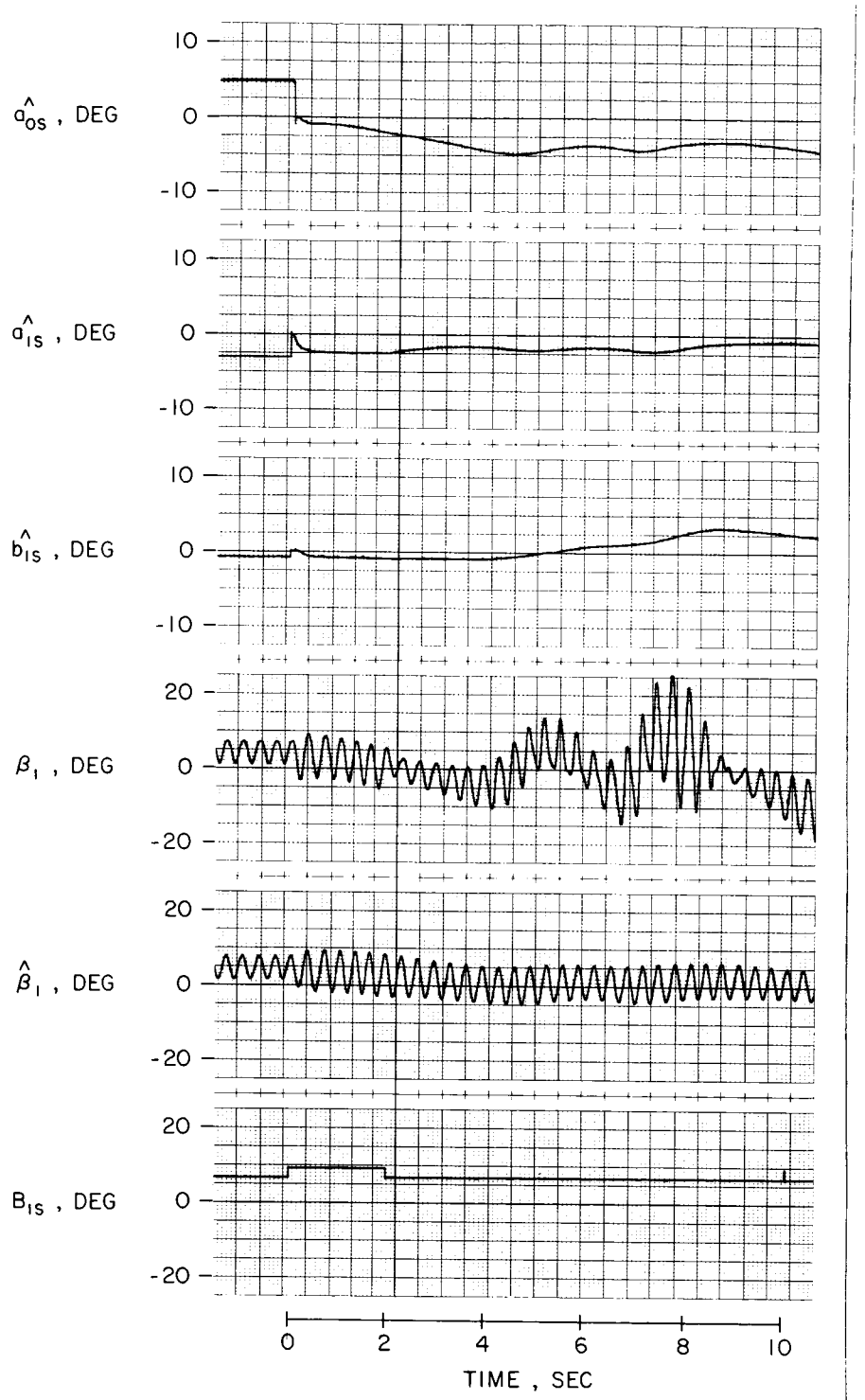

Figure 8. Nonlinear Model Tip-Path-Plane Time Histories Using the Static Fourier Resolver in the Dynamic Mode (CH-53A at 100 Kt).

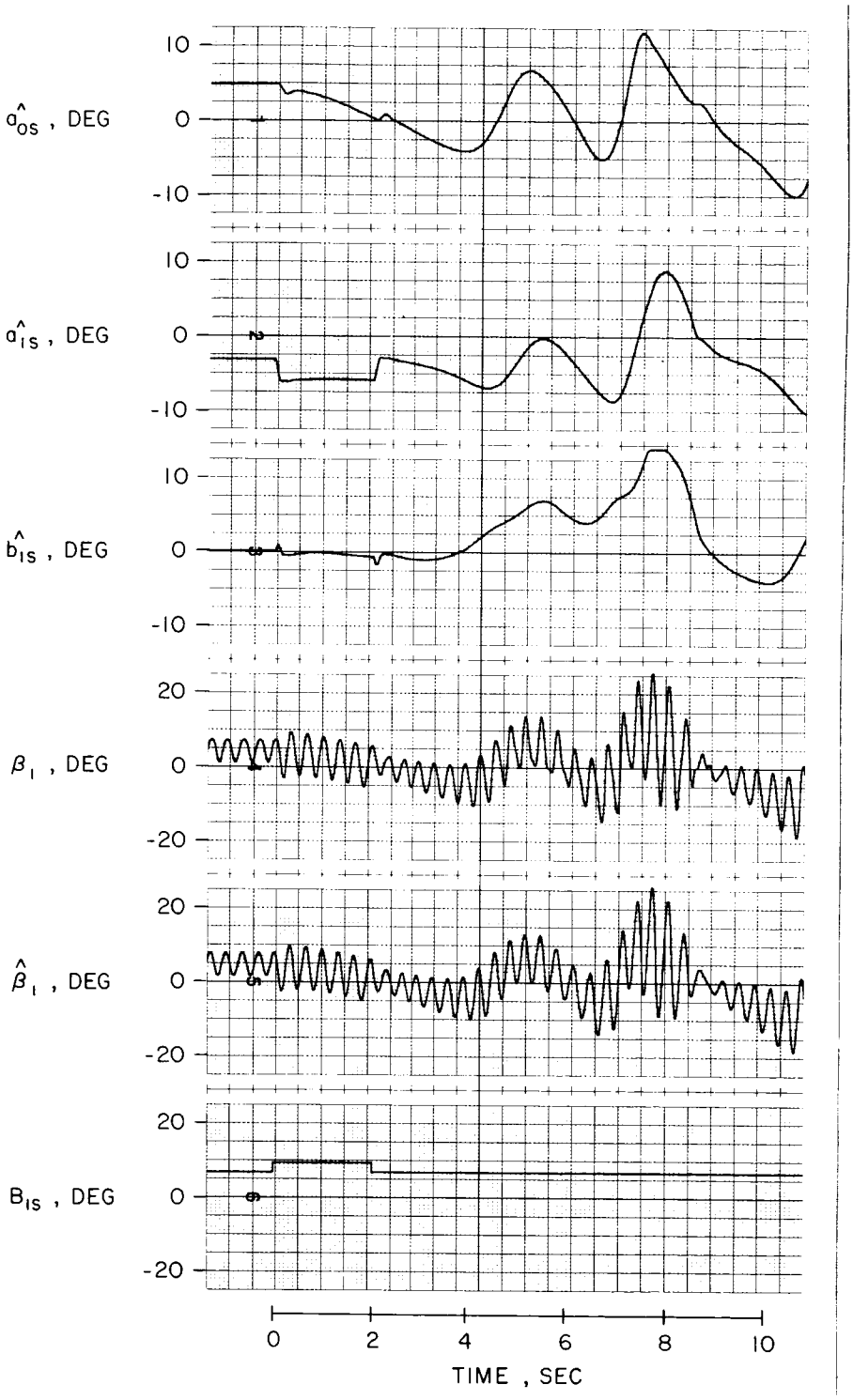

Figure 9. Nonlinear Model Tip-Path-Plane Time Histories Using the Time-Varying Fourier Resolver (CH-53A at 100 Kt).

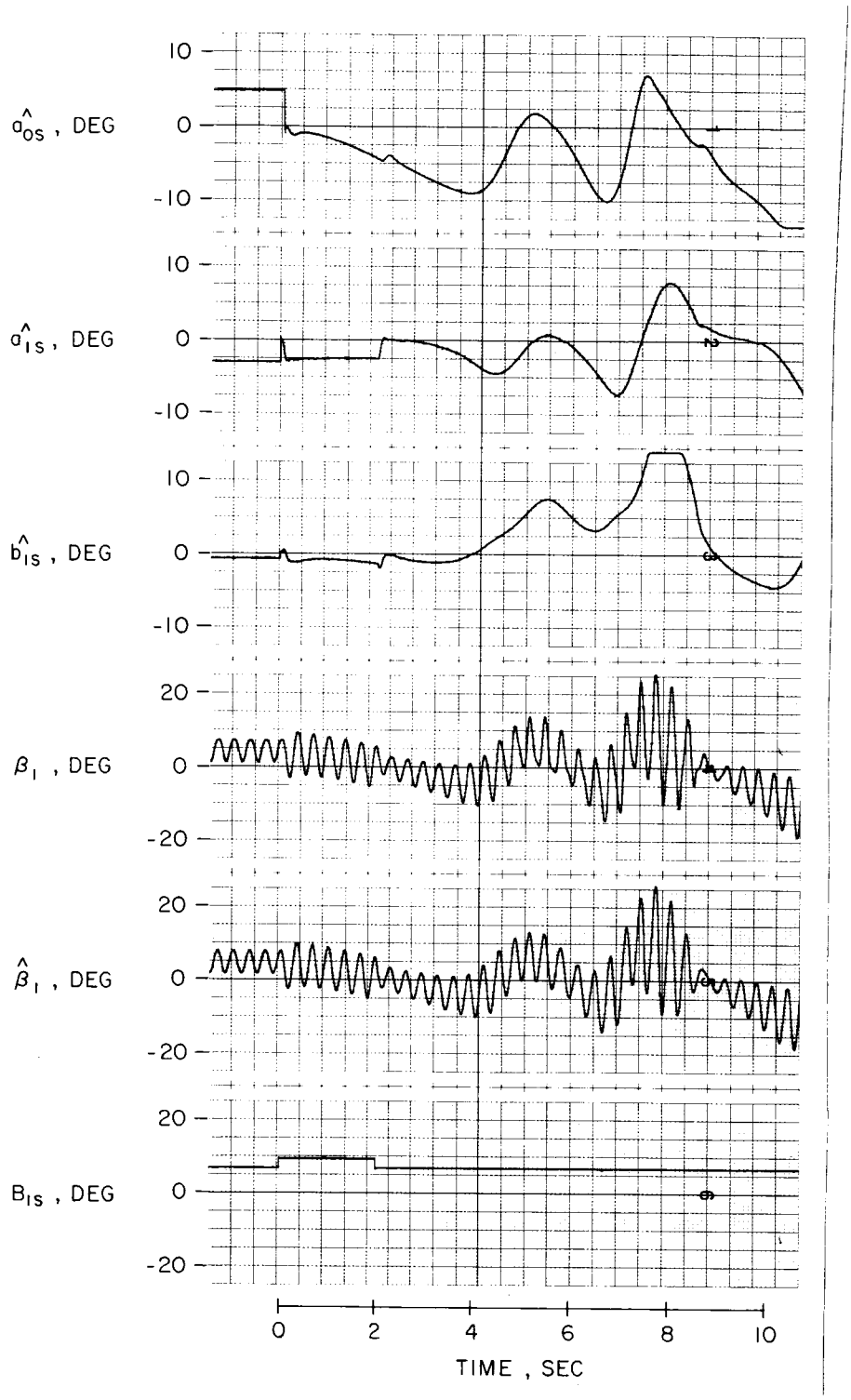

Figure 10. Nonlinear Model Tip-Path-Plane Time Histories Using the Kalman Resolver, R/Q = 1/100 (CH-53A at 100 Kt).

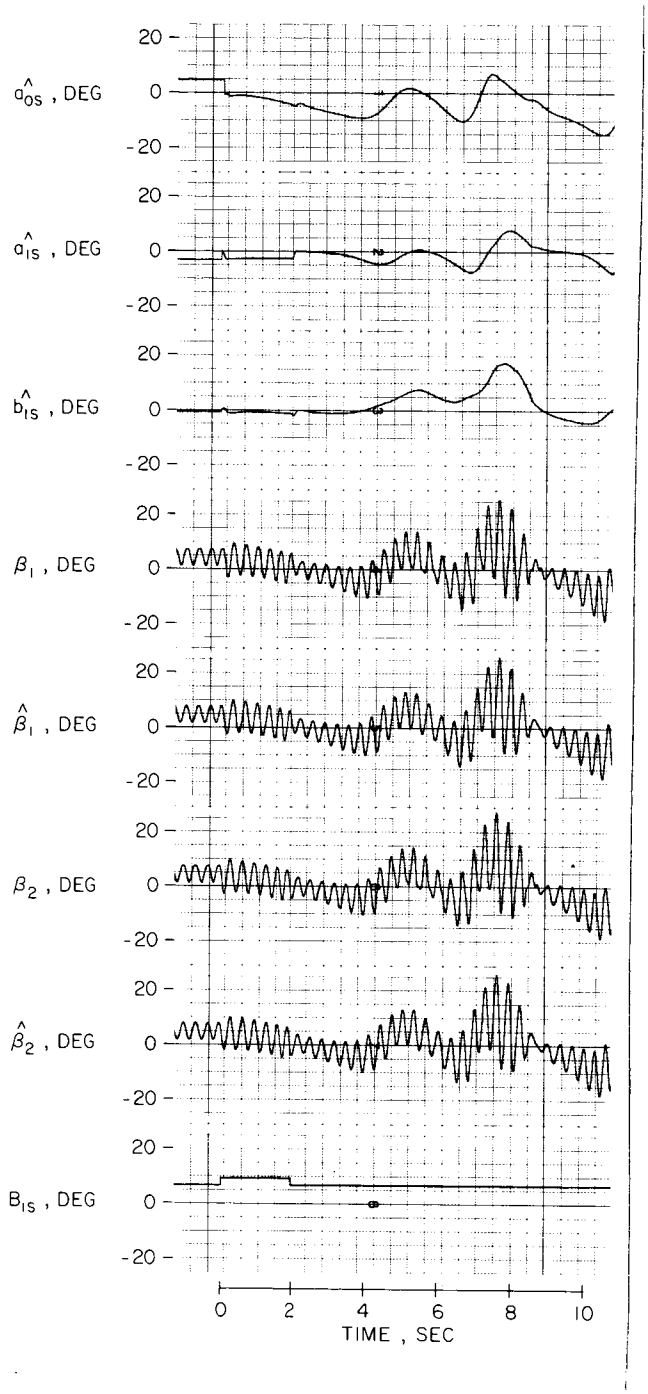

Figure 11. Nonlinear Model Tip-Path-Plane Time Histories Using the Kalman Resolver Sampling 6 Blades, R/Q = 1/100 (CH-53A at 100 Kt).

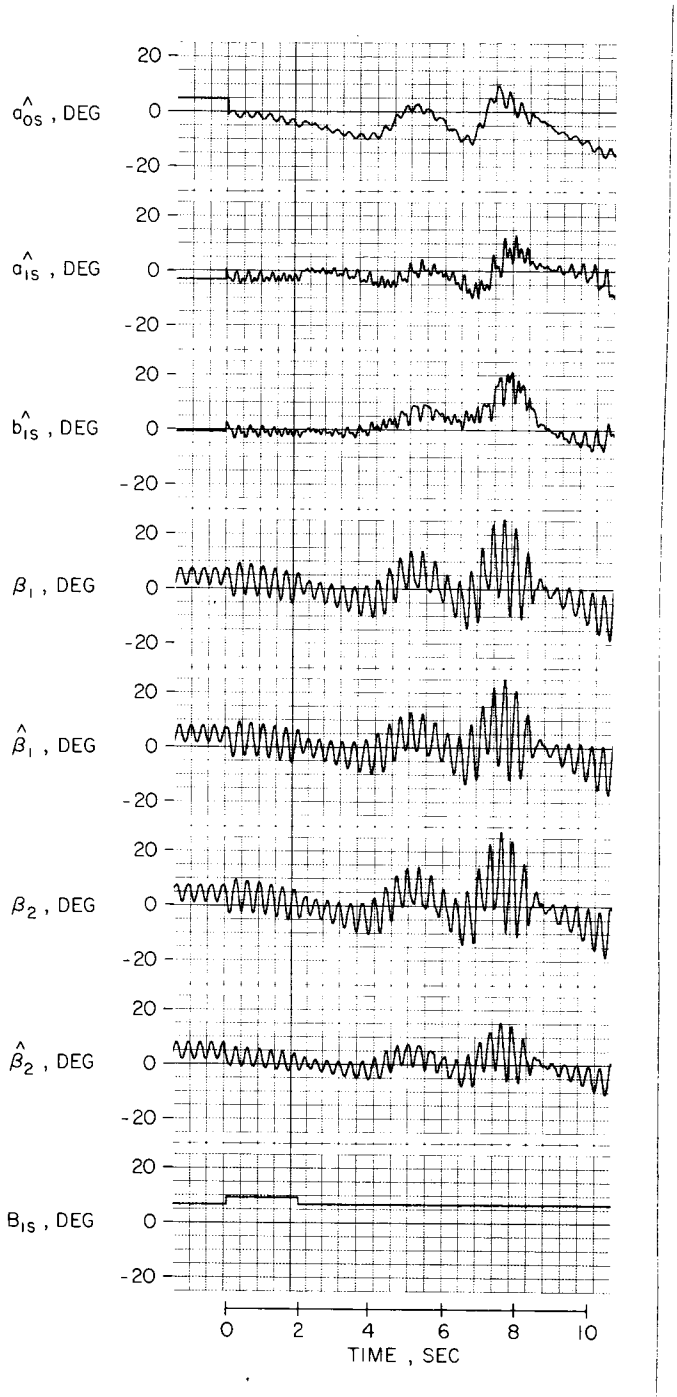

Figure 12. Nonlinear Model Tip-Path-Plane Time Histories Using the Kalman Resolver Sampling 5 Blades, R/Q = 1/100 (CH-53A at 100 Kt).

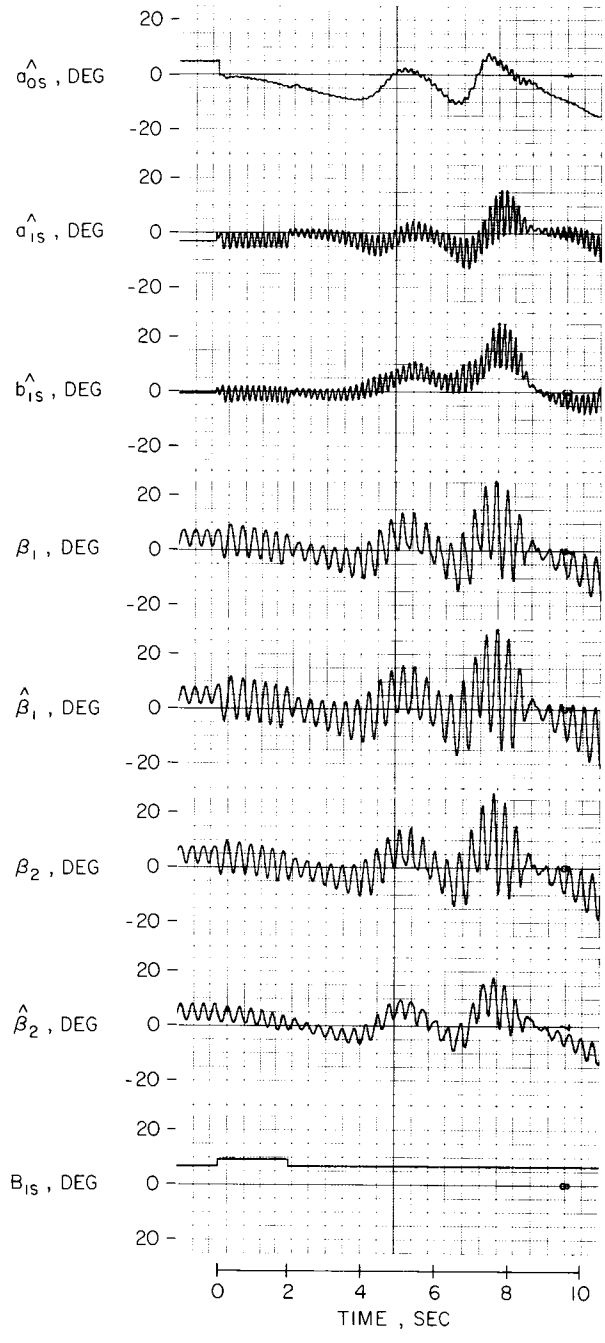

Figure 13. Nonlinear Model Tip-Path-Plane Time Histories Using the Kalman Resolver Sampling 4 Blades, R/Q = 1/100 (CH-53A at 100 Kt).

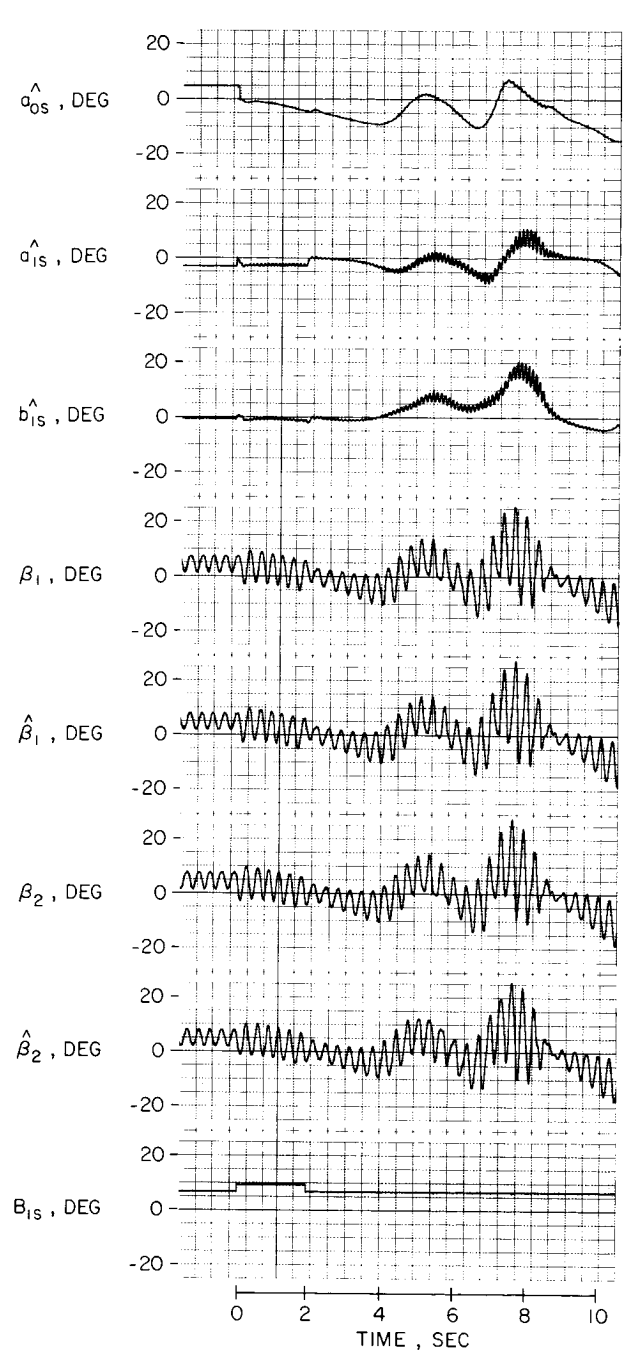

Figure 14. Nonlinear Model Tip-Path-Plane Time Histories Using the Kalman Resolver Sampling 3 Blades, R/Q = 1/100 (CH-53A at 100 Kt).

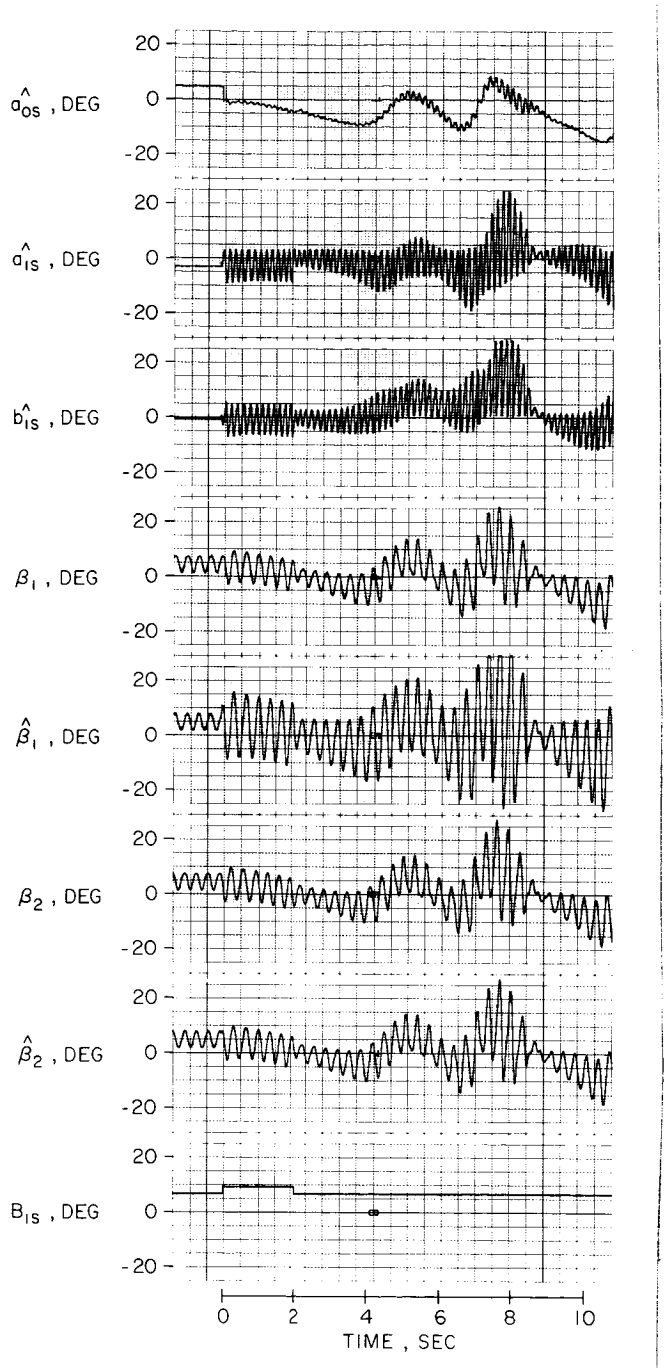

Figure 15. Nonlinear Model Tip-Path-Plane Time Histories Using the Kalman Resolver Sampling 2 Blades, R/Q = 1/100 (CH-53A at 100 Kt).

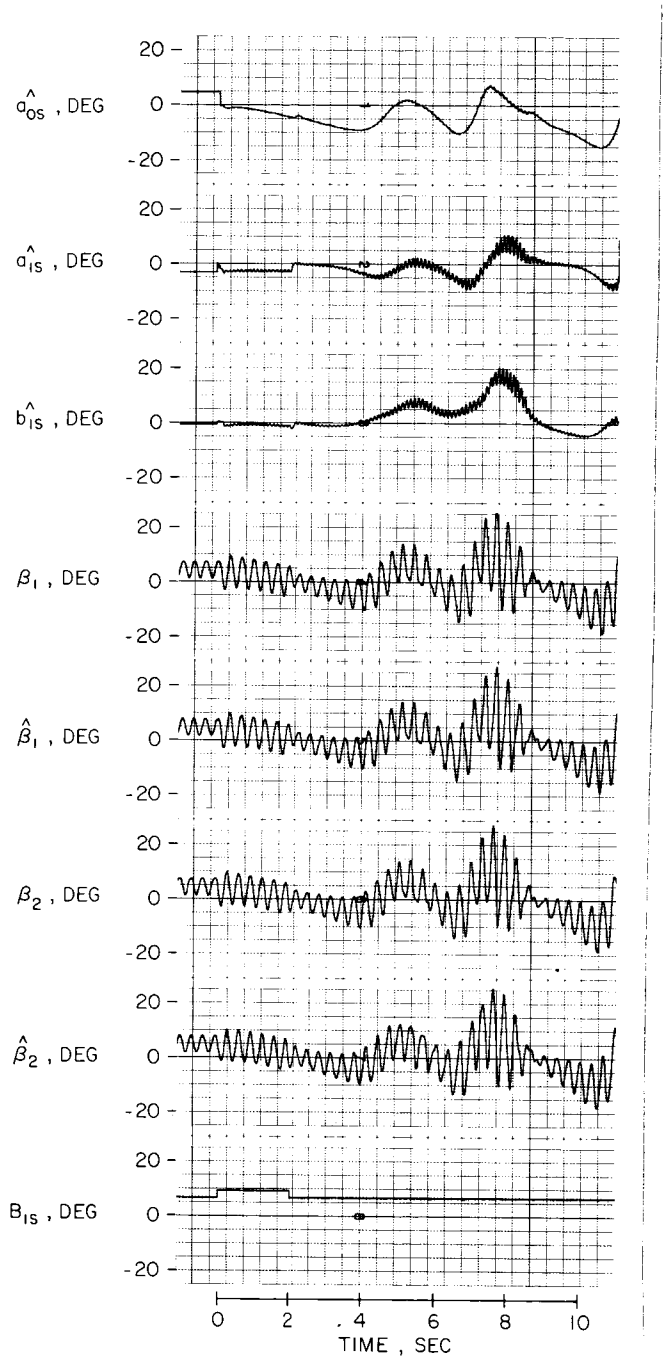

Figure 16. Nonlinear Model Tip-Path-Plane Time Histories Using the Time-Varying Fourier Resolver Sampling 3 Blades (CH-53A at 100 Kt).

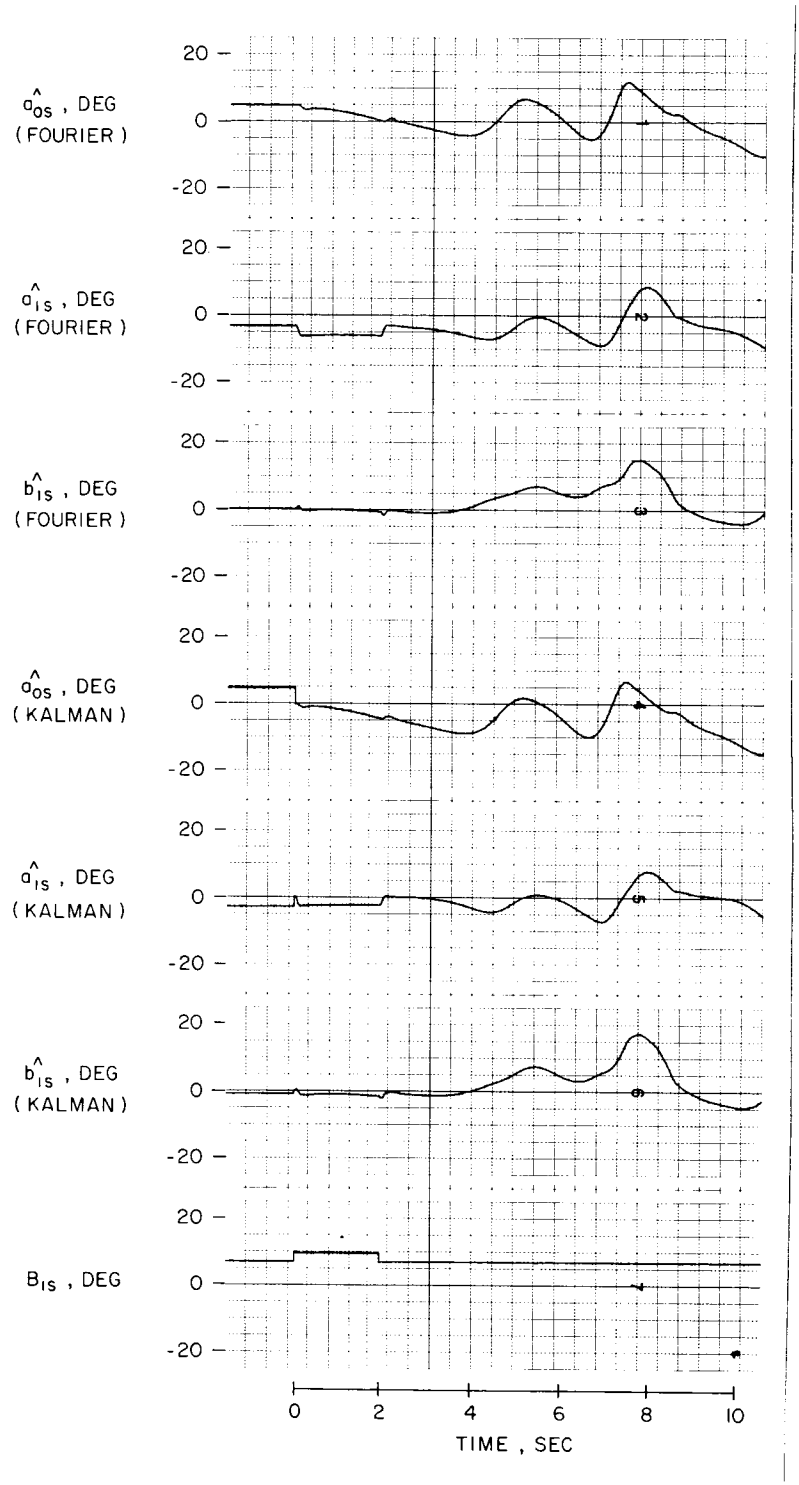

Figure 17. Nonlinear Model Tip-Path-Plane Time Histories Using the Kalman (R/Q = 1/100) and Time-Varying Fourier Resolvers Sampling 24 Times Per Revolution (CH-53A at 100 Kt).

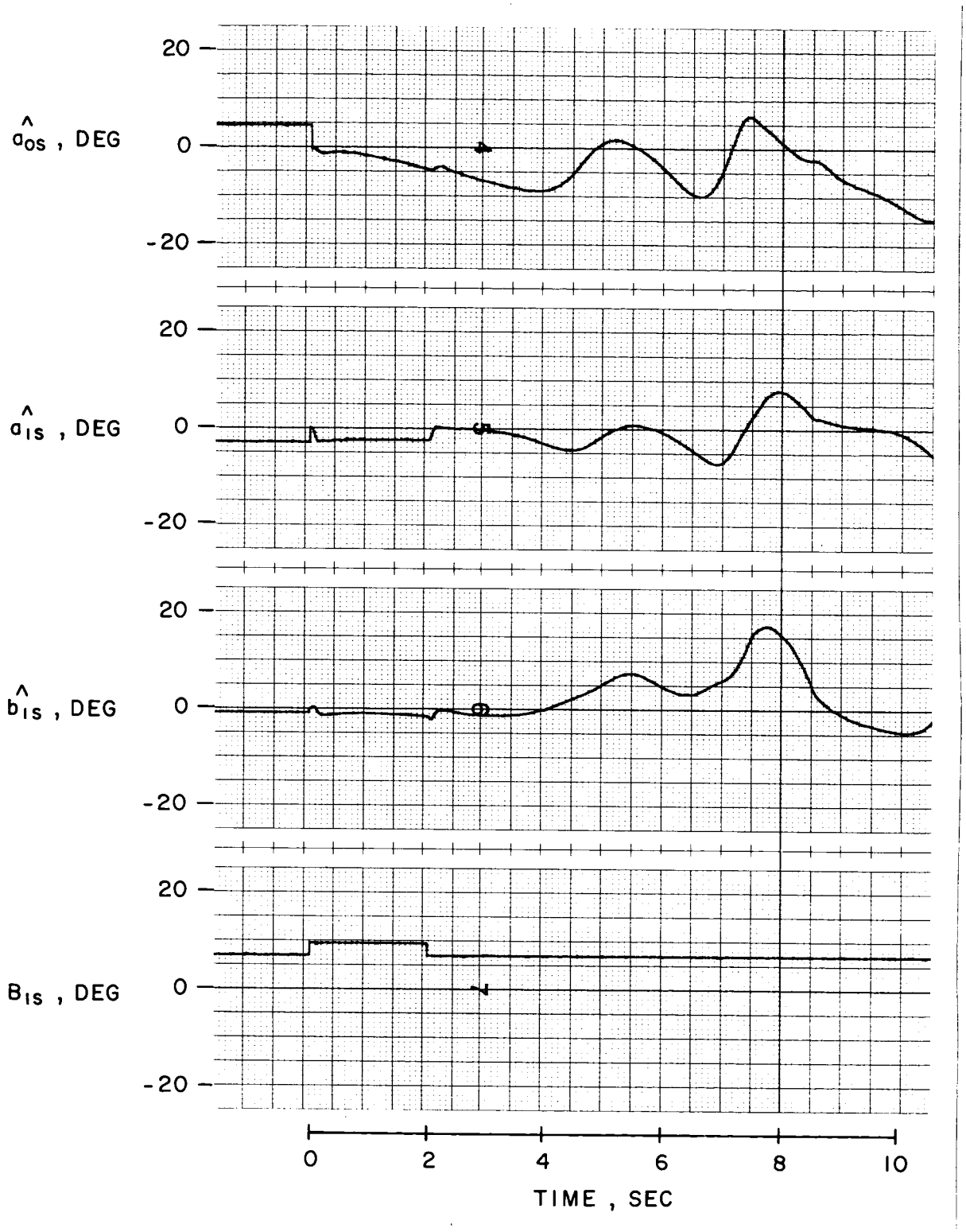

Figure 18. Nonlinear Model Tip-Path-Plane Time Histories Using the Kalman Resolver Sampling 12 Times Per Revolution, R/Q = 1/100 (CH-53A at 100 Kt).

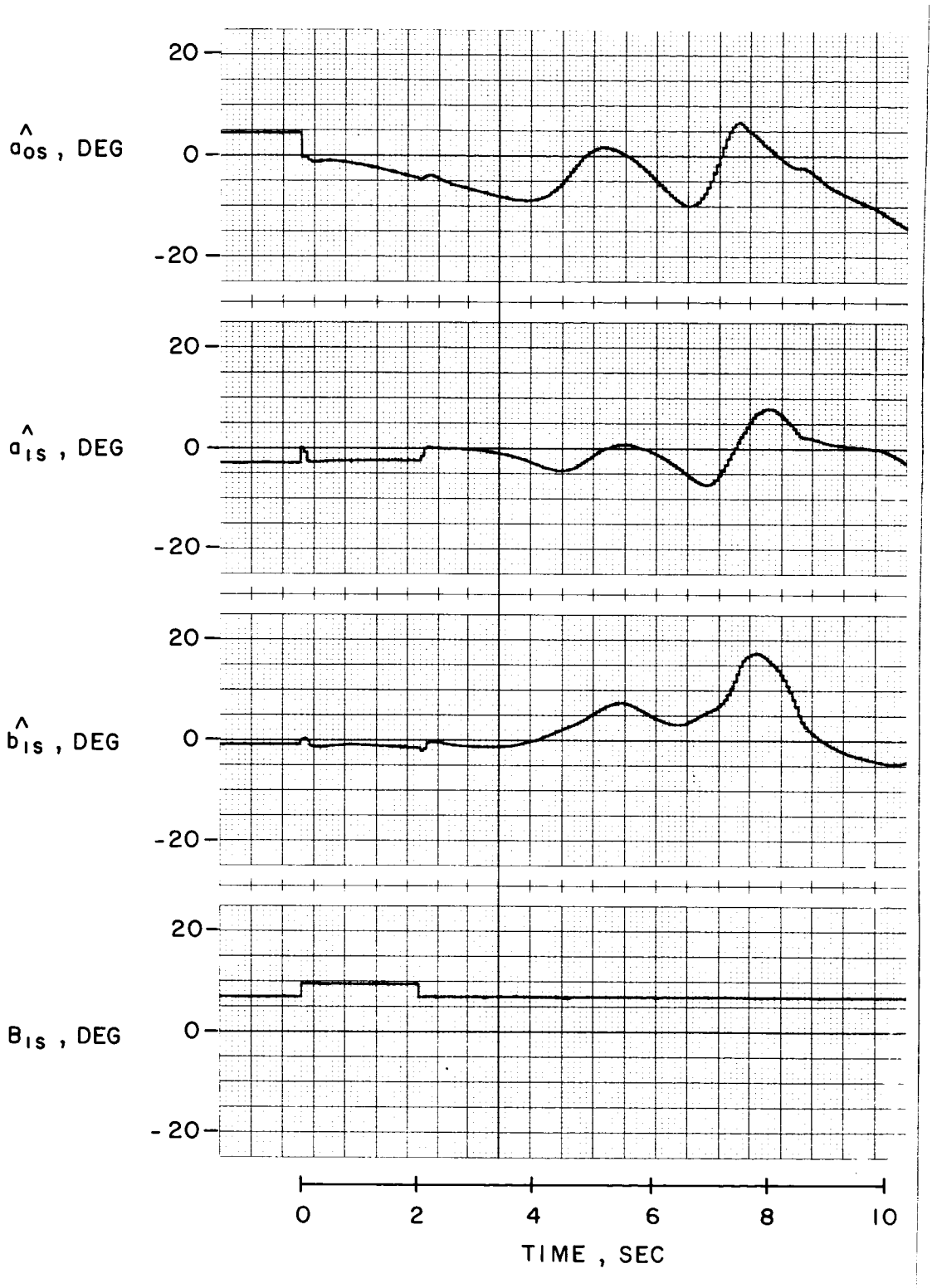

Figure 19. Nonlinear Model Tip-Path-Plane Time Histories Using the Kalman Resolver Sampling 6 Times Per Revolution, R/Q = 1/100 (CH-53A at 100 Kt).

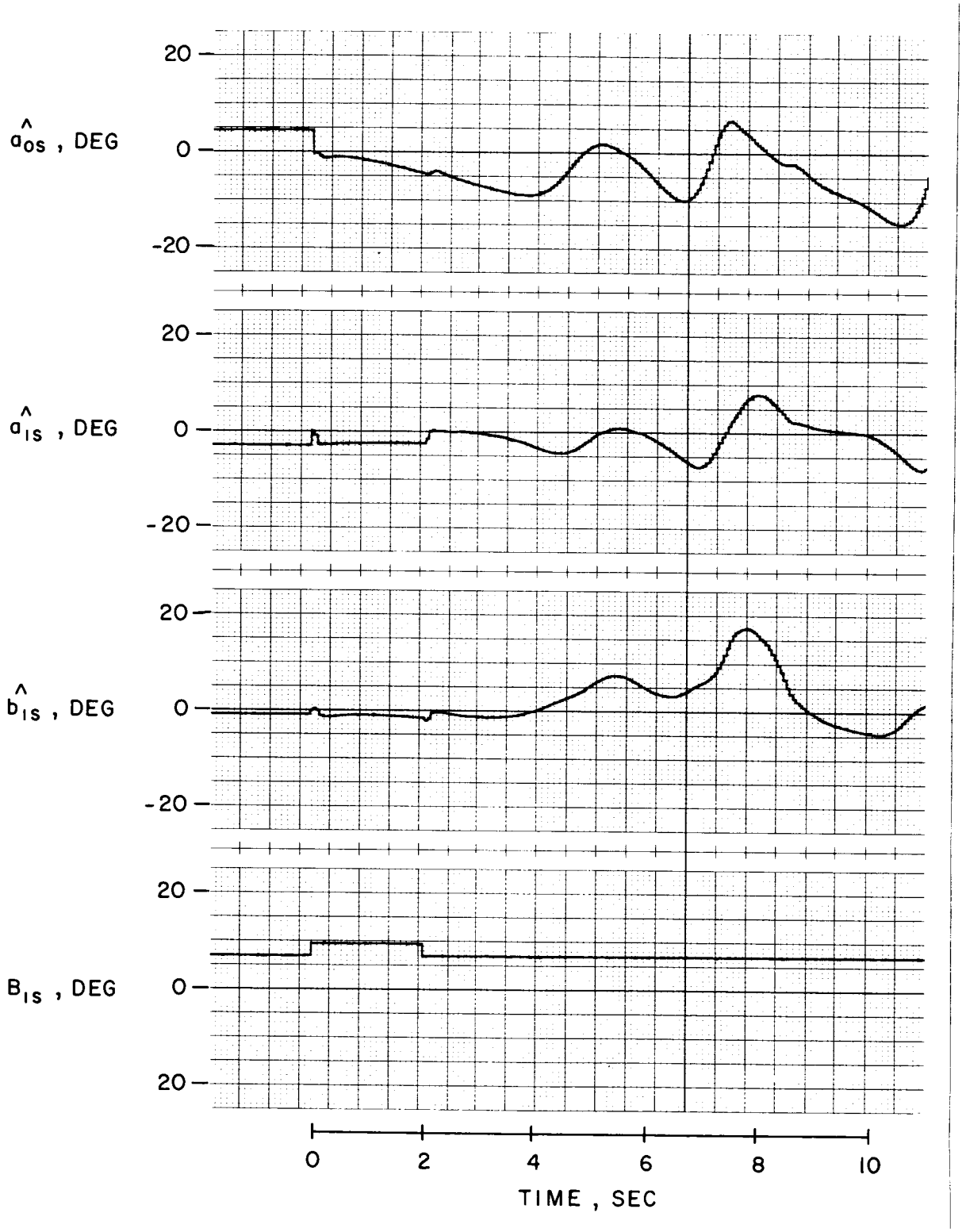

Figure 20. Nonlinear Model Tip-Path-Plane Time Histories Using the Time-Varying Fourier Resolver Sampling 6 Times Per Revolution (CH-53A at 100 Kt).

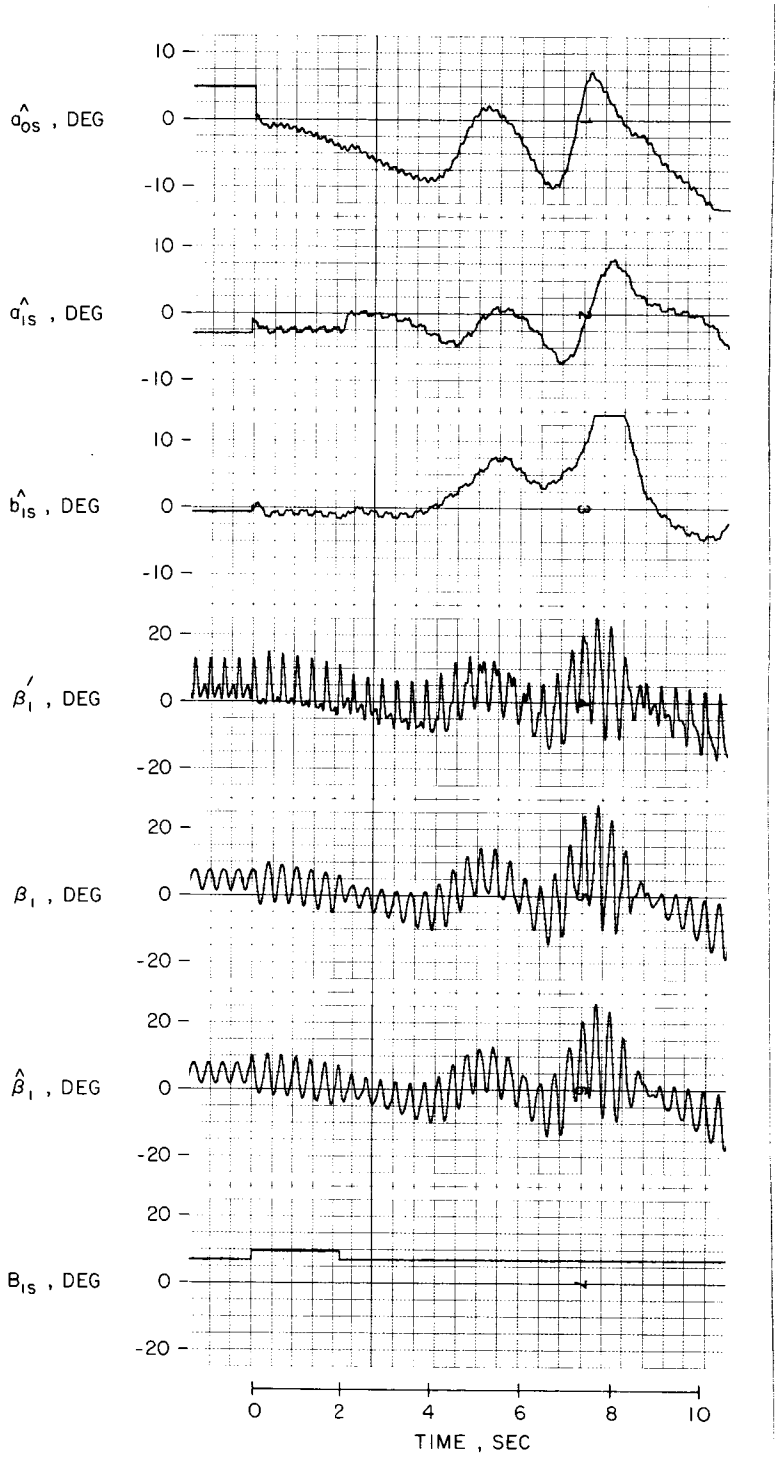

Figure 21. Nonlinear Model Tip-Path-Plane Time Histories Using the Kalman Resolver Sampling Contaminated Data, R/Q = 100 (CH-53A at 100 Kt).

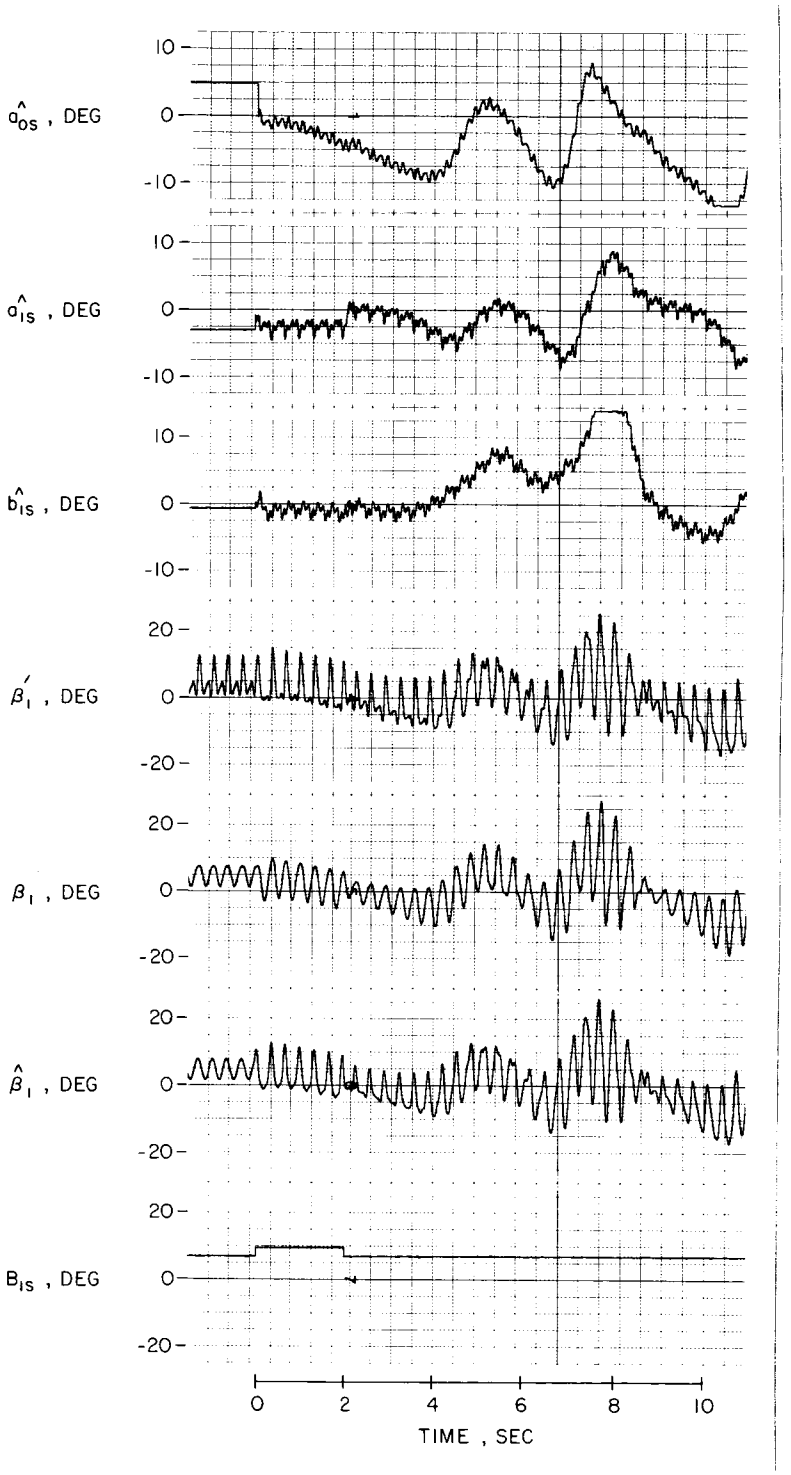

Figure 22. Nonlinear Model Tip-Path-Plane Time Histories Using the Time-Varying Fourier Resolver Sampling Contaminated Data (CH-53A at 100 Kt).

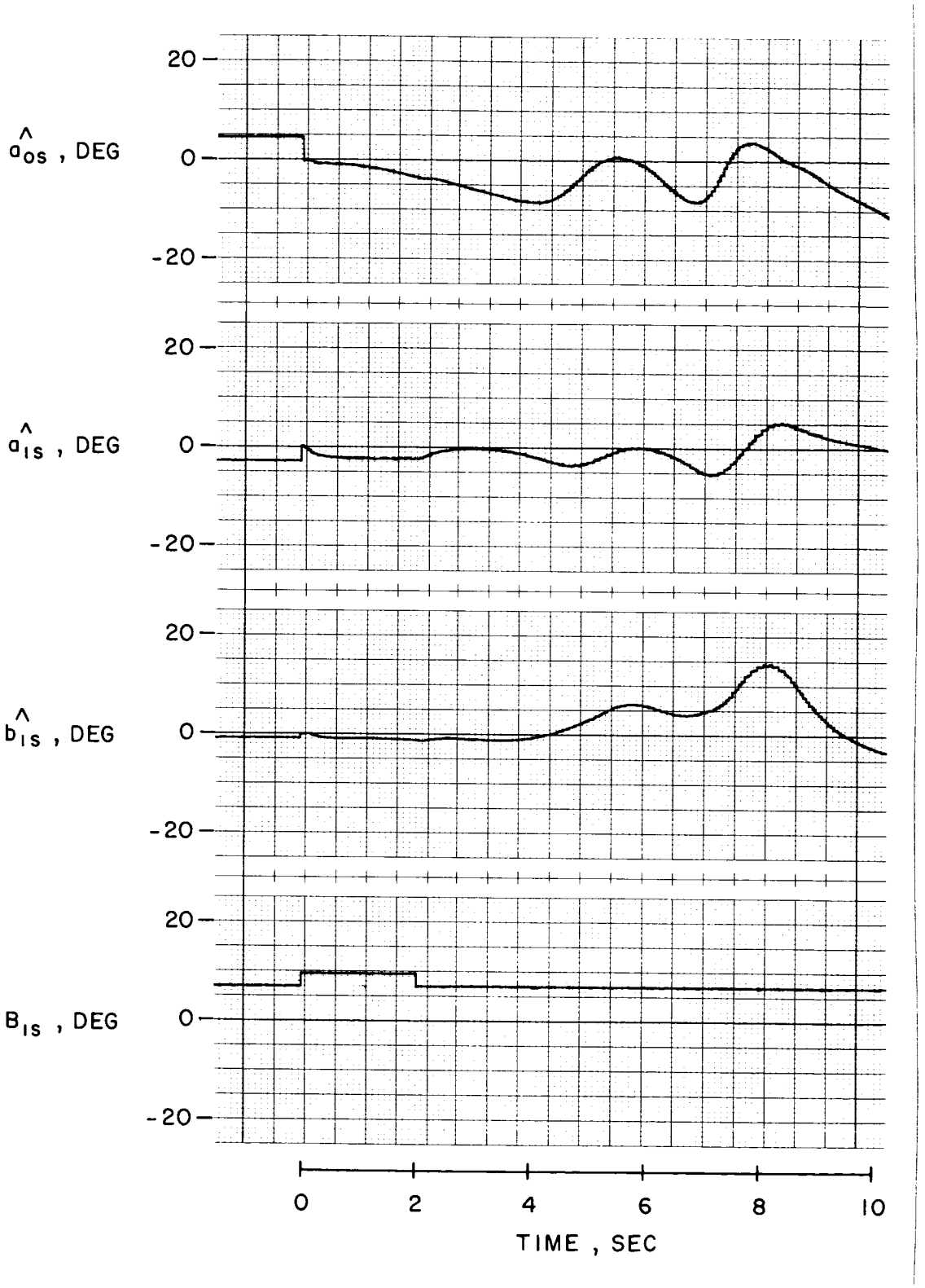

Figure 23. Nonlinear Model Tip-Path-Plane Time Histories Using the Kalman Resolver With An Effective Filter of $R/Q = 100$, Sampling 3 Blades 6 Times Per Revolution (CH-53A at 100 Kt).

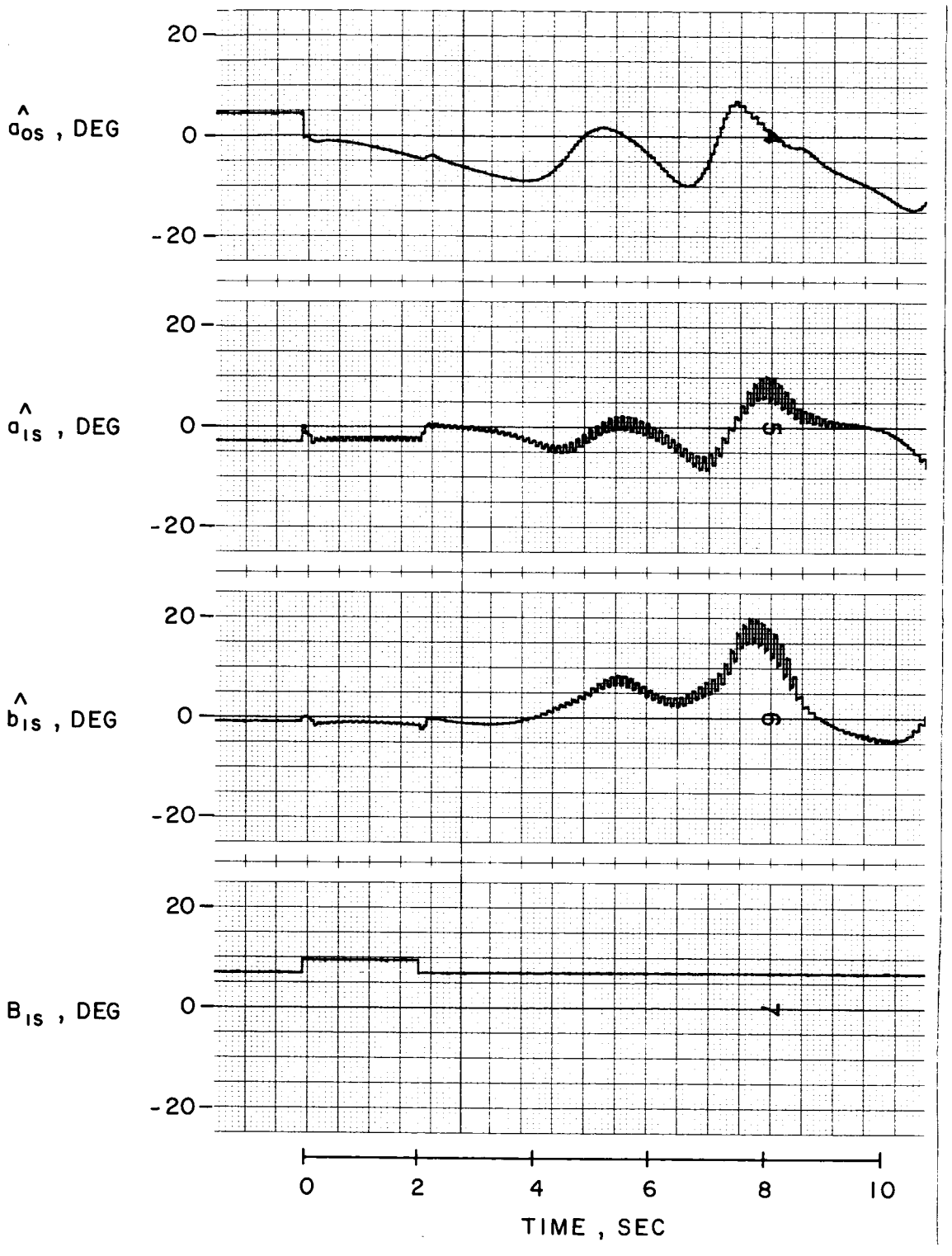

Figure 24. Nonlinear Model Tip-Path-Plane Time Histories Using the Kalman Resolver With An Effective Filter of R/Q = 1/100, Sampling 3 Blades 6 Times Per Revolution (CH-53A at 100 Kt).

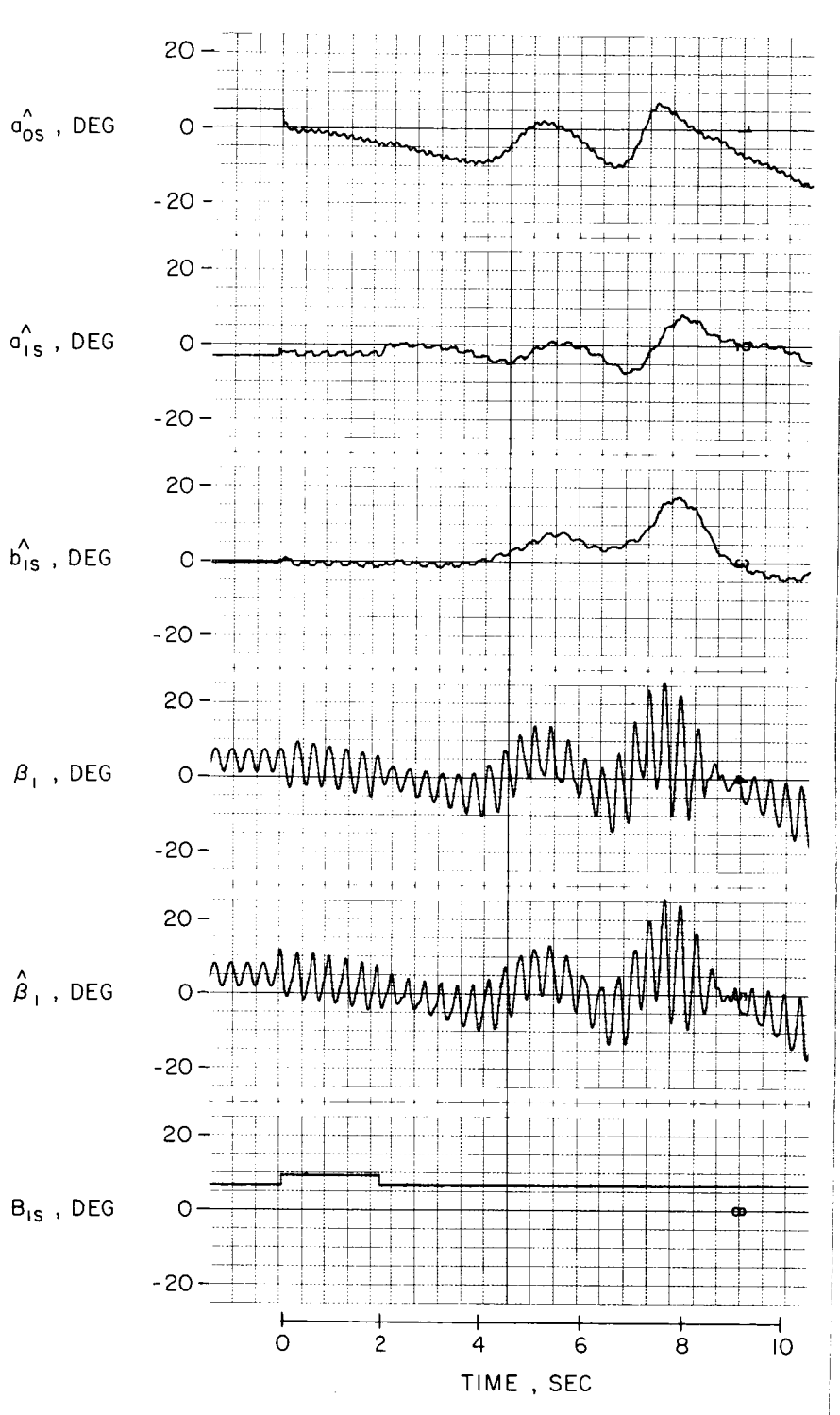

Figure 25. Nonlinear Model Tip-Path-Plane Time Histories Using the Kalman Resolver, R/Q = 100, Sampling Contaminated Data of 3 Blades 24 Times Per Revolution (CH-53A at 100 Kt).

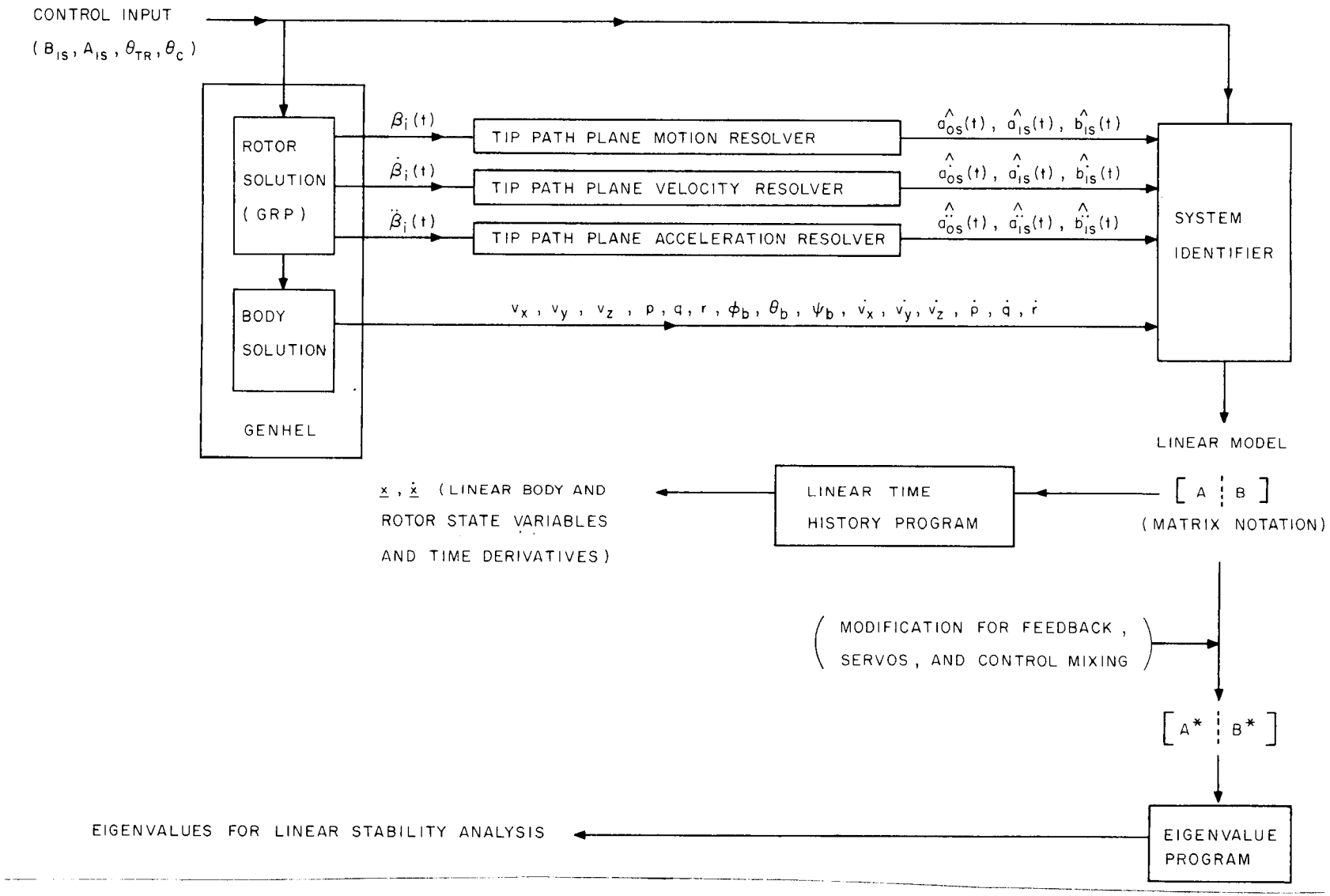

Figure 26. Identification of Linear Model and Preparation for Stability Analysis.

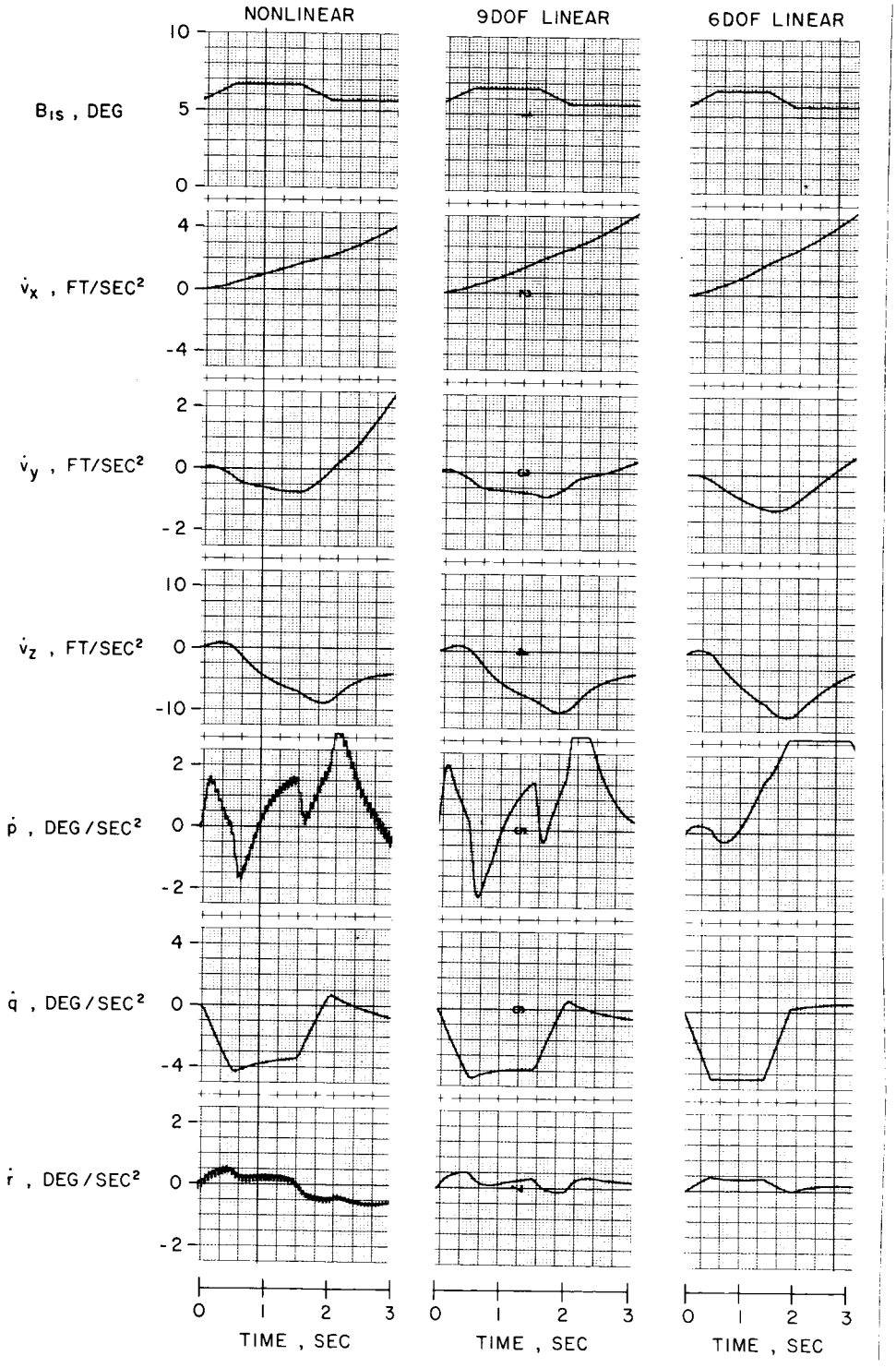

Figure 27. Comparison of Acceleration Time Histories Obtained from the Nonlinear Simulation and the Nine and Six Degree-of-Freedom Linear Models.

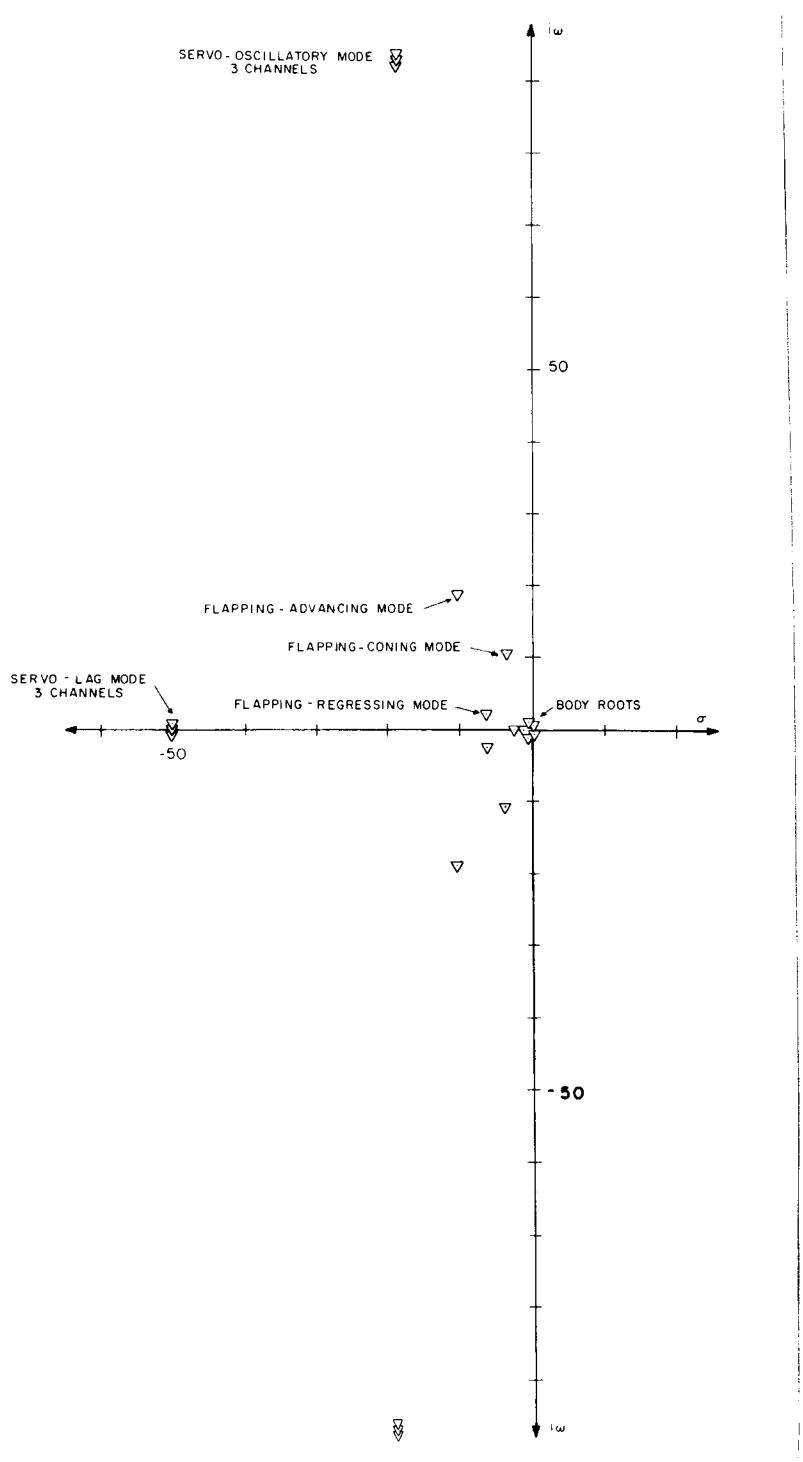

Figure 28. CH-53A Rotor/Fuselage/Control System Open Loop Roots at Hover (33,500 lb, 348 fscg).

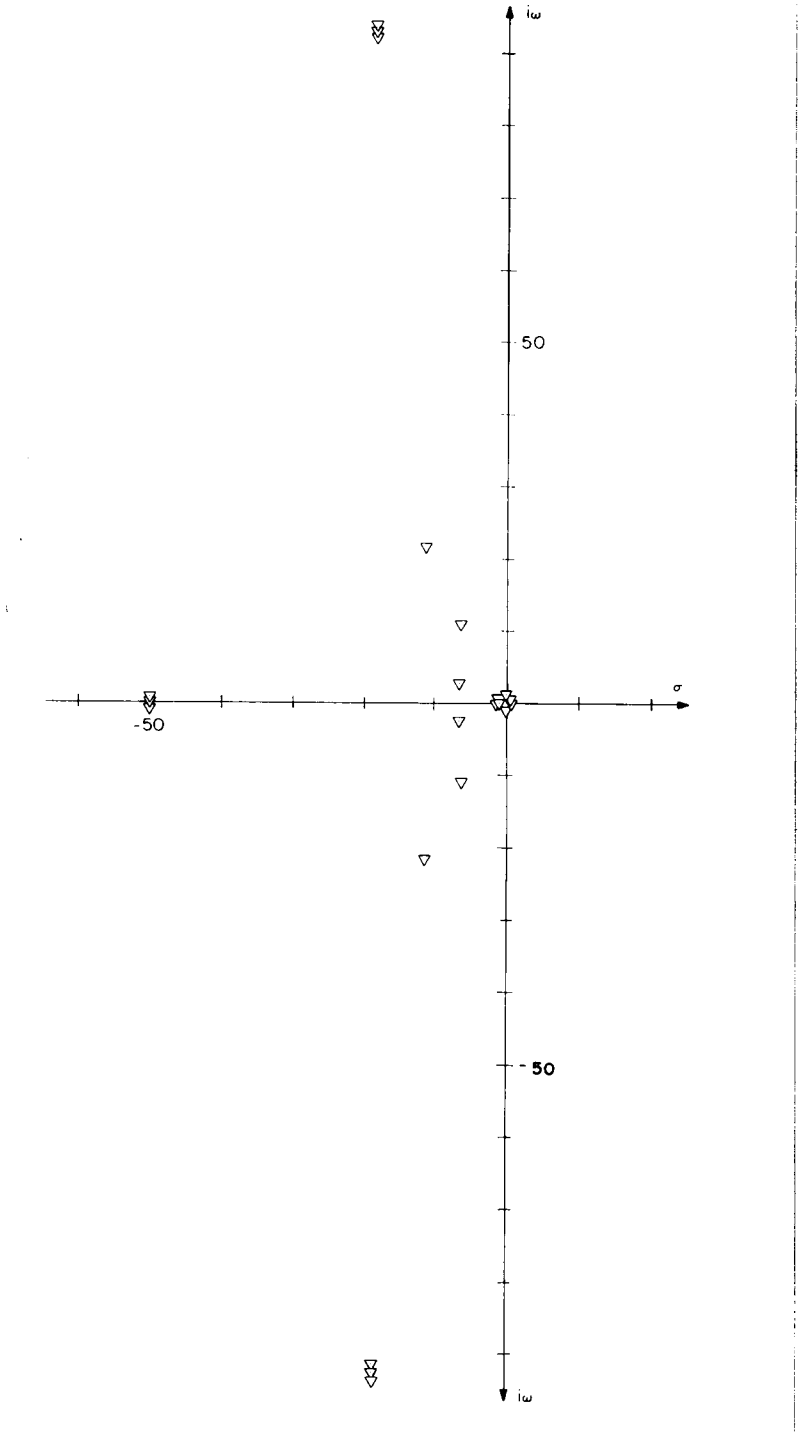

Figure 29. CH-53A Rotor/Fuselage/Control System Open Loop Roots at 100 Kt (33,500 lb, 348 fscg).

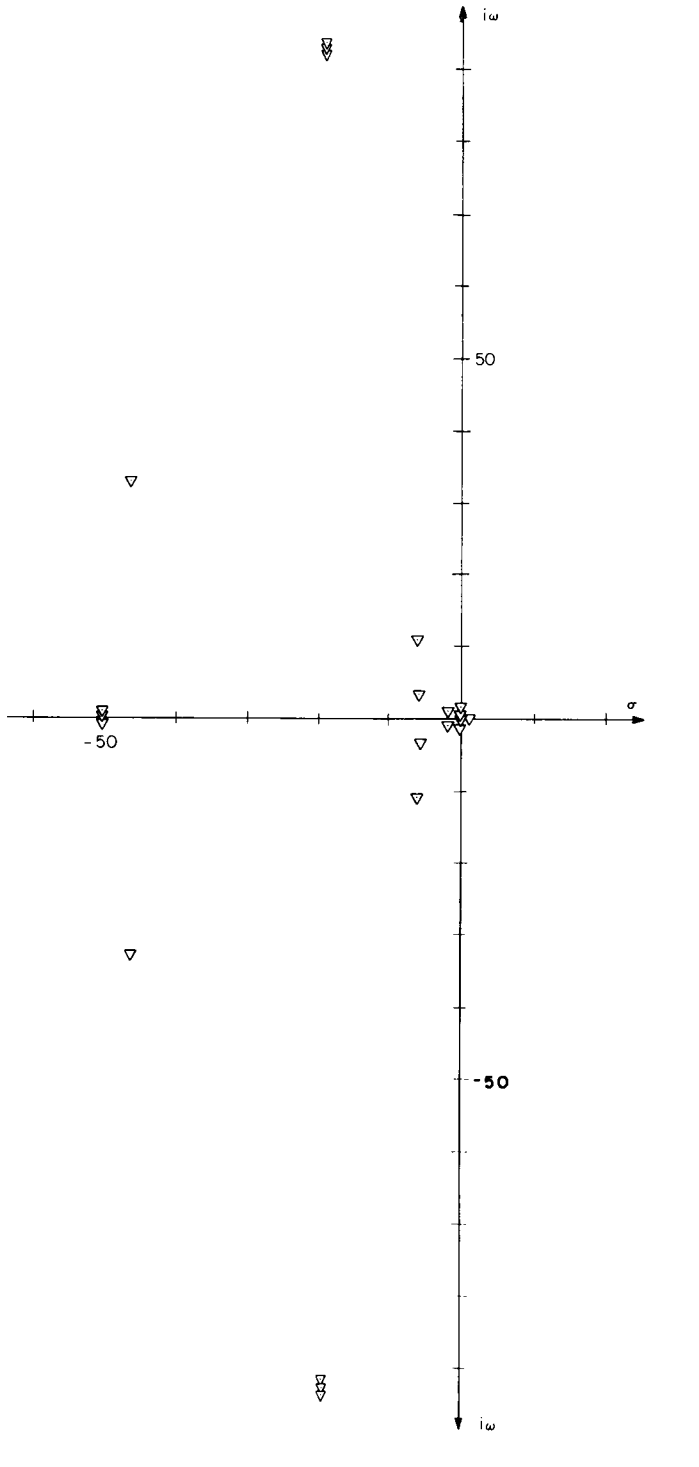

Figure 30. CH-53A Rotor/Fuselage/Control System Open Loop Roots at 150 Kt (33,500 lb, 348 fscg).

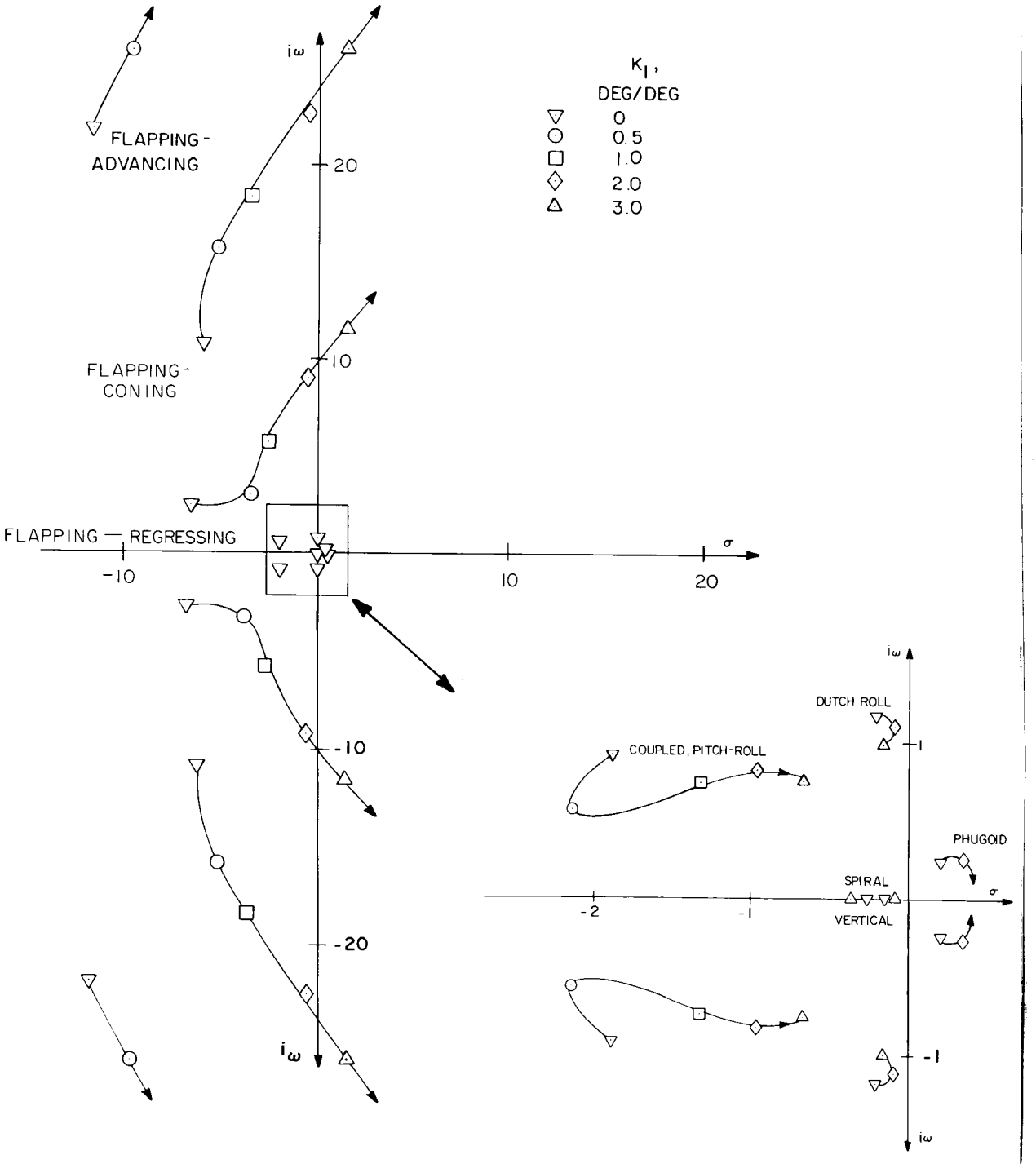

Figure 31. Closed Loop Locus of Roots for CH-53A with Delta-3 Feedback, Servos Included (100 Kt, 33,500 lb, 348 fscg).

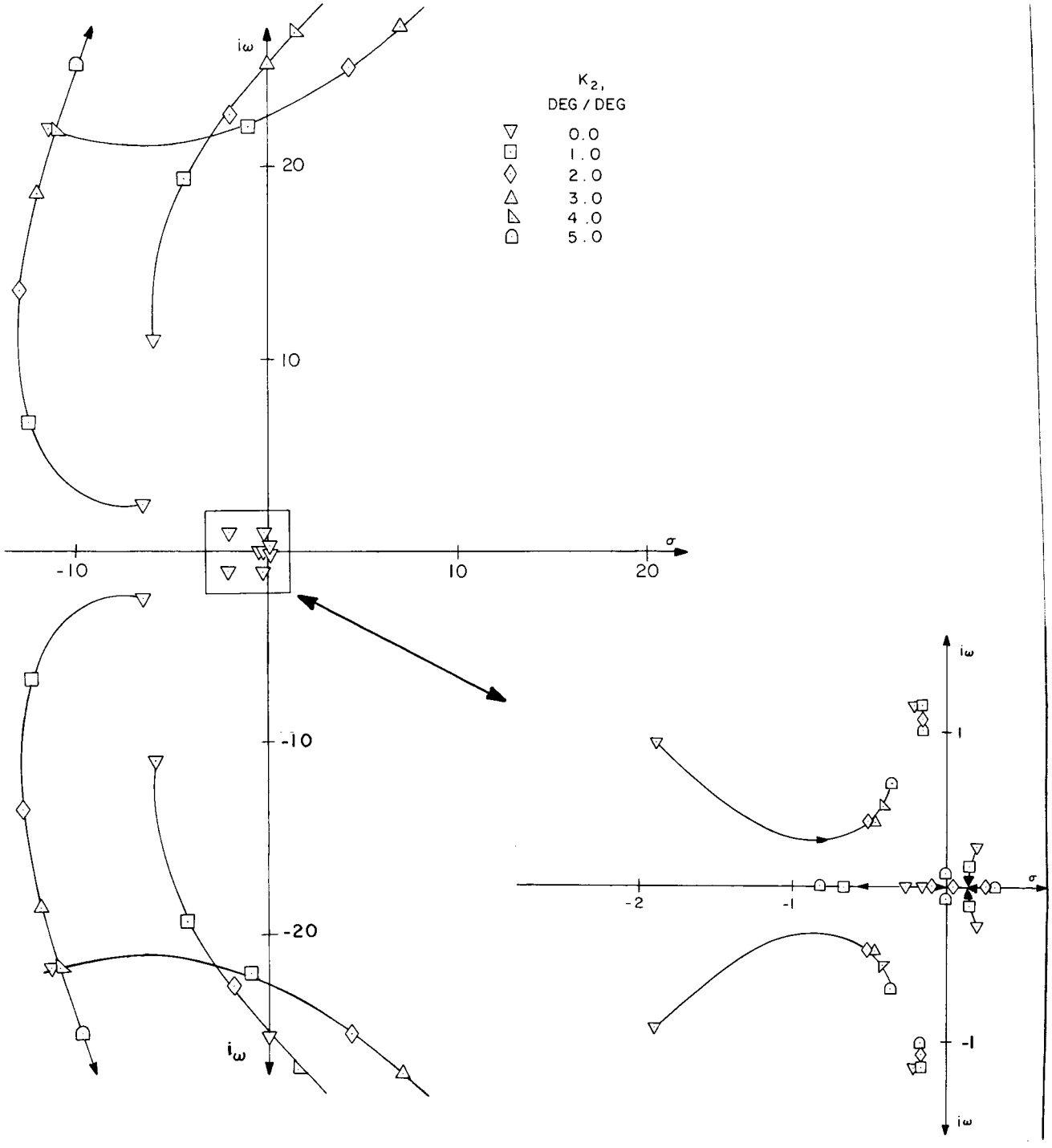

Figure 32. Closed Loop Locus of Roots for CH-53A with Oehmichen Feedback, Servos Included (100 Kt, 33,500 lb, 348 fscg).

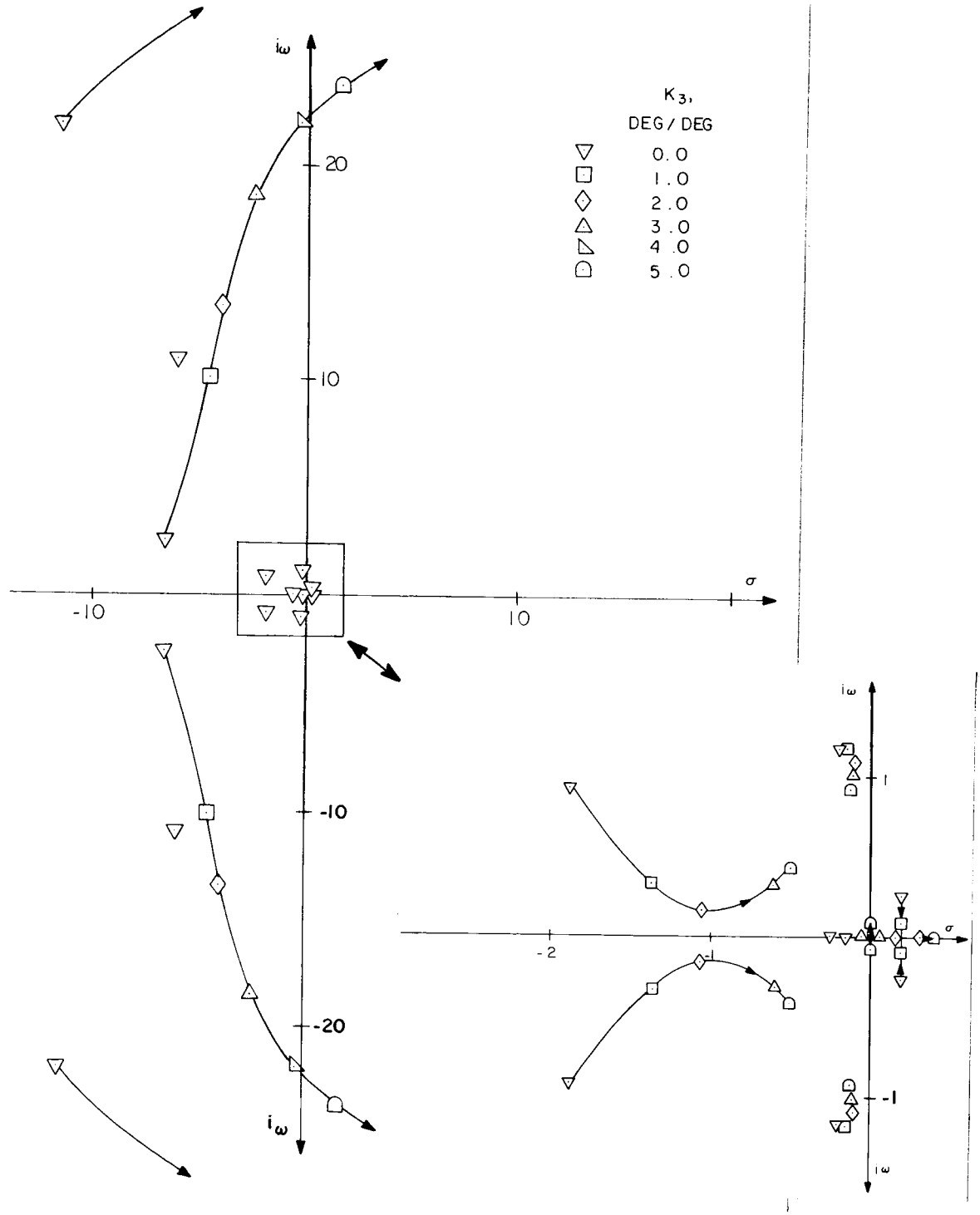

Figure 33. Closed Loop Locus of Roots for CH-53A with Delta-3/Oehmichen Feedback, Servos Included (100 Kt, 33,500 lb, 348 fscg).

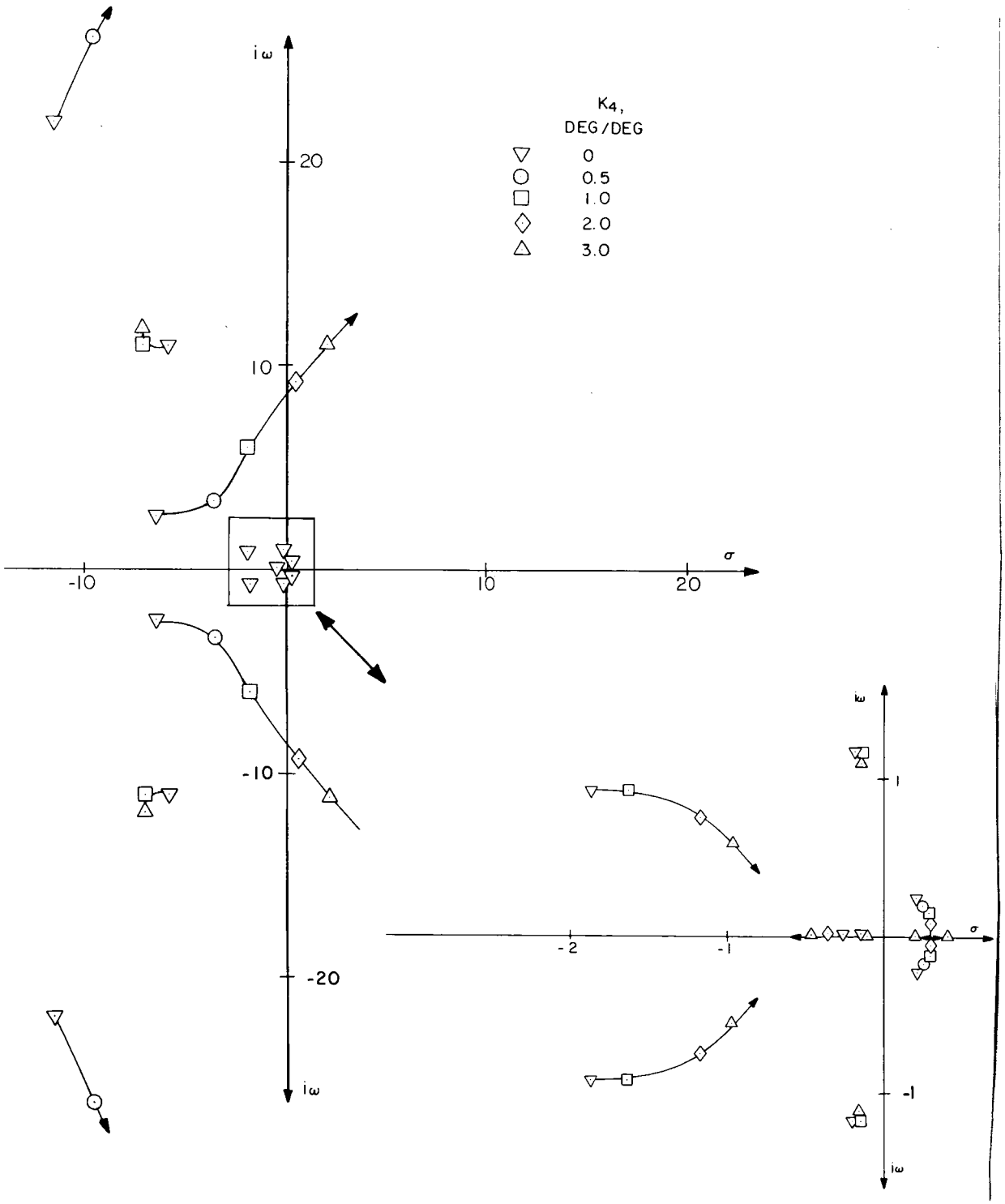

Figure 34. Closed Loop Locus of Roots for CH-53A with Type I Proportional Feedback, Servos Included (100 Kt, 33,500 lb, 348 fscg).

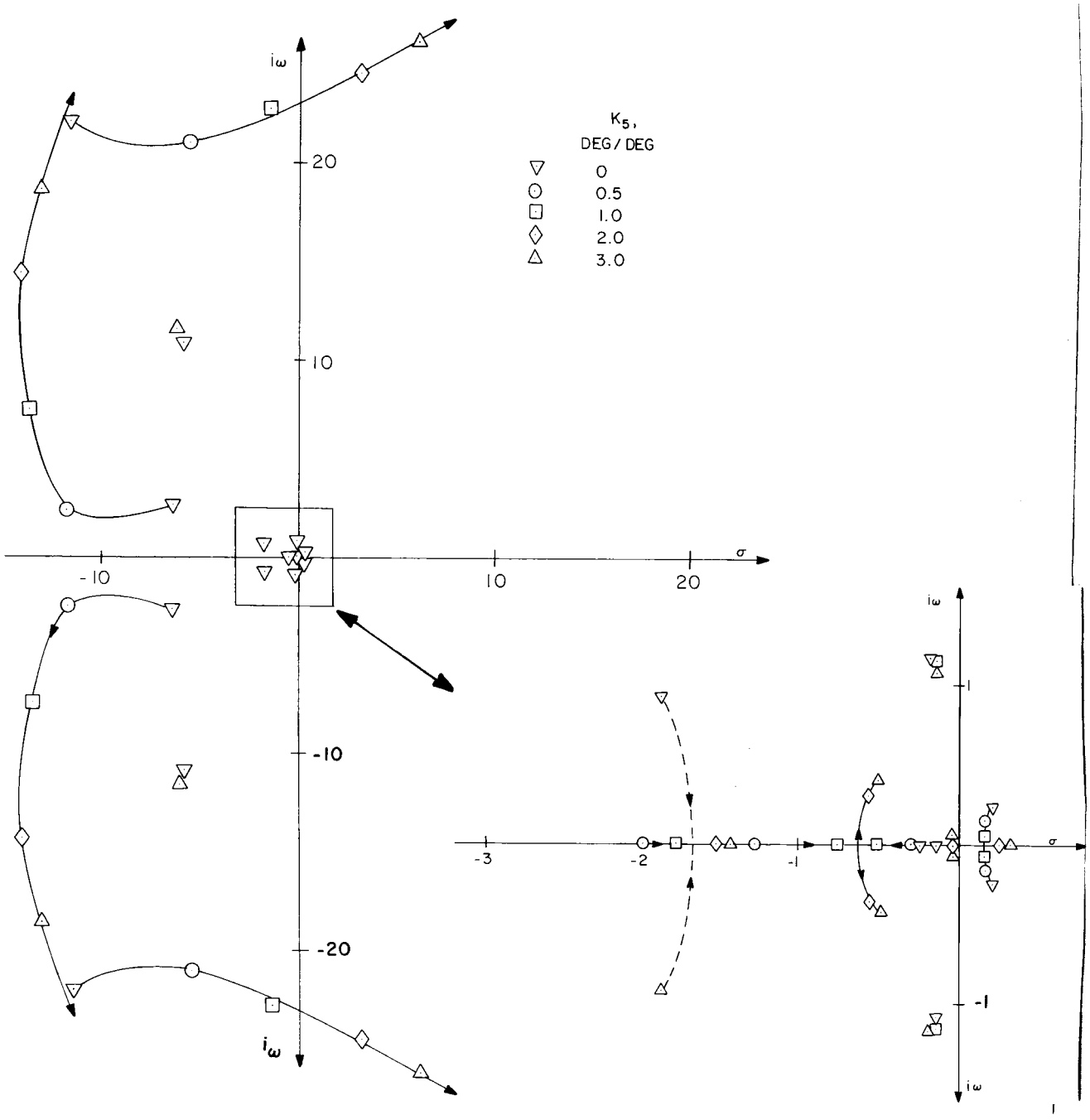

Figure 35. Closed Loop Locus of Roots for CH-53A with Type II Proportional Feedback, Servos Included (100 Kt, 33,500 lb, 348 fscg).

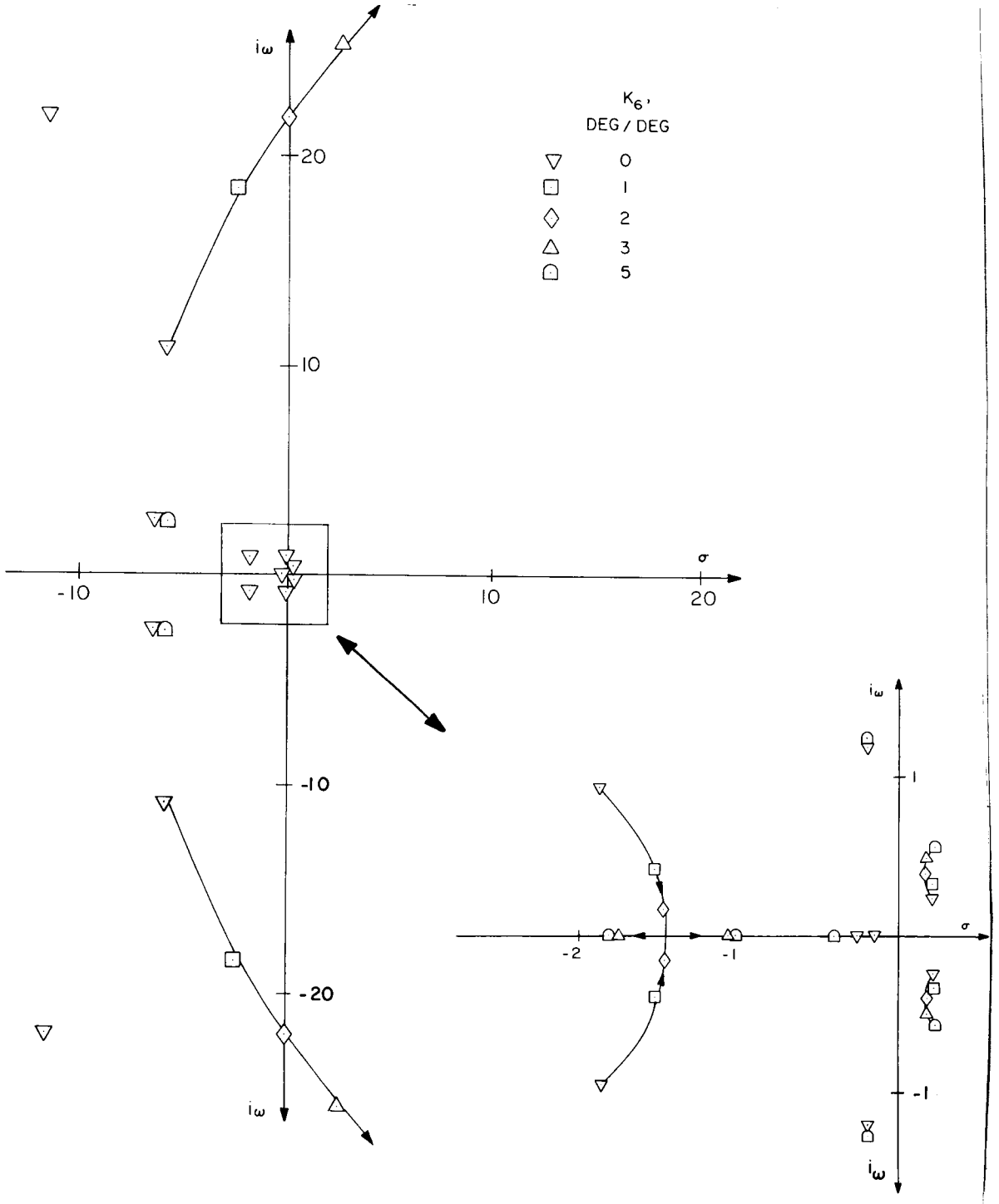

Figure 36. Closed Loop Locus of Roots for CH-53A with Pure Pitch-Cone Feedback, Servos Included (100 Kt, 33,500 lb, 348 fscg).

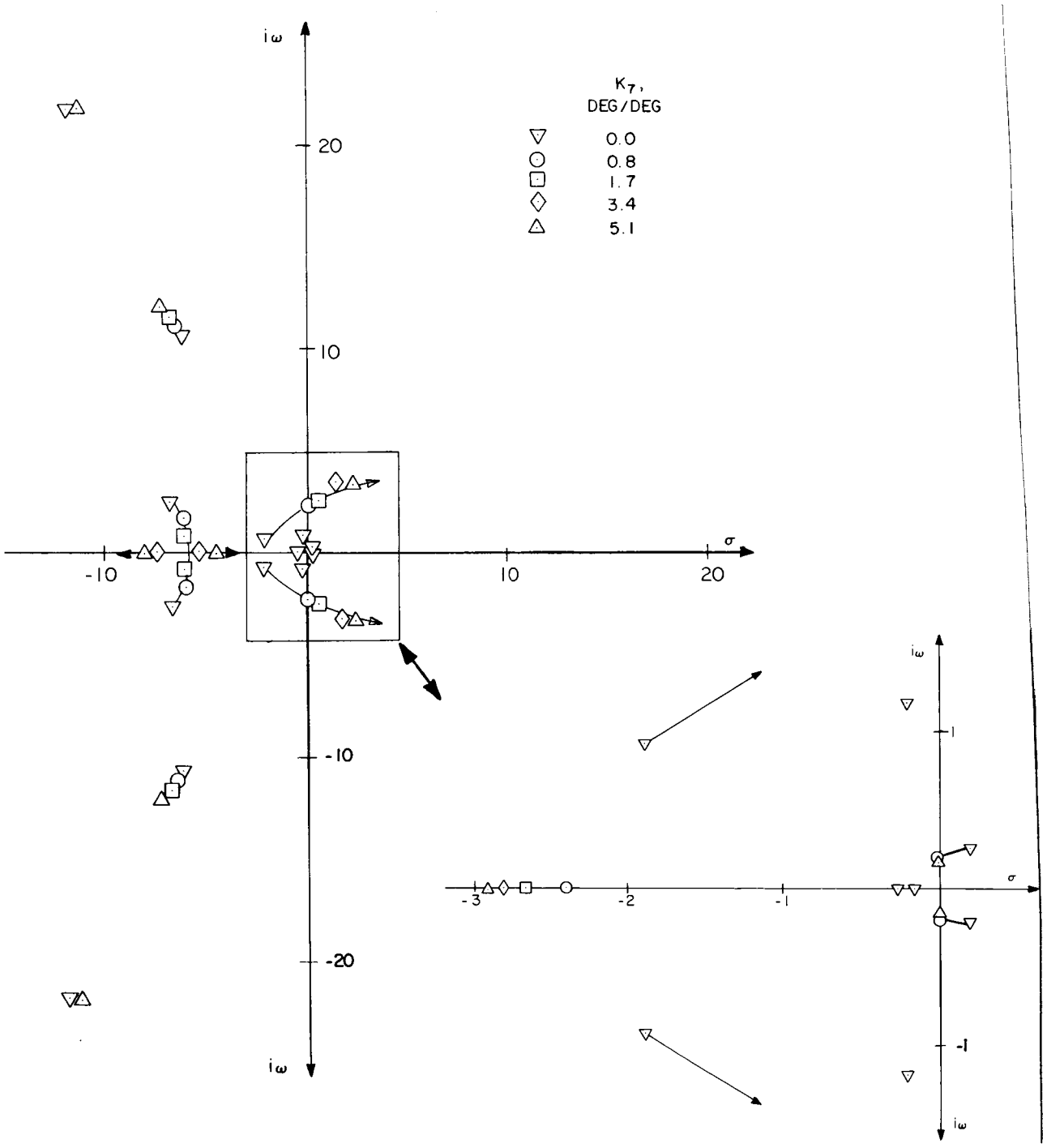

Figure 37. Closed Loop Locus of Roots for CH-53A with Angle-of-Attack Feedback, Servos Included (100 Kt, 33,500 lb, 348 fscg).

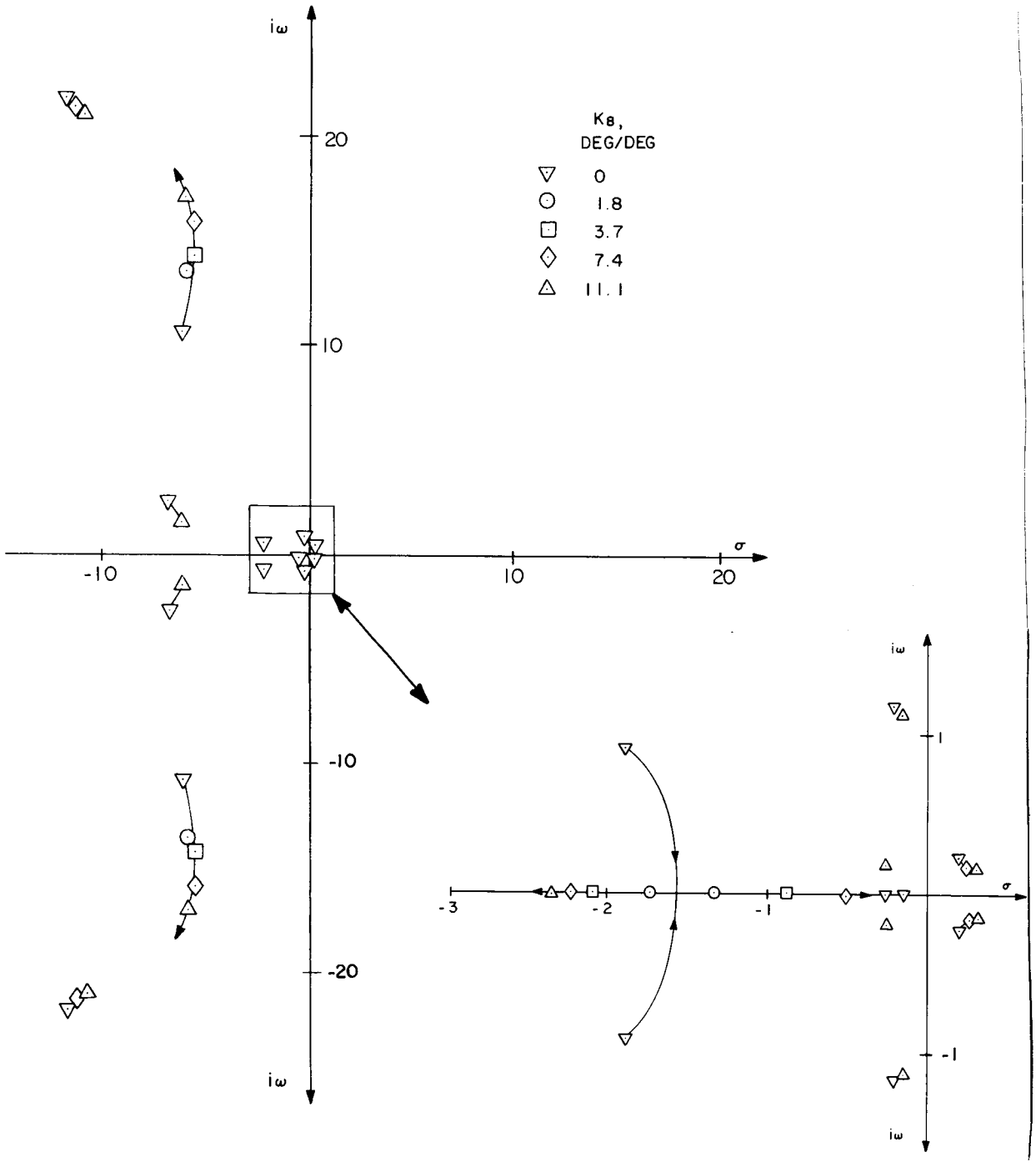

Figure 38. Closed Loop Locus of Roots for CH-53A with Normal Load Factor Feedback, Servos Included (100 Kt, 33,500 lb, 348 fscg).

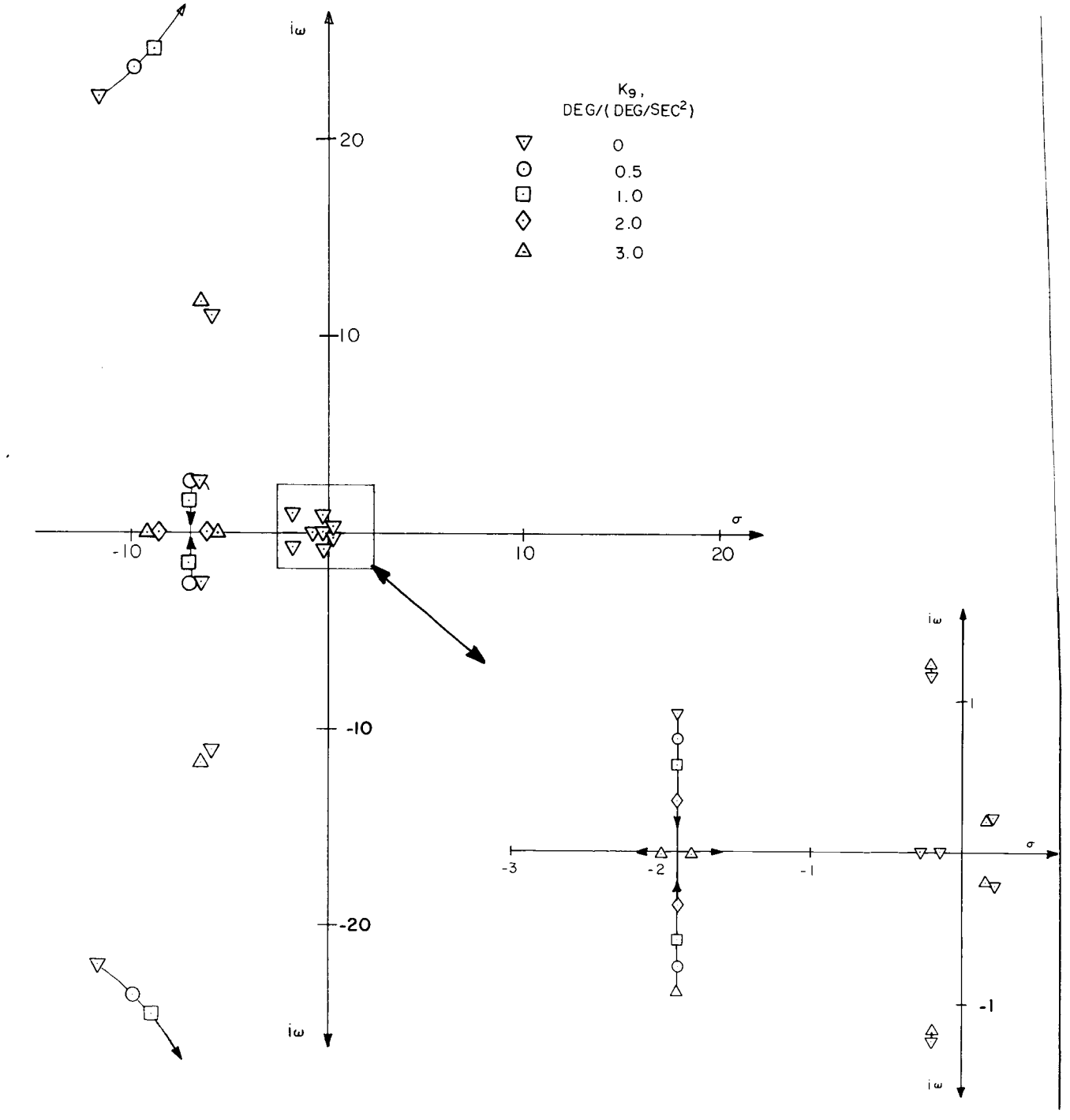

Figure 39. Closed Loop Locus of Roots for CH-53A with Pitch Acceleration Feedback, Servos Included (100 Kt, 33,500 lb, 348 fscg).

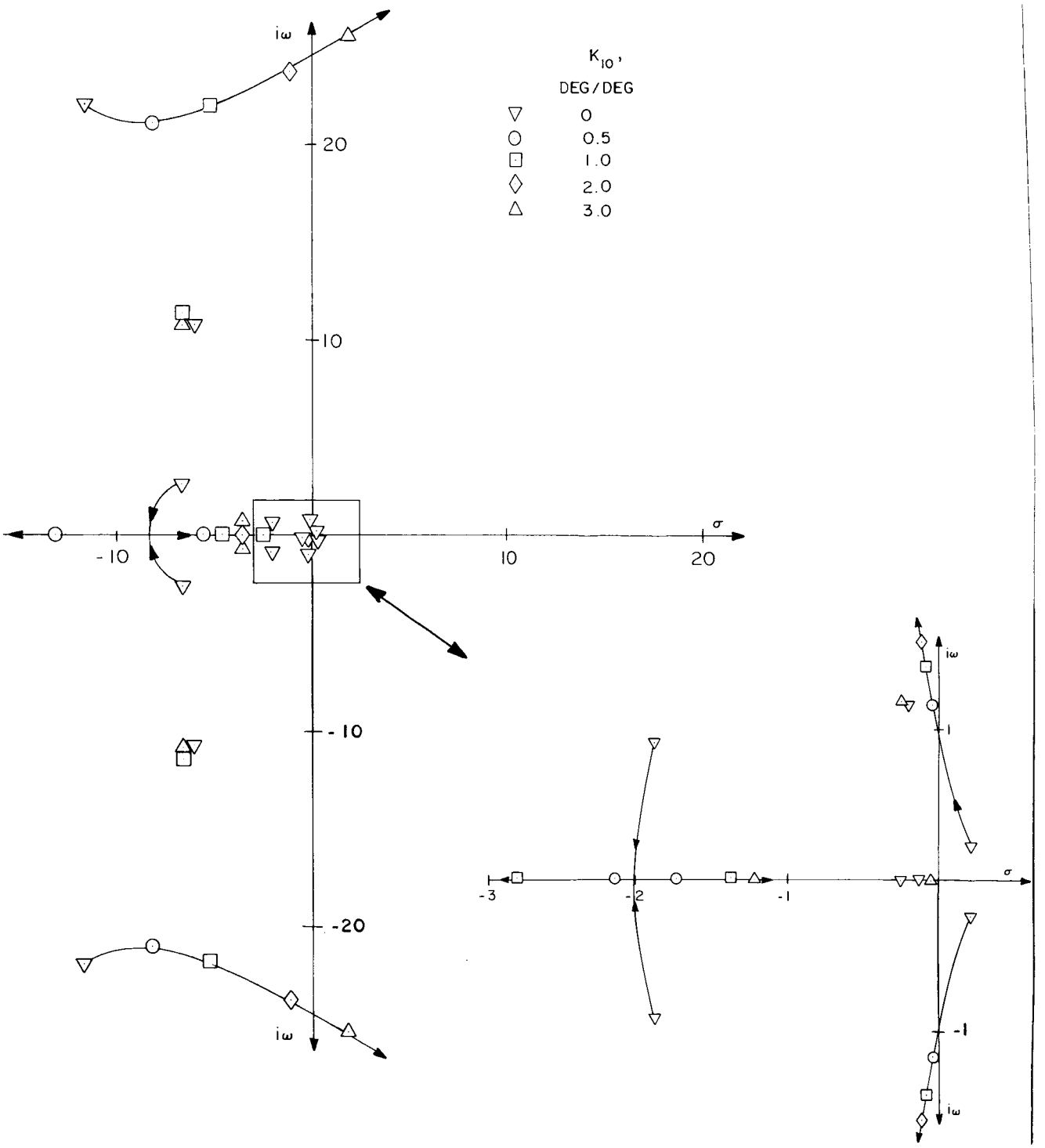

Figure 40. Closed Loop Locus of Roots for CH-53A with Rotor Vector Control Feedback, Servos Included (100 Kt, 33,500 lb, 348 fscg).

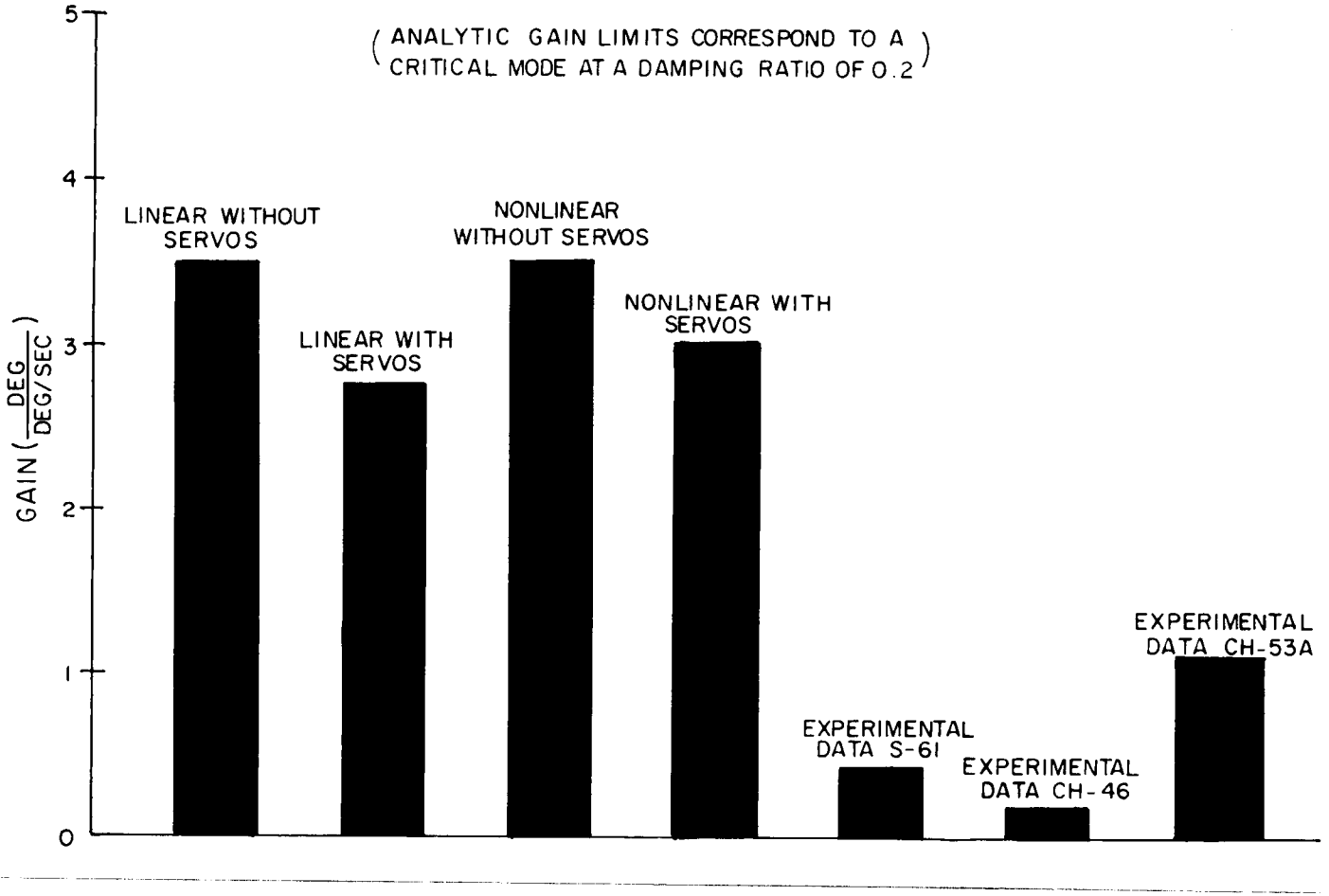

Figure 41. Theoretical and Empirical Gain Limits for Pitch Angular Rate Feedback.

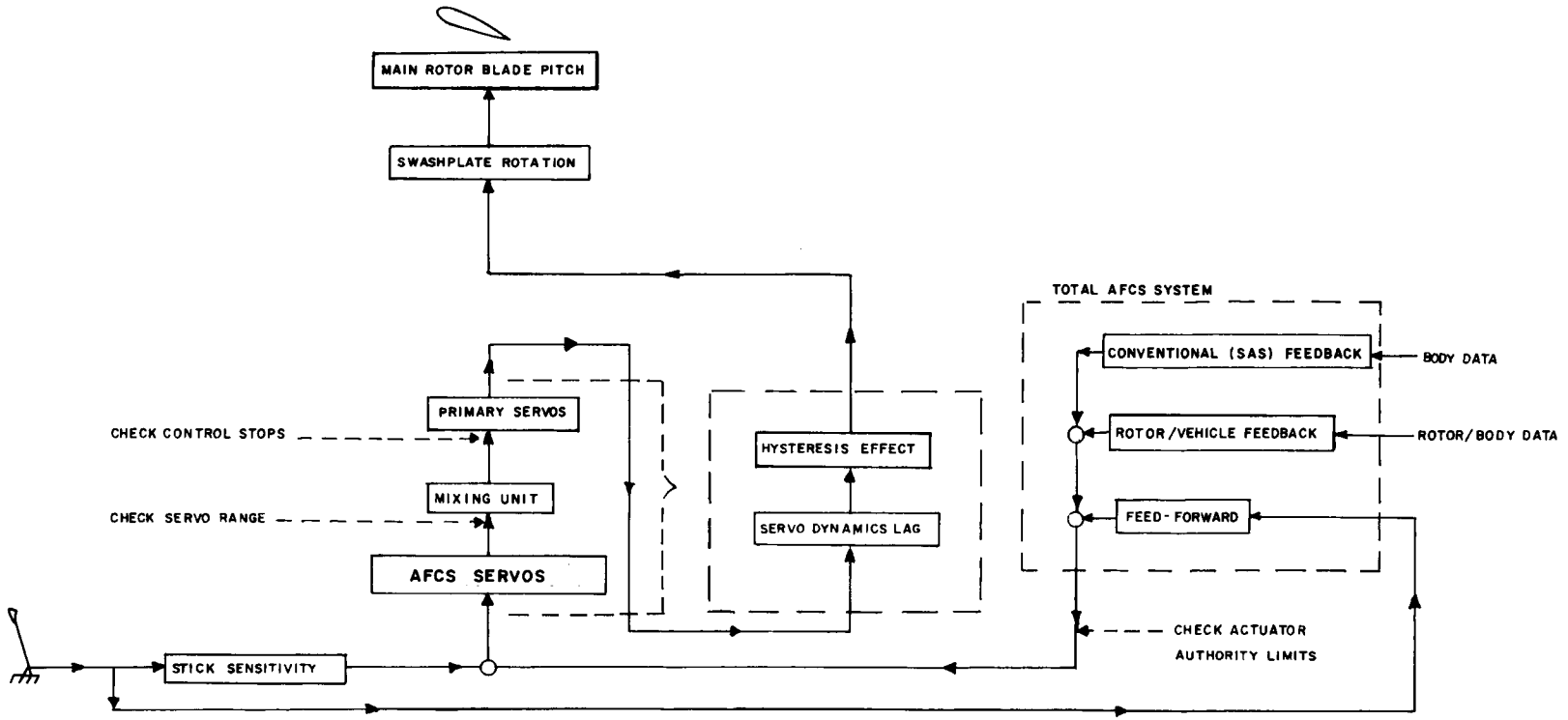

Figure 42. Nonlinear CH-53A Control System Representation.

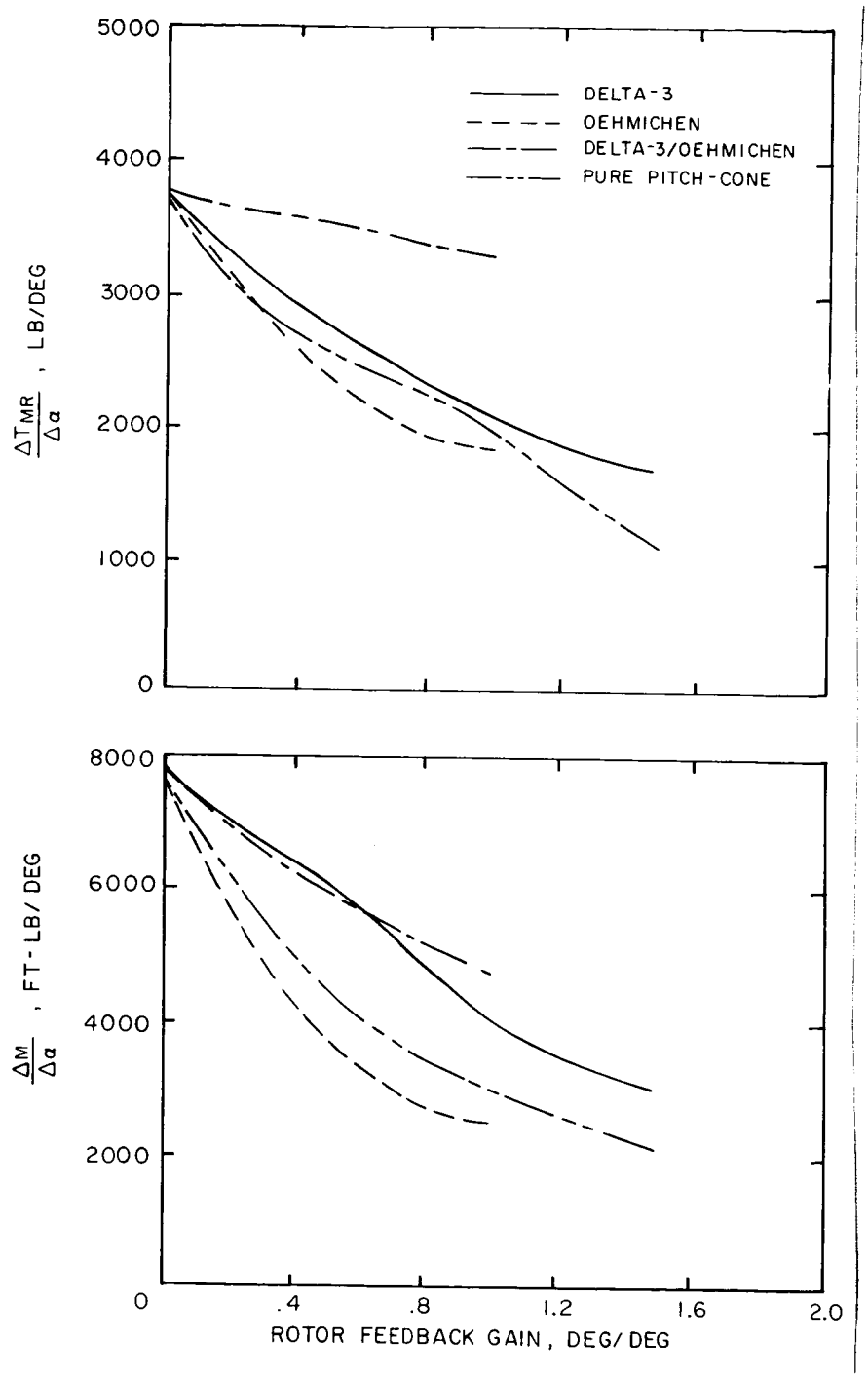

Figure 43. Quasi-Static Thrust and Pitching Moment Response of CH-53A Non-linear Model (150 Kt, 33,500 lb, 348 fscg) Due to Gust Disturbance, as a Function of Various Rotor Feedback Gains.

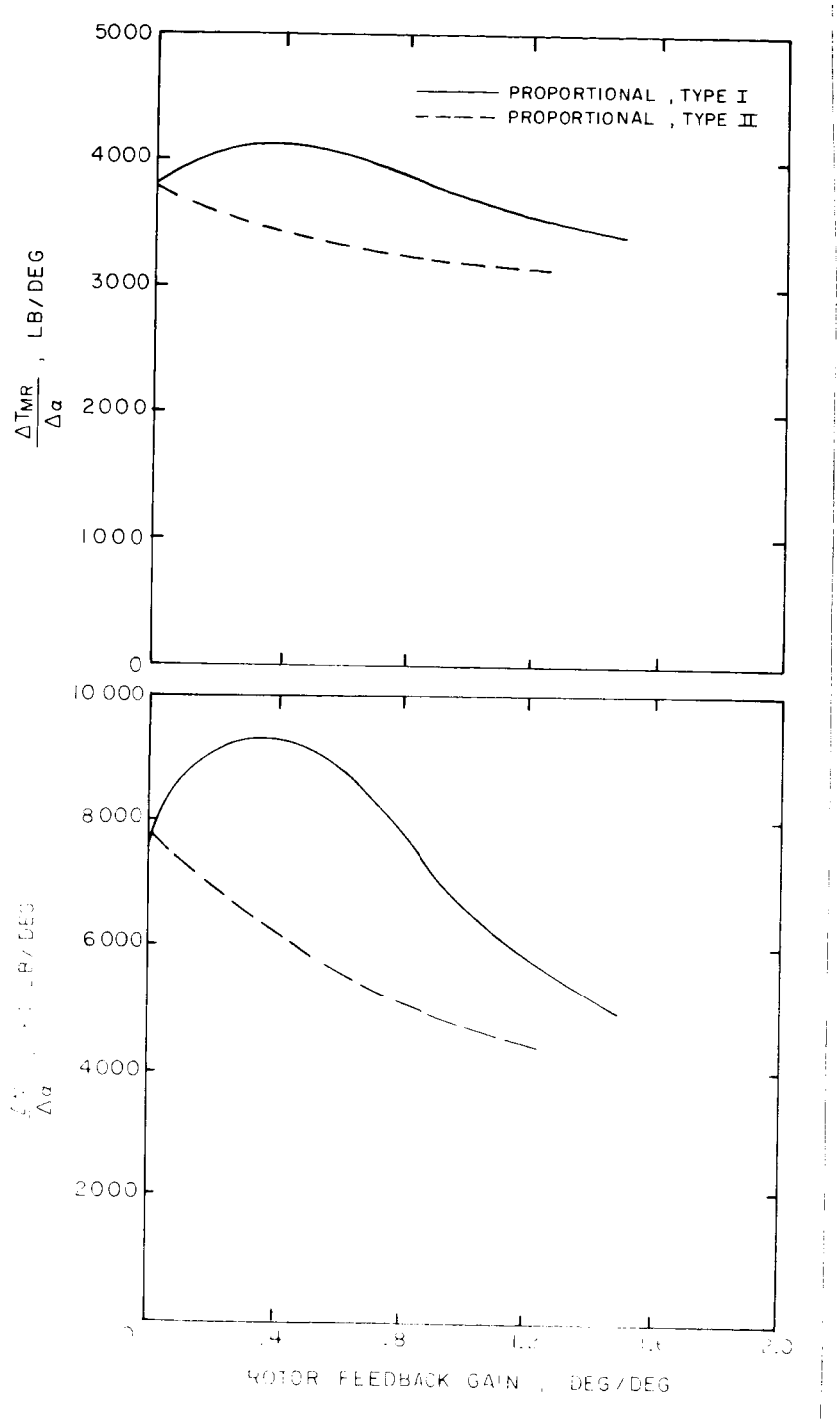

Figure 44. Quasi-Static Thrust and Pitching Moment Response of CH-53A Nonlinear Model (150 Kt, 33,500 lb, 348 fscg) Due to Gust Disturbance, as a Function of Various Rotor Feedback Gains.

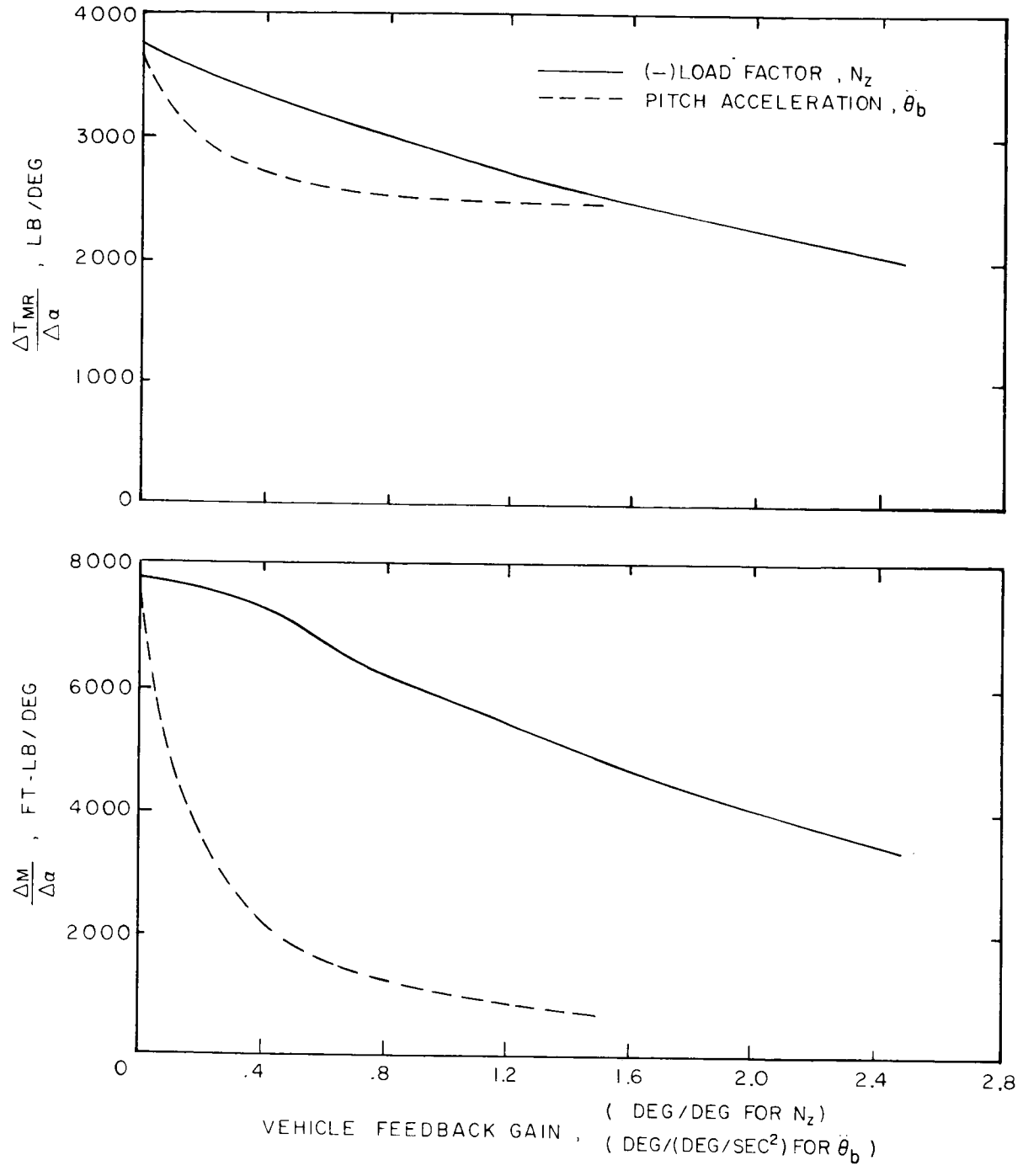

Figure 45. Quasi-Static Thrust and Pitching Moment Response of CH-53A Nonlinear Model (150 Kt, 33,500 lb, 348 fscg) Due to Gust Disturbance, as a Function of Normal Load Factor and Pitch Acceleration Feedback Gains.

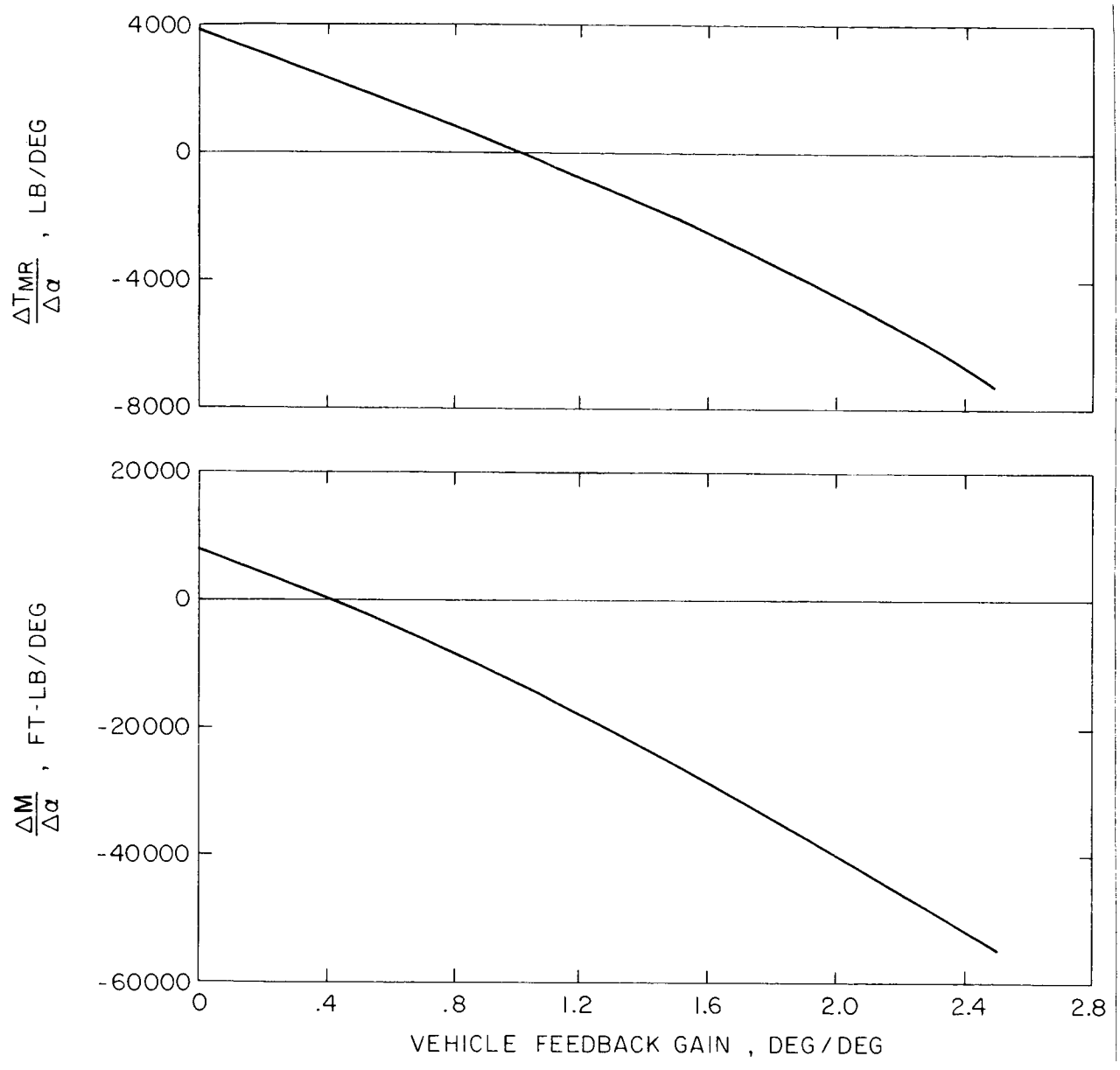

Figure 46. Quasi-Static Thrust and Pitching Moment Response of CH-53A Non-linear Model (150 Kt, 33,500 lb, 348 fscg) Due to Gust Disturbance, as a Function of Angle-of-Attack Feedback Gain.

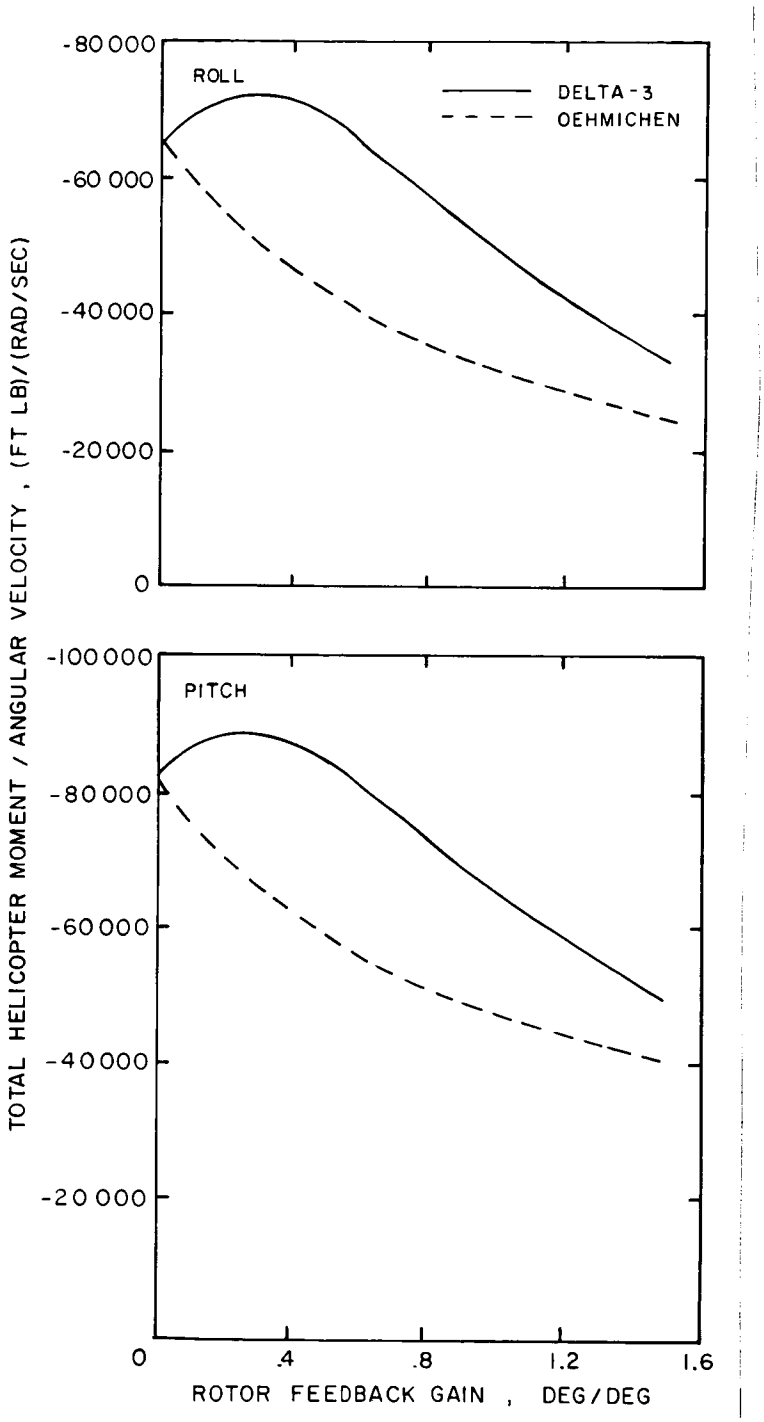

Figure 47. Roll and Pitch Damping of CH-53A Nonlinear Model (Hover, 33,500 lb, 348 fscg) as a Function of Delta-3 and Oehmichen Feedback Gains.

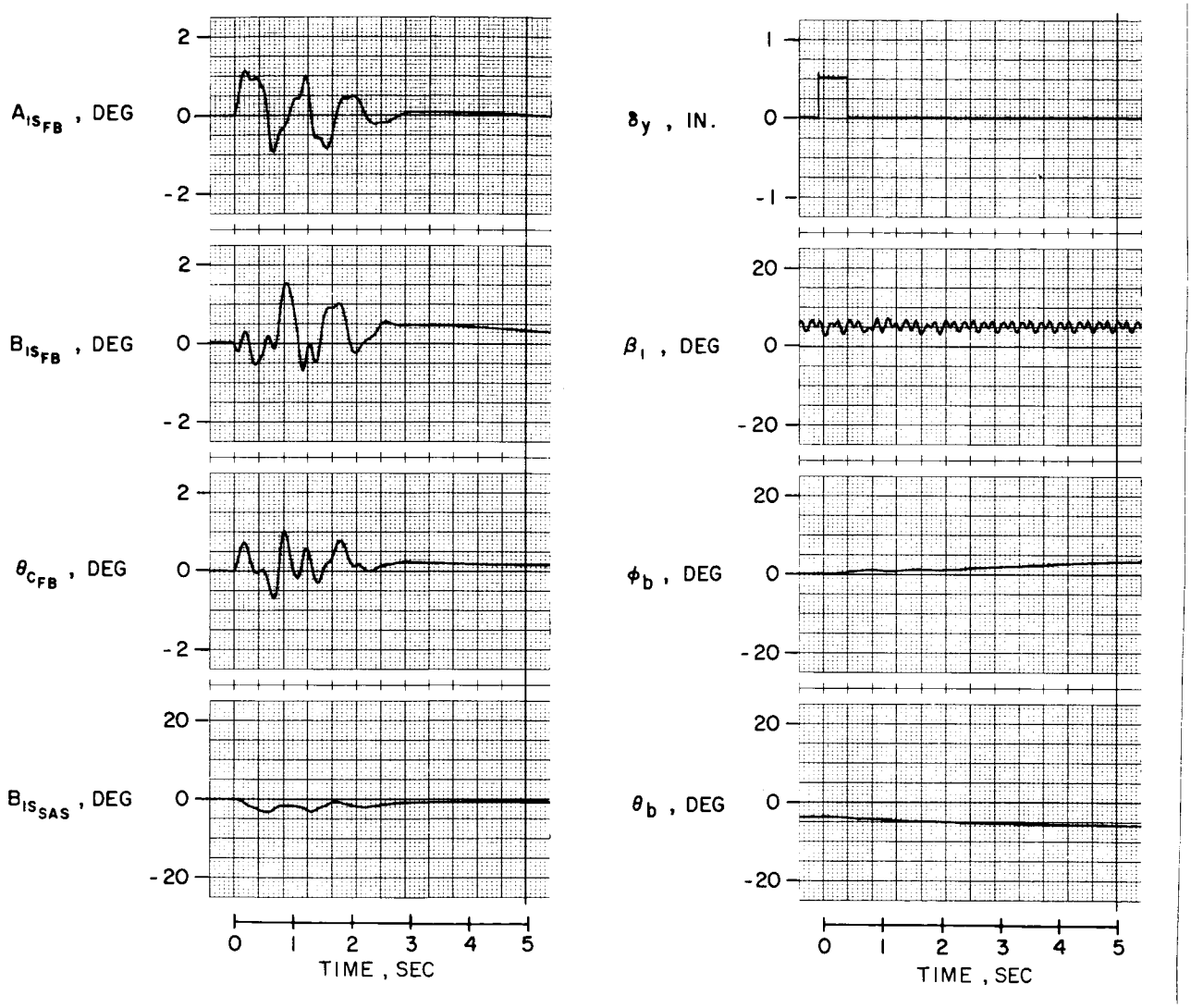

Figure 48. Stability Time Histories of CH-53A Nonlinear Model (33,500 lb, 348 fscg), Including Servos, at 150 Kt, Employing Delta-3 Feedback with K_1 = 1.75 deg/deg, Sampling 6 Blades 24 Times Per Revolution (Zero Roll Initial Trim).

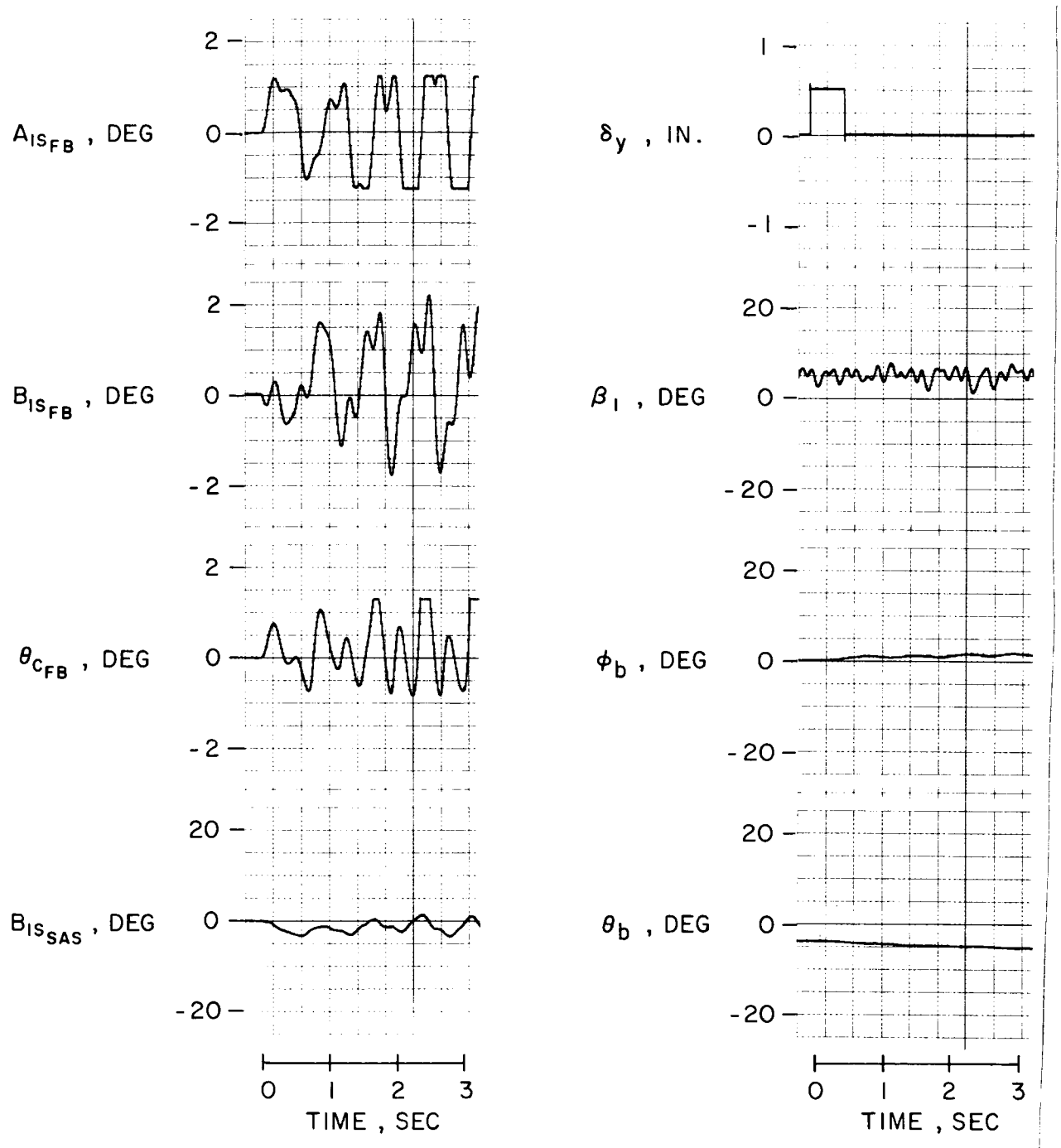

Figure 49. Stability Time Histories of CH-53A Nonlinear Model (33,500 lb, 348 fscg), Including Servos, at 150 Kt, Employing Delta-3 Feedback With K_1 = 1.85 deg/deg, Sampling 6 Blades 24 Times Per Revolution (Zero Roll Initial Trim).

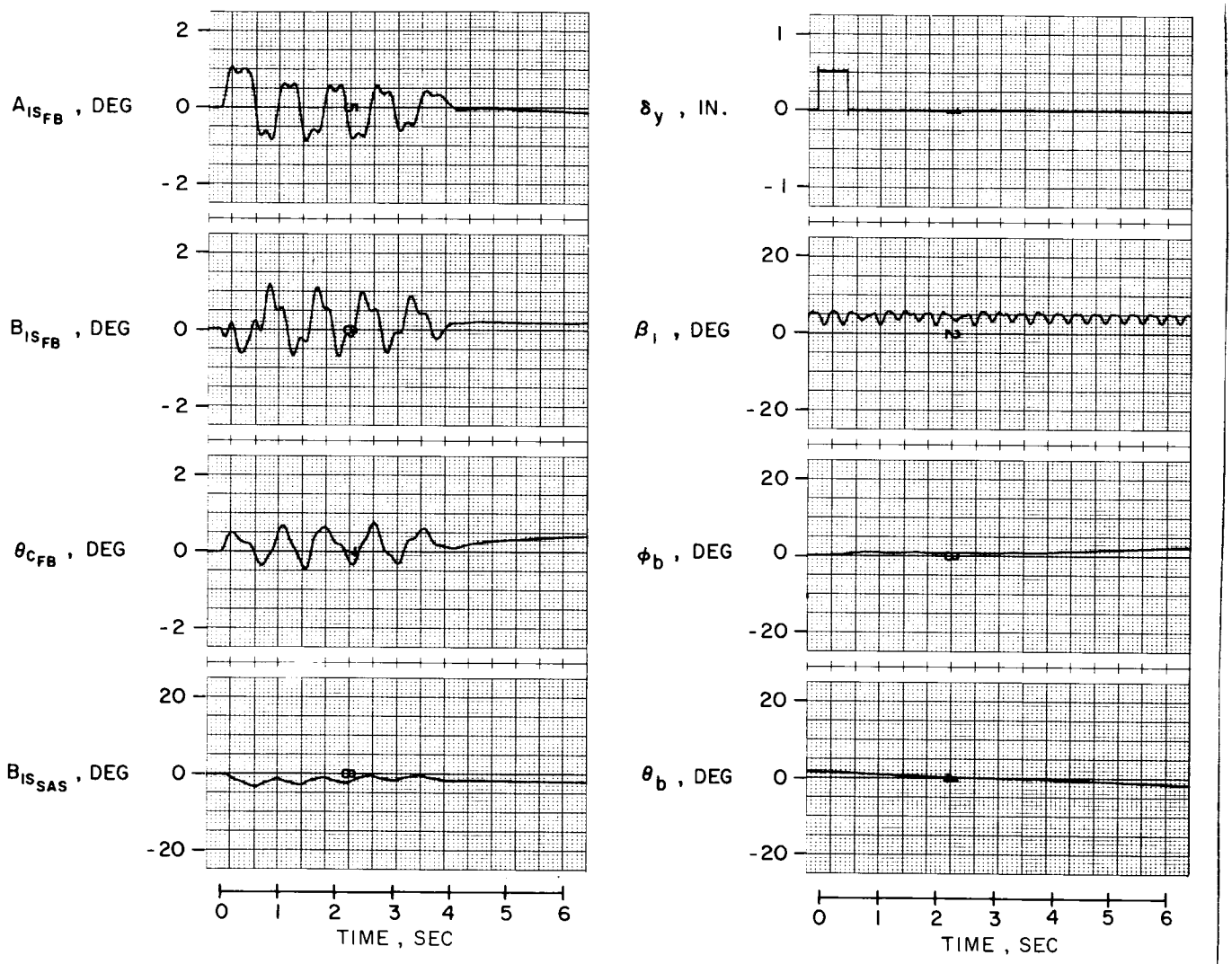

Figure 50. Stability Time Histories of CH-53A Nonlinear Model (33,500 lb, 348 fscg), Including Servos, at 100 Kt, Employing Delta-3 Feedback With K_1 = 1.85 deg/deg, Sampling 6 Blades 24 Times Per Revolution (Zero Roll Initial Trim).

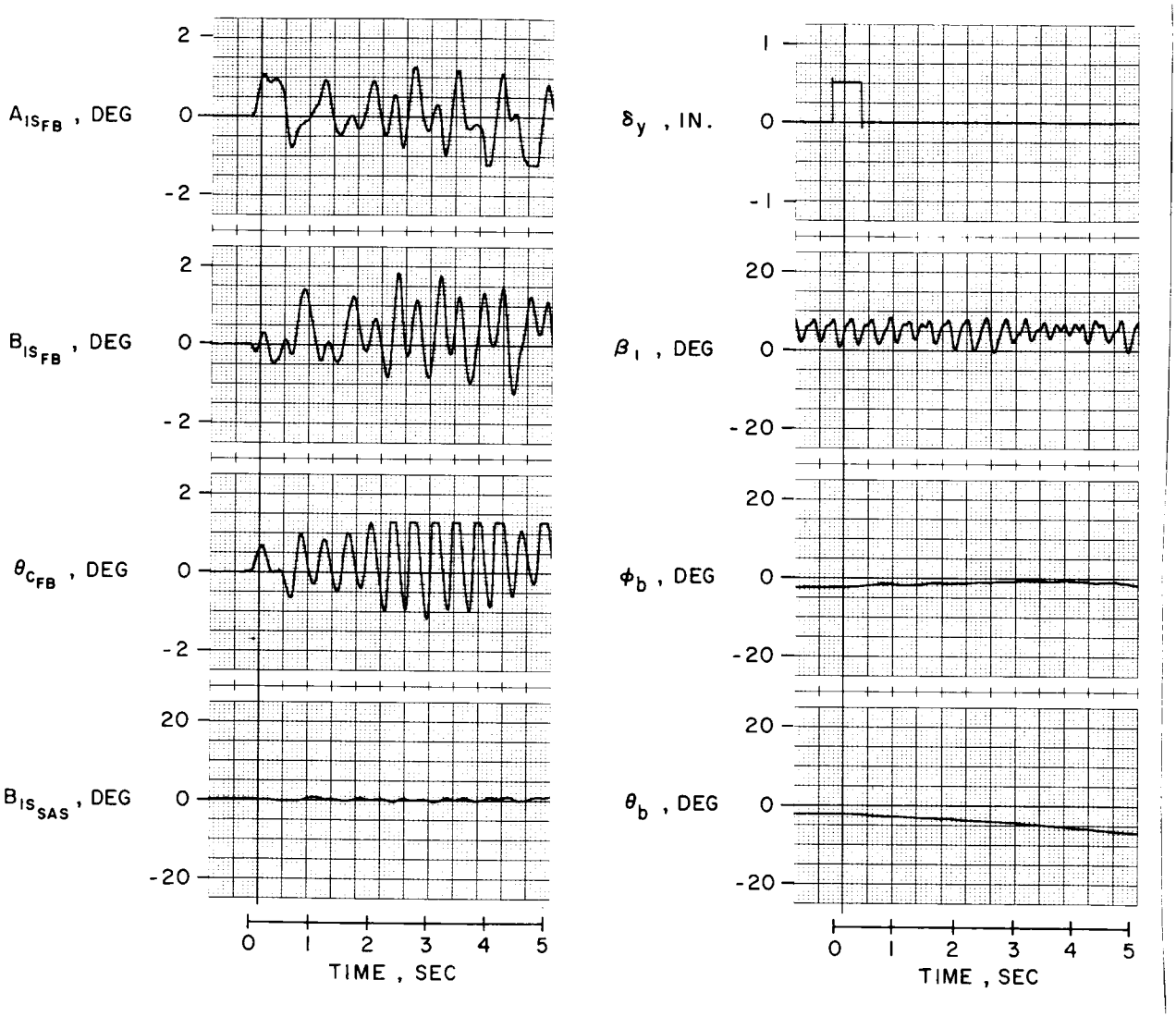

Figure 51. Stability Time Histories of CH-53A Nonlinear Model (33,500 lb, 348 fscg), Including Servos, at 150 Kt, Employing Delta-3 Feedback With K_1 = 1.65 deg/deg, Sampling 6 Blades 24 Times Per Revolution (Zero Sideslip Initial Trim).

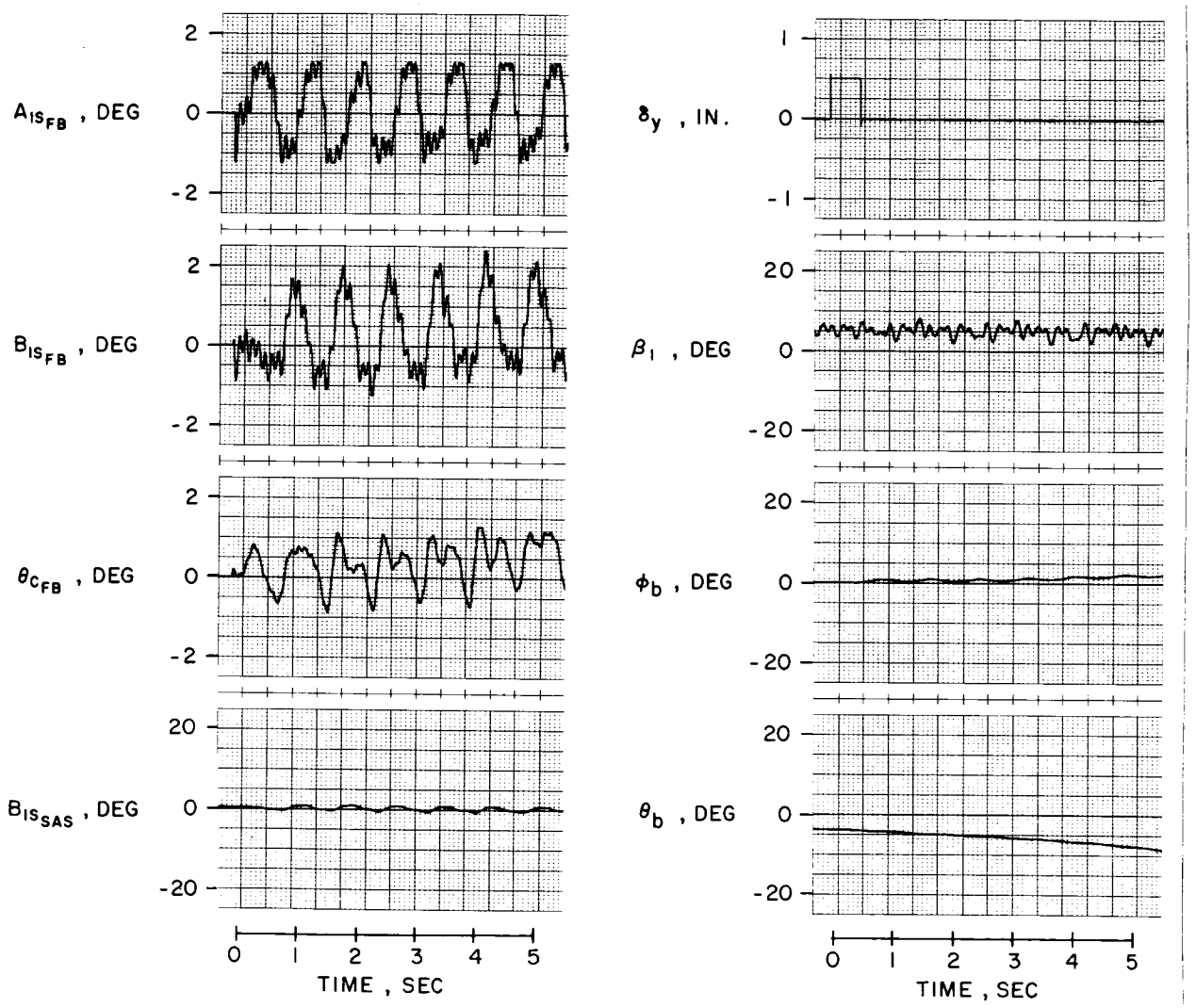

Figure 52. Stability Time Histories of CH-53A Nonlinear Model (33,500 lb, 348 fscg), Including Servos, at 150 Kt, Employing Delta-3 Feedback With K_1 = 1.75 deg/deg, Sampling 3 Blades 24 Times Per Revolution (Zero Roll Initial Trim).

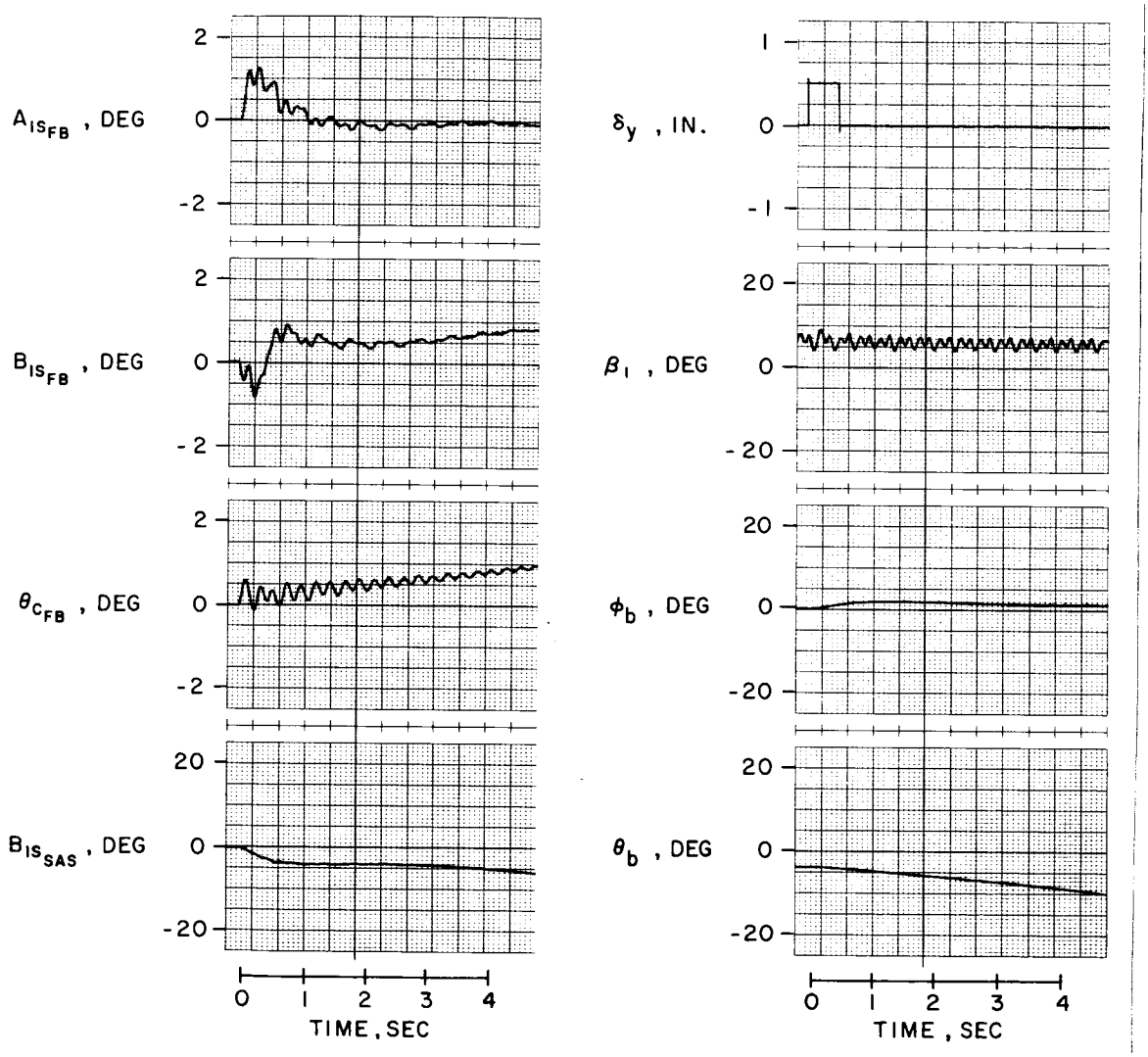

Figure 53. Stability Time Histories of CH-53A Nonlinear Model (33,500 lb, 348 fscg), Without Servos, and No Hysteresis, at 150 Kt, Employing Delta-3 Feedback with K_1 = 2.0 deg/deg, Sampling 6 Blades 24 Times Per Revolution (Zero Roll Initial Trim).

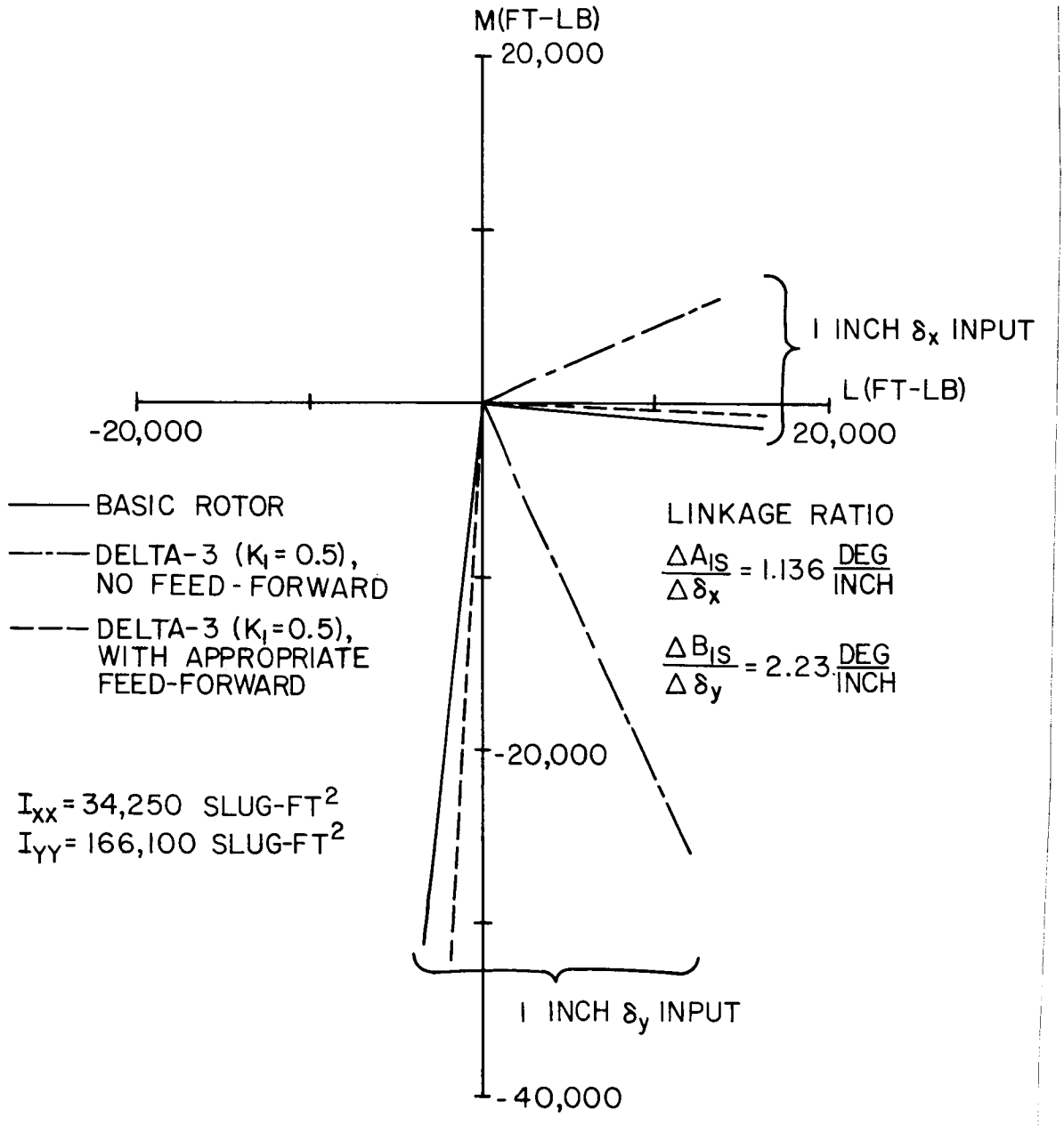

Figure 54. Quasi-Static Rolling and Pitching Moment Response of CH-53A Nonlinear Model (33,500 lb, 348 fscg) in Hover Due to Lateral and Longitudinal Cyclic Stick Step Inputs, as a Function of Delta-3 Feedback and Stick Feed-Forward.

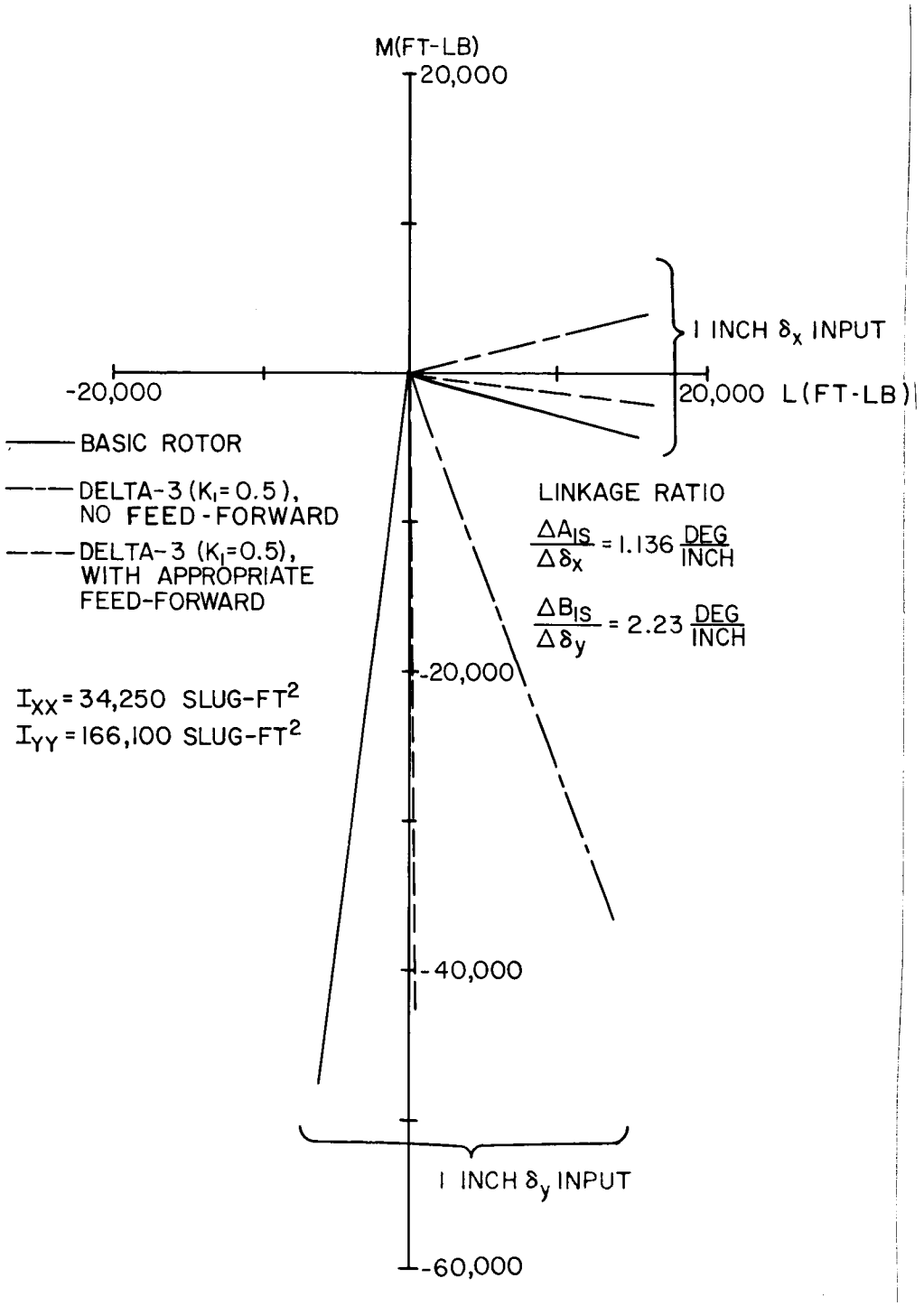

Figure 55. Quasi-Static Rolling and Pitching Moment Response of CH-53A Nonlinear Model (33,500 lb, 348 fscg) at 150 Kt Due to Lateral and Longitudinal Cyclic Stick Step Inputs, as a Function of Delta-3 Feedback and Stick Feed-Forward.

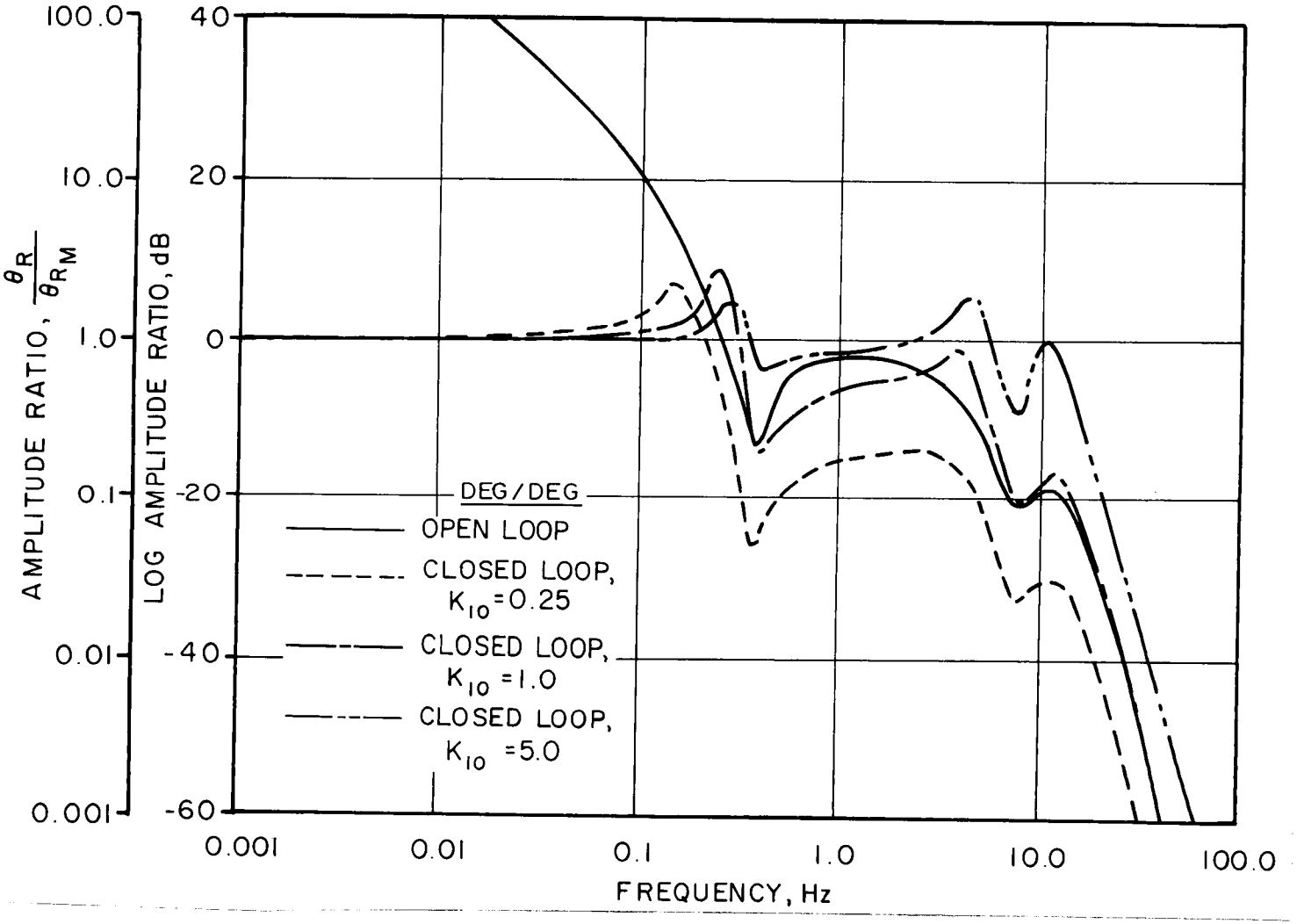

Figure 56. Linear Model Frequency Response of the CH-53A in Hover Employing Rotor Vector Control Feedback, as a Function of Feedback Gain.

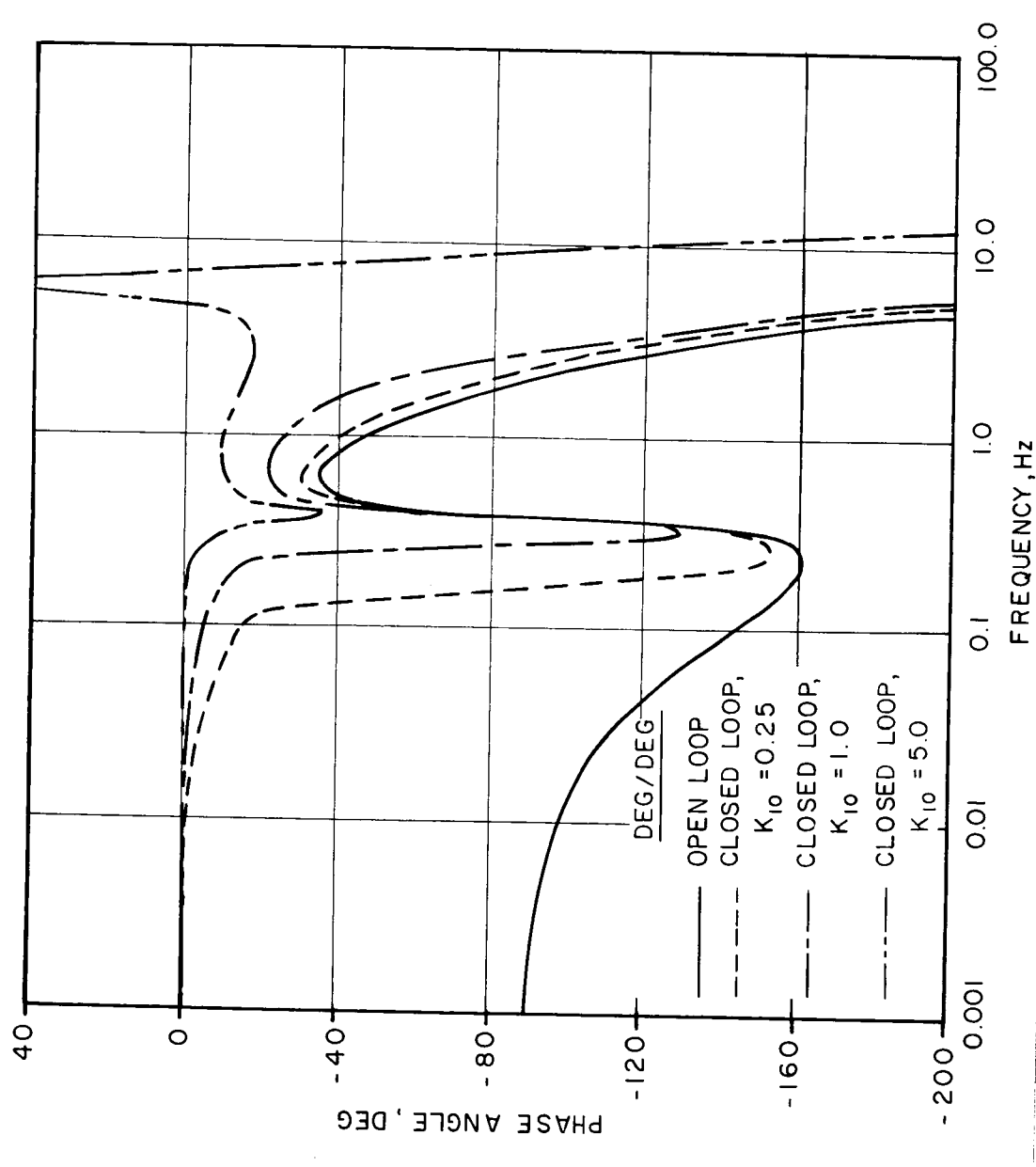

Figure 56. Concluded.

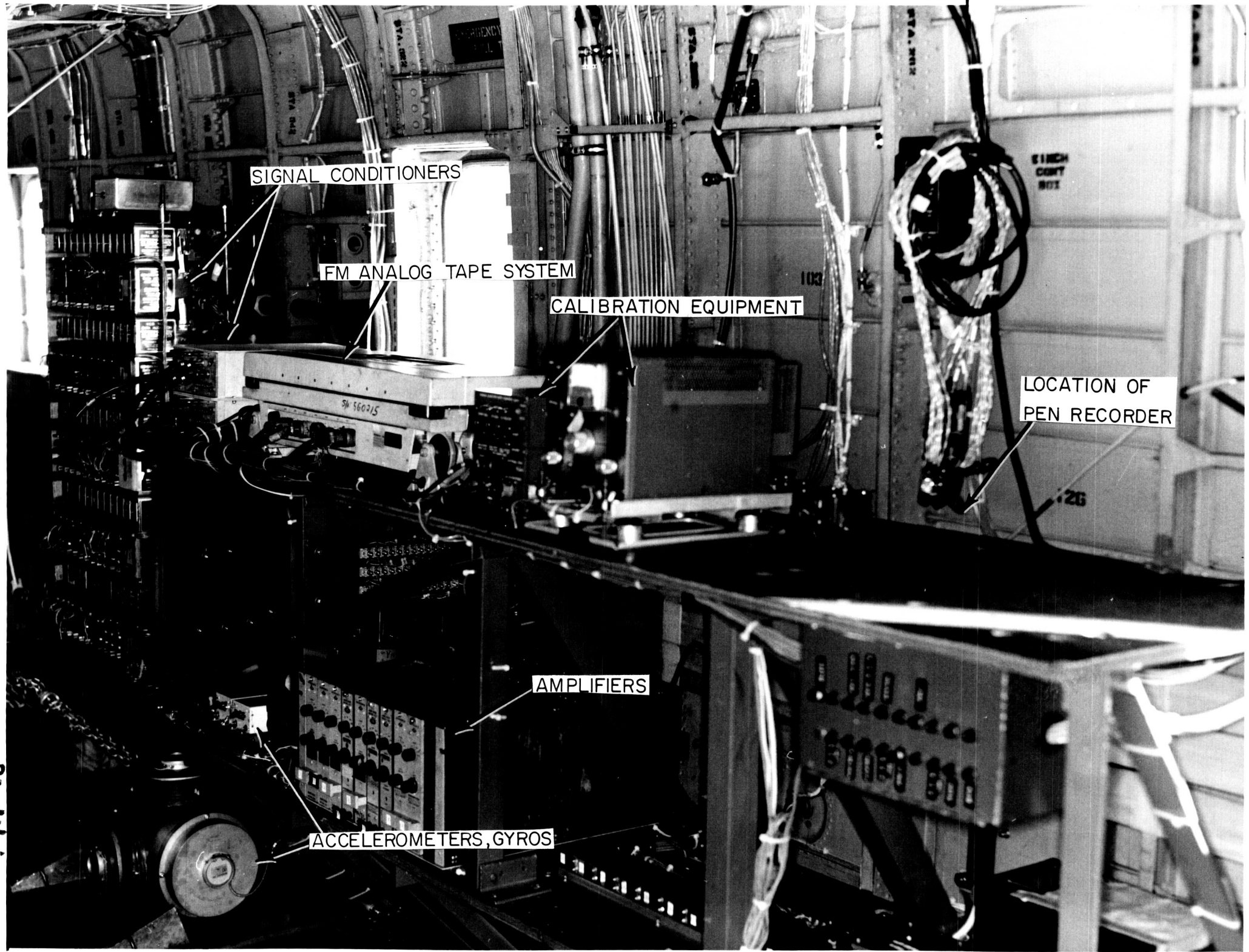
SIGNAL CONDITIONERS
FM ANALOG TAPE SYSTEM
CALIBRATION EQUIPMENT
LOCATION OF PEN RECORDER
AMPLIFIERS
ACCELEROMETERS, GYROS

Figure 57

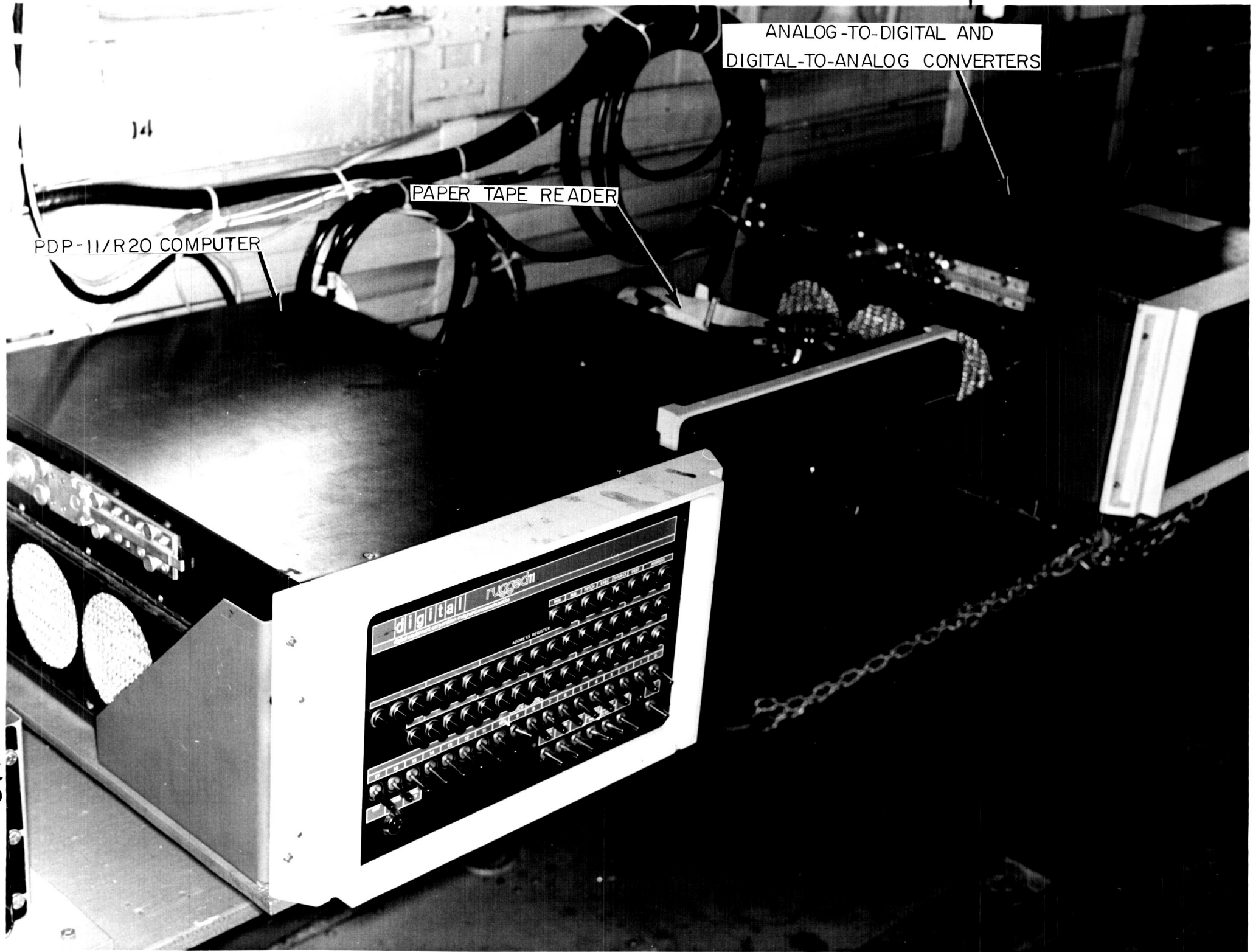
ANALOG-TO-DIGITAL AND
DIGITAL-TO-ANALOG CONVERTERS
PAPER TAPE READER
PDP-11/R20 COMPUTER

Figure 58

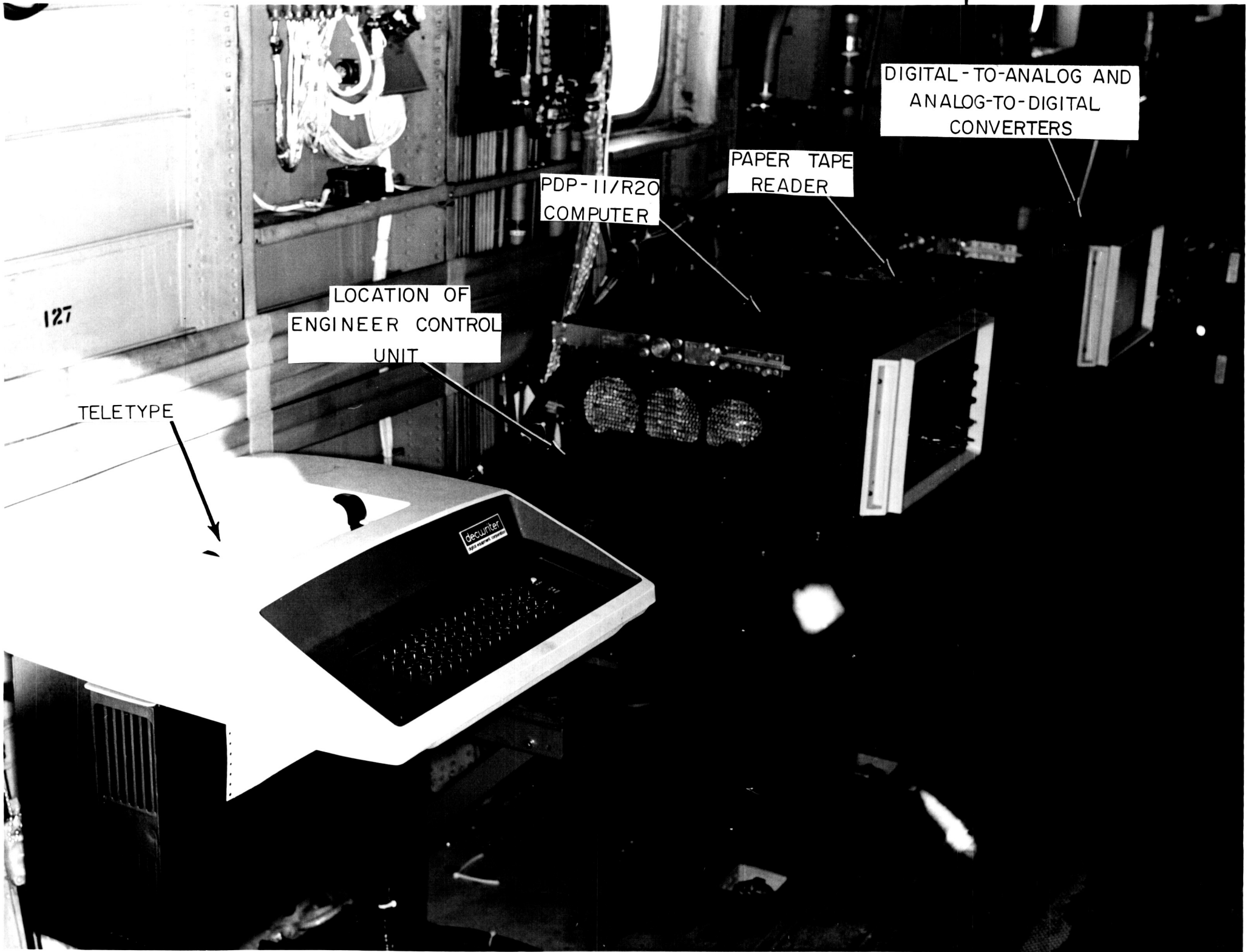
DIGITAL-TO-ANALOG AND
ANALOG-TO-DIGITAL
CONVERTERS
PAPER TAPE
READER
PDP-11/R20
COMPUTER
LOCATION OF
ENGINEER CONTROL
UNIT
TELETYPE
127
decwriter

Figure 59

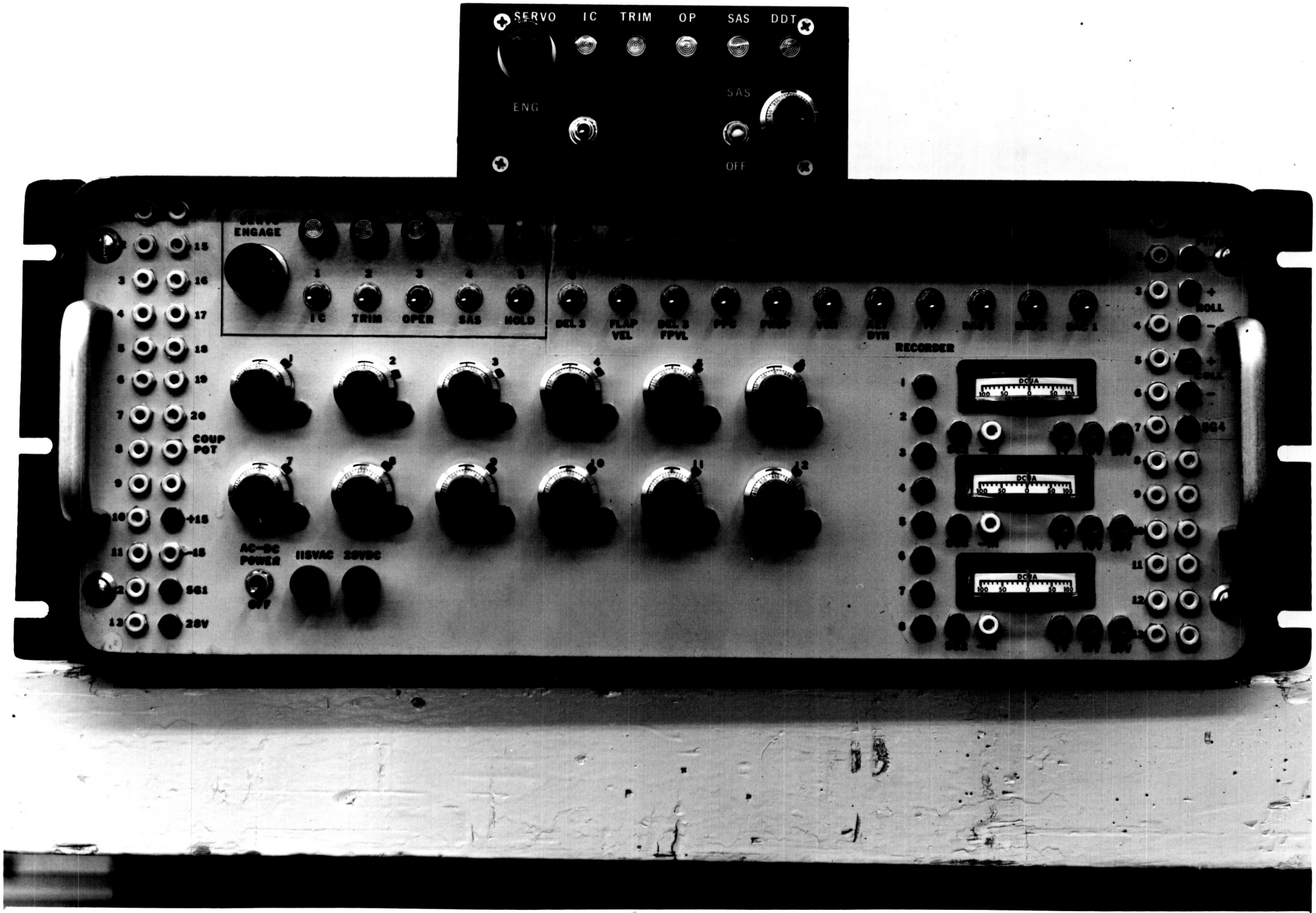
SERVO
IC
TRIM
OP
SAS
DDT
ENG
SAS
OFF
SERVO ENGAGE
1
2
3
4
5
IC
TRIM
OPER
SAS
HOLD
DEL 3
FLAP VEL
DEL 2 FPVL
RECORDER
COUP POT
+15
-15
SG1
28V
AC-DC POWER
OFF
115VAC
28VDC
ROLL
SG4

Figure 60

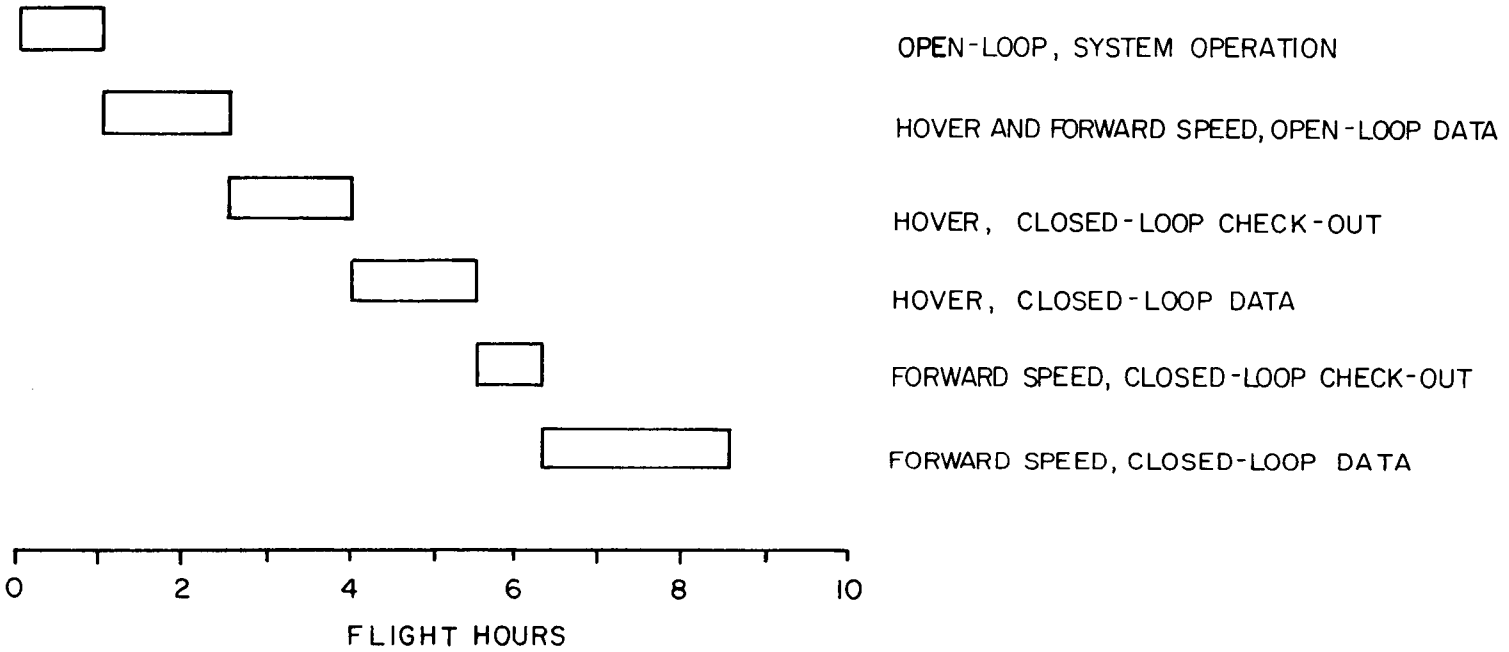

Figure 61. Rotor/Vehicle State Feedback Hours of Flight Testing.

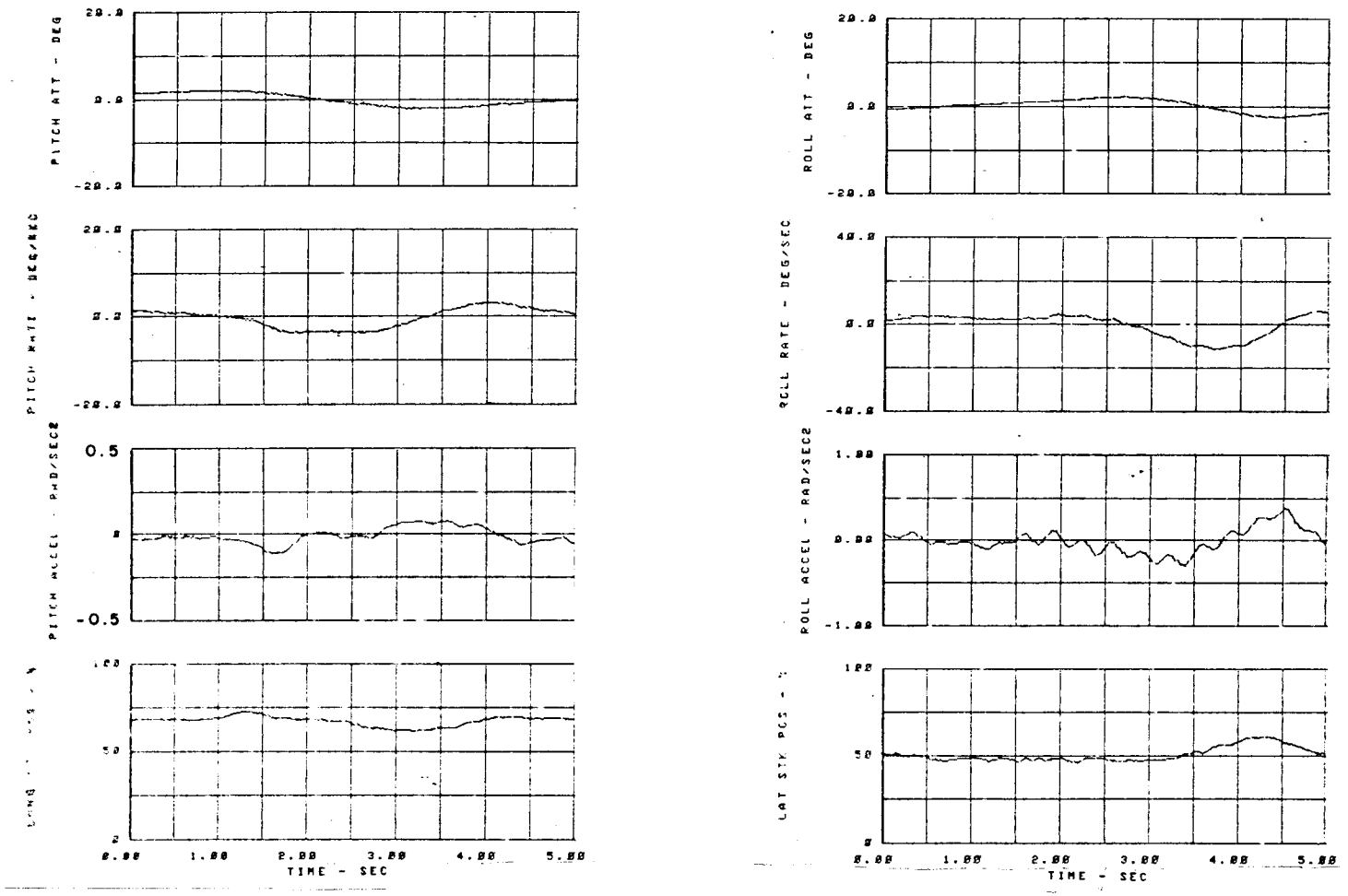

Figure 62. Example of Processed Rotor/Vehicle State Feedback Flight Investigation Time History Data (CH-53A at 100 Kts With Delta-3 = 0.5 deg/deg).

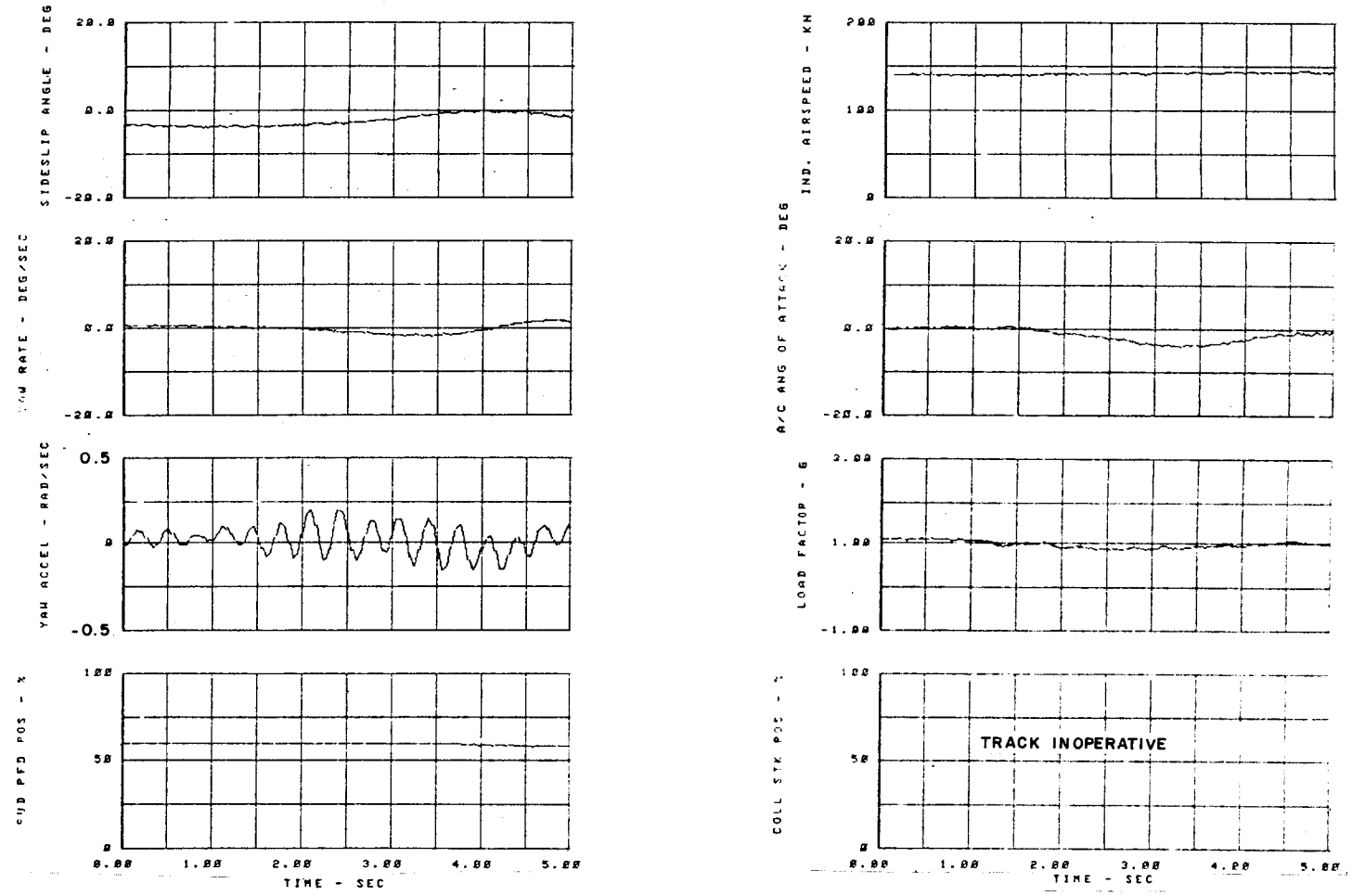

Figure 62. - Continued.

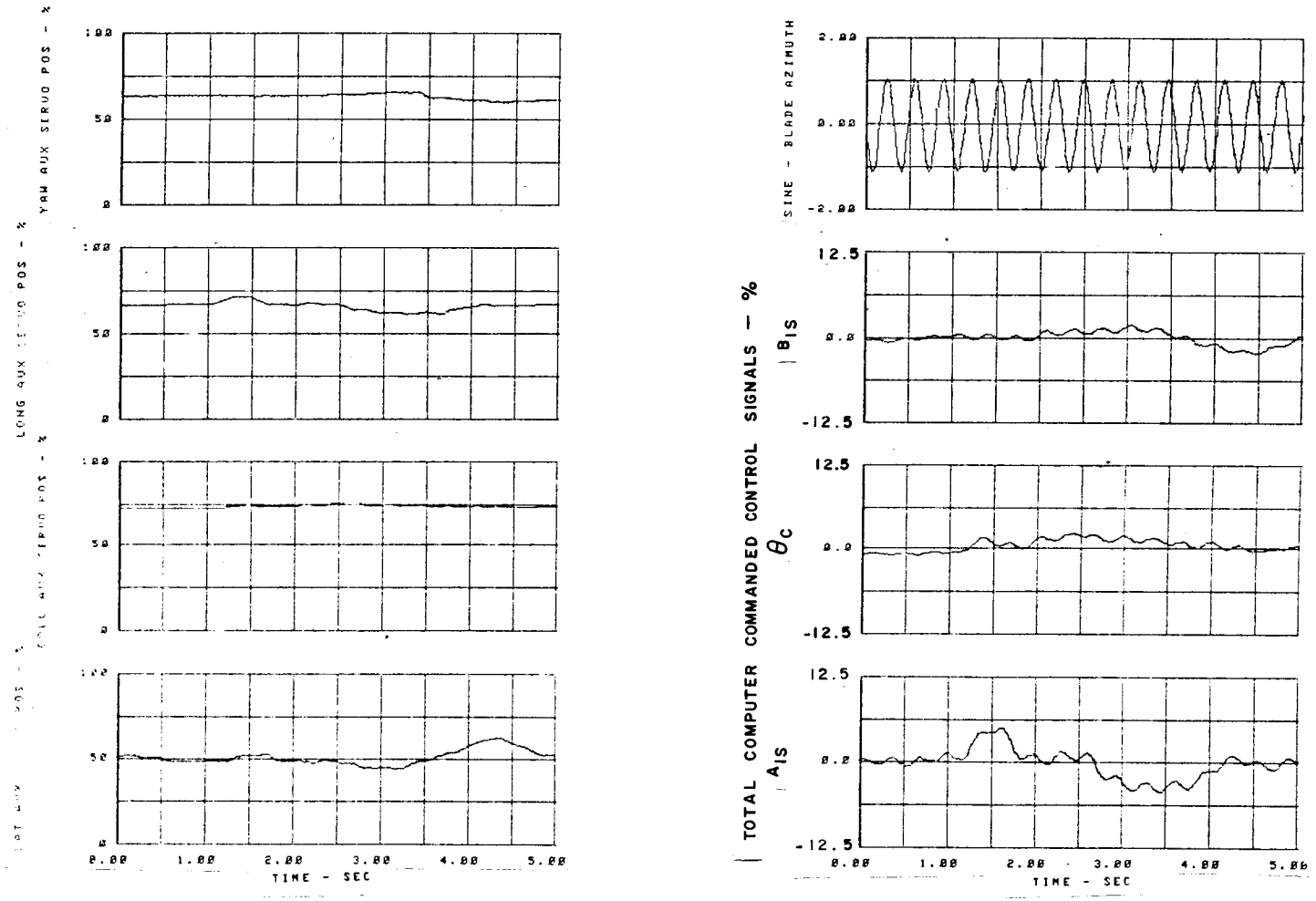

Figure 62. - Continued.

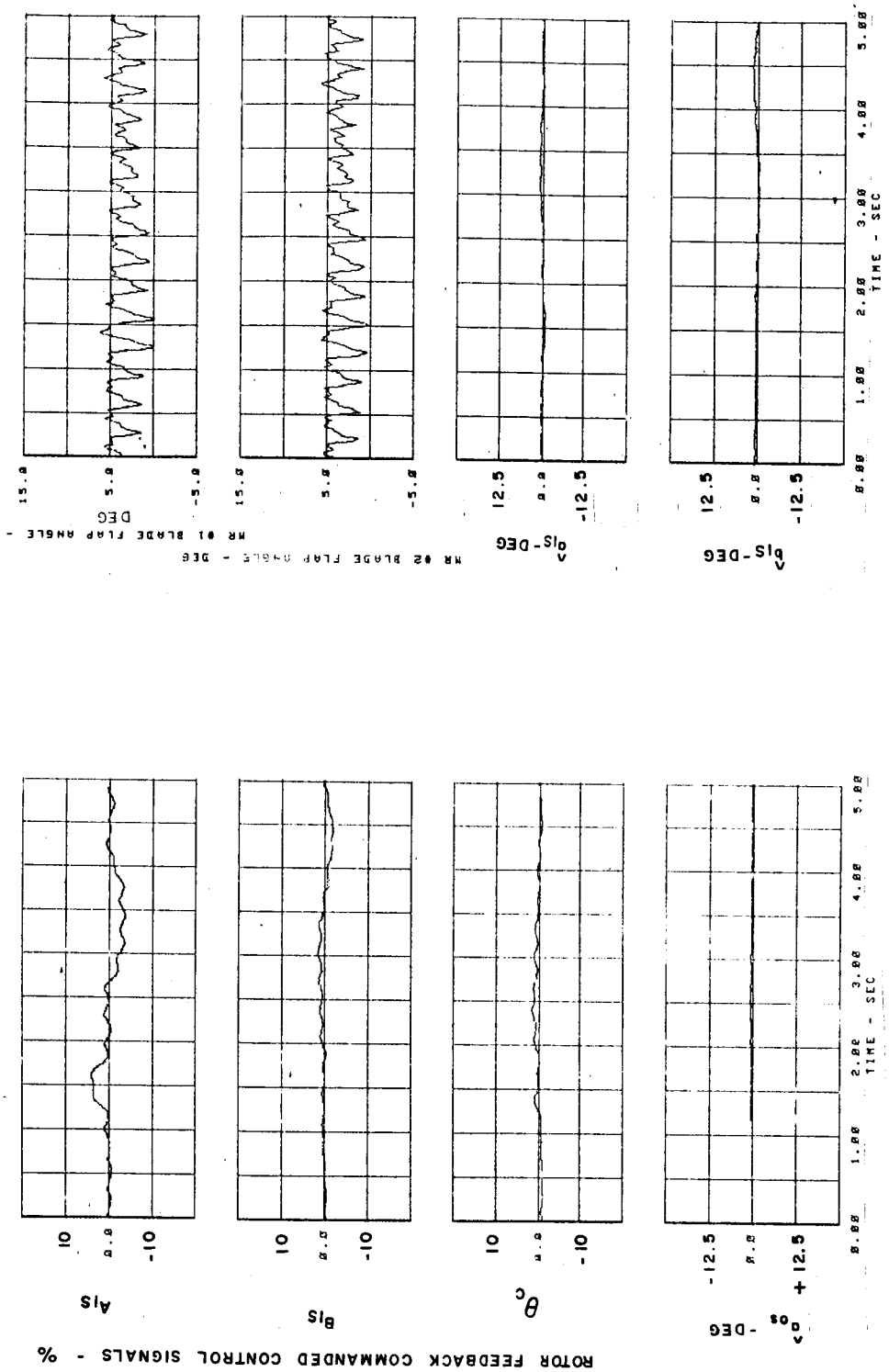

Figure 62. - Continued.

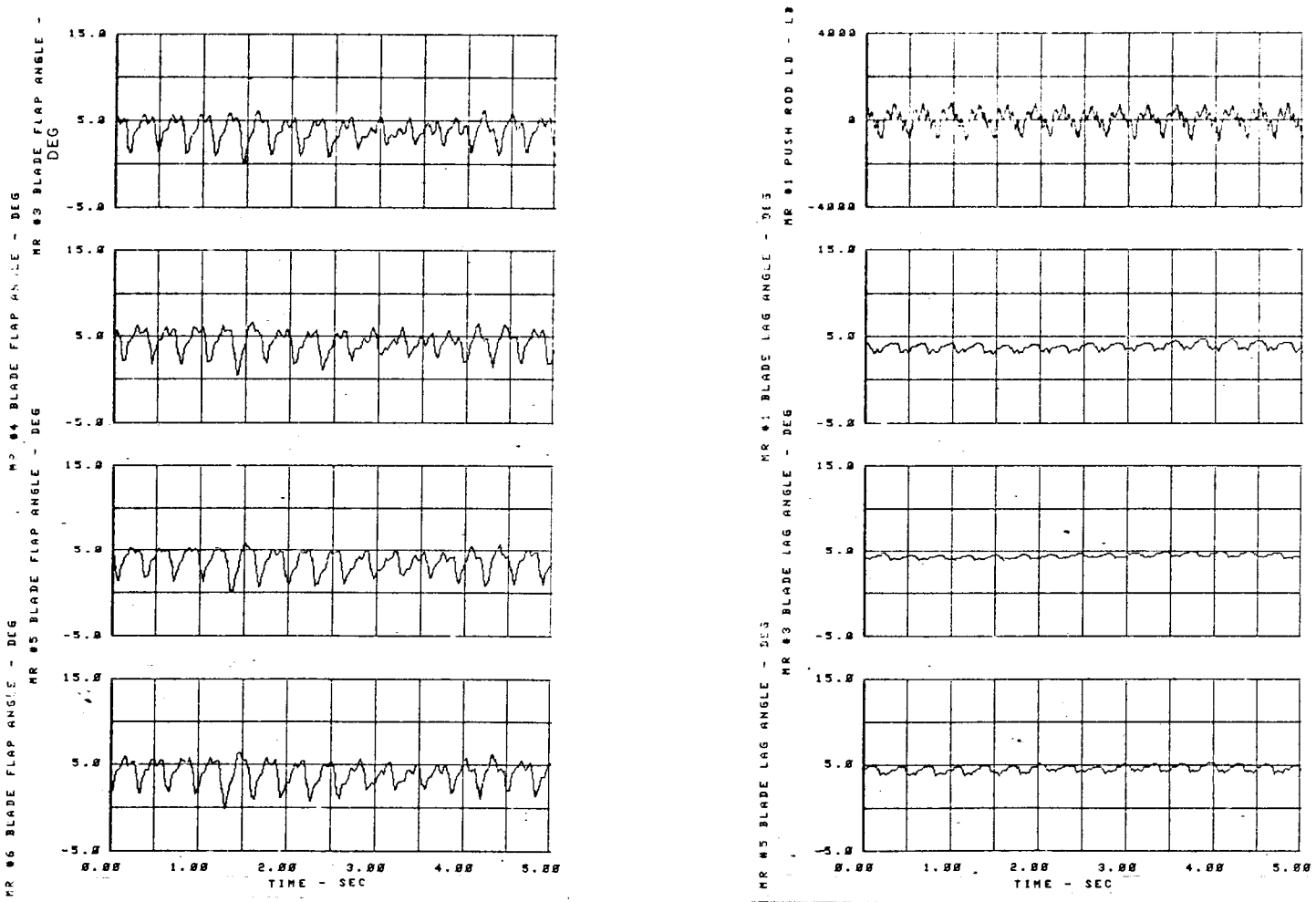

Figure 62. - Concluded.

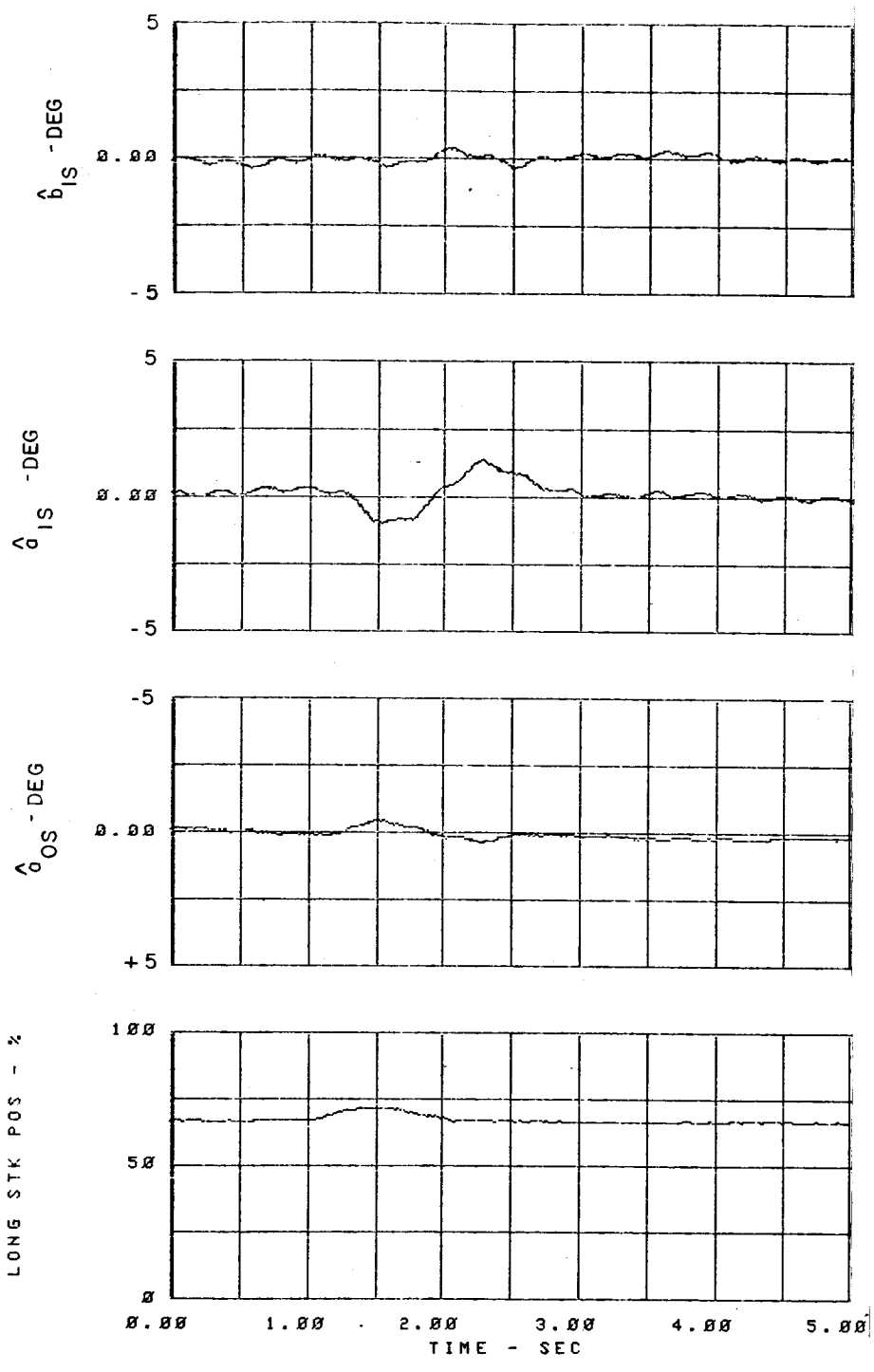

Figure 63. Change in Tip-Path-Plane Coefficients from Trim Estimated in Flight by the Kalman Filter (CH-53A at 150 Kts).

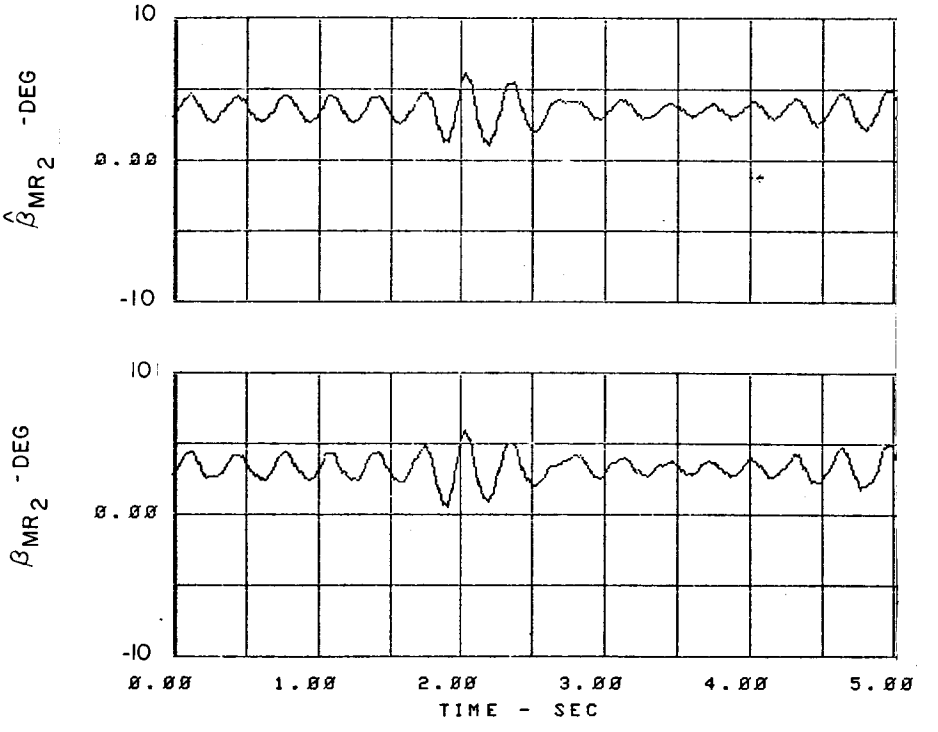

Figure 64. Blade Flapping Reconstructed from Estimated Tip-Path-Plane Coefficients vs Actual Blade Flapping in Flight for CH-53A in Hover.

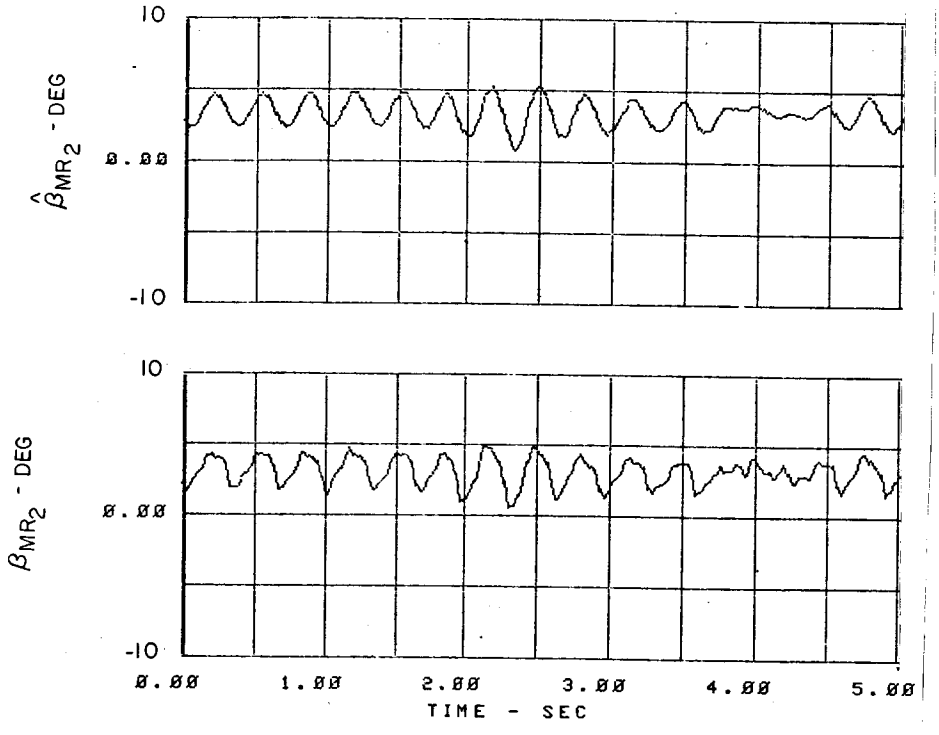

Figure 65. Blade Flapping Reconstructed from Estimated Tip-Path-Plane Coefficients vs Actual Blade Flapping in Flight for CH-53A at 100 Kts.

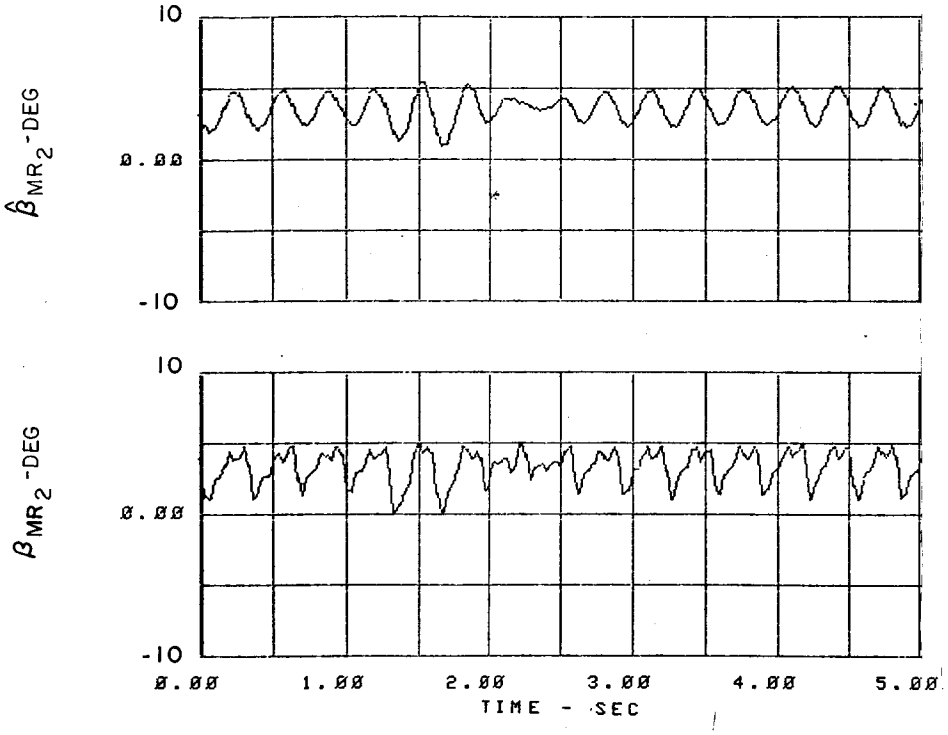

Figure 66. Blade Flapping Reconstructed from Estimated Tip-Path-Plane Coefficients vs Actual Blade Flapping in Flight for CH-53A at 150 Kts.

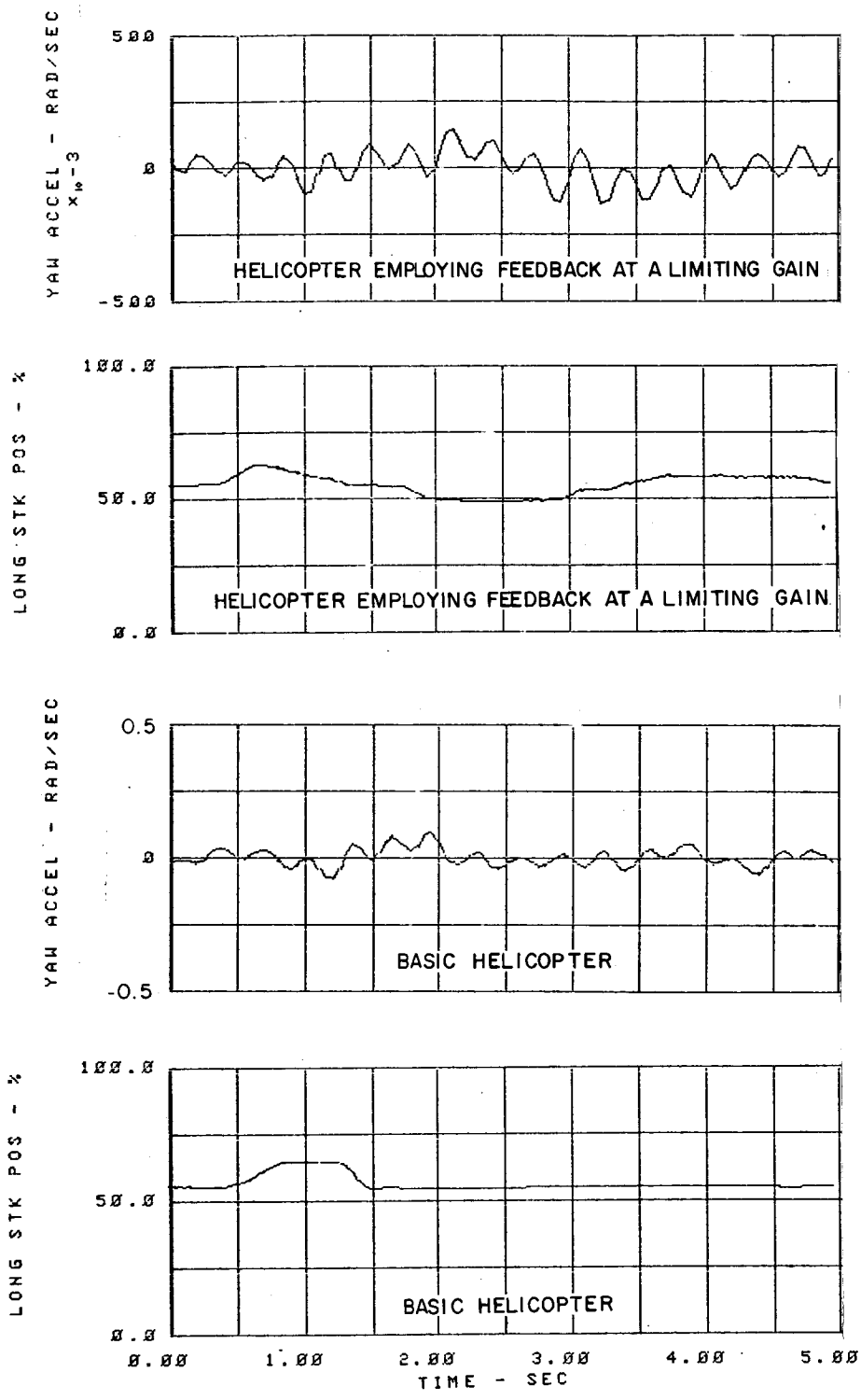

Figure 67. Yaw Response for Helicopter Employing Feedback at a Limiting Gain (Delta-3 = 0.6 deg/deg) Compared to Yaw Response of Basic Helicopter (CH-53A Test Data at 100 Kts).

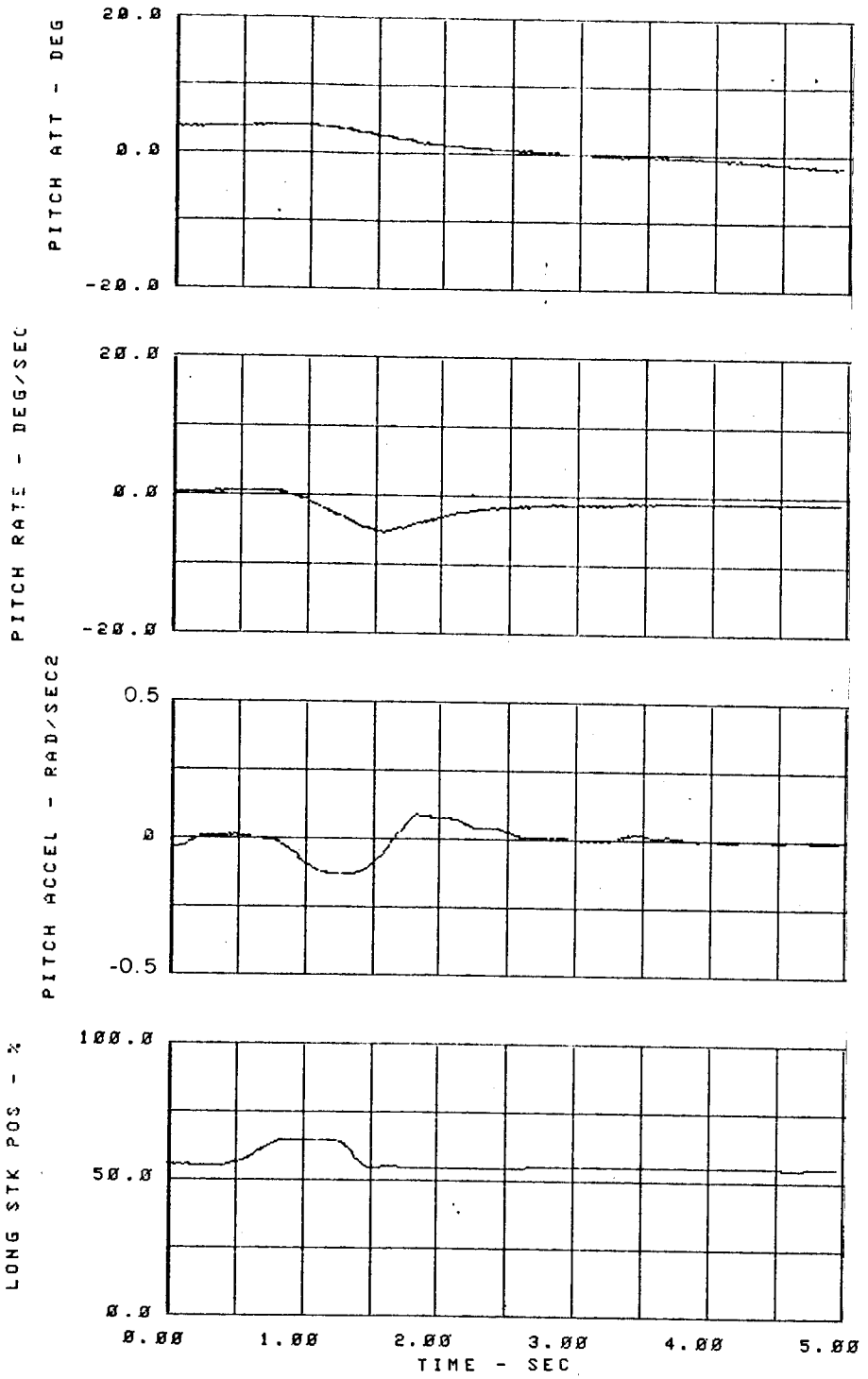

Figure 68. Pitch and Roll Response of Basic Helicopter (Without Conventional SAS) to a Forward Cyclic Stick Input (CH-53A Test Data at 100 Kts).

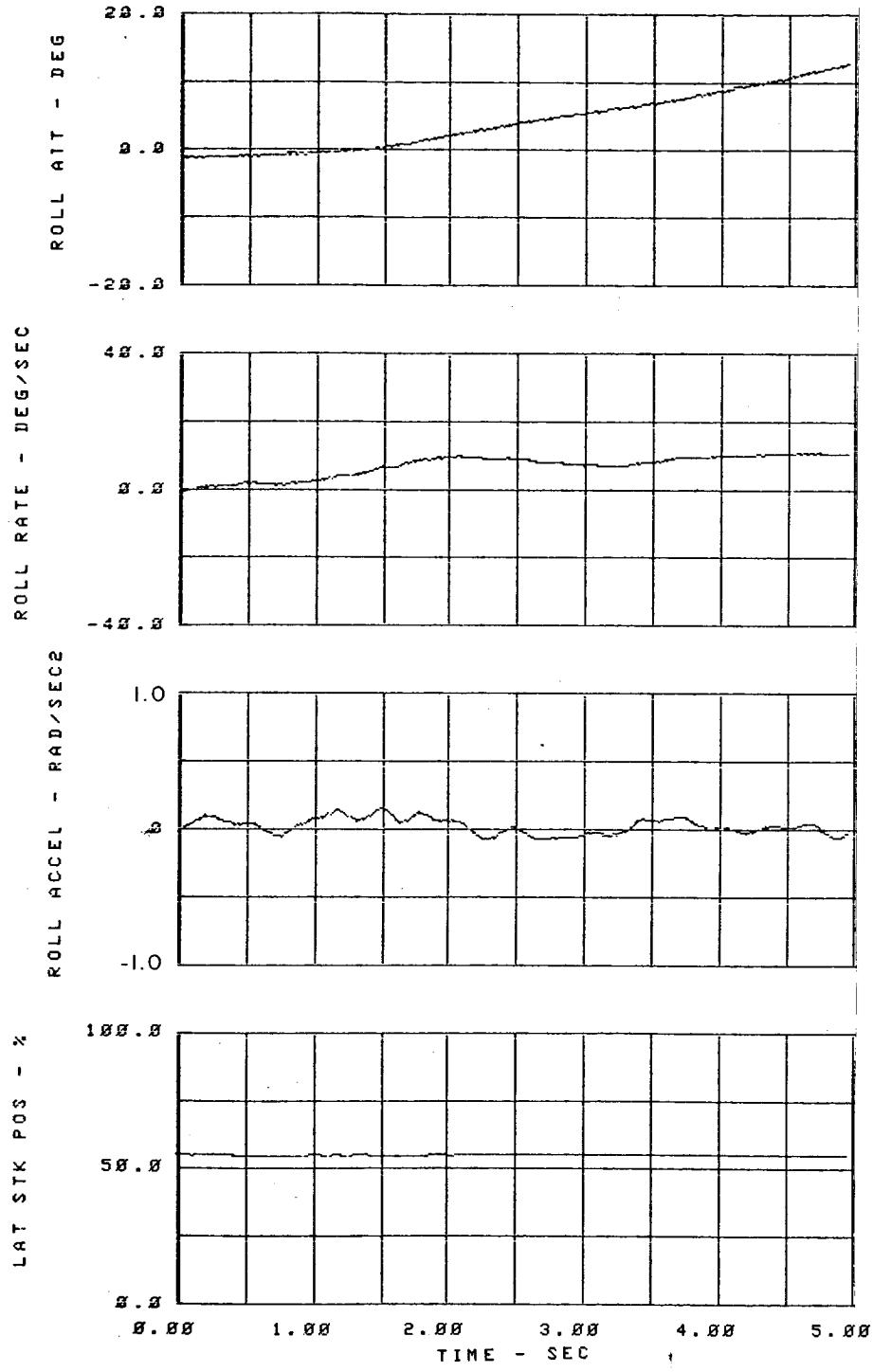

Figure 68. - Concluded.

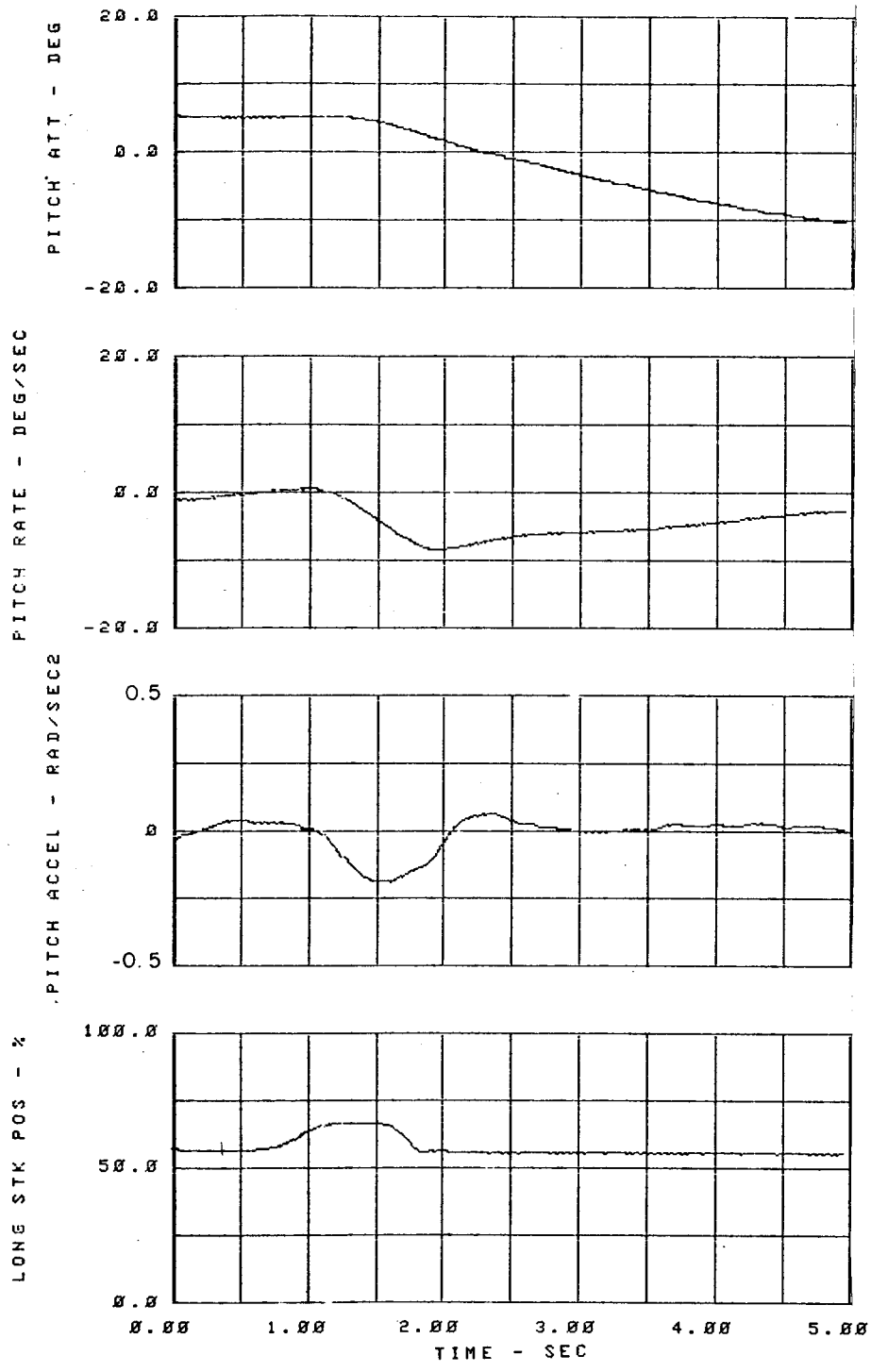

Figure 69. Pitch and Roll Response of Helicopter with Delta-3 Feedback = 0.2 deg/deg, to a Forward Cyclic Stick Input (CH-53A Test Data at 100 Kts).

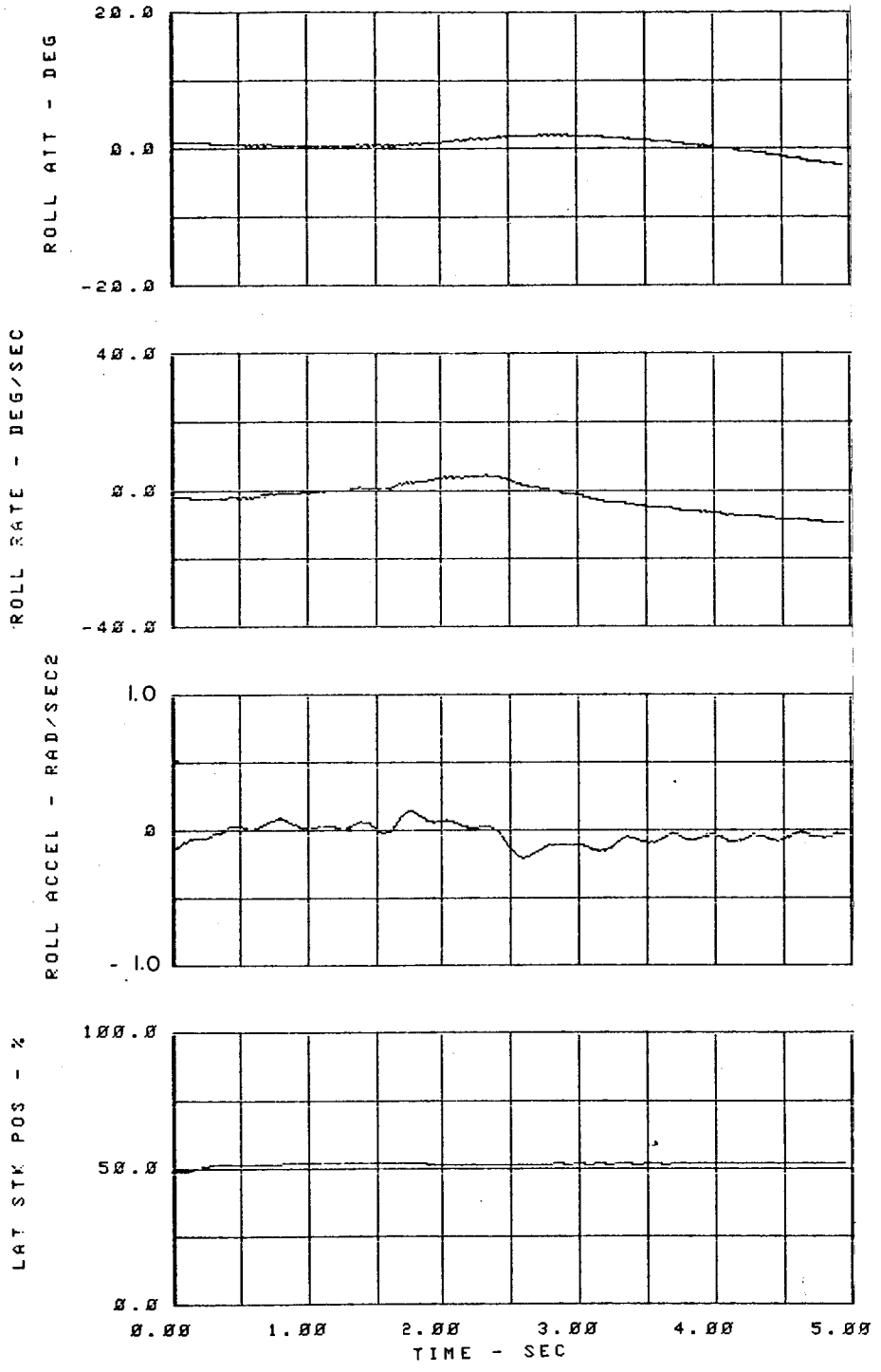

Figure 69. - Concluded.

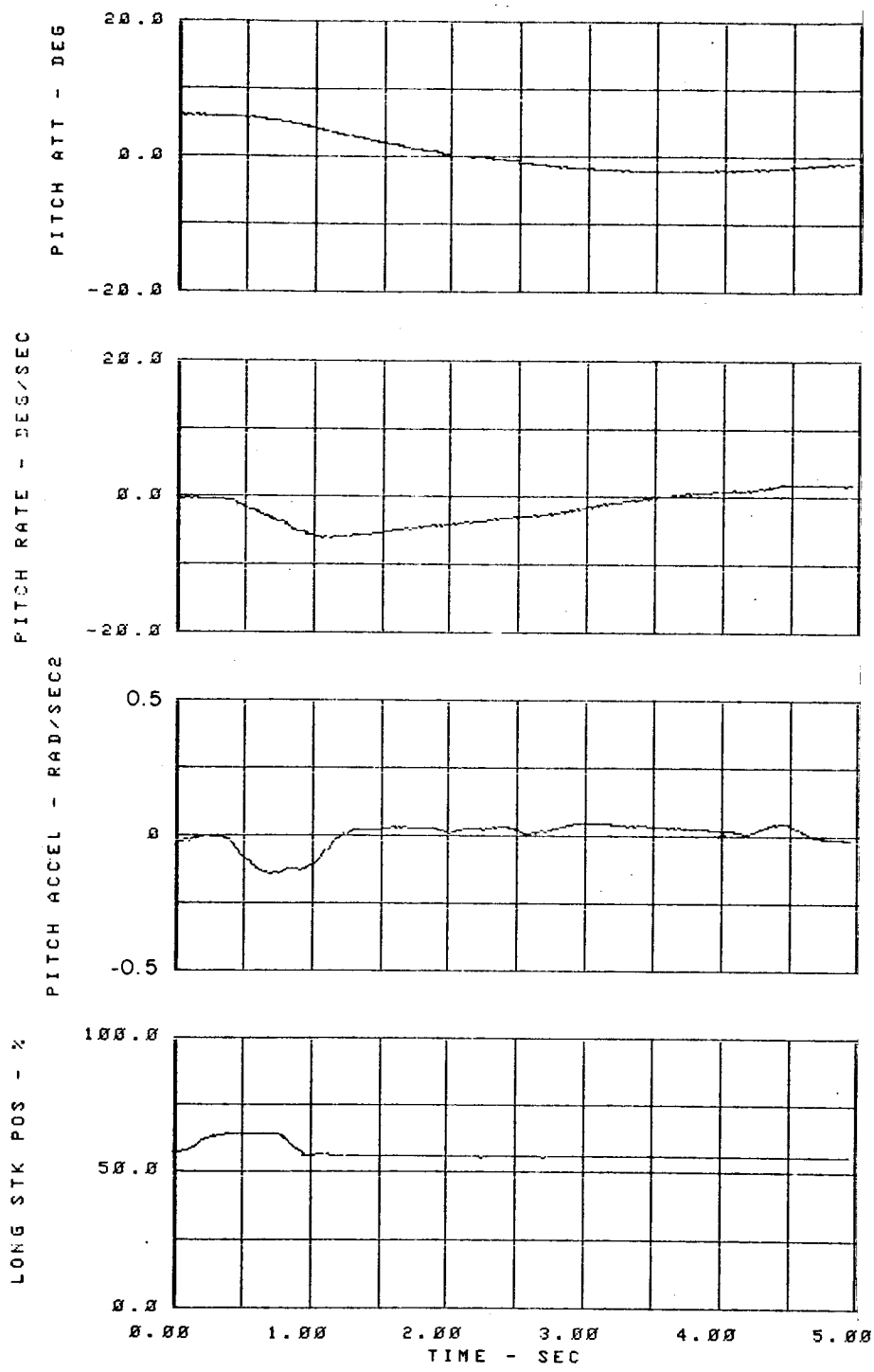

Figure 70. Pitch and Roll Response of Helicopter with Delta-3 Feedback = 0.4 deg/deg, to a Forward Cyclic Stick Input (CH-53A Test Data at 100 Kts).

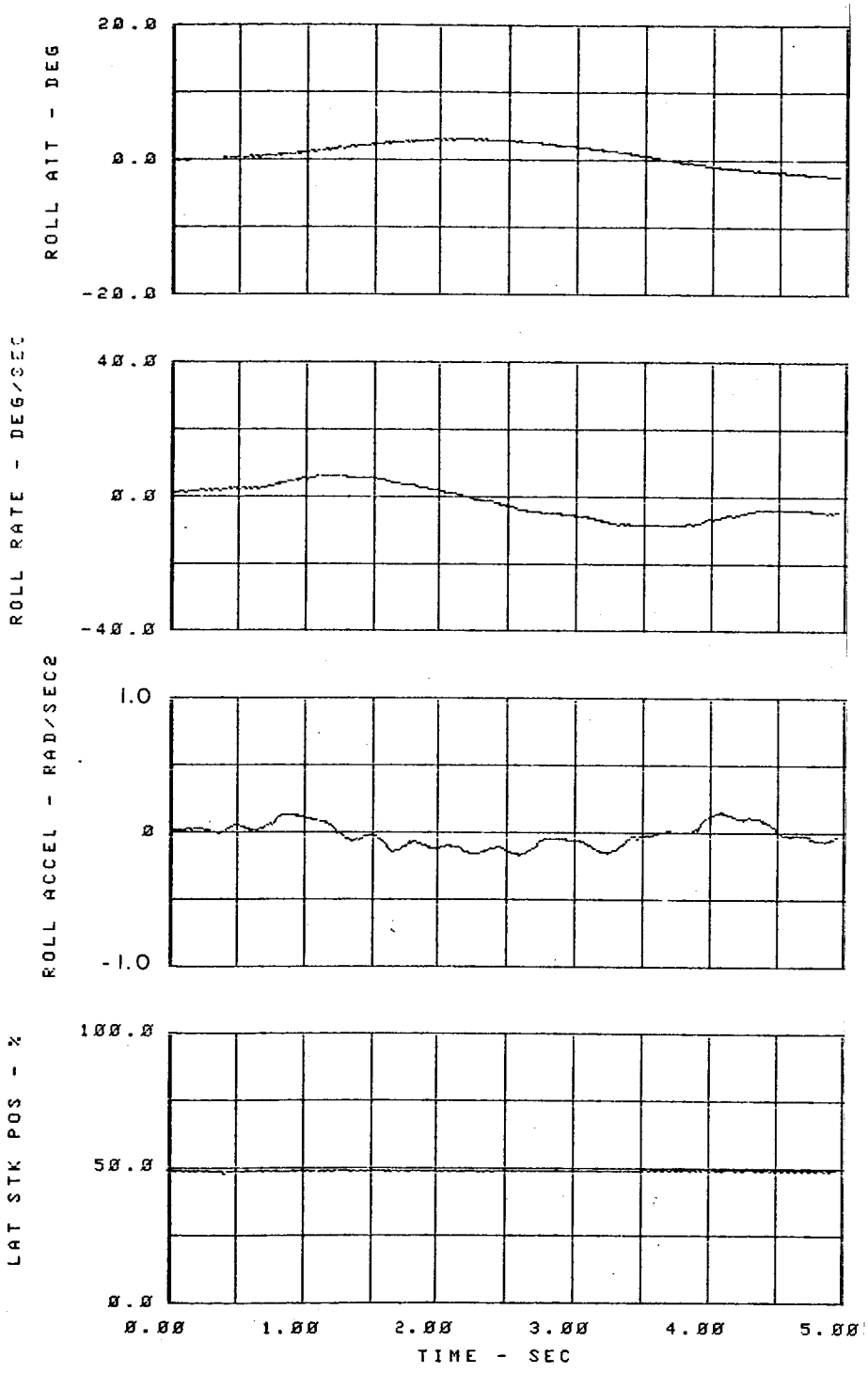

Figure 70. - Concluded.

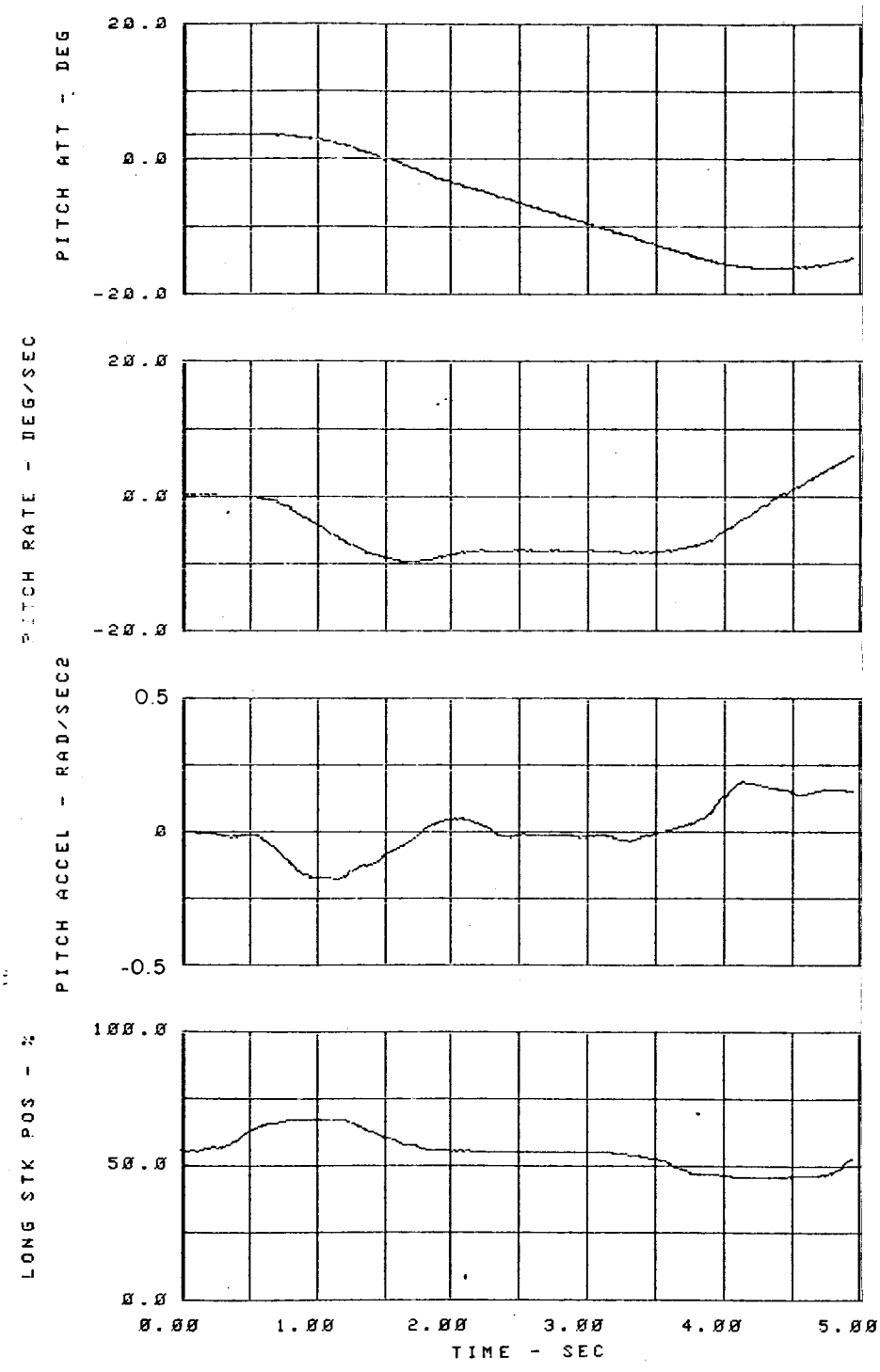

Figure 71. Pitch and Roll Response of Helicopter with Delta-3 Feedback = 0.6 deg/deg, to a Forward Cyclic Stick Input (CH-53A Test Data at 100 Kts).

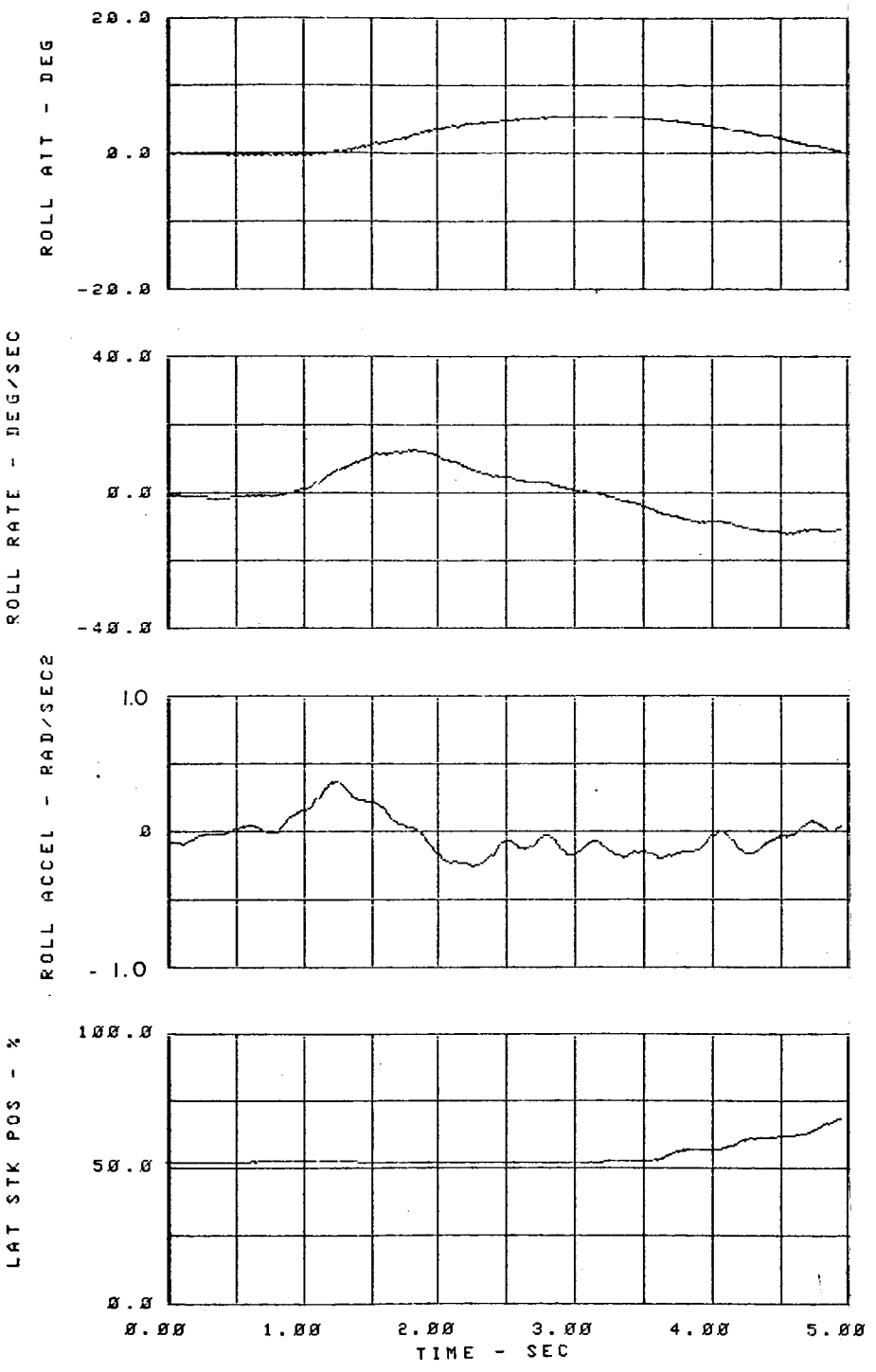

Figure 71. - Concluded.

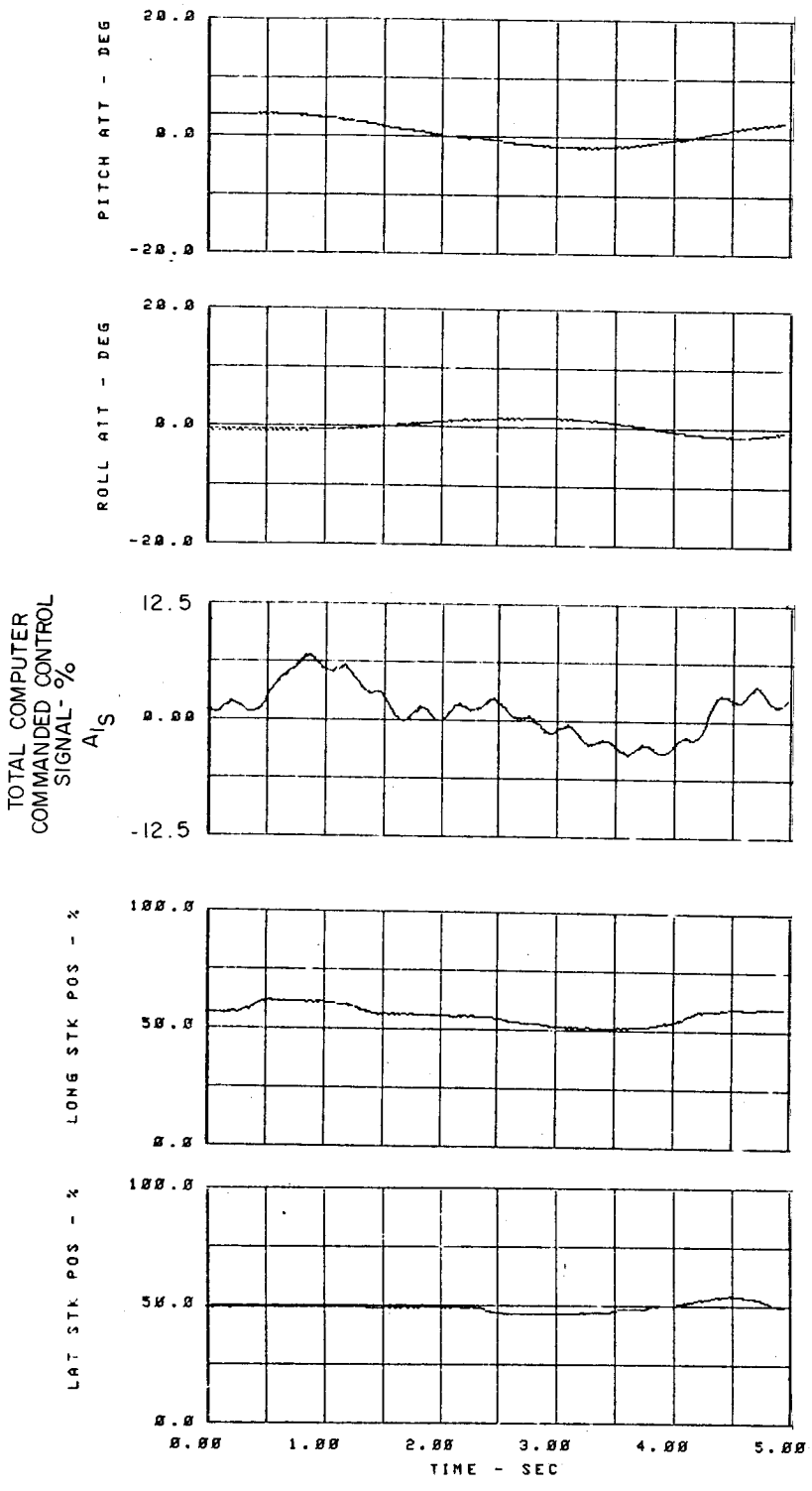

Figure 72. Cross-Coupled Response of Helicopter With Delta-3 Feedback (0.5 deg/deg), to a Forward Cyclic Stick Input (CH-53A Test Data at 100 Kts).

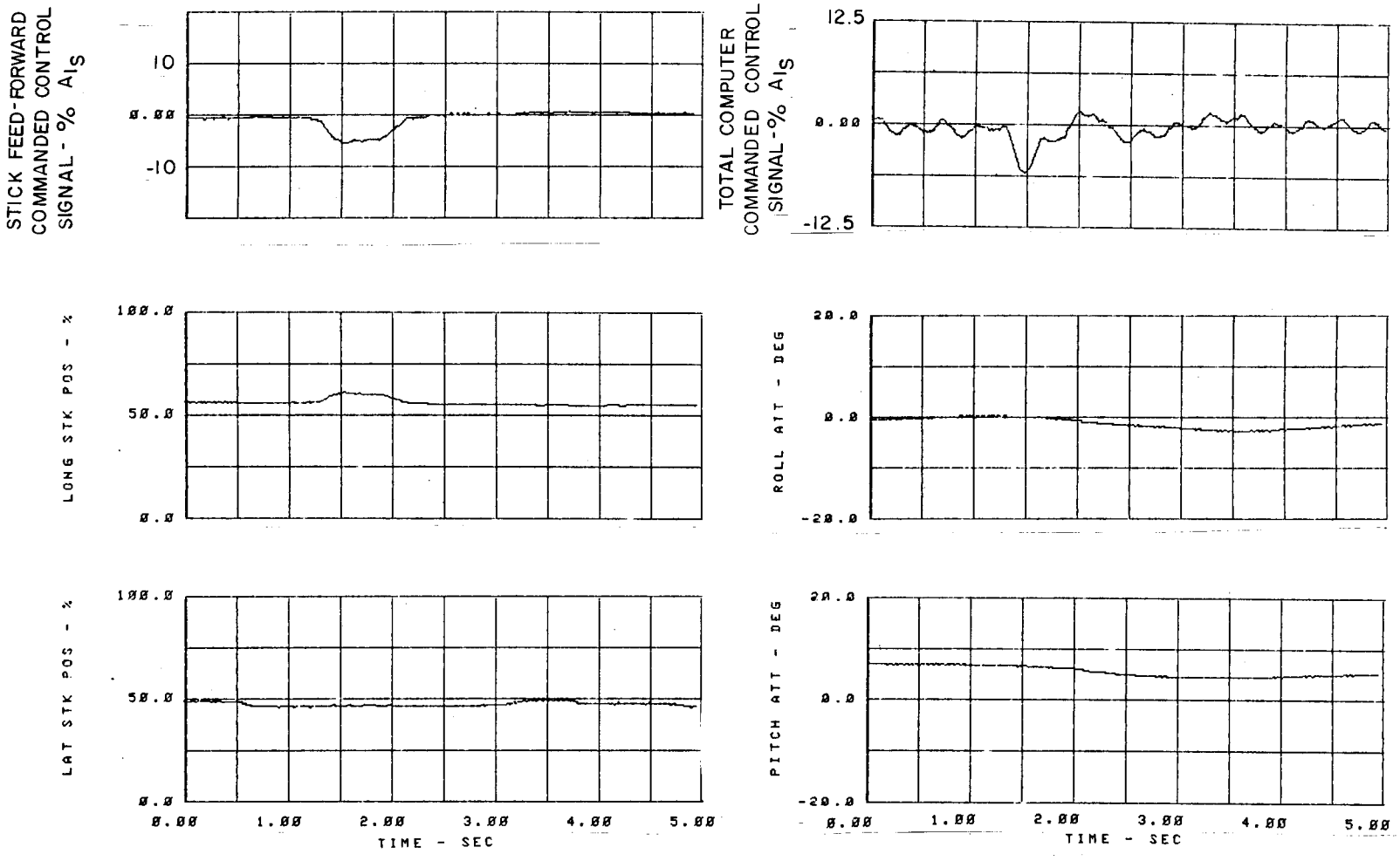

Figure 73. Cross-Coupled Response of Helicopter With Delta-3 Feedback (0.5 deg/deg) and Stick Feed-Forward, to a Forward Cyclic Stick Input (CH-53A Test Data at 100 Kts).

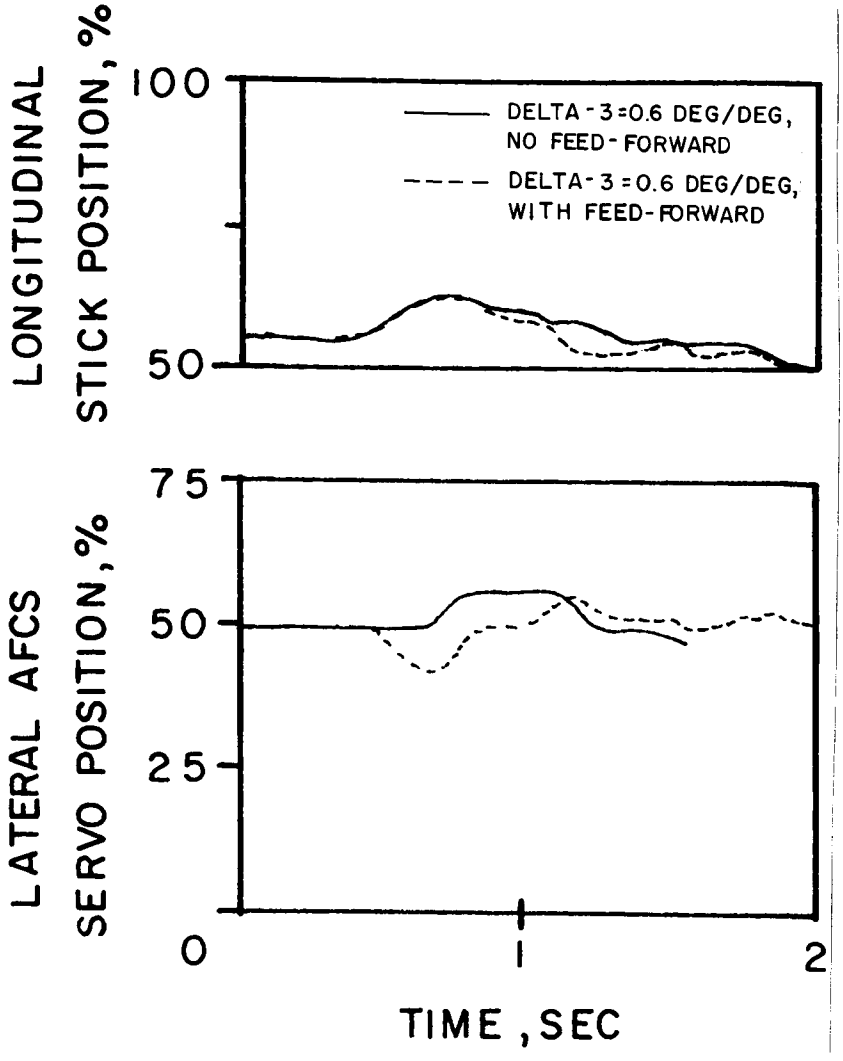

Figure 74. Time Difference Between Rotor Feedback and Stick Feed-Forward Inputs (CH-53A Test Data at 100 Kts).

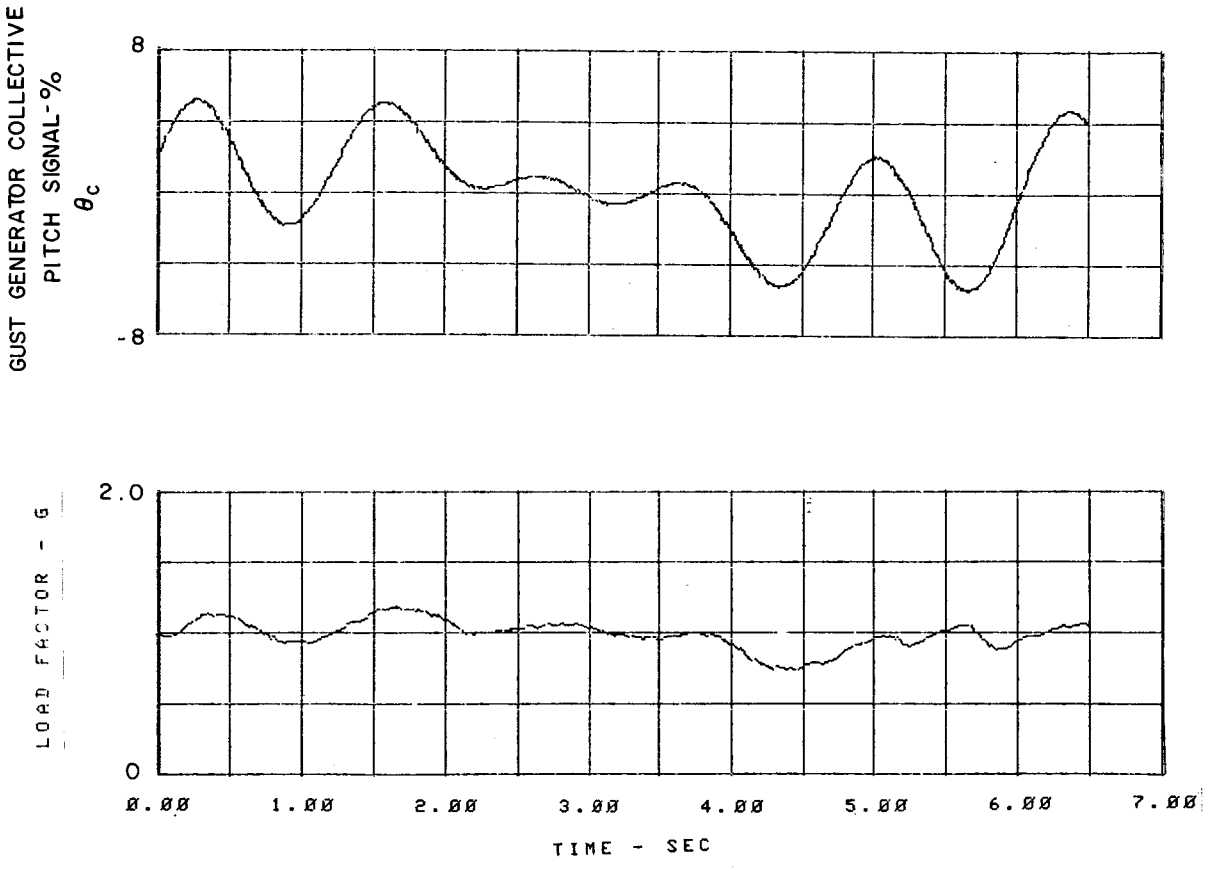

Figure 75. Simulated Gust Disturbance Collective Pitch Input and Basic Helicopter Normal Load Factor Response (CH-53A Test Data at 150 Kts).

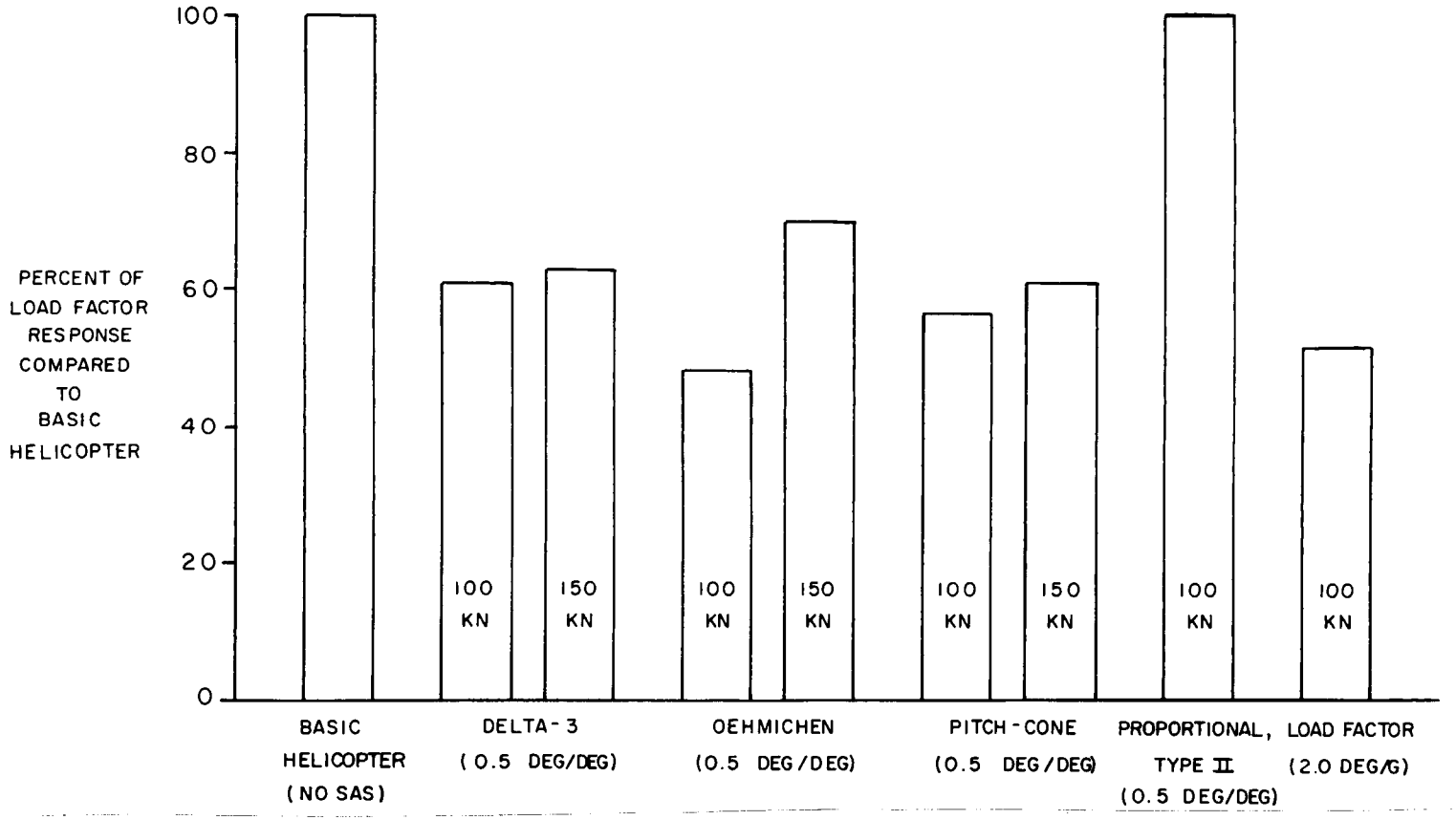

Figure 76. Reduction in Transient Normal Load Factor Response Due to Gust Disturbance For Various Feedback Schemes (Based on CH-53A Test Data).